STUDIES TOWARD A UNIFIED SYNTHESIS OF APOPTOLIDINONE C AND GLYCOSYLATED VARIANTS

By

Katherine Melissa Chong

Dissertation

Submitted to the Faculty of the

Graduate School of Vanderbilt University

in partial fulfillment of the requirements

for the degree of

DOCTOR OF PHILOSOPHY

in

Chemistry

August 31, 2017

Nashville, Tennessee

Approved:

Gary A. Sulikowski, Ph.D.

Brian O. Bachmann, Ph.D.

Lawrence J. Marnett, Ph.D.

Steven D. Townsend, Ph.D.

To my grandparents who sacrificed everything

To my parents for their amazing love, patience, and support

To my baby brothers, whom I will always love and care for

And

To Thomas Struble, whom I could never live without

ACKNOWLEDGEMENTS

I am thankful to my advisor Dr. Gary Sulikowski for his guidance and support throughout my graduate career. From my first day until my final defense, Gary has always believed in me. His relentless pursuit toward perfection in education has always been a compelling example for our group. His passion to understand and create unique synthetic transformations, tactics, and strategies is contagious and has formed me into the chemist I am today. And his unwavering support has shaped a confidence in me that hadn't existed before graduate school, and for that I am truly grateful.

I am grateful to my committee members Dr. Brian Bachmann, Dr. Steven Townsend, and Dr. Larry Marnett, for their time, dedication, support, and guidance. Their helpful conversations at meetings through my graduate career and random hallway conversations have paved the way for my thesis work. In particular, I want to thank Larry for always making time for me, Brian for mentoring me on the chemical biology side of our work, and Steve for providing me with innumerable opportunities even without my asking. You have always been frank but overwhelmingly supportive. I could not have made it thus far without your sponsorship. So much of my success in graduate school has been a direct extension of the help you've provided me.

For instilling a love and excitement for fundamental scientific research, I must acknowledge Dr. Bruce Armitage, who first took me into his group as an undergraduate. The education I received with the Armitage group, and especially with Dr. Gloria Silva, still dictates the attitude I carry toward research today. The deep respect for the practice of education and patience toward research that I learned from Bruce, Gloria, and the group,

has carried me through graduate school and hopefully will continue, far beyond. I owe a great deal of gratitude to Karen Stump, who at Carnegie Mellon, pushed me the most to pursue higher education. And Karen taught me how to care for people, an invaluable lesson that I will never forget.

It takes a village to raise a chemist and I have been so fortunate to be surrounded by talented and supportive chemists at all times of my graduate career. I must thank, David Earl, Dr. James Salovich, Dr. Rocco Gogliotti, Dr. Somnath Jana, Dr. Kwangho Kim, Dr. Plamen Christov, Dr. Yasunori Toda, Dr. Kazuyuki Tokumaru, Dr. Joseph Panarese, Dr. Matt O'Reilly, Dr. Matthew Windsor, Dr. Marta Wenzler, Dr. Ian Romaine, and Dr. Matthew Leighty, for investing the time to answer my questions, talk about chemistry and life, and teach me the ropes.

Throughout my time at Vanderbilt University, I've also had the pleasure of working with some of the best collaborators including, David Earl of the Bachmann group and Sai Leelatian of the Irish group. Without their help, this project would never have made it off the ground. Within the Sulikowski group, I need to acknowledge, celebrate, and thank several members of "team apo." My deepest of thanks must be extended toward Robby Davis, whose work on the synthesis of the apoptolidinone fragments is never acknowledged enough. For helpful conversations regarding new synthetic routes, past apoptolidin routes, writing and applying for grants and fellowships, and completing this very thesis, I am indebted to your support. You have been the easiest collaborator to work with and an excellent friend. I would also like to acknowledge several undergraduate summer researchers, REU students, and visiting scholars who I have had the pleasure of

working with on the apoptolidin project: Megumi Ito, BinHua Li, and Peter Hall. I want to wish you all the best as you set forth into the future.

To get through the trials and tribulations that make up the bulk of daily graduate school life, I must thank my entire group, past and present. In particular, I want to thank Dr. Brendan Dutter, Robby Davis, Jenny Benoy, Jason Hudlicky, Chris Fullenkamp, Quinn Bumpers, Zach Austin, Alex Allweil, and Jade Williams. Thank you all for living in such a vibrant world of possibilities with me. I have enjoyed all our conversations from new retrosynthetic connections for our projects to theorizing a world in which we all have lab-related superpowers. Thank you for enduring my endless "knock-knock" and punny jokes. Together we've created such a fun atmosphere that is intellectually stimulating yet without pretense. I will miss our group the most and I'm sad to be leaving such an easy environment to work in. I believe in all your individual future successes and hope that you can keep up the atmosphere for years to come. Don't lose sight of who you were when you first came to graduate school but don't stop growing as a person and chemist either.

I have always tried to get out of my comfort zone by moving to new cities where I know no one. Five years after moving to Nashville, as I embark on a new journey to a new city, I'm sad to leave behind the new friendships I've made. To Chelsea Davis, Madeline Long, and Alexis Wong who have always listened when I needed to be heard and helped me remember to have fun; to me, you are family. To Matt and Madison Knowe for being some of the first friends I made in Nashville. To Evan Gizzie and Wes Bauer for being the older brothers I never had but always (kind of, sometimes, but definitely) wanted. When I look back on graduate school, I'll think of it fondly because of the fun times we all shared. To

Keersten Ricks and Emilianne McCranie Limbrick for always looking out for me. And to Mike Turo, Gail and Mike Danneman, Brandon Vara, Chris Gulka, Jade Bing, Andrew Kantor, Andrew Flach, Rob Hinkle, Emily Buttgieg, Alex Lamars, and especially Ms. Carol Simpson for your invaluable friendship.

Family is not an important thing. It is everything. I am who I am today thanks to my mother, my father, my brothers, and my grandparents. They have given me everything and the education I have is all thanks to them. My grandparents and parents have sacrificed everything they had to ensure a better future for their family. A lifetime would not be a sufficient amount of time to repay every thing my parents have given and taught me. I will always be indebted to their unconditional love and support. Through all they've been through in a lifetime, they can always find the patience to let me figure things out on my own. Learning to walk the line between two societies: American and Chinese was not an easy task, but growing up, you never gave up on me. Through the ups and downs of graduate school, you championed on my behalf and taught me to never give up on my goals. One day, I hope to echo, even to a small degree, the amount of firm yet humble confidence and determination you both exude. My parents have always been and will always be my greatest role models in life.

I also need to thank my younger brothers, Matthew and Brian Chong, who have always kept my ego in check – unimpressed by anything their older sister has ever done! You both will always be my baby brothers and I will never stop fighting for you.

I need to thank my cousin Dr. Candice Yip, who to this day still treats me like a younger sister. Thanks for standing up for me in high school, for pushing me through graduate school, for listening, and for always being there.

I have been fortunate to inherit a great deal of friends I now consider family. I want to thank Darcy, Ed, Molly, Neil, Mikee, Monica, and Jim Struble for always treating me like family. To Darcy especially for always picking up my phone calls on my way home from work, for listening to me always, and for being the best friend anyone could ask for. To Molly Struble, for always bringing me down to earth. And to all the Strubles, for caring for me like family.

My journey through graduate school could never have been complete without my boyfriend, Thomas Struble. You have stood with me at my best and my worst, and you have never left my side. At my ugliest, you still accepted, supported, and befriended me. You have always been relentless in your belief in me that so much of my strength these past five years has really come from you. This degree is as much yours as it is mine; I could not have made it through graduate school without you. You are my best friend and my other half – my best half.

Life is really simple but we insist on making it complicated.

– Confucius

TABLE OF CONTENTS

LIST OF TABLES

LIST OF FIGURES

CHAPTER I

INTRODUCTION TO APOPTOLIDIN: ISOLATION, BIOSYNTHETSIS, STRUCTURE AND ACTIVITY RELATIONSHIP, AND BIOACTIVITY HISTORY

1.1 Apoptolidin isolation and biosynthesis

Apoptolidin A **1.1** was first isolated by Seto and coworkers from a soil microbe classified as an actinomycete, of the species *Nocardiopsis sp*. Apoptolidin A **1.1** was named according to its selective apoptotic activity against E1A induced rat glial cells over untransformed cells.[1] Its structure was fully elucidated one year from its isolation [2] and to date, over ten structurally similar apoptolidins have been described **1.1-1.14** (Fig. 1) [3-10]. The apoptolidin family is characterized by their inclusion of a 20 or 21- membered macrolactone core (isoapoptolidins), fully substituted hemi-ketal pyran ring, 30 stereogenic elements (25 stereocenters, 5 double bonds), and variable glycosylation that may include the addition of three carbohydrate units at the C9- and C27- positions. The members of this family differ at several positions including the C6-, C2'-, C16-, C19-, C27- positions, E/Z geometry about C2-3, and *O*-acyl migration of the C1 carbonyl onto either the C19- or C20- hydroxyls. More recently, Mahmud and coworkers at Oregon State University have isolated and identified three additions to the apoptolidin family, including: 2'-*O*-succinylated- and 3'-*O*-succinylated- apoptolidins **1.12 – 1.13**, and linear fully glycosylated apoptolidin seco-acid **1.14** from an *Amycolatopsis sp.* ICBB 8242. [10]

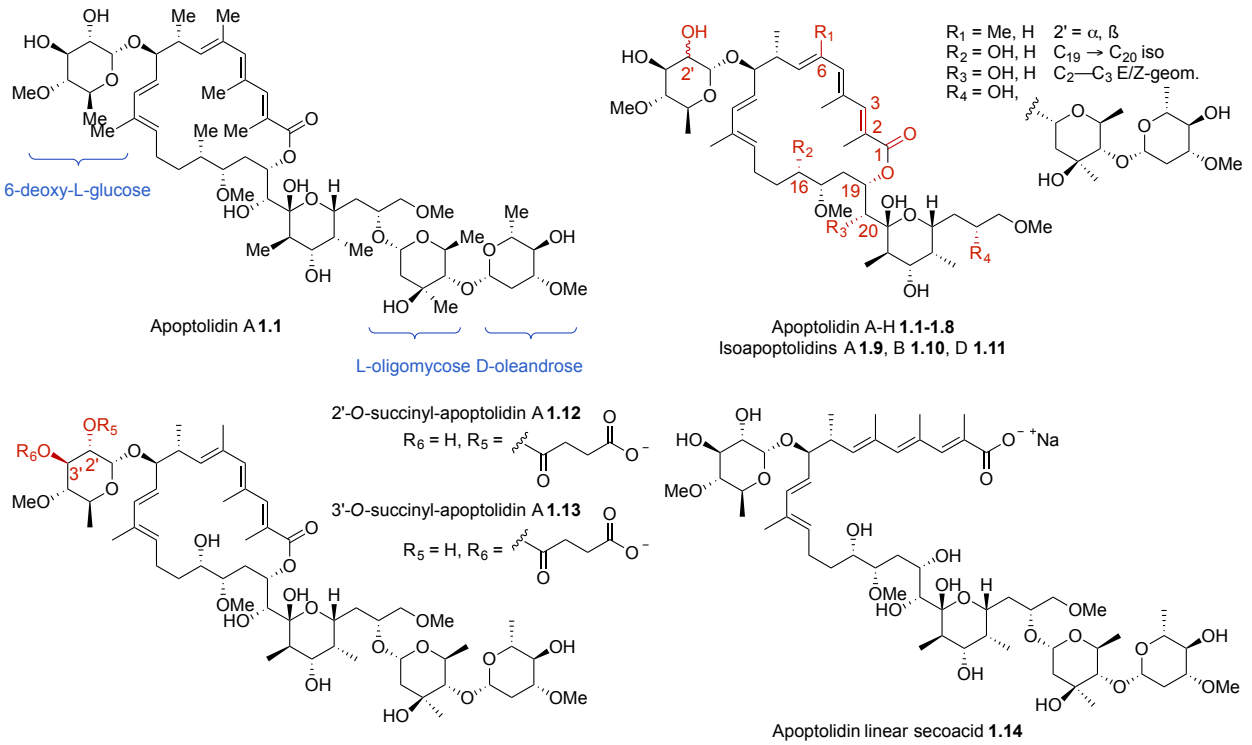

Figure 1.1. Members of the apoptolidin family of macrolides.

The apoptolidin family is derived from a polyketosynthase (PKS) cluster, annotated by Bachmann and coworkers (Fig 1.2 and 1.3). [11] Its genome is comprised of a non-iterative type-I PKS with 13 homologating modules and spans approximately 39 open reading frames (ORF), including nine type-I PKS, six oxidoreductase, four methyltransferase, and three glycosyl trasnferase genes. Of the 65 domains that encode for the biosynthesis of the macrolide apoptolidin core, four have been predicted to be inactive (denoted in black, Fig. 1.2) Interestingly, the apoptolidin biosynthesis begins with a (2R)-methoxymalonyl-acyl carrier protein (ACP) loading module (Fig. 1.3). Though atypical, this precursor has been observed in various type-I polyketide biosynthesis (e.g. FK520, soraphen, and ansamitocin). [40] The apoptolidin gene cluster also includes a single cluster of putative sugar biosynthetic genes that encode for its three sugar appendages: 6-deoxy-4-*O*-L-methyl glucose, L-

olivomycose and D-oleandrose (Fig. 1.1), and is flanked by two glycosyl transferases. A third glycosyl transferase is located within the putative PKS cluster. Lastly, there are two putative *O*-methyl transferases and two candidates for C-H oxidation of the C16- and C20-positions via ApoP, a P_{450} gene that is similar to an oxidase used in the biosynthesis of the erythromycin macrolide core, and ApoD1-3 gene, non-heme iron-dependent oxidase that is similar to those used in aryl oxidations.

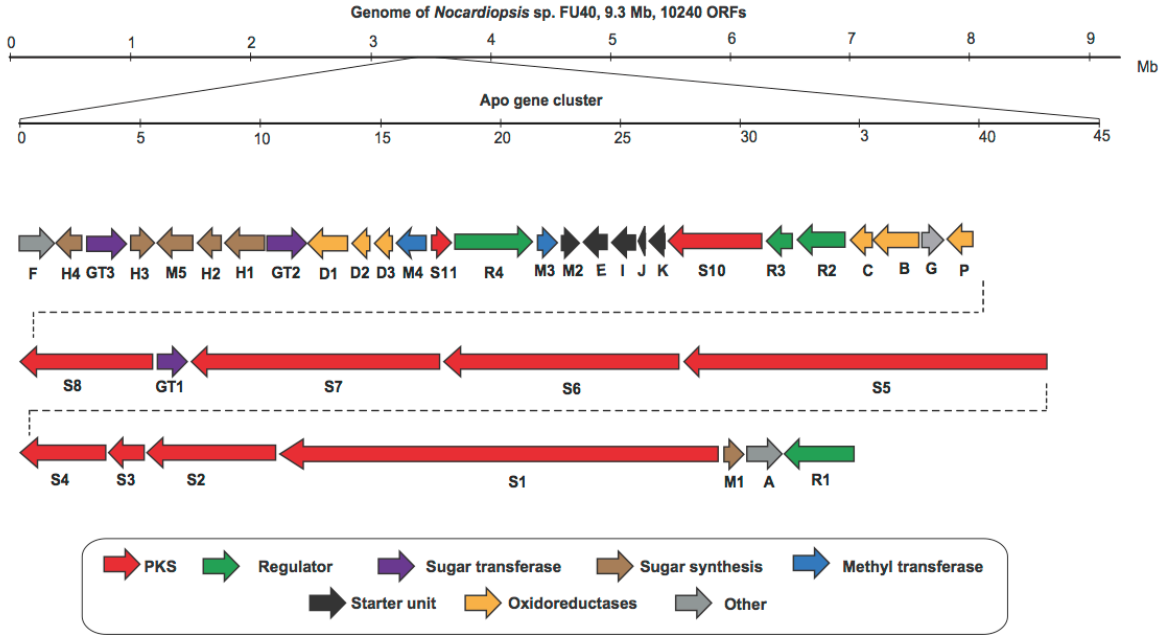

Figure 1.2. Organization of apoptolidin gene cluster in *Nocardiopsis* sp. FU 40. [11]

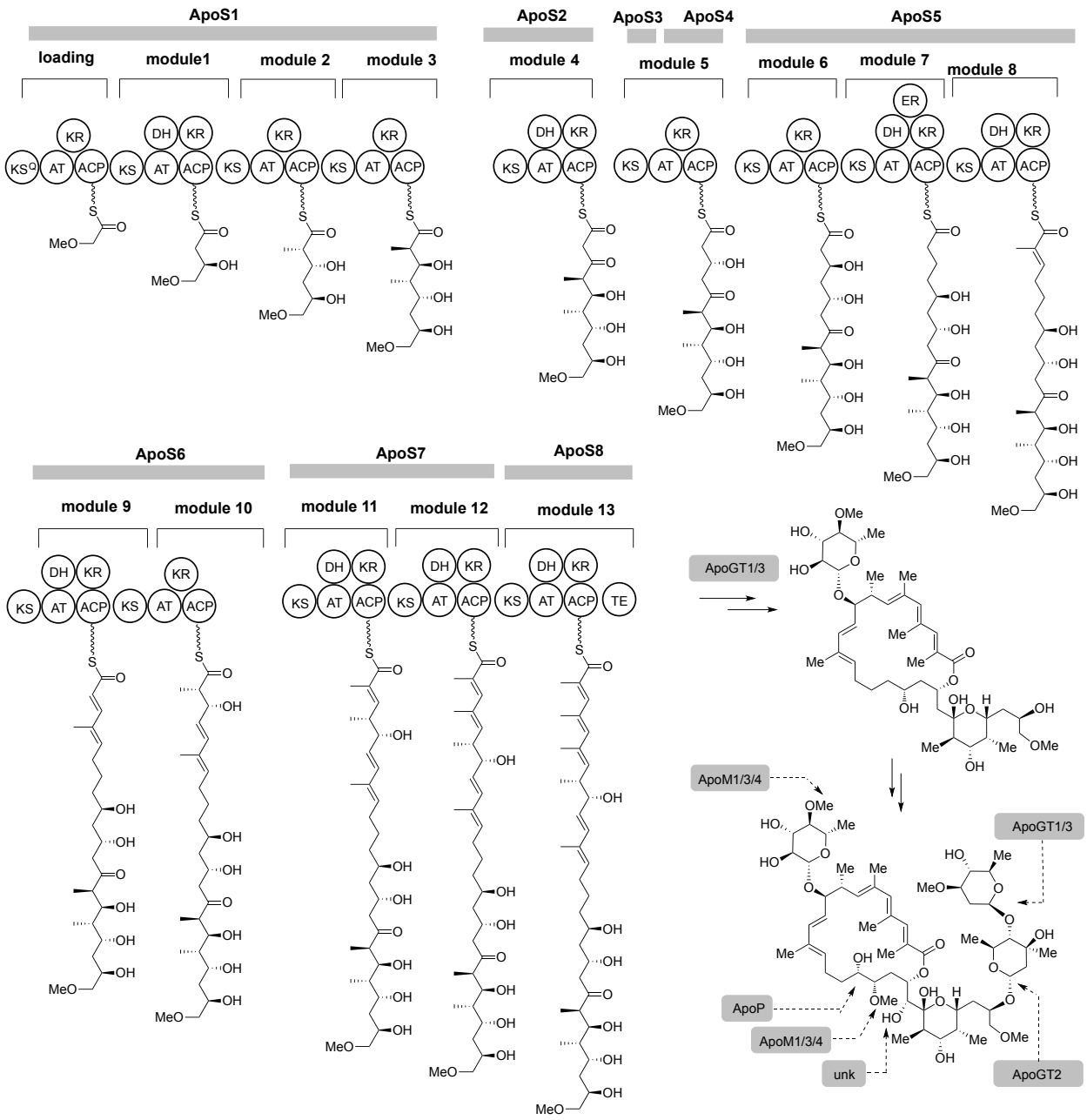

Figure 1.3. Hypothetical biosynthetic pathway leading to apoptolidin A. [11]

1.2 Apoptolidin structure and activity relationship: the apoptolidin family

Structural differences among the naturally occurring members of the apoptolidin family **1.1-1.14** have revealed a great deal of insight into the importance of various structural features within the molecule for bioactivity (Fig. 1.4). [3-11]

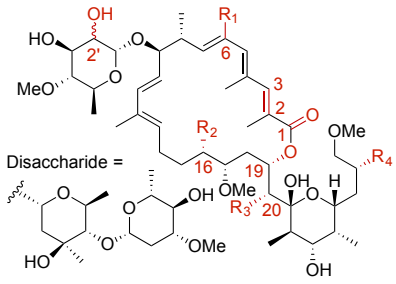

Apoptolidin A **1.1** (R_1 = Me, R_2 = OH, R_3 = OH, R_4 = Disaccharide, C2' = β, C_{19} O-Acyl, C_2-C_3 = E geom)
Apoptolidin B **1.2** (R_1 = Me, **R_2 = H**, R_3 = OH, R_4 = Disaccharide, C2' = β, C_{19} O-Acyl, C_2-C_3 = E geom)
Apoptolidin C **1.3** (R_1 = Me, **R_2 = H, R_3 = H**, R_4 = Disaccharide, C2' = β, C_{19} O-Acyl, C_2-C_3 = E geom)
Apoptolidin D **1.4** (**R_1 = H**, R_2 = OH, R_3 = OH, R_4 = Disaccharide, C2' = β, C_{19} O-Acyl, C_2-C_3 = E geom)
Apoptolidin E **1.5** (R_1 = Me, R_2 = OH, R_3 = OH, R_4 = Disaccharide, **C2' =** α, C_{19} O-Acyl, C_2-C_3 = E geom)
Apoptolidin F **1.6** (R_1 = Me, **R_2 = H, R_3 = H, R_4 = OH, C2' =** α, C_{19} O-Acyl, C_2-C_3 = E geom)
Apoptolidin G **1.7** (R_1 = Me, R_2 = OH, R_3 = OH, R_4 = Disaccharide, C2' = β, C_{19} O-Acyl, **C_2-C_3 = Z geom**)
Apoptolidin H **1.8** (R_1 = Me, R_2 = OH, R_3 = OH, **R_4 =OH**, C2' = β, C_{19} O-Acyl, C_2-C_3 = E geom)
Isoapoptolidin A **1.9** (R_1 = Me, R_2 = OH, R_3 = OH, R_4 = Disaccharide, C2' = β, **C_{20} O-Acyl**, C_2-C_3 = E geom)
Isoapoptolidin B **1.10** (R_1 = Me, **R_2 = H**, R_3 = OH, R_4 = Disaccharide, C2' = β, **C_{20} O-Acyl**, C_2-C_3 = E geom)
Isoapoptolidin D **1.11** (**R_1 = H**, R_2 = OH, R_3 = OH, R_4 = Disaccharide, C2' = β, **C_{20} O-Acyl**, C_2-C_3 = E geom)

	F_OF_1-ATPase IC_{50} (μM)[x]	H292 Cells IC_{50} (nM)[x,x]	HeLa Cells IC_{50} (nM)[x]	H292 Cells GI_{50} (μM)[x]	H292 Cells EC_{50} (nM)
Apoptolidin A **1.1**	0.7 ± 0.5	16[x]	39	0.032 ± 0.003	50 (60 - 210)[x]
Apoptolidin B **1.2**				0.007 ± 0.004	
Apoptolidin C **1.3**				0.024 ± 0.005	
Apoptolidin D **1.4**					110 (60 - 210)[x]
Apoptolidin E **1.5**					> 500[x]
Apoptolidin F **1.6**					< 100[x]
Apoptolidin G **1.7**		150[x]			
Apoptolidin H **1.8**		610[x]			
Isoapoptolidin A **1.9**	17 ± 5				
Isoapoptolidin B **1.10**					
Isoapoptolidin D **1.11**					
2'-*O*-Succ-Apoptolidin A **1.12**		91	240		
3'-*O*-Succ-Apoptolidin A **1.13**		82	260		
Apoptolidin A Secoacid **1.14**		> 1000	> 1000		

Figure 1.4. Structure-activity relationship (SAR) of members of the apoptolidin family of macrolides.

While members of the apoptolidin family reportedly exhibit similar cytotoxicity against tumor cell lines, it is important to note that certain structural features directly impact observed potency. *O*-acyl migration from the C19- to the C20- hydroxyl, resulting in ring expansion to the isoapoptolidins, has been shown to exist in equilibrium (K_{eq} = 0.616) when kept at ambient temperature as a dilute aqueous solution (Dulbecco's phosphate-buffered saline). This ring expansion giving isoapoptolidin A **1.9**, stable at -20 °C in methanol or dichloromethane, is slightly less active (IC_{50} = 17 μM, F_oF_1-ATPase assay) than

apoptolidin A **1.1** (IC_{50} = 0.7 μM, F_oF_1-ATPase assay). Under assaying conditions, which occur in less than 20 min, less than 12% conversion to isoapoptolidin A **1.9** was observed by Wender and coworkers. [2] Independently, Sulikowski and coworkers [3] isolated isoapoptolidin A **1.9** and noticed that ring expansion from apoptolidin A **1.1** to isoapoptolidin A **1.9** could be promoted under base catalyzed conditions (triethylamine in methanol) to give a 1.4:1 mixture, in favor of the latter analogue. Koert and coworkers note that the treatment of apoptolidin **1.1** with pH=7 buffer at 37 °C for 20 hours results in the formation of a mixture of apoptolidin **1.1** and isoapoptolidin **1.9**. [17]

Additionally, apoptolidins kept in the presence of light, result in the isomerization of the C2-C3 double bond from (E)- to (Z)- geometry. The first suggestion of this photochemical liability was described in the dissertation of Jankowski at Stanford University [41] when isolating and assaying apoptolidins B **1.2** and C **1.3**. Analyzing the cytotoxicity of apoptolidin C **1.3**, in particular, they noted the formation of an unknown isomer with significantly decreased bioactivity. Utilizing spectroscopic analysis, Bachmann and coworkers [6] later determined this isomerization to occur across the C2-C3 double bond, from the (E)- geometry of apoptolidin A **1.1** to the (Z)-geometry of apoptolidin D **1.4**. While apoptolidin D **1.4** can only be isolated from the FU40 extract in < 5 mg/L, irradiation of apoptolidin A **1.1**, can give apoptolidin D **1.4** in about a 5:1 ratio. Compared to apoptolidin A **1.1** (IC_{50} = 16 nM, H292), apoptolidin D **1.4** has significantly decreased activity (IC_{50} = 150 nM, H292), making the geometry about the C2-C3 double bond extremely important for bioactivity.

Apoptolidins F **1.6** and H **1.8**, lacking the C27- disaccharide, both exhibit significantly reduced bioactivities. Wender and coworkers [7] report apoptolidin F **1.6** to have greater than an order of magnitude loss in potency (>500 nM, H292) as compared with apoptolidin A (50 nM, H292). Sulikowski and coworkers [8] report that apoptolidin H **1.8** can be obtained through targeted gene deletion of the GT2 glycosyl transferase gene by double cross over homologous recombination. Mutasynthetic removal of the C27 disaccharide, results in significantly lowered potency (610 nM, H292), on par with that of apoptolidin F **1.6**. It is important to note that while apoptolidin F **1.6** can be extracted from the crude fermentation extract of the *Nocardiopsis sp.* FU40 (< 5 mg/L), apoptolidin H **1.8** was accessed via targeted gene deletion (50-100 mg/L).

Recently isolated *O*-succinylated apoptolidin A compounds **1.12-1.13** show a slight reduction in bioactivity (91 nM and 82 nM in H292 for 2'-*O*-succinylated **1.12** and 3'-*O*-succinylated **1.13** apoptolidins, respectively). Mahmud and coworkers, [9] note that succinylated apoptolidins **1.12-1.13** may also be hydrolyzed to the more active apoptolidin A **1.1**, and note that these succinylated compounds may act more like prodrugs. Real time analysis of cellular respiration of H292 cells upon treatment of compounds **1.12-1.13** show succinylated apoptolidins to be weak mitochondrial inhibitors. Mahmud and coworkers hypothesize that the succinylation event may play a role in self-resistance and/or act as an export mechanism. Individual incubation of *O*-succinylated apoptolidins **1.12-1.13** in RPMI-1640 mammalian culture conditions for 72 hours led to approximately 30% conversion of **1.12** or **1.13** to apoptolidin A **1.1**. The linear apoptolidin A glycosylated secoacid **1.14** appeared to be inactive when tested against H292 and HeLa cancer cells (> 1 μM). This seems to suggest the extreme importance of the intact macrocyclic ring.

1.3 Apoptolidin structure and activity relationship: chemical functionalization of apoptolidins

Since the isolation of the apoptolidins, in addition to understanding its structure-activity relationship (SAR) by isolating structural analogues of the apoptolidin family, chemical modification of apoptolidin A **1.1** through semi-synthetic means has also revealed a great deal of structural information about the apoptolidins (Fig. 1.5). Work completed by the Sulikowski [4] and Wender [12-13] groups have shown that through functionalization of the decorating hydroxyls of apoptolidin, their role in terms of bioactivity can be decoded.

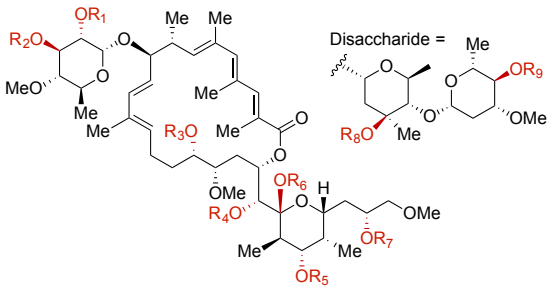

Functionalized Apoptolidins **1.15-1.25**

1.1 ($R_1 = R_2 = R_3 = R_4 = R_5 = R_6 = H$, R_7 = Disaccharide, $R_8 = R_9 = H$)
1.15 (**$R_1 = R_2 = R_3 = R_4 = R_5$ = Ac**, $R_6 = H$, R_7 = Disaccharide, **$R_8 = R_9$ = Ac**, + **$^-$OAc**)[4]
1.16 (**$R_1 = R_2 = R_3 = R_4 = R_5$ = Ac**, R_6 = **R_7 = H**)[4]
1.17 (**$R_1 = R_2 = R_3 = R_4 = R_5$ = Ac,** $R_6 = H$, **R_7 = Ac**)[4]
1.18 (**$R_1 = R_2 = R_3 = R_4 = R_5 = H$, R_6 = Me**, R_7 = Disaccharide, $R_8 = R_9 = H$)[12-13]
1.19 (**R_1 = Bz**, $R_2 = R_3 = R_4 = R_5 = R_6 = H$, R_7 = Disaccharide, $R_8 = R_9 = H$)[12-13]
1.20 ($R_1 = R_2 = R_3 = R_4 =$ H, **R_5 = Ac**, $R_6 = H$, R_7 = Disaccharide, $R_8 = H$, **R_9 = Ac**)[12-13]
1.21 ($R_1 = R_2 = H$, $R_3 = R_4 = R_5 = R_6 = H$, R_7 = Disaccharide, $R_8 = H$, **R_9 = Ac**)[12-13]
1.22 ($R_1 = R_2 = H$, **R_3 = Ac**, $R_4 = R_5 = R_6 = H$, R_7 = Disaccharide, $R_8 = R_9 = H$)[12-13]
1.23 ($R_1 = H$, **R_2 = Ac**, $R_3 = R_4 = R_5 = R_6 = H$, R_7 = Disaccharide, $R_8 = R_9 = H$)[12-13]
1.24 ($R_1 = R_2 = R_3 = H$, **R_4 = Ac**, $R_5 = R_6 = H$, R_7 = Disaccharide, $R_8 = R_9 = H$)[12-13]
1.25 ($R_1 = R_2 = R_3 = H$, **R_4 = Me**, $R_5 = R_6 = H$, R_7 = Disaccharide, $R_8 = R_9 = H$)[12-13]

	F_OF_1-ATPase K_i (μM)	F_OF_1-ATPase IC_{50} (μM)
Apoptolidin A **1.1**	0.38[4]	0.7 ± 0.5[12-13]
1.15	>100[4]	
1.16	>100[4]	
1.17	>100[4]	
1.18		2.3 ± 0.5[12-13]
1.19		0.3 ± 0.5[12-13]
1.20		0.4 ± 0.5[12-13]
1.21		0.8 ± 0.5[12-13]
1.22		0.8 ± 0.5[12-13]
1.23		0.4 ± 0.5[12-13]
1.24		1.1 ± 0.5[12-13]
1.25		2.8 ± 0.5[12-13]

Figure 1.5. Functionalized apoptolidins via chemical modification for SAR understanding.

Per-acetylation of the apoptolidins by Sulikowki and coworkers, [4] show the importance of the hydroxyls for binding to their proposed target. Per-acetylation of the

fully glycosylated apoptolidin **1.15** and C9- monoglycosylated apoptolidin **1.16-1.17**, leads to a large decrease in binding affinity to F_oF_1-ATPase *in vitro* (K_i > 100 μM) as compared to the free hydoxylated apoptolidin A **1.1** (K_i = 0.38 μM).

Mono- or di- functionalization of the adorning apoptolidin hydroxyls, affect only a slight decrease in activity. Through collaboration, the Wender and Miller groups [12-13] showed that selective functionalization of apoptolidin A could be achieved **1.18-1.25**. While selective acylation or methylation generally gives little change in bioactivity, methylation at the C20- hydroxyl results in the largest loss in activity (IC_{50} = 2.8 ± 0.5 μM, F_oF_1-ATPase assay). This effect is larger than that seen with per-methylated apoptolidin **1.18** (IC_{50} = 2.3 ± 0.5 μM, F_oF_1-ATPase assay). This could suggest that the size of the C20-hydroxyl is important for binding to its target as deletion of this functional group, as in apoptolidin C **1.3**, does not directly impact bioactivity. The increase in steric bulk at this position with the introduction of a methoxy group could be encumbering enough to prevent favorable binding to its molecular target. Additionally, functionalization at the C2', C3', and C23- hydroxyls have the least impact on bioactivity, suggesting these could potentially be sites for further functionalization to create molecular probes of apoptolidin.

In three separate reports by the Wender, Seto, and Khosla groups, [14-16] drastic chemical modification was performed on apoptolidin A to access diverse macrolide analogs (Fig. 1.6). While these changes to the overall apoptolidin core are much more severe, cleavage of the hemi-ketal and disaccharide moiety result in about a 20 fold decrease in potency (IC_{50} = 13 – 32 μM, F_oF_1-ATPase assay, **1.26-1.28**) as compared to apoptolidin A (IC_{50} = 0.7 μM). Ring expansion of macrolide unit **1.26** under basic conditions to give **1.29**,

showed a decrease in potency (IC_{50} = 34 μM, F_oF_1-ATPase assay) as compared to its 20-membered analogue **1.26** (IC_{50} = 13 μM). δ-lactone **1.30** showed a marked decrease in potency (IC_{50} = 190 μM, F_oF_1-ATPase assay), suggesting the apoptolidin macrolide is crucial for binding to its target. Diels alder adduct **1.31** gave only a slight decrease in potency (IC_{50} = 2.3 μM, F_oF_1-ATPase assay) as compared to its parent (IC_{50} = 0.7 μM), showing the relative unimportance of the dienyl unit of apoptolidin A. [14-15]

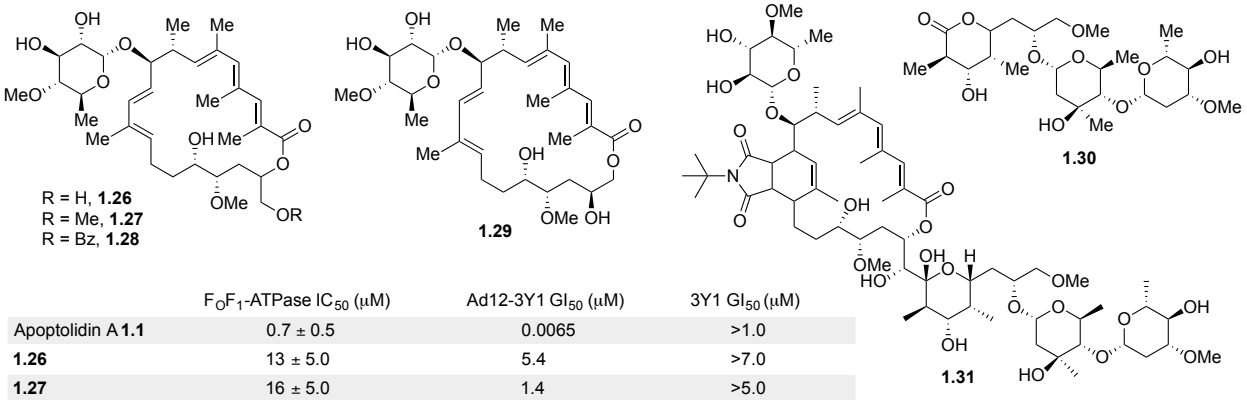

	F_OF_1-ATPase IC_{50} (μM)	Ad12-3Y1 GI_{50} (μM)	3Y1 GI_{50} (μM)
Apoptolidin A **1.1**	0.7 ± 0.5	0.0065	>1.0
1.26	13 ± 5.0	5.4	>7.0
1.27	16 ± 5.0	1.4	>5.0
1.28	32 ± 5.0	2.4	>16
1.29	34 ± 5.0		
1.30	190 ± 50	>12	>12
1.31	2.3	3.2	>5

Figure 1.6. Chemical modification to the marcolide core of apoptolidin A

Functionalized apoptolidins **1.26-1.29** were accessed via oxidative cleavage of fully pentatriethylsilyl protected apoptolidin A **1.32**, followed by sodium borohydride reduction to give a mixture of protected C9- glycosylated macrolide core **1.33** and δ-lactone **1.34** (Fig. 1.7). Functionalization of the free hydroxyl, followed by silyl deprotection gave functionalized macrolides **1.26-1.28**. Ring expansion under basic conditions of macrolide **1.26**, gave 21-membered lactone **1.29**. Silyl deprotection of protected δ-lactone **1.34** was used to give the desired δ-lactone **1.30**. Finally, [4+2] cycloaddition between apoptolidin A and N-*tert*-butyl maleimide gave the Diels Alder adduct **1.31**.

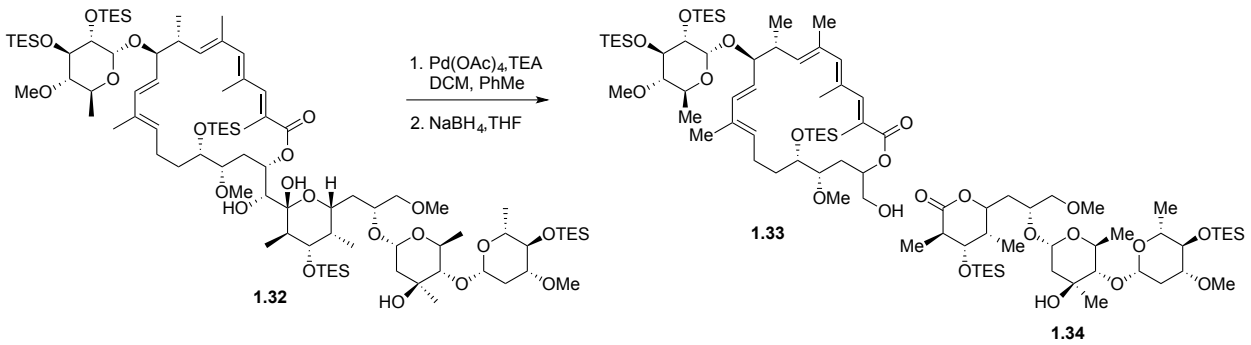

Figure 1.7. Oxidative cleavage of apoptolidin A

Lastly, interestingly through total synthesis of the apoptolidin aglycone, apoptolidinone, [17-29] biological testing of apoptolidinones A **1.1**, C **1.3**, and D **1.4** show the aglycone of apoptolidin to be completely inactive (> 10 μM, H292). [9]

1.4 Apoptolidin mechanism of cytotoxic and cytostatic effects

Several early papers reported apoptolidin A **1.1** has been shown to selectively induce apoptosis in several cultured cancer cell models over "healthy" cell models. In 1997, Seto and coworkers [1] demonstrated that E1A-transformed rat glial cells treated with 1 μM of apoptolidin A **1.1**, exhibited visual signs of apoptotic cell death such as condensed chromatin, fragmented nuclei, and a large amount of DNA laddering, after 24 hours. Additionally, **1.1** showed significant cytotoxicity towards E1A-transformed rat glial cells (IC_{50} = 11 nM) as compared to untransformed cells (IC_{50} = 100 μM).

In 2000, Khosla and coworkers [30] reported apoptolidin to be among the top 0.1% most cell-line selective cytotoxic agents of the 37,000 molecules screened by the National Cancer Institute (NCI) 60 human cancer cell line panel. In this report, Khosla and

coworkers attribute apoptolidin's (**1.1**) selective activity as derived from targeting F_oF_1-ATP synthase (F_oF_1-ATPase), due to apoptolidin's (**1.1**) structural similarity to known F_oF_1-ATPase targeting polyketides (i.e. ossamycin **1.35**, cytovaricin **1.36**, and oligomycin A **1.37**, Fig. 1.8). Analysis of the data from the NCI60 cell line panel, showed a statistically significant correlation among leukemia cell lines that exhibited sensitivity to apoptolidin and expression levels of encoding genes for the subunit 6 of the mitochondrial F_oF_1-ATPase. It is important to note, that this subunit of F_oF_1-ATPase has been reported to act as the binding site for macrolides such as oligomycin A **1.37**. Additionally, a high degree of correlation among screened leukemia cell lines between apoptolidin sensitivity and their expression for enzymes involved in central carbon metabolism such as pyruvate kinase and aspartate aminotransferase, was also observed.

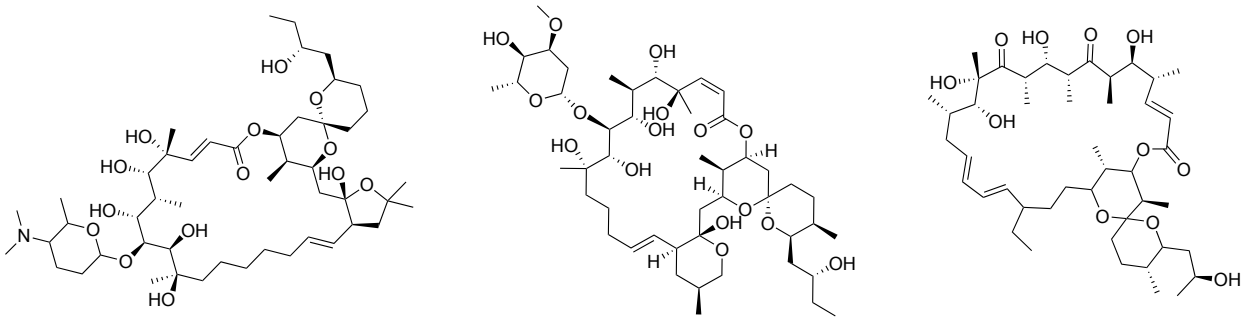

Figure 1.8. Structurally similar polyketides to the apoptolidin family.

The Khosla group concluded their report by hypothesizing that apoptolidin's cancer cell selectivity can be explained through inhibition of mitochondrial oxidative phosphorylation, similar to that of oligomycin A **1.37**. This metabolic preference can be correlated well with a mitochondrial target such as F_oF_1-ATPase. And while most cancer cells maintain a high level of anaerobic carbon metabolism, cancer cells that are more

glycolytic in nature can be chemically sensitized to apoptolidin A **1.1** by co-treatment with nontoxic, small molecule inhibitors of cellular glycolysis, such as oxamate **1.39** and 2-deoxyglucose **1.38** (Fig. 1.9). [30]

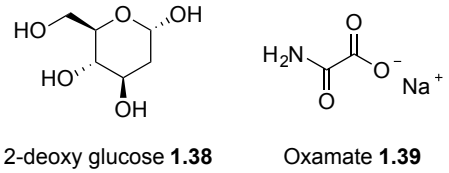

2-deoxy glucose **1.38** Oxamate **1.39**

Figure 1.9. Small molecular inhibitors of cellular glycosylsis: 2-deoxy glucose and oxamate.

In a separate report, Khosla and coworkers [31] determined that apoptolidin A **1.1** cytotoxicity is most likely apoptotic in nature. The mechanism of apoptosis is highly complex and sophisticated cascade of events but research to date has indicated that there are two main modes of apoptotic cell death: the extrinsic death receptor pathway or the intrinsic mitochondrial pathways (Fig. 1.10). [38]

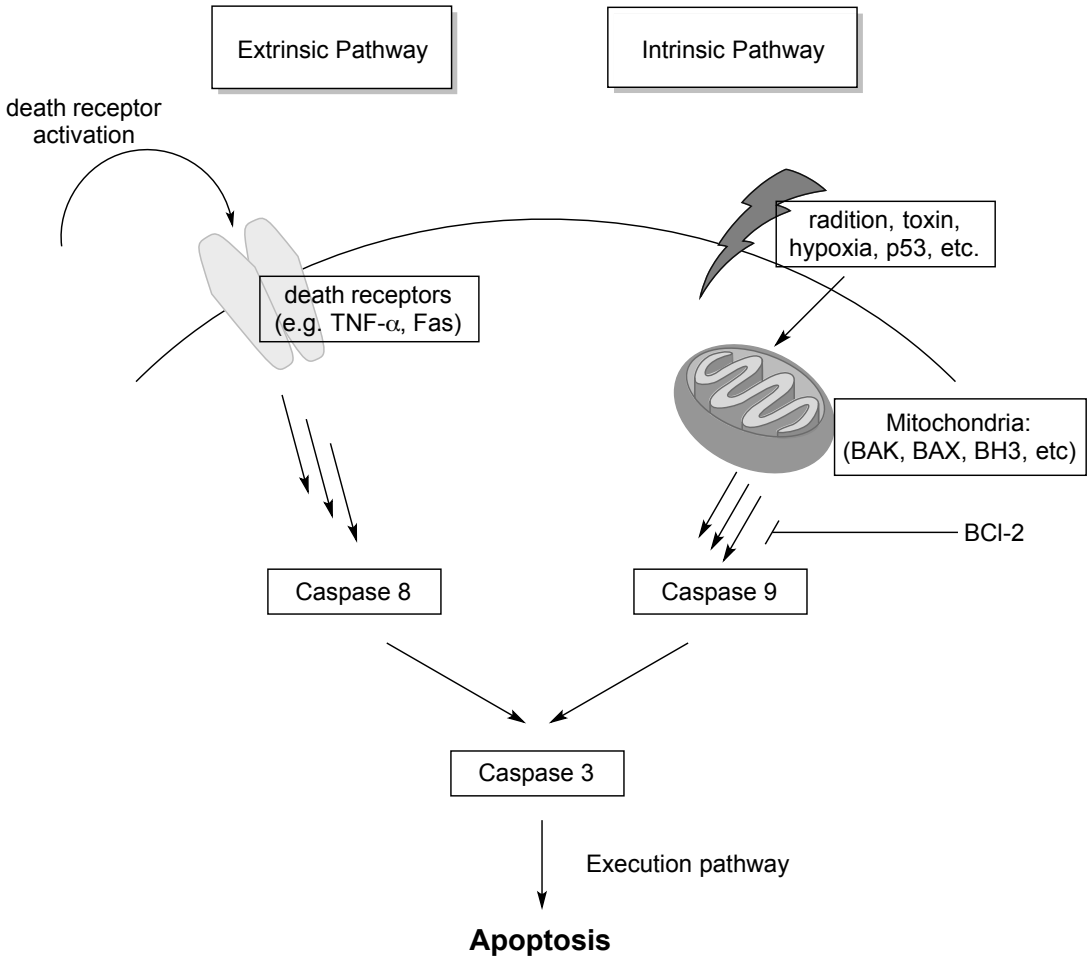

Figure 1.10. Overview of extrinsic and intrinsic apoptotic pathway.

In order to probe the mechanism of apoptolidin A **1.1** apoptotic cell death, Khosla and coworkers conducted a series of experiments. Using a mouse B lymphoma cell line (LYas), which showed a surprising degree of sensitivity to apoptolidin as compared to LYas cells transfected with Bcl-2, they demonstrated that apoptolidin's cytotoxicity toward LYas cells was inhibited by the presence of anti-apoptotic protein Bcl-2. Its specific mechanism of cell death was determined using flow cytometry to measure cell surface staining (FACS) using propidium iodide in conjunction with annexin V. These experiments showed propidium iodide and annexin V positive staining upon treatment of apoptolidin (200 nM) after 3 hours, supporting an apoptotic mechanism of cell death. [37] To further support a

mitochondrial apoptotic mechanism of cell death, LYas cells were co-treated with apoptolidin (**1.1**) and known caspase-9 inhibitor etoposide **1.40** or caspase-9 specific peptide inhibitor z-LEHD.fmk **1.41**, showing a significant loss in activity. In contrast, LYas cells solely treated with apoptolidin resulted in PARP cleavage, a biochemical event that occurs through the mitochondrial intrinsic pathway and results in apoptosis.

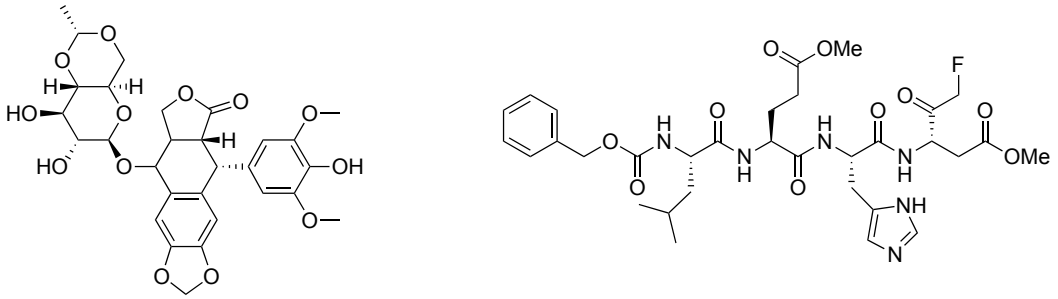

Figure 1.11. Caspase-9 inhibitors: etoposide and z-LEHD.fmk.

Interestingly, using an isogenic pair of wild type and double knock out human colorectal cells (HCT116) p53 +/+ and p53 -/-, apoptolidin was observed to exhibit apoptotic activity independent of p53 status. While p53 dependent apoptosis is not well understood, cells that engage in p53 dependence typically act through the intrinsic cell death pathway. This pathway is typically regulated by BCL-2 as BCL-2 overexpression inhibits this pathway of apoptosis (Fig. 1.10). [32]

In November of 2014, in a collaboration between the Sulikowski, Bachmann, and Marnett groups, a report [9] showed that differentially glycosylated apoptolidins A and H tagged with Cy3 fluorophores **1.42-1.43** (Fig. 1.12) resulted in specific cell localization to the mitochondria of H292 human lung cancer cells, about thirteen years post initial reports hypothesizing a cancer cell selective apoptolidin induced apoptotic mechanism of cell death

via mitochondrial F_oF_1-ATPase. These fluorescent apoptolidin analogues showed comparable activity to their natural parents and a high degree of overlap with a fluorescent mitochondrial stain (MitoTracker® **1.46**). However, cells treated solely with fluorescent Cy3 linker (BNE-Cy3 **1.44**) showed significant and specific mitochondrial localization. While cationic dyes such as Cy3 **1.45** often localize to the mitochondria, the BNE-Cy3 **1.44** linker also proved to be non-toxic to cells (EC_{50} = 4.6 μM, H292).

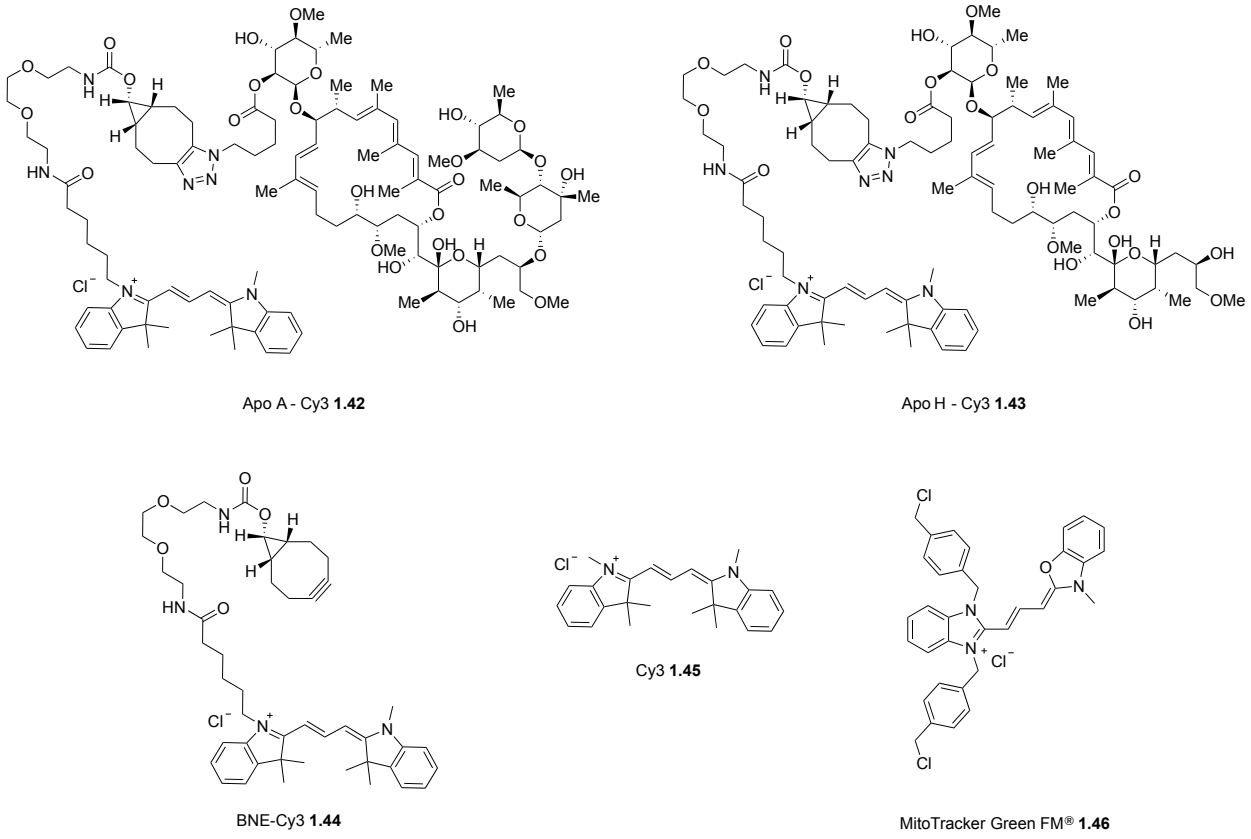

Figure 1.12. Fluorescent apoptolidin and related small molecule probes.

In addition, Sulikowski and coworkers showed that cancer cell confluence directly impacted apoptolidin activity. By treating H292 cells at low confluence (20k cells/well or less), a cytostatic effect was observed with cell viability maintaining about 50% viability as compared to control cells (DMSO treated). However, H292 cells grown to a higher

confluence (25k cells/ well) demonstrated potent apoptolidin-induced cytotoxicity. Using this model for consistent measurements for apoptolidin-induced cell death, activity was measured according to glycosylation state (Fig. 1.13). Notably, Sulikowski and coworkers observed a direct correlation between apoptolidin glycolytic state and cytotoxicity with the fully glycosylated apoptolidins showing sub-nanomolar activity (IC_{50} = 16 nM, **1.1**, H292 cells, human lung cancer) and the aglycone losing most of its parent activity (> 10 μM, **1.48** H292).

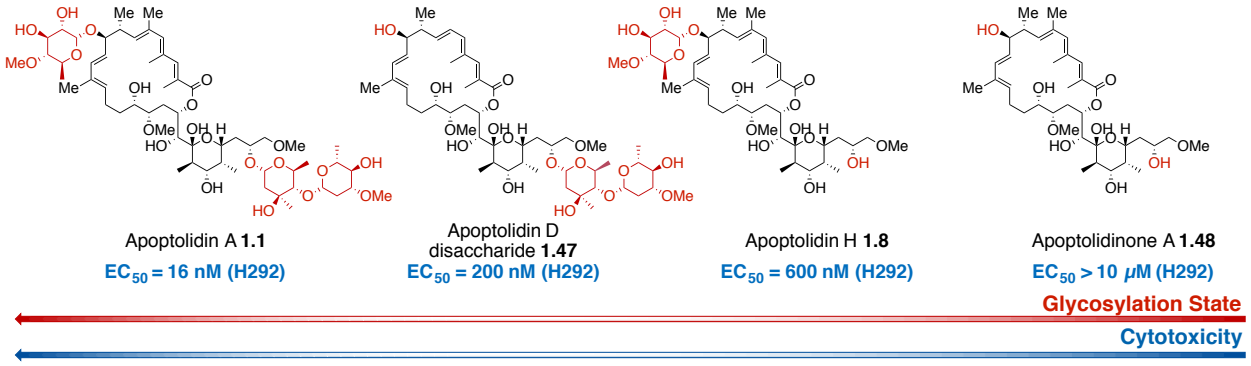

Figure 1.13. Correlation between apoptolidin glycosylation state and bioactivity.

In December of 2014, Ishmael and coworkers [33] analyzed apoptolidin activity in several cancer cell lines, including human gliablastoma, lung cancer, and mouse embryonic fibroblasts (MEFs). Apoptolidin A **1.1** treatment of human gliablastoma (U87-MG and SF-295) and lung cancer (H292 and H460) cell types resulted in decreased viability in a time and concentration dependent manner, consistent with previous reports. However, they also observed that gliablastoma cells proved to be resistant to short exposure times to apoptolidin **1.1** and **1.3**. Due to this observed phenomena, Ishmael and coworkers probed changes in cell metabolism of live cells overtime after treatment with apoptolidin. Their findings were consistent with that of a mitochondrial ATPase inhibitor. U87-Mg, H292, and

H460 cells all showed decreased in rates of oxidative phosphorylation and increased rates of glycosylsis. While this trend is consistent with previous reports of an apoptolidin F_oF_1-ATPase target, comparisons between apoptolidin A **1.1** and oligomycin A **1.37** revealed significant differences in activity and metabolic changes within the four cell lines used. It has long been established that oligomycin A **1.37** targets F_oF_1-ATPase. [39] Notably, they observed that the metabolic phenotype of a cell line was a critical determinant for apoptolidin sensitivity, rather than histological similarities among cell lines. They ascribe this phenomenon to be the basis for apoptolidin's cancer cell selectivity among cell lines.

In addition, Ishmael and coworkers also determined that apoptolidin treatment to U87-MG gliablastoma cells and MEF mouse embryonic cells resulted in the indirect activation of 5' AMP-activated protein kinase (AMPK) leading towards autophagy, without significant molecular target of rapamycin C1 (mTORC1) activation. In U87-MG and MEF cells, apoptolidin treatment results in the phosphorylation of phosphorylated acetyl-CoA carboxylase (ACC) and UNC-like-51 kinase (ULK1), leading toward the phosphorylation of 5' AMP-activated protein kinase (AMPK). Additionally, wild type MEFs exhibited clear activation of AMPK while AMPKα-null MEFs showed no signs of phosphorylation of ACC with either apoptolidin A **1.1** or oligomycin A **1.37**. These events were also only observed with cell lines that showed a large metabolic preference toward oxidative phosphorylation (wild type MEFs and U87-MG) over glycolysis (AMPKα-null MEFs and SF-295). This could be attributed to a secondary autophagic response towards apoptolidin-induced cellular stress. This is consistent with other reports of a diverse group of natural products, which have been shown to activate AMPK indirectly as a result of compromising mitochondrial function. [34, 35]

In January of 2016, collaboration between the Sulikowski, Bachmann, and Irish groups [36] resulted in work showing that fluorescent differentially glycosylated apoptolidins are selectively taken up into several cancer cell lines (A549, U87, LN229, and SW620) over healthy cell models (peripheral blood mononuclear cells, PBMC), 10 min after treatment. Cell microscopy imaging showed specific uptake of the fluorescent probes into human lung cancer cells (A549) and gliablastoma cells (U87). Single-cell fluorescent phospho- specific flow cytometry (phospho-flow) was then used to quantitate the uptake of fluorescent apoptolidins in the four cell lines as plotted against up-regulation of phosphorylated ACC, 1 hour after treatment. Phospho-flow analysis after apoptolidin treatment showed almost compete uptake of apoptolidin into healthy PBMCs and all tested cancer cell lines (>98%). However, healthy PBMCs showed minimal response to apoptolidin in terms of phosphorylated ACC (p-ACC) while all cancer cells showed a portion of cell subset, which showed high p-ACC signal. LN229 gliablastoma cells showed the highest increase in the abundance of this subset of apoptolidin-sensitive cells, from 2.74% (DMSO control) to 12.39% and 15.28% for fully glycosylated fluorescent apoptolidin A **1.42** and C9-monoglycosylated apoptolidin H **1.43**, respectively.

1.5 Conclusion

Although isolated twenty years ago, the mechanism for apoptolidin's observed selective cancer cell toxicity remains mostly unanswered. As more data regarding structure-activity relationships between apoptolidin structure and function, the better insight we gain into utilizing this knowledge to create cancer cell selective small molecule

therapeutics. The apoptolidin macrolide family represents an immense opportunity to probe cancer cell mechanistic pathways.

1.6 Notes and references

1. Kim, J. W.; Adachi, H.; Shin-Ya, K.; Yoichi, H.; Seto, H., Apoptolidin, a New Apoptosis Inducer in Transformed Cells from *Nocardiopsis* sp. *J. Antibiot.* **1997**, 50, 628-630.

2. Hayakawa, Y.; Kim, J. W.; Adachi, H.; Shin-ya, K.; Fujita, K.; Seto, H., Structure of Apoptolidin, a Specific Apoptosis Inducer in Transformed Cells *J. Am. Chem. Soc.* **1998**, 120, 3524-3525.

3. Wender, P. A.; Gulledge, A. V.; Jankowski, O. D.; Seto, H., Isoapoptolidin: Structure and Activity of the Ring-Expanded Isomer of Apoptolidin *Org. Lett.* **2002**, 4, 3819-3822.

4. Pennington, J. D.; Williams, H. J.; Salomon,A. R.; Sulikowski, G. A., Toward a Stable Apoptolidin Derivative: Identification of Isoapoptolidin and Selective Deglycosylation of Apoptolidin *Org. Lett.* **2002**, 4, 3823-3825.

5. Wender, P. A.; Sukopp, M.; Longcore, K. Apoptolidins B and C: Isolation, Structure Deterimination, and Biological Activity *Org. Lett.* **2005**, 7, 3025-3028.

6. Wender, P. A.; Longcore, K. E., Isolation, Structure Determination, and Anit-Cancer Activity of Apoptolidin D *Org. Lett.* **2007**, 9, 691-694

7. Wender, P. A., Longcore, K. E. Apoptolidins E and F, New Glycosylated Macrolactones Isolated from *Nocardiopsis* sp *Org. Lett.* **2009**, 23, 5474-5477.

8. Bachmann, B. O.; McNees, R.; Melancon, B. J.; Ghidu, V. P.; Clark, R.; Crews, B. C.; Deguire, S. M.; Marnett, L. J.; Sulikowski, G. A., Light-Induced Isomerization of Apoptolidin A leads to Inversion of C2-C3 Double Bond Geometry *Org. Lett.* **2010**, 12, 2944-2947.

9. Deguire, S. M.; Earl, D. C.; Du, Y.; Crews, B. A.; Jacobs, A. T.; Ustione, A.; Daniel, C.; Chong, K. M.; Marnett, L. J.; Piston, D. W.; Bachmann, B. O.; Sulikowski, G. A., Fluorescent Probes of the Apoptolidins and their Utility in Cellular Localization Studies *Angew. Chem. Int. Ed.* **2015**, 54, 961-964.

10. Sheng, Y.; Fotso, S.; Serill, J. D; Shahab, S.; Santosa, D. W.; Ishmael, J. E.; Proteau, P. J.; Zabriskie, T. M.; Mahmud, T., Succinylated Apoptolidins from *Amycolatopsis* sp. ICBB 8242 *Org. Lett.* **2015**, 17, 2526-2529.

11. Du, Y.; Derewacz, D. K.; Deguire, S. M.; Teske, J.; Ravel, J.; Sulikowski, G. A.; Bachmann, B. O. Biosynthesis of apoptolidins in *Nocardiopsis* sp. FU 40 *Tetrahedron*, **2011**, 67, 6568-6575.

12. Wender, P. A.; Jankowski, O. D.; Tabet, E. A.; Seto, H. Toward a Structre-Activity Relationship for Apoptolidin: Selective Functionalization of the Hydroxyl Group Array *Org. Lett.* **2003**, 5, 487-490.

13. Lewis, C. A.; Longcore, K. E.; Miller, S. J.; Wender, P. A., An Approach to the Site-Selective Diversification of Apoptolidin A with Peptide-Based Catalysts *J. Nat. Prod.* **2009**, 72, 1864-1869.

14. Wender, P. A.; Jankowski, O. D.; Tabet, E. A.; Seto, H., Facile Synthetic Access to and Biological Evaluation of the Macrocyclic Core of Apoptolidin

15. Wender, P. A.; Jankowski, O.D.; Longcore, K. E.; Tabet, E. A.; Seto, H.; Tomikawa, T., Correlation of F_oF_1-ATPase Inhibition and Antiproliferative Activity of Apoptolidin Analogues *Org. Lett.* **2006**, 8, 589-592.

16. Saloman, A. R.; Zhang, Y.; Seto, H.; Khosla, C., Structure-Activity Relationships within a Family of Selectively Cytotoxic Macrolide Natural Products *Org. Lett.* **2001**, 3, 57-59.

17. Daniel, P. T.; Koert, U.; Schuppan, J., Apoptolidin: Induction of Apoptosis by a Natural Product *Angew. Chem. Int. Ed.* **2006**, 45, 872-893.

18. Schuppan, J.; wehlan, H.; Keper, S.; Koert, U. Synthesis of Apoptolidinone *Angew. Chem. Int. Ed.* **2001**, 40, 2063-2066.

19. Wehlan, H.; Dauber, M.; Mujica Fernaud, M.-T.; Schuppan, J.; Mahrwald, R.; Ziemer, B.; Juarez Garcia, M.-E.; Koert, U. Total synthesis of Apoptolidin *Angew. Chem. Int. Ed.* **2004**, 43, 4597-4601.

20. Schuppan, J.; Wehlan, H.; Keiper, S.; Koert, U. Apoptolidinone A: Synthesis of the Apoptolidin A Aglycone *Chem. Eur. J.* **2006**, 12, 7364-7377.

21. Nicolaou, K. C.; Li, Y.; Fylaktakidou, K. C.; Mitchell, H. J.; Wei, H.-X.; Weyershausen, B. Total Synthesis of Apoptolidin: Part 1. Retrosynthetic Analysis and Construction of Building Blocks *Angew. Chem. Int. Ed.* **2001**, 40, 3849-3854.

22. Nicolaou, K. C.; Li, Y.; Fylaktakidou, K. C.; Mitchell, H. J.; Sugita, K. Total Synthesis of Apoptolidin: Part 2. Coupling of Key Building Blocks and Completion of the Synthesis *Angew. Chem. Int. Ed.* **2001**, 40, 3854-3857.

23. Nicolaou, K. C.; Fylaktakidou, K. C.; Monenschein, H.; Li, Y.; Weyershausen, B.; Mitchell, H. J.; Wei, H.-X.; Guntupalli, P.; Hepworth, D.; Sugita, K. Total Synthesis of Apoptolidin: Construction of Enantiomerically Pure Fragments *J. Am. Chem. Soc.* **2003**, 125, 15433-15442.

24. Nicolaou, K. C.; Li, Y.; Sugita, K.; Monenschein, H.; Guntupalli, P.; Mitchell, H. J.; Fylaktakidou, K. C.; Vourloumis, D.; Giannakakou, P.; O'Brate, A. Total Synthesis of Apoptolidin: Completion of the Synthesis and Analogue Synthesis and Evaluation *J. Am. Chem. Soc.* **2003**, 125, 15443-15454.

25. Wu, B.; Liu, Q.; Sulikowski, G. A. Total Synthesis of Apoptolidinone *Angew. Chem. Int. Ed.* **2004**, 43, 6673-6675.

26. Ghidu, V. P.; Wang, J.; Wu, B.; Liu, Q.; Jacobs, A.; Marnett, L. J.; Sulikowski, G. A. Synthesis and Evaluation of the Cytotoxicity of Apoptolidinones A and D *J. Org. Chem.* **2008**, 73, 4949-4955.

27. Crimmins, M. T.; Christie, H. s.; Chaudhary, K.; Long. A. Enantioselective Synthesis of Apoptolidinone: Exploiting the Versatility of Thiazolidinethione Chiral Auxiliaries *J. Am. Chem. Soc.* **2005**, 127, 13810-13812.

28. Crimmins, M. T.; Christie, H. S.; Long. A.; Chaudhary, K. Total Synthesis of Apoptolidin A *Org. Lett.* **2009**, 11, 831-834.

29. Vargo, T. R.; Hale, J. S.; Nelson, S. G. Catalytic Asymmetric Aldol Equivalents in the Enantioselective Synthesis of the Apoptolidin C Aglycone *Angew. Chem. Int. Ed.* **2010**, 49, 8678-8681.

30. Salomon, A. R.; Voehringer, D. W.; Herzenberg, L. A.; Khosla, C. Understanding and exploiting the mechanistic basis for selectivity of polyketide inhibitors of F_oF_1-ATPase *Proc. Natl. Acad. Sci. U. S. A.* **2000**, 97, 14766-14771.

31. Salomon, A. R.; Voehringer, D. W.; Herzenberg, L. A.; Khosla, C. Apoptolidin, a selective cytotoxic agent, is an inhibitor of F_oF_1-ATPase *Chem. Biol.* **2001**, 8, 71-80.

32. Chipuk, J. E.; Green, D. R. *Cell Death Differ.* **2006**, 6, 994-1002.

33. Serrill, J. D.; Tan, M.; Fotso, S.; Sikorska, J.; Kasanah, N.; Hau, A. M.; McPhail, K. L.; Santosa, D. A.; Zabiskie, T. M.; Mahmud, T.; Viollet, B.; Proteau, P. J.; Ishmael, J. E. Apoptolidins A and C activate AMPK in metabolically sensitive cell types and are mechanistically distinct from oligomycin A. *Biochem. Pharmacol.* **2015**, 3, 251-265.

34. Hardie, D. G.; Ross, F. A.; Hawley, S. A. AMP-activated protein kinase: a target for drugs both ancient and modern *Chem. Biol.* **2012**, 19, 1222-1236.

35. Russo, G. L.; Russo, M.; Ungaro, P. AMP-activated protein kinase: a target for old drugs against diabetes and cancer *Biochem. Pharmacol.* **2013**, 86, 339-350.

36. Chong, K. M.; Leelatian, N.; Deguire, S. M.; Brockman, A. A.; Earl, D.; Ihrie, R. A.; Irish, J. M.; Bachmann, B. O.; Sulikowski, G. A. The use of fluorescently-tagged apoptolidins in cellular uptake and response studies *J. Antibiot.* **2016**, 69, 327-330.

37. While this technique has widely been used to determine whether cell death is occurring through apoptosis or necrosis, recent reports have shown that FACS is often unable to stain live and early apoptotic cells due to their intact membrane. Late stage apoptotic cells often result in false positives for necrotic cell death as propidium iodide has been shown to intercalate into RNA. Getun, I. V.; Torres, B.; Bois, P. R. Flow cytometry purification of mouse meiotic cells *J. Vis. Exp.* **2011**, 50, e2602.

38. Elmore, S. Apoptosis: A Review of Programmed Cell Death *Toxicol. Pathol.* **2007**, 35, 495-516.

39. Symersky, J.; Osowski, D.; Walters, D. E.; Mueller, D. M. Oligomycin frames a common drug-binding site in the ATP synthase *Proc. Natl. Acad. Sci. U. S. A.* **2012**, 35, 13961-13965.

40. Chan, Y. A.; Thomas, M. G. Formation and Characterization of Acyl Carrier Protein-Linked Polyketide Synthase Extender Units *Methods Enzymol.* **2009**, 459, 143-163.

41. Jankowski, O. D. Exploring the Chemistry and Biology of Apoptolidin. Ph.D. Stanford University, Stanford, CA, 2004.

CHAPTER II

STRUCTURE-ACTIVITY RELATIONSHIP STUDIES: GLYCOCONJUGATES AGLYCA AND THEIR BIOACTIVITY

2.1 Importance of glycosylation in medicinally relevant natural products

The discovery and development of glycosylated natural products to improve human health can be found throughout medical history. Glycosylated natural products such as calicheamicin **2.1** (anticancer), amphotericin B **2.2** (antifungal), lomaiviticin **2.3** (antitumor), daunomycin **2.4** (a.k.a. daunorubicin, anticancer), bleomycin **2.5** (anticancer), and everninomicin **2.6** (antibiotic) are examples of well-known secondary metabolites containing important sugar residues (Fig. 2.1). [1]

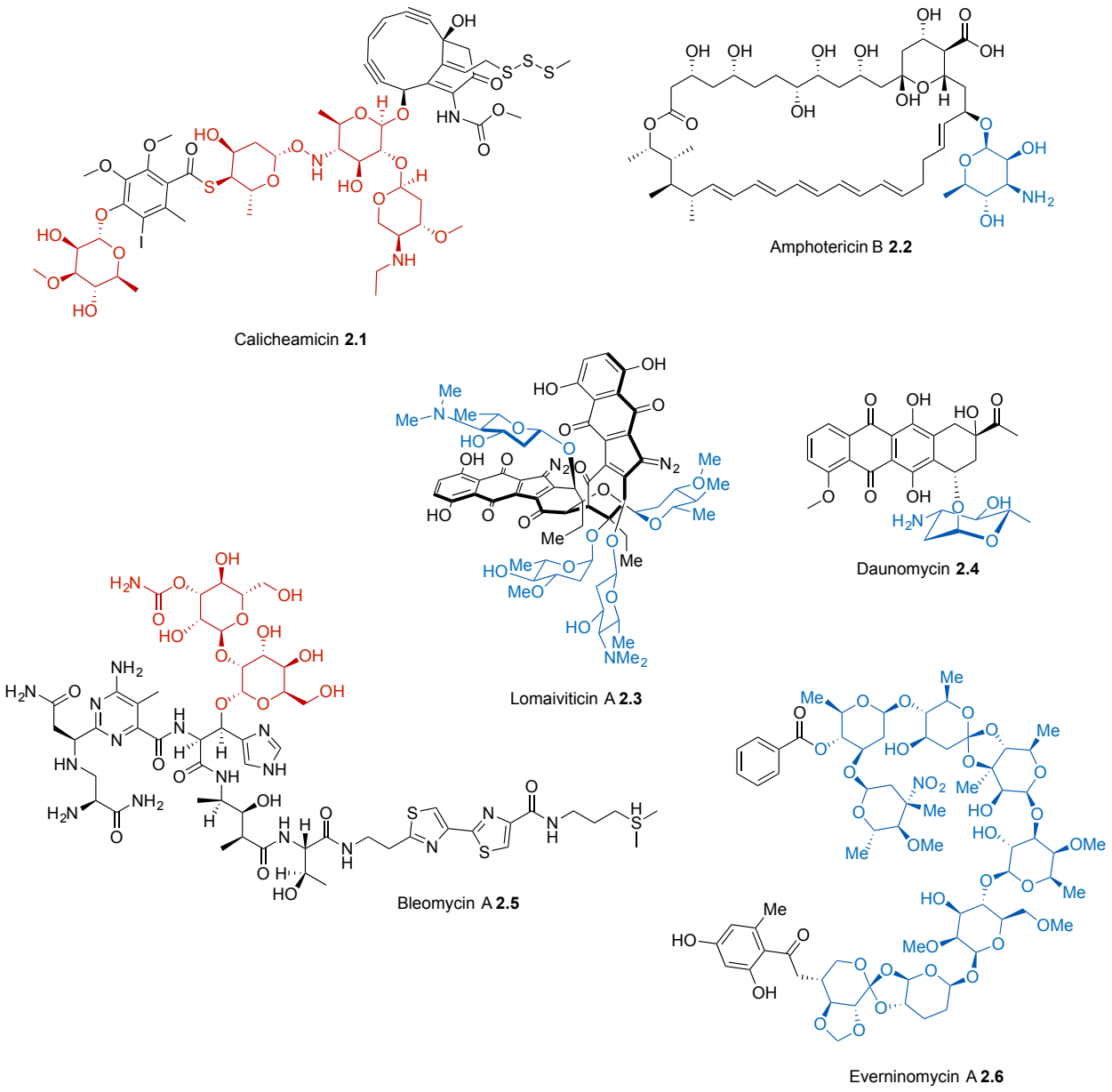

Figure 2.1. Glycosylated medicinally relevant natural products.

Generally widely accepted, the carbohydrate units of and/or decorating natural product scaffolds are thought to increase binding to their molecular targets, improve cell permeability, and improve solubility. In some cases, polysaccharides are thought to help increase the overall molecular weight of the natural product, as these high molecular weight species can passively accumulate in tumor tissues due to their poor vascularization

and therefore enhanced permeability, as compared to healthy cells, which often have significant barriers to high molecular weight species. [2] Other reports show that the decreased number of lymphatic vessels in tumor cells allows for increased retention of these secondary metabolites in the interstitial space of cells. [3, 4] Conjugation of antibodies to drugs have also shown slower release times from its carrier, giving sustained high intra-tumoral concentrations and lower plasma concentrations of the active drug. [5]

While it is generally accepted that sugars play a major role in contributing to overall natural product pharmacokinetics, these hypotheses largely remain unproven. There is a lack of detailed understanding at the molecular level of the importance of glycosylation and identity among secondary metabolites, as it relates to overall *in vitro* and *in vivo* activity of bioactive natural products. Exceptions to this generality include the calicheamicins **2.1** and bleomycins **2.5**, as these families of natural products have been studied extensively. [6-16] SAR studies of these natural products have produced a detailed understanding of target engagement and relationship of glycosylation to its efficiency and selectivity (Fig. 2.2). [14]

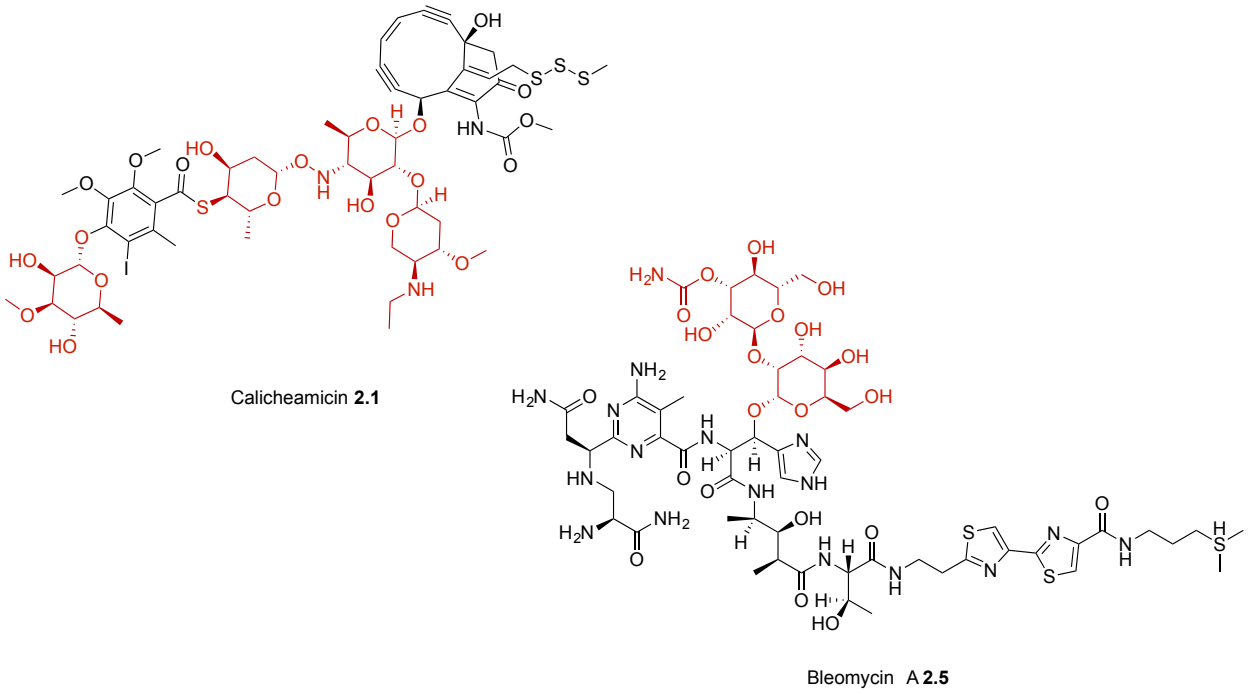

Figure 2.2. Chemical structures of calicheamicin and bleomycin.

2.2 A case study: structure and function of the calicheamicins

Calicheamicin **2.1** was first discovered in the mid-1980's by a scientist on vacation in Kerrville, Texas. The scientist had collected a sample of the soil and sent it back for testing to discover an extremely potent cytotoxic agent (optimal dose = 0.5 – 1.5 μg/k, ca. 4000x more potent than doxorubicin). [6] While calicheamicin **2.1** does not show selectivity for cancer cells by itself, when bound to a humanized monoclonal antibody, it can be directed toward leukemia cells in patients diagnosed with acute myeloid leukemia. [17] Calicheamicin **2.1** itself is an extremely potent cytotoxic agent. The generally accepted mechanism of calicheamicin **2.1** binding to DNA first involves non-specific binding of calicheamicin **2.1** to the minor groove, followed by tracking along the groove or outer

surface of the helix until a target site is reached. Either during this process or once bound, reduction of the calicheamicin trisulfide **2.7** most likely via glutathione, triggers an intramolecular thiol conjugate addition followed by a Bergman cyclization, resulting in the formation of a di-radical species **2.10** (Fig. 2.3). The orientation of the resulting diradical intermediate **2.10** within the minor groove results in ribose hydrogen atom abstraction of each strand of duplex DNA. This results in lethal double-stranded DNA cleavage leading to apoptosis. This pathway is the basis for calicheamicin's potent cellular toxicity. [17]

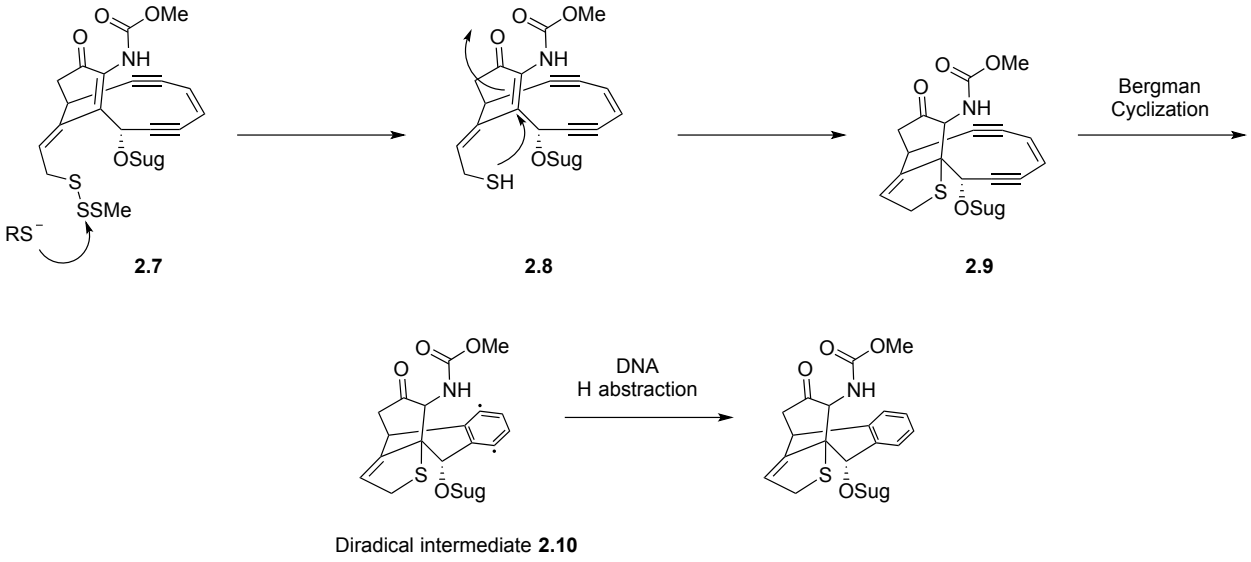

Figure 2.3. Mechanism for calicheamicin cellular toxicity via dsDNA cleavage.

Interestingly, studies have shown that the aryl tetrasaccharide of calicheamicin binds in the same orientation with or without the aglycone. [18-21] Kahne and coworkers have shown that the aryl tetrasaccharide exhibits a surprisingly large amount of rigidity and does not undergo any major conformational changes when calicheamicin binds to DNA. Instead, they suggest that DNA undergoes a conformational change in the presence of the rigid tetrasaccharide due to the steric pressure on the pyrimidine strand, leading toward widening of the minor groove. [22, 23] Additionally Danishefsky and coworkers have shown

that the aglycone of calicheamicin **2.1** may bind to DNA but with a much weaker interaction and a loss of DNA cleavage specificity. Thus in the case of calicheamicin **2.1**, the tetrasaccharide unit is necessary for tight DNA binding and double-stranded DNA cleavage specificity. [24]

2.3 A case study: structure and function of the bleomycins

Bleomycin **2.5** is a glycopeptide first isolated in 1966 by Umezawa and coworkers [25] and later marketed in Japan as a drug under the tradename "Blenoxane" by Nippon Kayaku in 1966. Since its initial isolation and discovery as an anti-cancer agent, Blenoxane (a mixture of bleomycin A2 **2.11** and bleomycin B2 **2.12**) [14] has become an integral part of combination therapy to treat a number of cancers including Hodgkin's lymphoma, non-Hodgkin's lymphoma, testicular cancer, breast cancer, cervical cancer, head and neck cancer, pleural effusions from metastatic tumors, and AIDS-related sarcoma intracranial germ cell tumors (Fig 2.4). [26] Most notable of these treatments is blenoxane's use alongside cisplatin and etoposide to treat testicular cancer, at a 90% curative effect. [14]

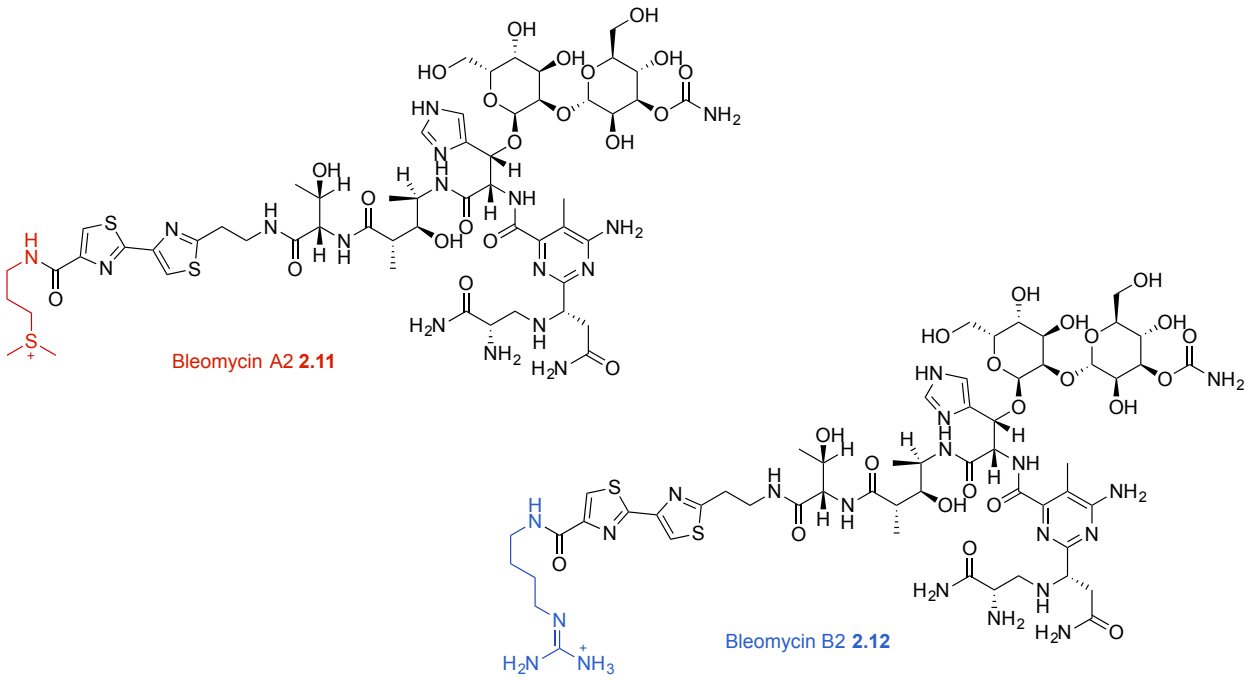

Figure 2.4. Chemical structure of Blenoxane®: Bleomycin A2 and B2.

The bleomycin family consists of a similarly shared aglycone core, differentiated by glycoslation pattern and charged tail. The structural features of the bleomycin family have been extensively studied and dissected into several functional domains (Fig. 2.5). [14]

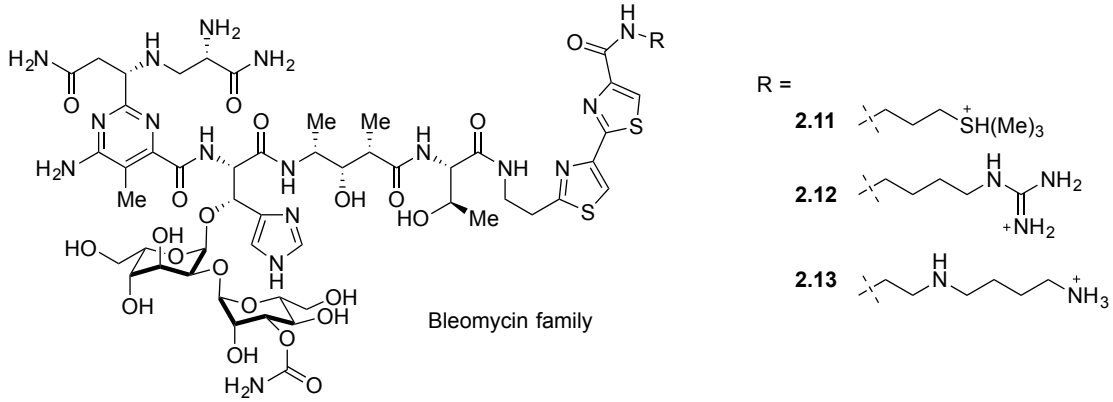

Figure 2.5. Chemical structure of bleomycin family.

The metal binding domain of bleomycin forms an octahedral complex with either iron(II) or copper(I) to form the active metallobleomycin species: bleomycin-Fe(III)-OOH

or bleomycin-Cu(I), the latter of which can be oxidized further resulting in reactive oxygen species (ROS). These active forms of bleomycin are believed to diffuse into the nucleus, bind to, and cleave double stranded DNA (dsDNA). [27, 28] This metal binding domain binds selectively to guanine sites, typically through intercalation or binding to the minor groove with the pyrimidine of bleomycin [29, 30] (Fig. 2.6A). Hydrogen atom abstraction by ROS leads toward the cleavage of DNA. [31, 32] The linker length of bleomycin has been found to be extremely important for binding to DNA as the charged bithiazole tail partially intercalates into DNA so that bleomycin can reorganize itself and cleave a second strand of DNA [33, 34] (Fig. 2.6B). While extensive SAR studies have been conducted on bleomycin, until recently little was known about its selective mechanism of cancer cell uptake and the functional role of its disaccharide.

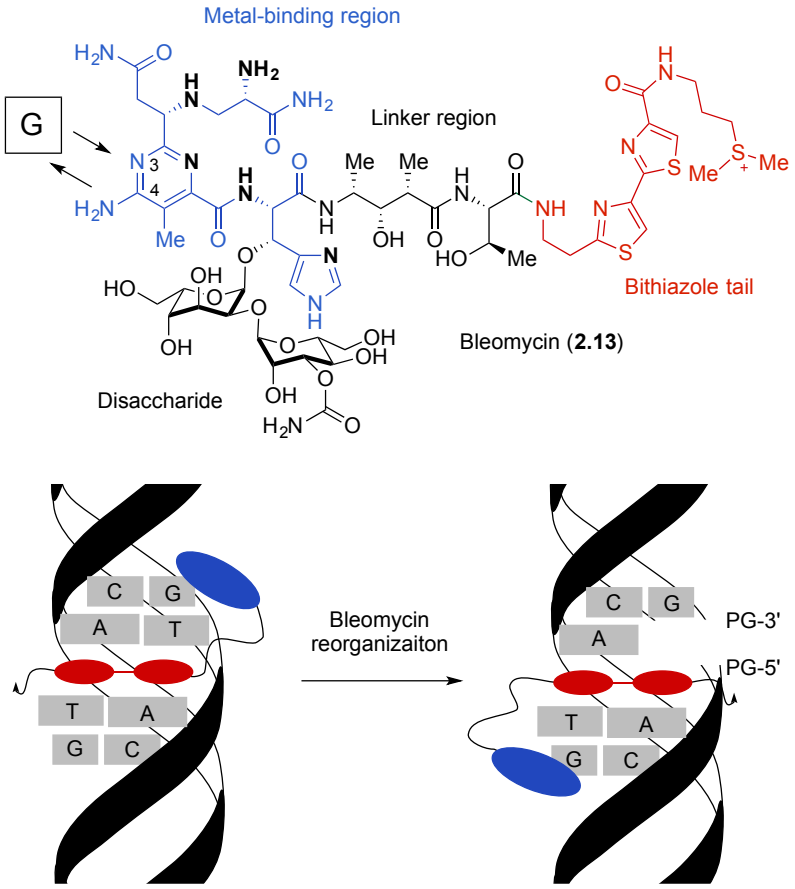

Figure 2.6. Bleomycin structure and function. A. SAR of bleomycin B. Mechanism for dsDNA clevage

In 2013, Hecht and coworkers showed that the disaccharide of bleomycin is necessary for selective tumor cell targeting. [35] Using fluorescent bleomycin, the aglycone of bleomycin, and the bleomycin disaccharide, Hecht and coworkers demonstrated that bleomycin glycovarints **2.13-2.16** (Fig. 2.7) selectively stain breast cancer cells (MCF-7) but not normal human breast cells (MCF-10A). Notably, the bleomycin aglycone showed little or no staining of either MCF-7 or MCF-10A cell lines.

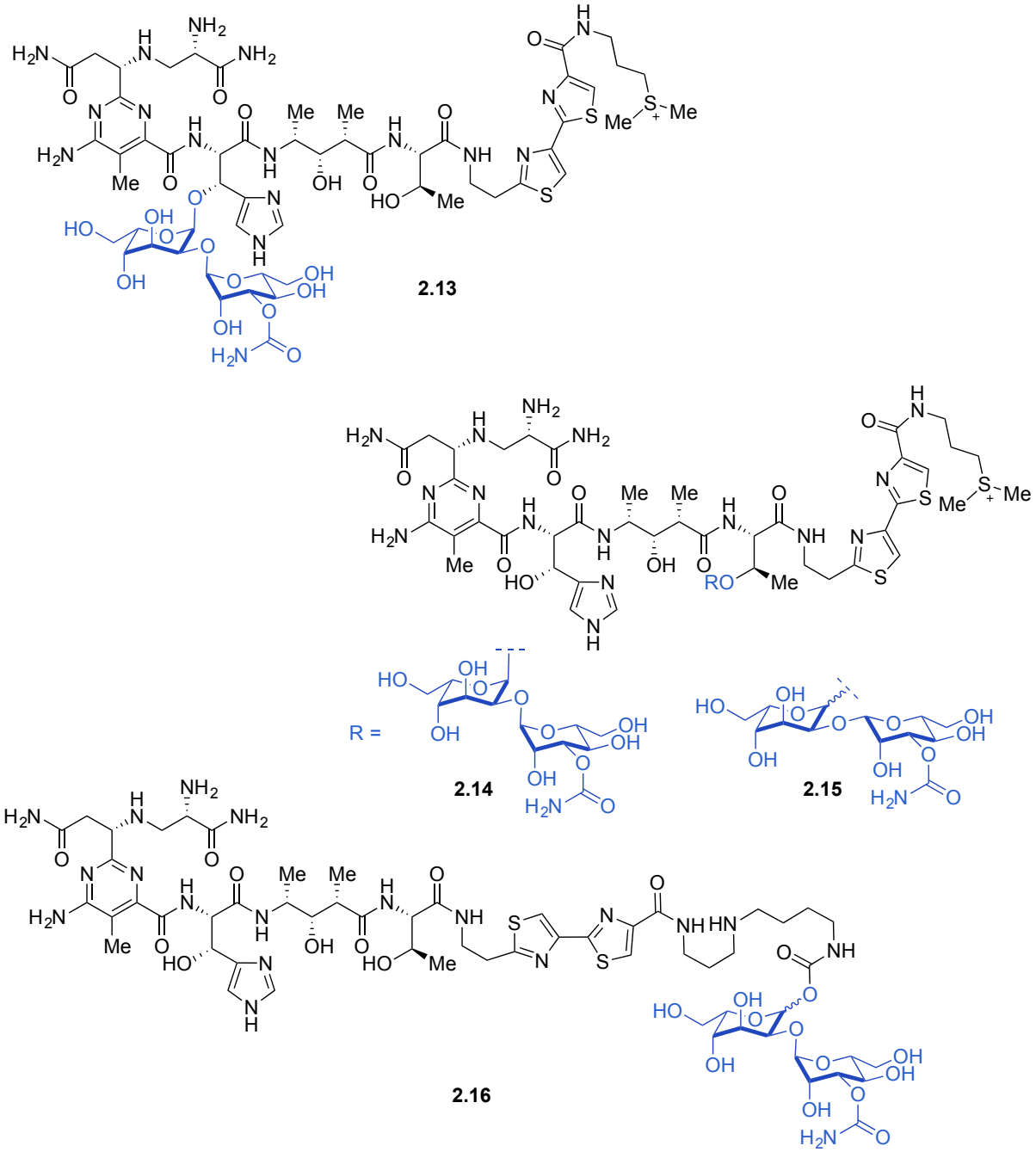

Figure 2.7. Structure of synthetic bleomycin glycovariants.

In 2015, the Hecht group [36] followed up these studies by creating fluorescent bleomycin monosaccharide analogues **2.7-2.9** (Fig. 2.8). These studies showed that the disaccharide portion of bleomycin could be simplified to the carbamoylmannose moiety of bleomycin and still exhibit selectivity toward cancer cell uptake in six different cancer cell

lines. Interestingly they found that the carbamoyl portion of the sugar was necessary for selective cancer cell uptake.

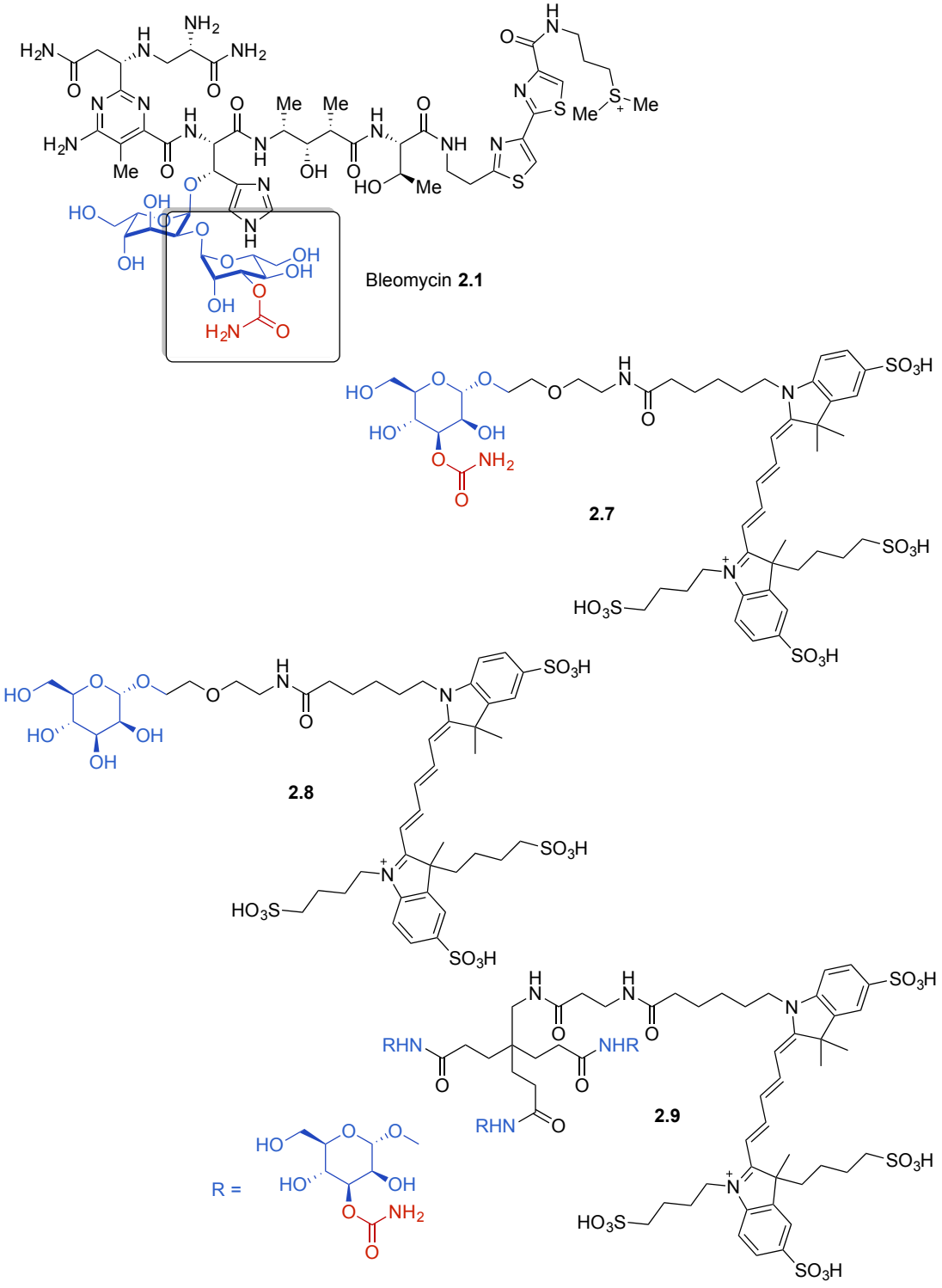

Figure 2.8. Fluorescent synthetic bleomycin monosaccharide analogues.

Recent findings by Hecht and coworkers [35-36] illustrate the potential to better understanding the importance of glycosylation to bioactivity. While there has been a recent

surge in the number of techniques to systematically explore the SAR of natural product glycosides, it remains an area of science little explored.

2.4 Recent advances in understanding the purpose of natural product glycosylation state

Groups such as those led by Jon Thorson and Tadashi Eguchi have sought to tackle this interesting yet much unexplored area of science by systematically diversifying glycans on known natural products via glycorandomization (Fig. 2.9). Glycorandomization allows for the creation of large libraries of differentially glycosylated macrolide aglycone that can be screened for bioactivity. [37]

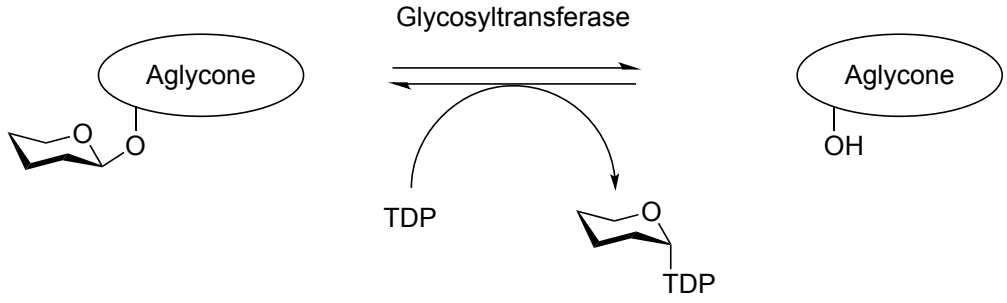

Figure 2.9. Overview of enzymatic glycorandomization.

In 2005, Eguchi and coworkers showed that using VinC, a glycosyltransferase of vicenilactam, in the presence of thimidine diphosphate (TDP), reversible glycosylation could be achieved to form the aglycone and TDP-activated glycoside. TDP-vicenisamine. TDP-vicenisamine could then be used to glycosylate five other aglyca (Fig. 2.10). [38]

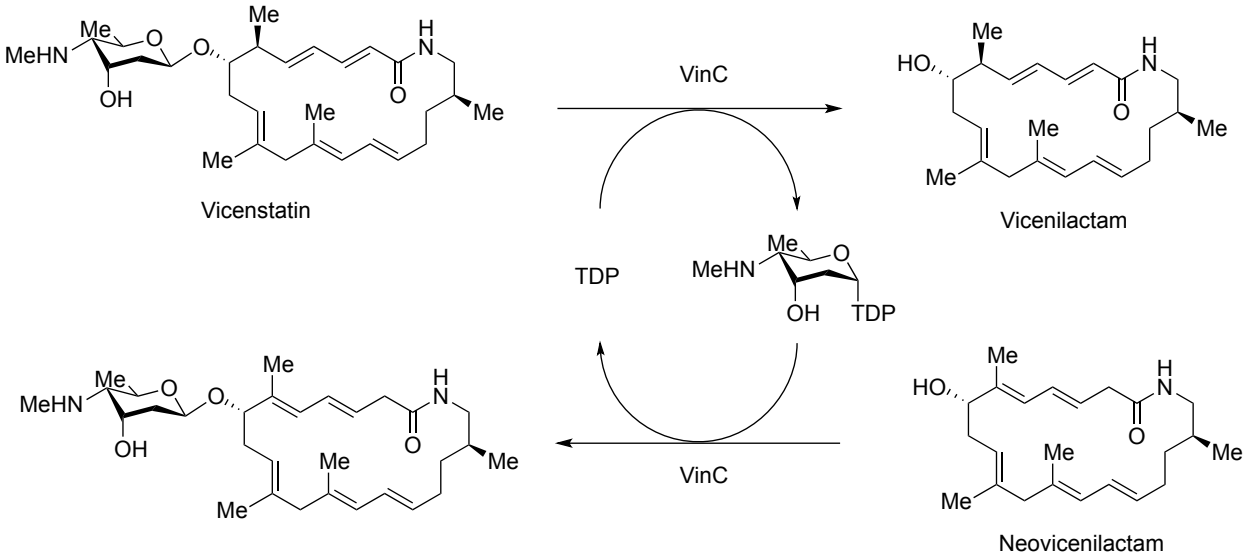

Figure 2.10. Demonstration of glycorandomization functionality toward accessing new aglyca.

In 2006, Thorson and coworkers showed glycosyltransferases from calicheamycin (CalG1 and CalG4) and vancomycin (GtfD and GtfE), allowed for increased expansion of this reversible glycosyltransferase activity, leading to the formation of 10 TDP sugars and 70 new calicheamycins. [39]

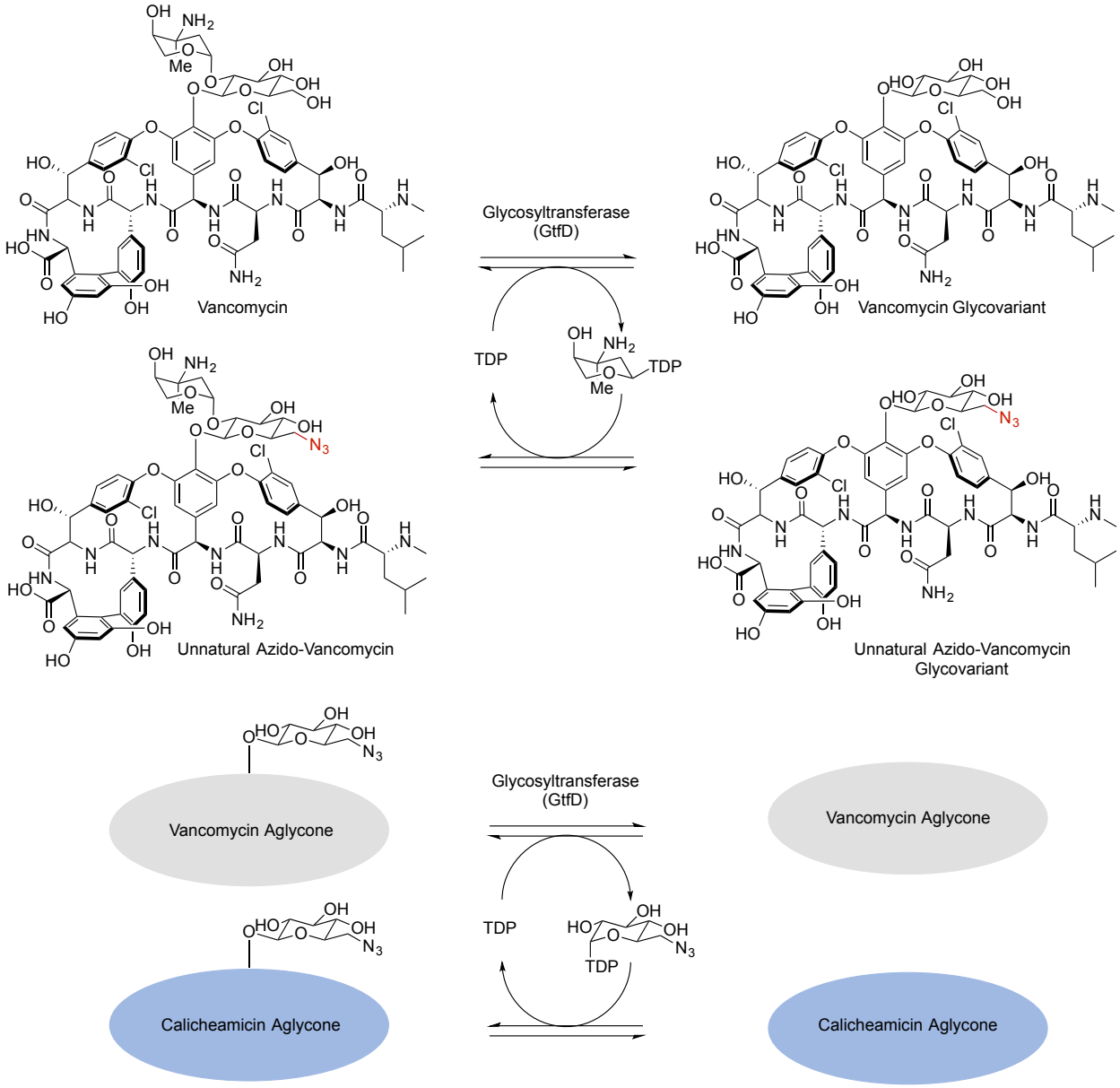

Figure 2.11. Demonstration of glycorandomization functionality toward accessing new aglyca con't.

Glycorandomization is a powerful new approach that could allow access to various activated glycosyl donors and aglyca not easily accessible. It significantly expands the scope and role of glycosyl transferases as catalysts for traditional organic reactions. This approach, however, does require large and variable amounts of isolated enzyme. Because of the size of the glycosyltransferase, large quantities of the enzyme catalyst are needed,

even for low catalyst loadings. Typically this approach requires knowledge of the natural product biosynthesis and/or a means of isolating the glycosyltransferase catalyst. And while glycorandomization represents an attractive technique to analyze glycosylation state such as those identifying new unnatural potent analogues of calicheamicin and vancomycin, it is still a recently developed technique that has yet to be applied toward other aglyca.

2.5 Exploring the function of apoptolidin glycosylation state

In 2009, through collaboration between the Bachmann, Sulikowski, and Marnett groups, [40] a hybrid chemical ketosynthase (PKS) "knockdown" approach (Fig. 2.14) was used to selectively glycosylate a synthetically produced aglycone of apoptolidin (apoptolidinone D, **2.20**). This technique was first utilized by the Omura group to convert a biologically inactive tylosin aglycone (protylonolide, **2.23**) into chimeramycin A **2.24** with a spiramycin A **2.25** producing organism (Fig. 2.12). [41] The Bachmann group [40] showed selective C27- glycosylation of apoptolidinone D is possible by co-treating its producing organism (FU40) with synthetic aglycone apoptolidinone D **2.20** and PKS inhibitor cerulenin **2.22**. Treatment of cerulenin **2.22** suppresses endogenous aglycone production from the producing organism. This allows for downstream machinery, such as a glycosyltransferase, to act upon an exogenously treated aglycone.

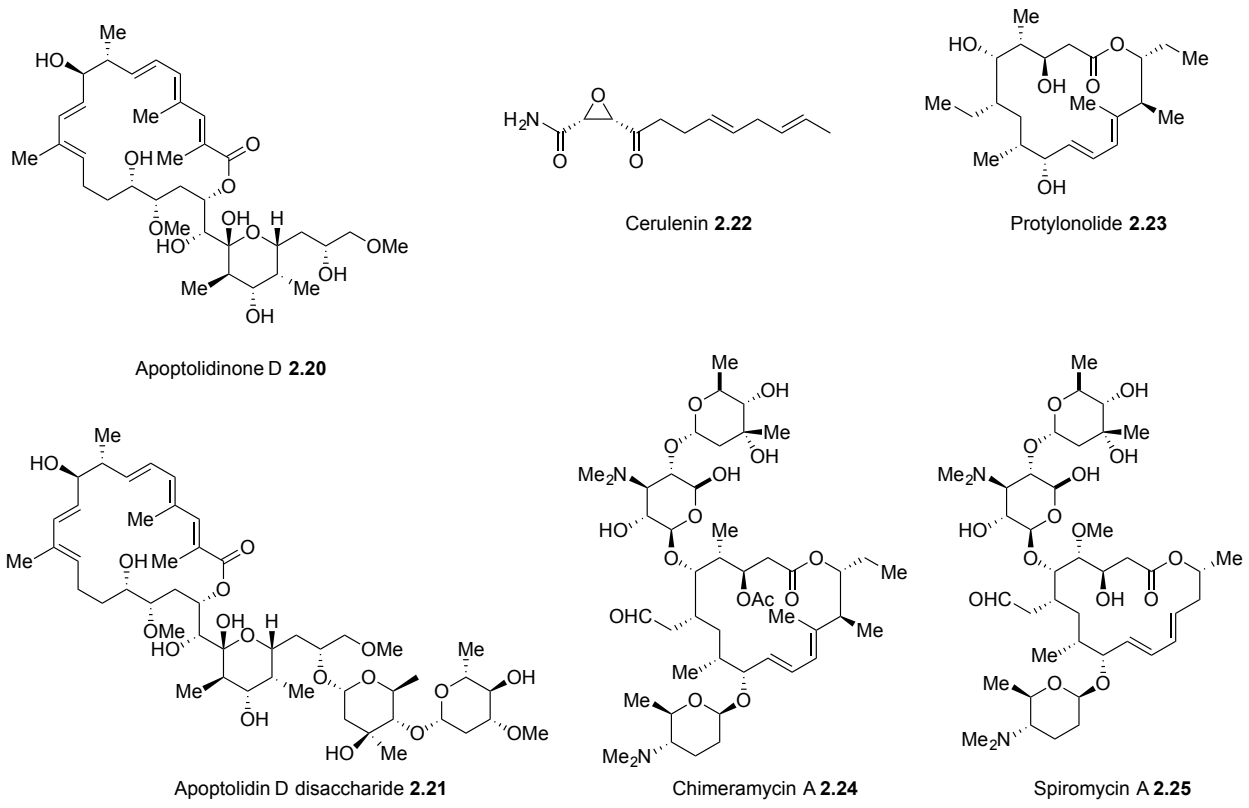

Figure 2.12. Glycovariants obtained via "chemical knockdown".

Selective C27- glycosylation, even in the presence of free hydroxyl groups within the molecule represents a powerful tool to further understand apoptolidin SAR and access apoptolidin glycovariants without any knowledge of the natural product biosynthetic pathway. From a total synthesis perspective, the construction of the complex molecular matrix of apoptolidin remains a tedious and daunting task. Utilizing the producing organism to synthesize the apoptolidin disaccharide and achieve its selective glycosylation is an attractive method to circumvent its chemical synthesis. It is however, unknown whether this technique can allow for a great amount of flexibility within the structure of the treated aglycone, as apoptolidin D **2.21** is a naturally occurring member of the apoptolidin family.

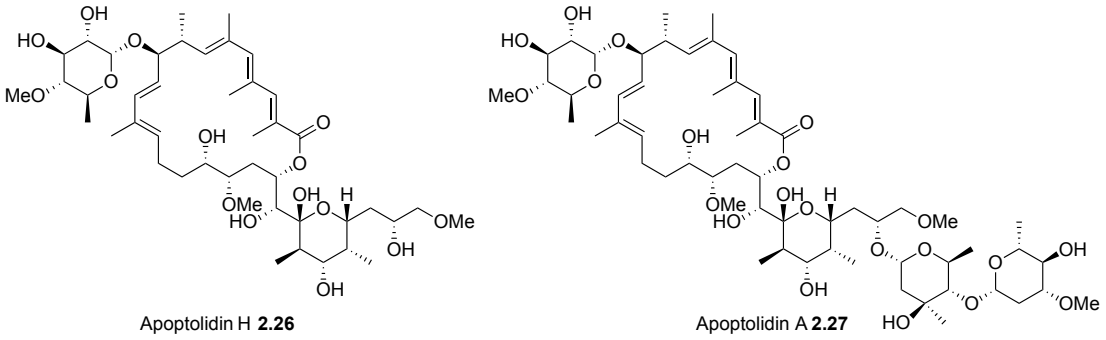

Figure 2.13. Apoptolidin glycovariants obtained via precursor-directed biosynthesis.

In 2011, Bachmann and coworkers [42] followed these studies in a seminal paper proposing the mechanism for apoptolidin biosynthesis by sequencing the FU40 gene cluster. Equipped with this knowledge, they showed that endogenous production of the apoptolidins could be shut down by targeting the last frame of its PKS, ApoS8 (Fig. 2.14). Using cosmids, the targeted gene was replaced by apramycin resistance gene markers using double crossover homologous recombination. The apramycin resistant mutant knockouts (FU40 ΔS8), showed no production of any of the apoptolidins but when treated with C9- glycosylated monosaccharide apoptolidin H **2.26**, could produce apoptolidin A **2.27** via C27- glycosylation (Fig. 2.13).

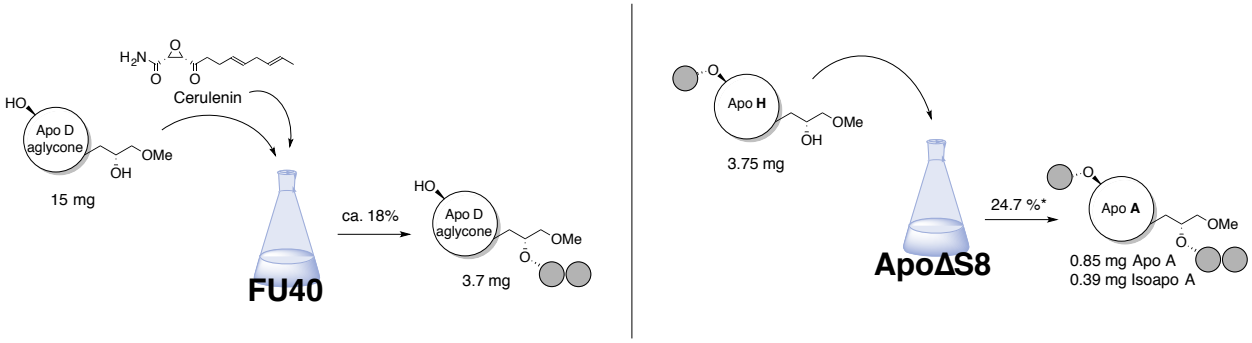

Figure 2.14. Demonstration of "chemical knockdown" and precursor directed biosynthesis to access apoptolidin glycovariants.

In contrast to the chemical "knockdown" hybrid approach (ca. 18%), this precursor directed biosynthetic approach allows for selective glycosylation of apoptolidin in ca. 24.7% yield (Fig. 2.14). Pulse feeding of both cerulenin **2.22** and the C9- glycosylated apoptolidin H **2.26** in the hybrid approach necessitates great care in effecting a chemical "knockdown" of the endogenous PKS system while reducing toxicity to the microorganism. Precursor directed biosynthesis circumvents the inherent toxicity of cerulenin **2.22**. These studies demonstrate an additional approach to "chemical knockdown" that could be used toward the selective C27- glycosylation of apoptolidin.

Additionally, collaboration between the Sulikowski and Bachmann groups [43] showed that using targeted gene deletion of one of the glycosyl transferases (ΔGT2), apoptolidin H **2.26** could be accessed (Fig.2.15). Mutasynthesis produces C9-monoglycosylated apoptolidin H **2.26** in 50-100 mg/L. This technique uses the same double crossover homologous recombination with apramycin resistant gene markers, developed by the Bachmann group toward the C27- glycosylation of apoptolidin H **2.26**.

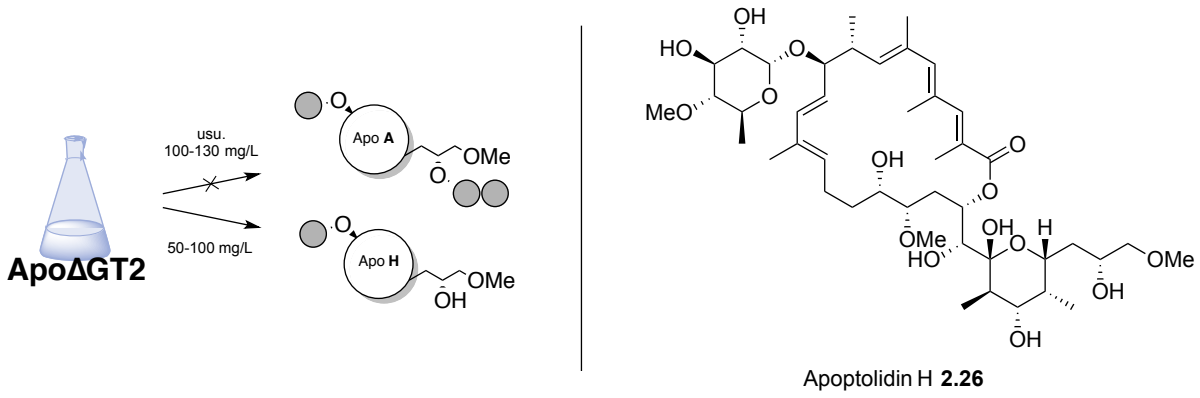

Figure 2.15. Demonstration of mutasynthesis to access apoptolidin glycovariants.

Lastly, the aglycone of apoptolidin (A **2.28**, C **2.29**, and D **2.30**, Fig. 2.16A) has been reached via total synthesis by several groups including those lead by Koert, Nicolaou, Crimmins, Sulikowski, and Nelson. [44-56] It is important to note that typical means of acid degradation of the fully glycosylated natural product **2.27** result in decomposition (Fig. 2.16B). Reports by Salomon and coworkers [57] have shown that acidic methanolysis of the fully glycosylated apoptolidin A results in the dehydration of the C23- hydroxyl group of the hemi-ketal ring and that the C9- sugar remains in tact before degradation of the macrolide is observed.

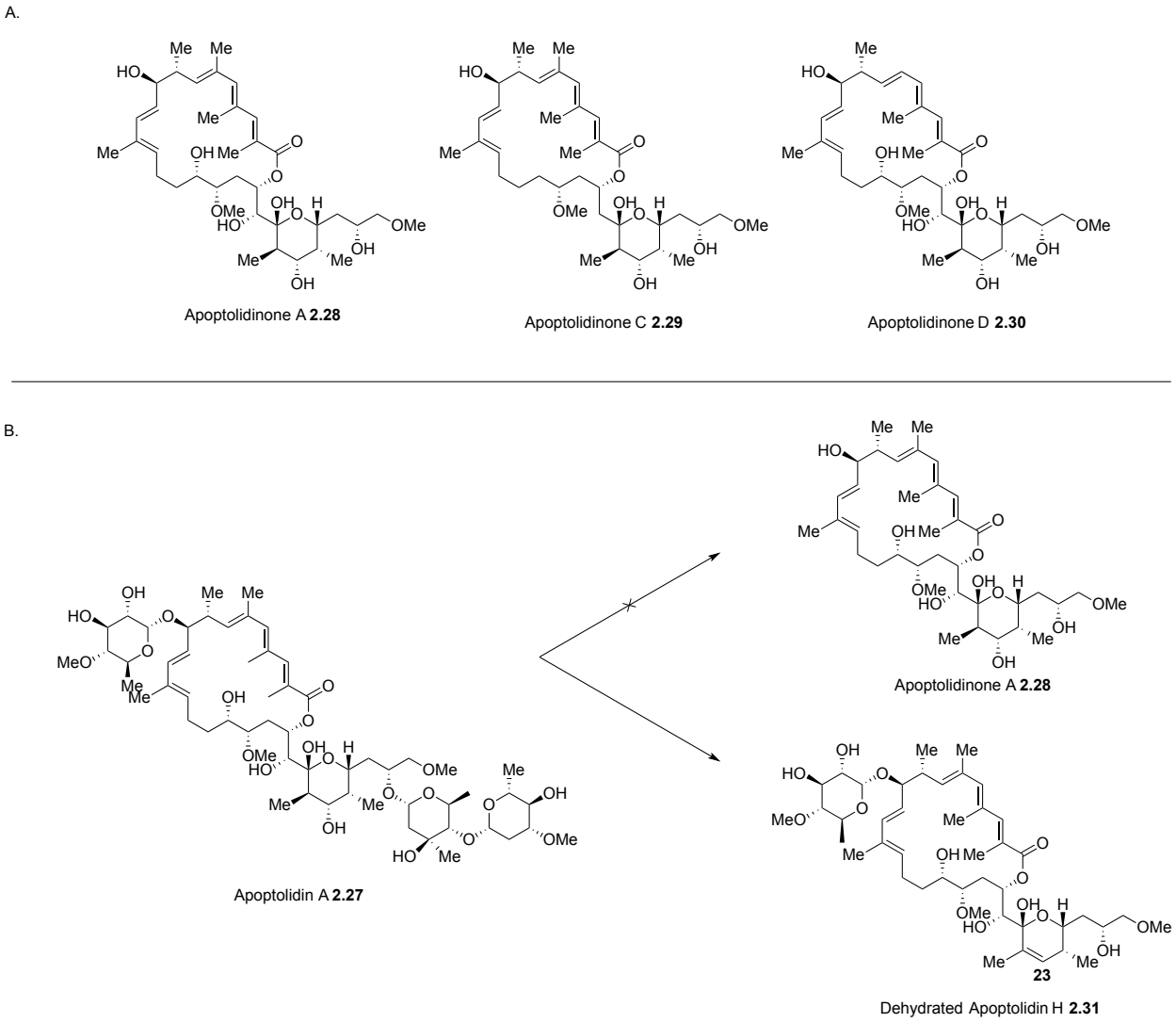

Figure 2.16. Chemical approaches toward acquiring the apoptolidin aglycone. A. Chemical structures of apoptolidinones A, C, and D accessed via total synthesis. B. Acidic degradation studies of apoptolidin A (apoptolidin A **2.27** treated with 0.2M HCl in methanol for 3h, 12% yield).

In 2015, using fully glycosylated apoptolidin A **2.27,** C27- glycosylated apoptolidin D disaccharide **2.21**, C9- glycosylated apoptolidin H **2.26**, and synthetic aglycone apoptolidinone A **2.28**, Sulikowski and coworkers [43] demonstrated apoptolidin cytotoxicity against H292 human lung cancer cells is dependent on glycosylation state (Fig. 2.17). Reports show apoptolidinone A **2.28**, which is devoid of all deoxy sugars, exhibit low cytotoxicity against H292 cells (EC_{50} > 10 μM), as compared to the fully glycosylated

apoptolidin A **2.27** (EC_{50} = 16 nM, H292). C27- glycosylated apoptolidin D disaccharide **2.21** retains some of its activity (EC_{50} = 200 nM, H292) and C9- mono-glycosylated apoptolidin H **2.26** loses much of its parent activity (IC_{50} = 810 nM, H292). Interestingly, when tested against F_oF_1-ATPase, apoptolidin H **2.26** exhibited similar activity (K_i = 13.7 μM) to the fully glycosylated apoptolidin A **2.27** (K_i = 4.9 μM). This data seems to suggest that the pharmacological importance of the apoptolidin disaccharide moiety is largely decoupled from its activity against its proposed molecular target, F_oF_1-ATPase.

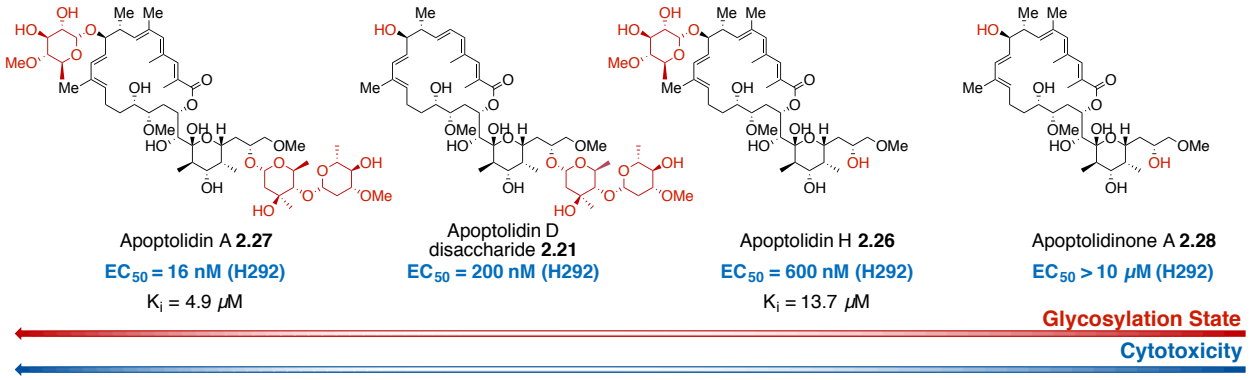

Figure 2.17. Exploring bioactivity as a function of glycosylation state.

2.6 Conclusion

The correlation between apoptolidin glycosylation state and subsequent bioactivity is a fascinating and compelling trend to further explore; it defines the basis for the thesis presented herein. Specifically, this thesis recounts work done towards the creation of molecular probes as varied by apoptolidin glycosylation state to understand the pharmacological relevance of the glycosidic appendages to the apoptolidin aglycone. In order to access fluorescent molecular probes of each glycosylation state of apoptolidin (tri-,

di-, mono-, and non- glycosylated apoptolidins), access to the aglycone is necessary. Fully glycosylated apoptolidin A **2.27** (tri-glycosylated) can be accessed as the natural major metabolite produced by *Nocardiopsis* sp. FU40. [58, 59] C27- glycosylated apoptolidin disaccharide **2.21** (di-glycosylated) can be accessed via chemical "knockdown" with cerulenin or precursor directed biosynthesis. [40, 42] And finally, mutasynthesis by GT2 glycosyltransferase knock out (FU40 ΔGT2) can be utilized to produce C9- glycosylated (mono-glycosylated) apoptolidin H **2.26**. [43] The aglycone **2.28** (non-glycosylated) can in theory be produced using several methods. However, acid mediated degradation of the fully glycosylated apoptolidin A **2.27**, does not give the desired apoptolidin A **2.28** but rather C23- dehydrated apoptolidin H **2.31** or decomposition (Fig. 2.16). [57] Additionally, efforts to either isolate active glycosyltranserases of FU40 or complete knockdown of the glycosyltransferases within the apoptolidin gene cluster have yet to be achieved. Thus total synthesis of the apoptolidin aglycone remains an attractive strategy and provides the basis for the work presented herein.

2.7 Notes and references

1. Thorson, J. S.; Vogt, T. Glycosylated Natural Products. In *Carbohydrate-Based Drug Discovery*; Wong C.-H.; Wiley-VCH Verlag GmBH & Co. KGaA: 2005, p. 685-711.

2. Dosio, F.; Brusa, P.; Cattel, L. Immunotoxins and Anticancer Drug Conjugate Assemblies: The Role of the Linkage between Components *Toxins*, **2011**, 3, 848-883.

3. Padera, T. P.; Kadambi, A.; di Tomaso, E.; Carreira, C. M.; Brown, E. B.; Boucher, Y.; Choi, N. C.; Mathisen, D.; Wain, J.; Mark, E. J.; Munn, L. L.; Jain, R. K. Lymphatic Metastasis in the Absence of Functional Intratumor Lymphatics *Science*, **2002**, 296, 1883-1886.

4. Leu, A. J.; Berk, D. A.; Lymboussaki, A.; Alitalo, K.; Jain, R. K. Absence of Functional Lymphatics within a Murine Sarcoma: A Molecular and Functional Evaluation *Cancer Res.* **2000**, 60, 4324-4327.

5. Singh, Y.; Palombo, M.; Sinko, P. J. Recent Trends in Targeted Anticancer Prodrug and Conjugate Design *Curr. Med. Chem.* **2008**, 15, 1802-1826.

6. Lee, M. D.; Dunne, T. S.; Siegel, M. M.; Chang, C. C.; Morton, G. O.; Borders, D. B. Calichemicins, a novel family of antitumor antibiotics. 1. Chemistry and partial structure of calichemicin γ_1^1 *J. Am. Chem. Soc.* **1987**, 109, 3464-3466.

7. ADC review. https://adcreview.com/uncategorized/calicheamicin/ (accessed July 25, 2017).

8. Maiese, W. M.; Lechevalier, M. P.; Lechevalier H. A.; Korshalla, J.; Kuck, N.; Fantini, A.; Wildey, M. J.; Thomas, J.; Greenstein, M. Calicheamicins, a novel family of antitumor antibiotics: taxonomy, fermentation and biological properties *J. Antibiot.* **1989**, 4, 558-563.

9. Watanabe, C. M.; Superkova, L; Schultz, P. G. Transcriptional effects of the potent enediyne anti-cancer agent Calicheamicin gamma(I) *Chem. Biol.* **2002**, 9, 245-251.

10. Ricart, A. D.; Tolcher, A. W. Technology insight: cytotoxic drug immunoconjugates for cancer therapty. *Nat. Clin. Pract. Oncol.* **2007**, 4, 245-255.

11. Nicolaou, K. C.; Smith, A. L.; Yue, E. W. Chemistry and biology of natural and designed enediynes *Proc. Natl. Acad. Sci. U. S. A.* **1993**, 90, 5881-5888.

12. Saunders, J. Anti-infectives: Chemical warfare *Nat. Rev. Micro.* **2003**, 1, 88.

13. Kalben, A.; Pal, S.; Andreotti, A. H.; Walker, S.; Gange, D.; Biswas, K. Calicheamicin-DNA Recognition: An analysis of Seven Different Drug-DNA Complexes *J. Am. Chem. Soc.* **2000**, 122, 8403-8412.

14. Chen, J.; Stubbe, J. Bleomycins: toward better therapeutics *Nat. Rev. Cancer* **2005**, 5, 102-112.

15. Bishun, N. P.; Smith, N. S.; Williams, D. C. Bleomycin (review) *Oncology* **1978**, 5, 228-234.

16. Blum, R. H.; Carter, S. K.; Agre, K. A clinical review of bleomycin—a new antineoplastic agent *Cancer* **1973**, 4, 903-914.

17. Cosgrove, J. P.; Dedon, P. C. Binding and Reaction of Calicheamicin and Other Enediyne Antibiotics with DNA In *Small Molecule DNA and RNA Binders: From Synthesis to Nucleic Acid Complexes*; Wiley-VCH Verlag GmbH & Co. KGaA: 2004, p. 609-642.

18. Ikemoto, N.; Kumar, R. A.; Ling, T. T.; Ellestad, G. A.; Danishefsky, S. J.; Patel, D. J. Calicheamicin-DNA complexes: warhead alignment and saccharide recognition of the minor groove *Proc. Natl. Acad. Sci. U. S. A.* **1995**, 92, 10506-10510.

19. Gomez Paloma, L.; Smith, J. A.; Chazin, W. J.; Nicolaou, K. C. Interactoin of Calicheamicin with Duplex DNA: Role of the Oligosaccharide Domain and Identification of Multiple Binding Modes *J. Am. Chem. Soc.* **1994**, 116, 3697-3708.

20. Bifulco, G.; Galeone, A.; Nicolaou, K. C.; Chazin, W. J.; Gomez-Paloma, L. Solution Structure of the Complex between the Head-to-Tail Dimer of Calicheamicin γ_1^I Oligosaccharide and a DNA Duplex Comtaining d(ACCT) and d(TCCT) High-Affinity Binding Sites *J. Am. Chem. Soc.* **1998**, 120, 7183-7191.

21. Bifulco, G.; Galeone, A.; Gomez-Paloma, L.; Nicolaou, K. C.; Chazin, W. J. Solution Structure of the Head-to-Head Dimer of Calicheamicin Oligosaccharide Domain and d(CGTAGGATATCCTACG)$_2$ *J. Am. Chem. Soc.* **1996**, 118, 8817-8824.

22. Walker, S. L.; Andreotti, A. H.; Kahne, D. E. NMR characterization of calicheamicin $\gamma 1^I$ bound to DNA *Tetrahedron* **1994**, 50, 1351-1360.

23. Walker, S.; Valentine, K. G.; Kahne, D. Sugars as DNA binders: a comment on the calicheamicin oligosaccharide *J. Am. Chem. Soc.* **1990**, 112, 6428-6429.

24. Drak, J.; Iwasawa N.; Danishefsky, S.; Crothers, D. M. The carbohydrate domain of calicheamicin $\gamma 1^I$ determines its sequence specificity for DNA cleavage *Proc. Natl. Acad. Sci. U. S. A.* **1991**, 88, 7464-7468.

25. Umezawa, H.; Maeda, K.; Takeuchi, T.; Okami, Y. New antibiotics, bleomycin A and B *J. Antibiot.* **1966**, 19, 200-209.

26. Drugs.com: Bleomycin Sulfate. https://www.drugs.com/monograph/bleomycin-sulfate.html (accessed July 25, 2017).

27. Kanao, M.; Tomita, S.; Ishihara, S.; Murakami, A.; Okada, H. Chelation of bleomycin with copper *in vivo Chemotherapy*, **1973**, 21, 1305-1310.

28. Burger, R. M.; Peisasch, J.; Horwitz, S. B. Activated bleomycin: a transient complex of drug, iron, and oxygen that degrades DNA *J. Biol. Chem.* **1981**, 256, 11636-11644.

29. Wu, W.; Vanderwaall, D. E.; Stubbe, J.; Kozarich, J. W.; Turner, C. J. Interaction of Co·bleomycin A2 (Green) with d(CCAGGCCTGG)$_2$: evidence for intercalation using 2D NMR *J. Am. Chem. Soc.* **1994**, 10843-10844.

30. Povirk, L. F.; Hogan, M.; Dattagupta, N. Binding of bleomycin to DNA: Intercalation of the bithiazole Rings. *Biochemistry* **1979**, 18, 96-101.

31. Povirk, L. F.; Wübker, W.; Köhnlein, W.; Hutchinson, F. DNA Double-strand breaks and alkali-labile bonds produced by bleomycin *Nucleic Acids Res.* **1977**, 4, 3573-3580.

32. Absalon, M. J.; Wu, W.; Kozarich, J. W.; Stubbe, J. Sequence-specific double-strand cleavage of DNA by Fe bleomycin. 2. Mechanism and dynamics *Biochemistry* **1995**, 34, 2076-2086.

33. Stubbe, J.; Kozarich, J. W.; Wu, W.; Vanderwall, D. E. Bleomycins: a structural model for specificity, binding, and double strand cleavage *Acc. Chem. Res.* **1996**, 29, 322-330.

34. Vanderwall, D. E.; Lui, S. M.; Wu, W.; Turner, C. J.; Kozarich, J. W.; Stubbe, J. A model of the structure of HOO-Co·bleomycin bound to d(CCAGTACTGG): recognition at the d(GpT) site and implications for double-stranded DNA cleavage. *Chem. Biol.* **1997**, 5, 373-387.

35. Yu, Z.; Schmaltz, R. M.; Bozeman, T. C.; Paul, R.; Rische, M. J.; Tsosie, K. S.; Hecht, S. M. Selective Tumor Cell Targeting by the Disaccharide Moiety of Bleomycin *J. Am. Chem. Soc.* **2013**, 135, 2883-2886.

36. Yu, Z.; Paul, R.; Bhattacharya, C.; Bozeman, T. C.; Rischel, M. J.; Hecht, S. M. Structural Features Facilitating Tumor Cell Targeting and Internalization by Bleomycin and Its Disaccharide *Biochemistry*, **2015,** 54, 3100-3109.

37. Bode, H. B.; Müller, R. Reversible Sugar Transfer by Glycosyltransferases as a Tool for Natural Product (Bio)synthesis *Angew. Chem. Int. Ed.* **2007**, 46, 2147-2150.

38. Minami, A.; Kakinuma, K.; Eguchi, T. Aglycon switch approach toward unnatural glycosides from natural glycoside with glycosyltransferase VinC *Tet. Lett.* **2005**, 46, 6187-6190.

39. Zhang, C.; Griffith, B. R.; Fu, Q.; Albermann, C.; Fu, X.; Lee, I.-K.; Li, L.; Thorson, J. S. Exploiting the Reversibility of Natural Product Glycosyltransferase-Catalyzed Reactions *Science*, **2006**, 313, 1291-2394.

40. Ghidu, V. P.; Ntai, I.; Wang, J.; Jacobs, A. T.; Marnett, L. J.; Bachmann, B. O.; Sulikowski, G. A. Combined Chemical and Biosynthetic Route to Access a New Apoptolidin Congener *Org. Lett.* **2009**, 11, 3032-3034.

41. Omura, S.; Sadakane, N.; Tanaka, Y.; Matsubara, H. Chimeramycins: New Macrolide Antibiotics Produced By Hybrid Biosynthesis *J. Antibiot.* **1983**, 36, 927-930.

42. Du, Y.; Derewacz, D. K.; Deguire, S. M.; Teske, J.; Ravel, J.; Sulikowski, G. A.; Bachmann, B. O. Biosynthesis of apoptolidins in *Nocardiopsis* sp. FU 40 *Tetrahedron*, **2011**, 67, 6568-6575.

43. Deguire, S. M.; Earl, D. C.; Du, Y.; Crews, B. A.; Jacobs, A. T.; Ustione, A.; Daniel, C.; Chong, K. M.; Marnett, L. J.; Piston, D. W.; Bachmann, B. O.; Sulikowski, G. A., Fluorescent Probes of the Apoptolidins and their Utility in Cellular Localization Studies *Angew. Chem. Int. Ed.* **2015**, 54, 961-964.

44. Daniel, P. T.; Koert, U.; Schuppan, J., Apoptolidin: Induction of Apoptosis by a Natural Product *Angew. Chem. Int. Ed.* **2006**, 45, 872-893.

45. Schuppan, J.; wehlan, H.; Keper, S.; Koert, U. Synthesis of Apoptolidinone *Angew. Chem. Int. Ed.* **2001**, 40, 2063-2066.

46. Wehlan, H.; Dauber, M.; Mujica Fernaud, M.-T.; Schuppan, J.; Mahrwald, R.; Ziemer, B.; Juarez Garcia, M.-E.; Koert, U. Total synthesis of Apoptolidin *Angew. Chem. Int. Ed.* **2004**, 43, 4597-4601.

47. Schuppan, J.; Wehlan, H.; Keiper, S.; Koert, U. Apoptolidinone A: Synthesis of the Apoptolidin A Aglycone *Chem. Eur. J.* **2006**, 12, 7364-7377.

48. Nicolaou, K. C.; Li, Y.; Fylaktakidou, K. C.; Mitchell, H. J.; Wei, H.-X.; Weyershausen, B. Total Synthesis of Apoptolidin: Part 1. Retrosynthetic Analysis and Construction of Building Blocks *Angew. Chem. Int. Ed.* **2001**, 40, 3849-3854.

49. Nicolaou, K. C.; Li, Y.; Fylaktakidou, K. C.; Mitchell, H. J.; Sugita, K. Total Synthesis of Apoptolidin: Part 2. Coupling of Key Building Blocks and Completion of the Synthesis *Angew. Chem. Int. Ed.* **2001**, 40, 3854-3857.

50. Nicolaou, K. C.; Fylaktakidou, K. C.; Monenschein, H.; Li, Y.; Weyershausen, B.; Mitchell, H. J.; Wei, H.-X.; Guntupalli, P.; Hepworth, D.; Sugita, K. Total Synthesis of Apoptolidin: Construction of Enantiomerically Pure Fragments *J. Am. Chem. Soc.* **2003**, 125, 15433-15442.

51. Nicolaou, K. C.; Li, Y.; Sugita, K.; Monenschein, H.; Guntupalli, P.; Mitchell, H. J.; Fylaktakidou, K. C.; Vourloumis, D.; Giannakakou, P.; O'Brate, A. Total Synthesis of

Apoptolidin: Completion of the Synthesis and Analogue Synthesis and Evaluation *J. Am. Chem. Soc.* **2003**, 125, 15443-15454.

52. Wu, B.; Liu, Q.; Sulikowski, G. A. Total Synthesis of Apoptolidinone *Angew. Chem. Int. Ed.* **2004**, 43, 6673-6675.

53. Ghidu, V. P.; Wang, J.; Wu, B.; Liu, Q.; Jacobs, A.; Marnett, L. J.; Sulikowski, G. A. Synthesis and Evaluation of the Cytotoxicity of Apoptolidinones A and D *J. Org. Chem.* **2008**, 73, 4949-4955.

54. Crimmins, M. T.; Christie, H. s.; Chaudhary, K.; Long. A. Enantioselective Synthesis of Apoptolidinone: Exploiting the Versatility of Thiazolidinethione Chiral Auxiliaries *J. Am. Chem. Soc.* **2005**, 127, 13810-13812.

55. Crimmins, M. T.; Christie, H. S.; Long. A.; Chaudhary, K. Total Synthesis of Apoptolidin A *Org. Lett.* **2009**, 11, 831-834.

56. Vargo, T. R.; Hale, J. S.; Nelson, S. G. Catalytic Asymmetric Aldol Equivalents in the Enantioselective Synthesis of the Apoptolidin C Aglycone *Angew. Chem. Int. Ed.* **2010**, 49, 8678-8681.

57. Saloman, A. R.; Zhang, Y.; Seto, H.; Khosla, C. Structure-Activity Relationships within a Family of Selectively Cytotoxic Macrolide Natural Products *Org. Lett.* **2001**, 3, 57-59.

58. Kim, J. W.; Adachi, H.; Shin-Ya, K.; Yoichi, H.; Seto, H., Apoptolidin, a New Apoptosis Inducer in Transformed Cells from *Nocardiopsis* sp. *J. Antibiot.* **1997**, 50, 628-630.

59. Hayakawa, Y.; Kim, J. W.; Adachi, H.; Shin-ya, K.; Fujita, K.; Seto, H., Structure of Apoptolidin, a Specific Apoptosis Inducer in Transformed Cells *J. Am. Chem. Soc.* **1998**, 120, 3524-3525.

CHAPTER III

DEVELOPMENT OF A ROUTE TOWARD THE WESTERN HEMISPHERE OF APOPTOLIDINONE C

3.1 Chemical synthesis of apoptolidinone A and C

Due to its complex structure and interesting bioactivity, apoptolidin A **3.1** has garnered much attention since its isolation in 1997. To date, three total syntheses have been accomplished by the Nicolaou, Koert, and Crimmins groups [1-7] and four synthesis of its aglycone (apoptolidinones A **3.2**, C **3.3**, and D **3.4)** by the Koert, Sulikowski, Crimmins, and Nelson groups, Fig. 3.1). [1, 8-13]

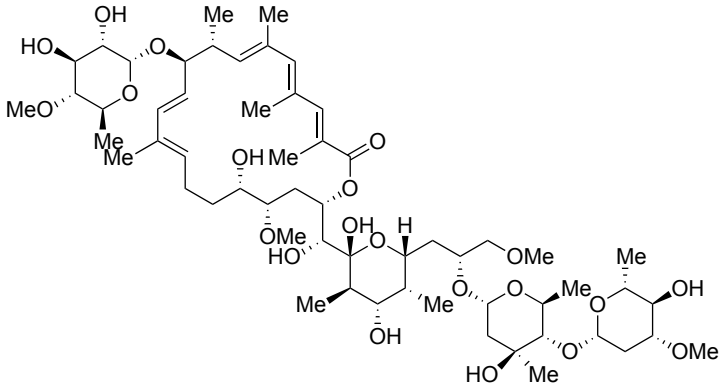

Apoptolidin A **3.1**

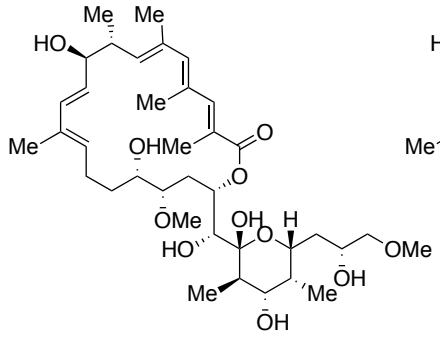

Apoptolidinone A **3.2**

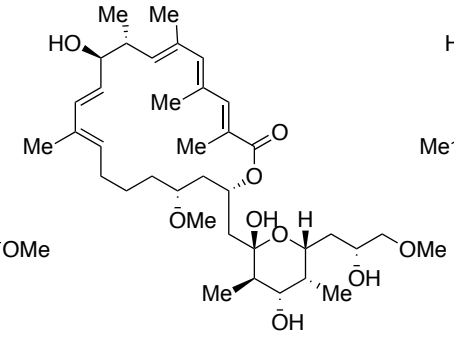

Apoptolidinone C **3.3**

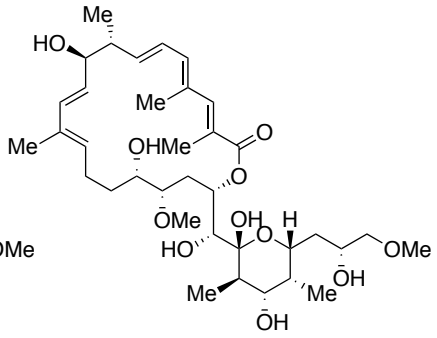

Apoptolidinone D **3.4**

Figure 3.1. Chemical structures of apoptolidin and related aglyca.

While the apoptolidins have been synthesized several times throughout history, efforts to achieve a highly convergent and efficient route toward the macrolide for late stage SAR studies are on going. Access to large quantities of the fully glycosylated apoptolidin A **3.1** and its glycovariants has yet to be reported. Solely focusing on the aglycone of apoptolidin A, it has been synthesized by the Koert, Sulikowski, and Crimmins groups. [1, 8-13] Overall yields range between 0.027% and 0.147% and contain 37-47 total steps and 18-26 longest linear sequences (Fig. 3.2).

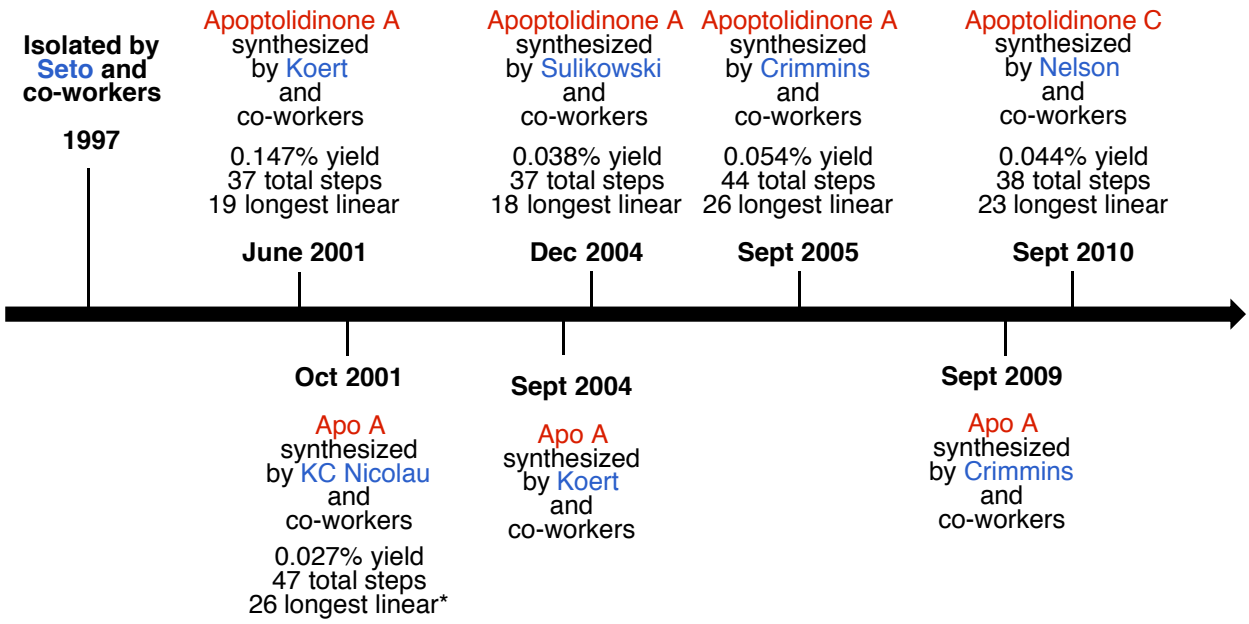

Figure 3.2. Historical timeline of completed syntheses of apoptolidin macrolides.

The Koert group first published their synthesis of apoptolidinone A in June of 2001, [8] four years after its initial isolation. Apoptolidinone A was synthesized by accessing the northern and southern hemispheres of apoptolidinone A and uniting the halves together through Stille coupling and macrolactonization (Fig. 3.3).

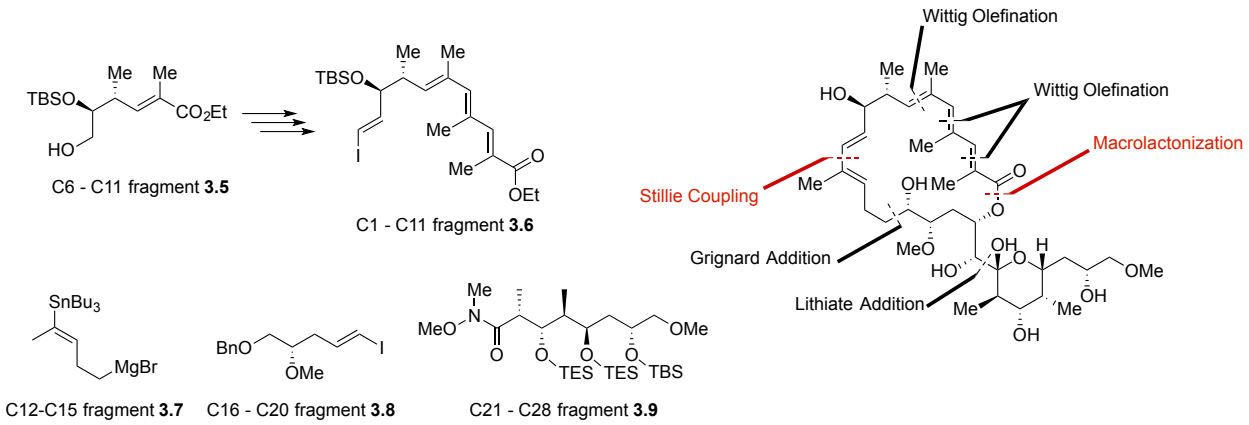

Figure 3.3. Koert's retrosynthetic analysis for apoptolidinone A.

The northern C1-C11 fragment **3.6** was constructed through iterative Wittig homologation of the C6-C10 fragment **3.5**. C6-C10 fragment **3.5** was synthesized beginning

from β-hydroxy lactone **3.10**. t-Butyldimethylsilyl (TBS) protection and semi-reduction arrived at lactol **3.11**. Wittig homologation followed by triethylsilyl (TES) protection gave alcohol **3.12** (Fig. 3.4).

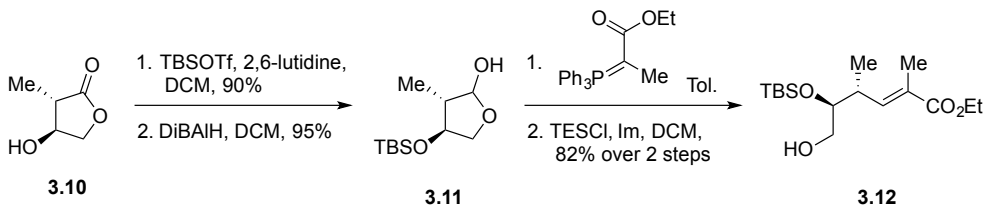

Figure 3.4. Koert's synthesis of C6-C10 fragment of apoptolidinone A.

C21-28 fragment **3.18** was assembled beginning with β-keto-ester **3.13** (Fig. 3.4). Noyori reduction followed by silyl protection and semi reduction gave aldehyde **3.14**. Evan's auxiliary mediated aldol with β-keto-imide auxiliary provided the aldol adduct in 91% yield and 96:4 dr. Hydroxy- directed reduction cleanly gave trans diol **3.17** in 98% yield and in 95:5 dr. Transamidation to the Weinreb amide followed by TES protection arrived at the C21-C28 fragment **3.18**.

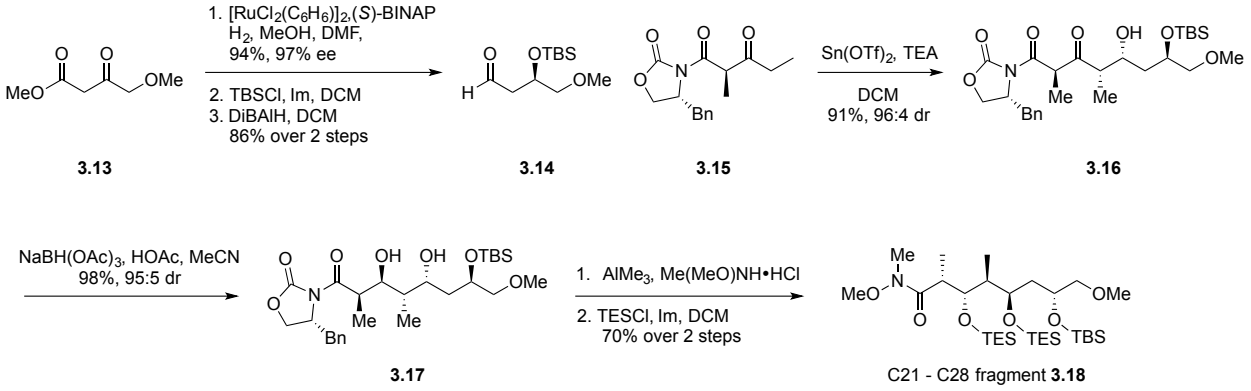

Figure 3.5. Koert's synthesis of C21-C28 fragment of apoptolidinone A.

The southern hemisphere of apoptolidinone A was assembled using iterative nucleophillic additions of fragments **3.19** and **3.24** (Fig. 3.6). Lithium halogen exchange

with vinyl iodide **3.19** and addition to Weinreb amide **3.20** gave α,β-ketone **3.21**. Comprehensive silyl deprotection resulted in the cyclization of the protected ketal ring to give **3.22**. Dihydroxylation and acetylation set the C19- and C20- hydroxyl group stereochemistry. Protecting group manipulation and oxidation provided electrophile **3.23** for nucleophillic addition of Grignard reagent **3.24**.

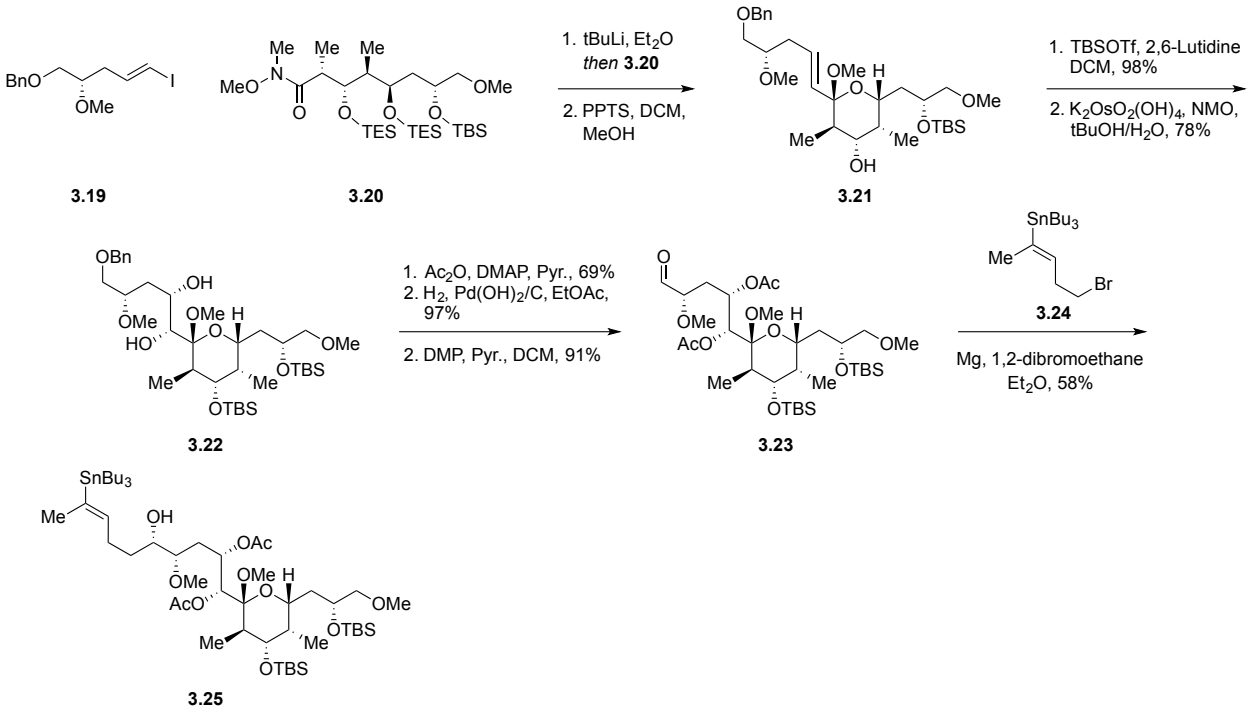

Figure 3.6. Koert's synthesis of apoptolidinone A southern hemisphere.

Completion of the aglycone was achieved via Copper (I) thiocarboxylate Stille coupling between northern fragment **3.6** and southern fragment **3.25** (Fig. 3.7). Hydrolysis, Yamaguchi macrolactonization, and global deprotection gave the apoptolidinone A **3.2** in 0.20% overall yield, 28 total steps, and a longest linear sequence of 20 steps.

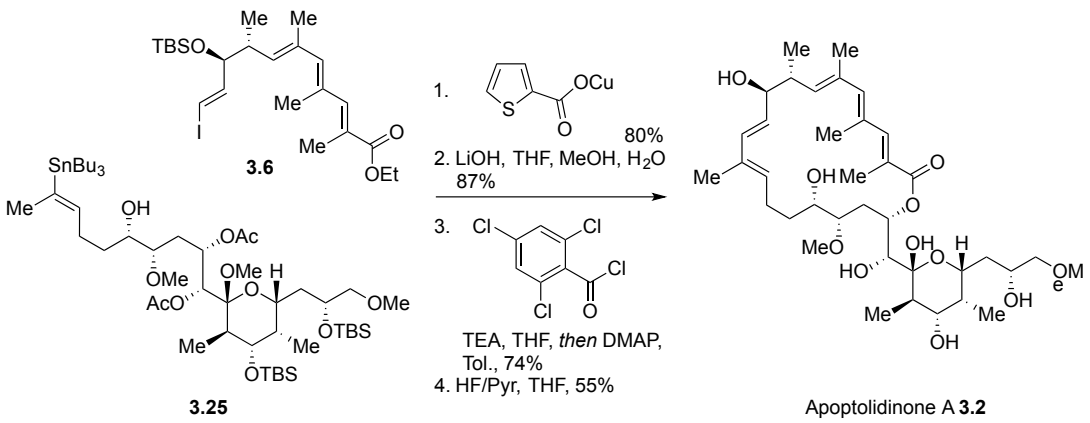

Figure 3.7. Koert's completion of apoptolidinone A.

In 2004, Sulikowski and coworkers [9] demonstrated synthesis of apoptolidinone A could be achieved by synthesizing western C6-C22 fragment **3.26**, northeastern C1-C5 **3.27**, and southeastern C23-C28 **3.28** fragments (Fig. 3.8). These three fragments were brought together utilizing a Mukaiyama aldol between the C22- and C23- carbons, esterification to combine C1-C5 fragment **3.27**, and Suzuki cross coupling to close the macrolide ring.

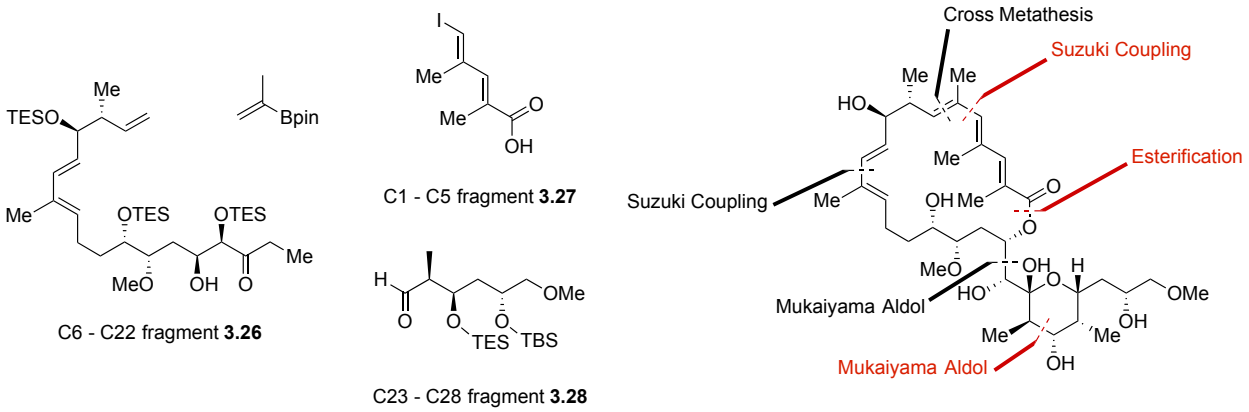

Figure 3.8. Sulikowski's retrosynthetic analysis for apoptolidinone A.

The synthesis of the C6-C22 fragment **3.26** was achieved from β-methoxy lactone **3.29** (Fig. 3.9). Semi-reduction, 1,3-dithiane opening, and oxidation revealed aldehyde **3.30**. Grignard formation and addition of bromide **3.31** to aldehyde **3.30** provided the vinyl

stannane **3.32**. Tin-iodine exchange and TES protection supplied the cross coupling partner **3.35** for Suzuki coupling with vinyl boronate **3.36**. Subsequent Mukaiyama aldol arrived at the C6-C22 fragment **3.39**.

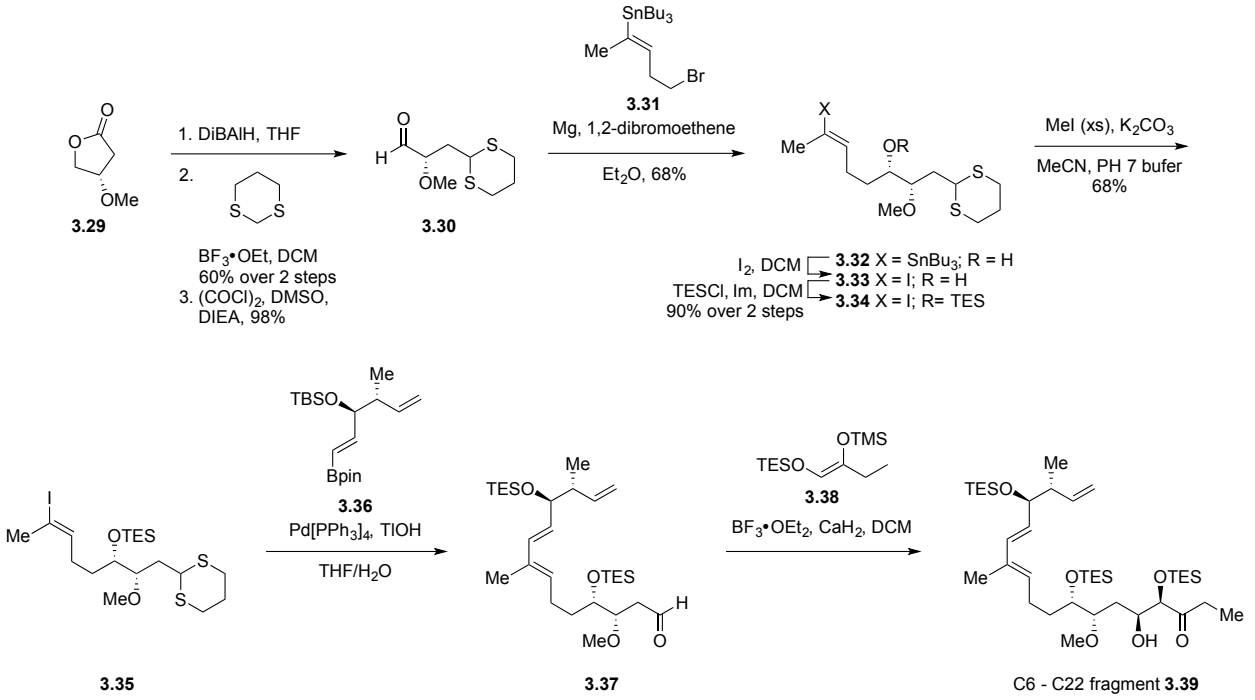

Figure 3.9. Sulikowski's synthesis of C6-C22 western fragment of apoptolidinone A.

With C6-C22 fragment **3.39** in hand, the macrolide was brought together via Yamaguchi esterification of **3.39** with C1-C5 fragment **3.40** (Fig. 3.10). Mukaiyama aldol between ketone **3.41** and aldehyde **3.42**, followed by cross metathesis to give the acyclic framework **3.43**. Final Suzuki cross coupling and global deprotection with concomitant cyclization of the pyran ring furnished the apoptolidinone A aglycone **3.2** in 0.078%, 34 total steps, and a longest linear sequence of 29 steps. Unique to this synthesis was the demonstration of comprehensive deprotection of the aglycone core resulting in simultaneous cyclization of the hemi-ketal ring. This means of concomitant ring cyclization avoids the need to protect the hemi-ketal moiety as a mixed ketal.

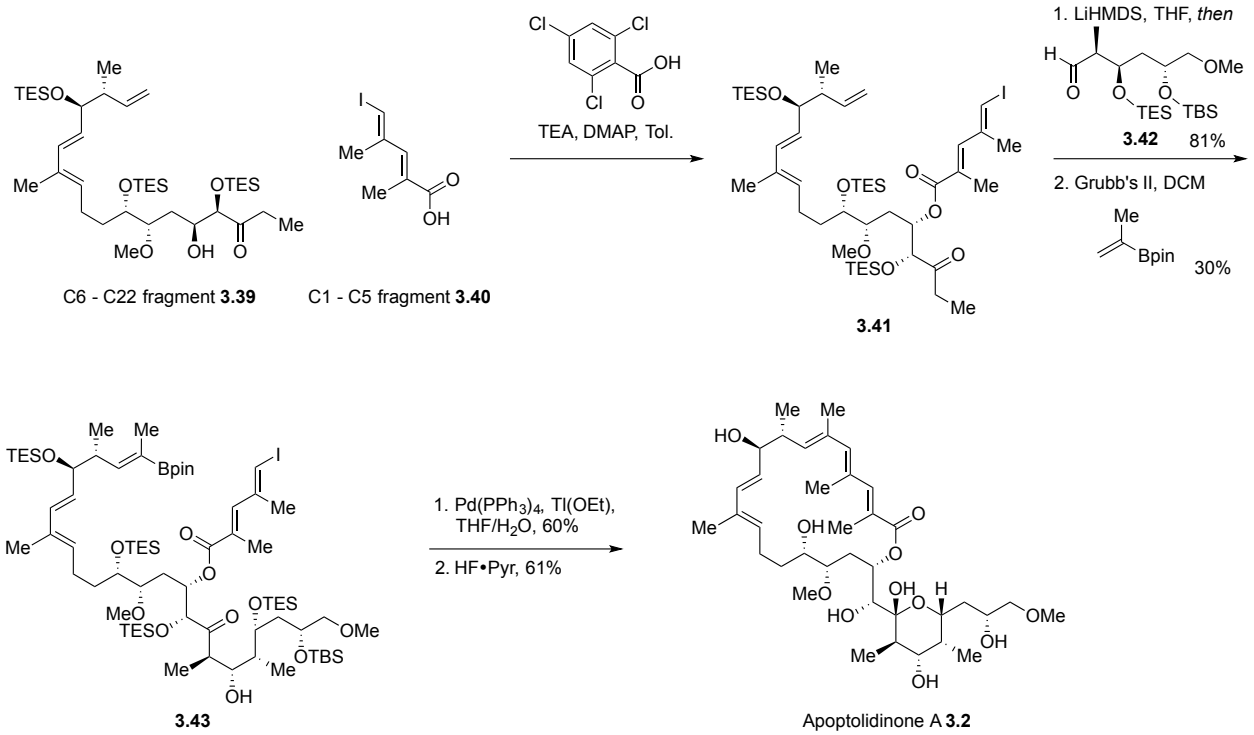

Figure 3.10. Sulikowski's completion of apoptolidinone A.

The Crimmins group synthesized apoptolidinone A in 2005 [7] by dividing the aglycone in roughly three equal parts: C1-C11 fragment **3.44**, C13-C19 fragment **3.47**, and C20-C28 fragment **3.48** (Fig. 3.11). These three fragments were brought together by Horner Wadsworth Emmons (HWE) olefination, cross methathesis, and macrolactonization. Similar to the Koert synthesis, [9] the hemi-ketal ring was formed prior to global deprotection with H_2SiF_6 in aqueous acetonitrile. Additionally saponification of the ethyl ester and carbonate moieties forms an analog **3.46** of the presumed seco-acid of apoptolidin A. Also, similar to the Koert synthesis of apoptolidinone A, [9] the northern hemisphere of the aglycone was synthesized by iterative Wittig homologation. Notably, the Crimmins group showcased the effective use of titantium mediated aldol methodology to set much of the molecule's stereocomplexity.

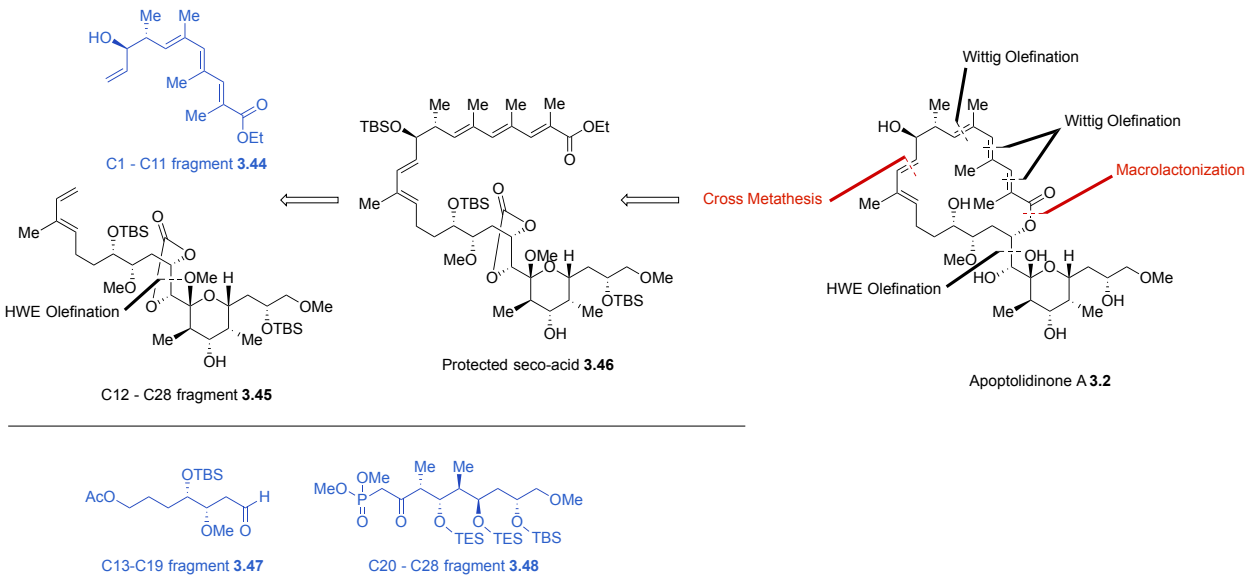

Figure 3.11. Crimmin's retrosynthetic analysis for apoptolidinone A.

Similar to syntheses by Koert [8, 9] and Sulikowski, [10, 11] the Crimmin's [12] group used iterative aldols to homologate the southern hemisphere of the aglycone. Instead of using Evan's tin and boron mediated aldol conditions, titanium mediated aldol reactions using thiazolidinthione auxiliaries directed stereoechemistry of the polyketide backbone. Interestingly, thiazolinthione auxiliaries can be removed with milder conditions, such as diisobutylaluminum hydride (DiBAlH) to obtain the aldehyde directly. In their synthesis of the southern half of apoptolidinone A, the Crimmin's group demonstrates effective use of titanium-mediated aldols. As a testament to the thiazolidinthione auxiliary utility, mild and direct addition from aldol adduct **3.53** to phosphonate **3.48** was achieved. Typical Evan's conditions would require transamidation to the Weinreb amide before alkylation. [38]

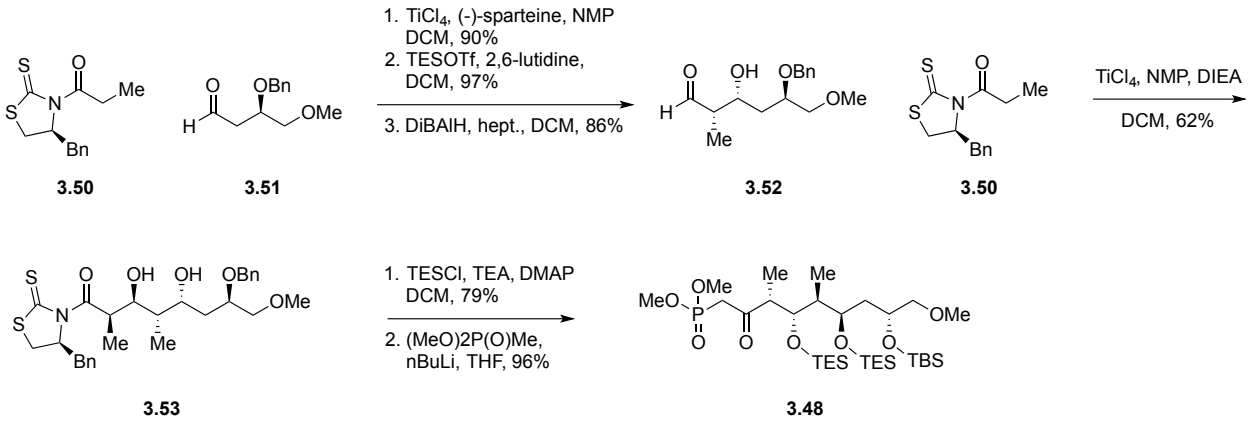

Figure 3.12. Crimmin's synthesis of C20-C28 phosphonate.

C13-C19 fragment **3.59** was prepared using auxiliary directed alkylation and redox manipulation to reach aldehyde **3.56** (Fig. 3.13). Titanium mediated allylation of **3.56** and TBS protection provided olefin **3.58**. Hydroboration-oxidation of the terminal olefin followed by protection and ozonolysis formed the desired aldehyde **3.59** for HWE olefination.

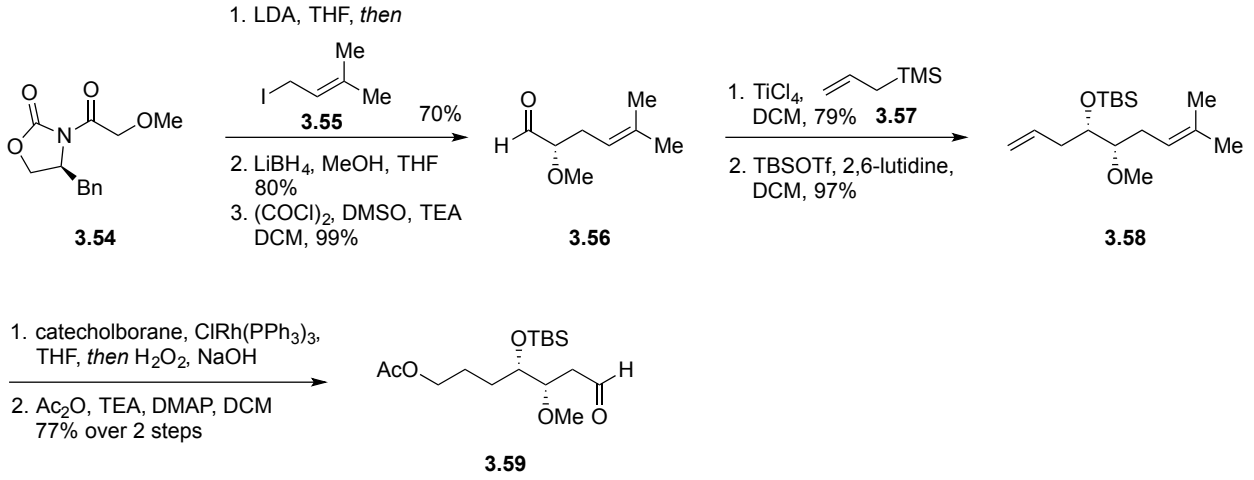

Figure 3.13. Crimmin's synthesis of C13-C19 fragment of apoptolidinone A.

To construct the southern hemisphere of apoptolidinone A, HWE olefination between aldehyde **3.59** and phosphonate **3.48** brought together the bulk of hemispheric

half (Fig. 3.14). Silyl deprotection resulted in ring cyclization and treatment with t-butyldimethylsilyl triflate gave ketal **3.49**. Dihydroxylation, as in the Nicolaou synthesis [2-5] toward apoptolidin A **3.1**, followed by acyl protection with triphosgene installed and protected the C19- and C20- hydroxyl groups. Protecting group manipulation and Wittig homologation then gave diene **3.53** to complete the southern hemisphere of apoptolidinone A.

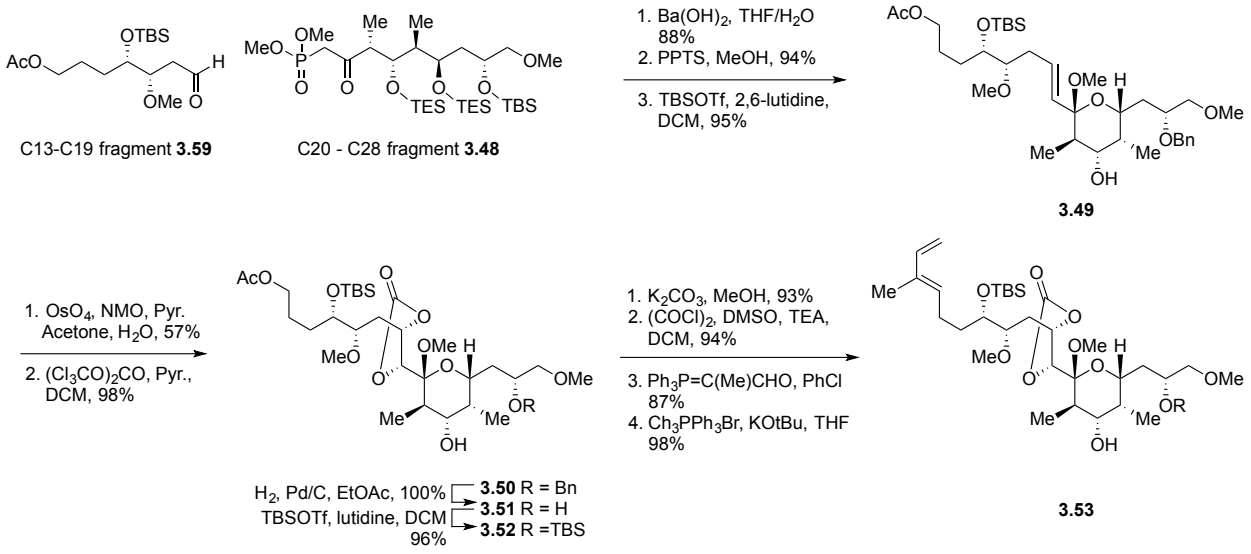

Figure 3.14. Crimmin's synthesis of the southern hemisphere of apoptolidinone A.

Preparation of the northern hemisphere of apoptolidinone A, began with crotonaldehyde and the necessary auxiliary for titanium-mediated anti-syn aldol. The resulting aldol adduct **3.54** was semi-reduced, subjected to iterative Wittig homologation, and deprotected to provide C1-C10 fragment **3.44**.

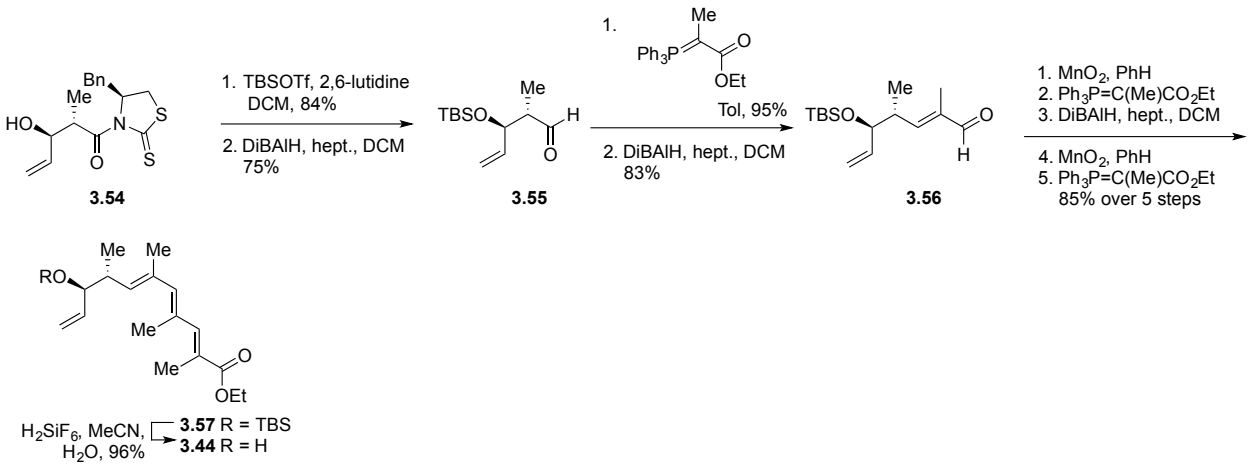

Figure 3.15. Crimmin's synthesis of the northern hemisphere of apoptolidinone A.

The northern **3.44** and southern **3.58** hemispheres were brought together via cross metatheses using the Grubb's second generation catalyst. The resulting seco-acid analogue was protected to give **3.59**. Saponification, Yamaguchi macrolactonization, and global deprotection gave the desired aglycone, apoptolidinone A **3.2**.

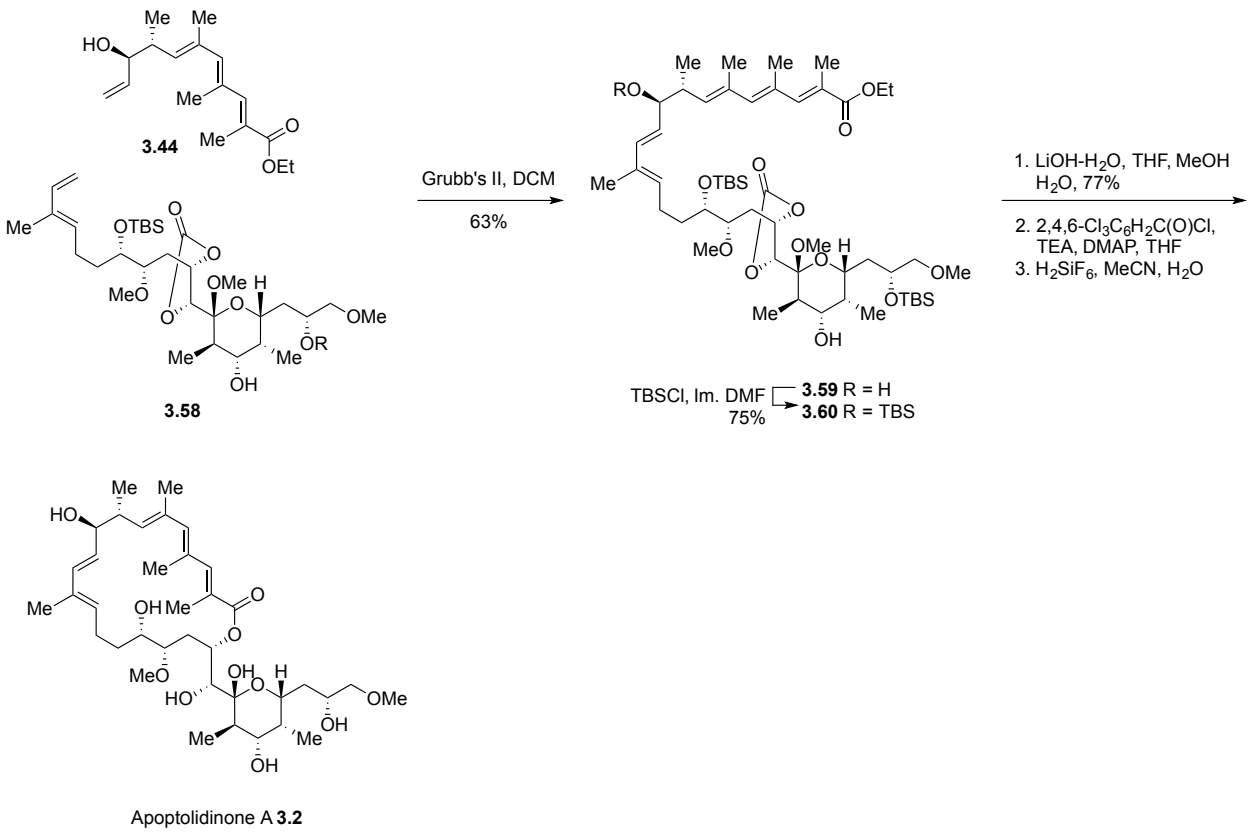

Figure 3.16. Crimmin's completion of apoptolidinone A.

The Nelson group has accomplished the synthesis of apoptolidinone C using four main fragments **3.63**-**3.66** (Fig. 3.17A). Macrolide construction featured a Stille coupling between the northern and southern fragments followed by macrolactonization and global deprotection, similar to the strategy employed by the Koert group. [8] However, unlike the strategies employed by the Koert, Sulikowski, [11] and Crimmins [12] groups, Nelson and coworkers [13] utilized catalytic enantioselective aldol surrogates to construct the polyketide backbone (Fig. 3.17B). Specifically, the Nelson group has developed a catalytic asymmetric acyl halide-aldehyde cyclocondensation (AAC) reaction, which utilize cinchona alkaloid Lewis base complexes **3.67**-**3.68** or aluminum (III) Lewis acid complexes **3.69**.

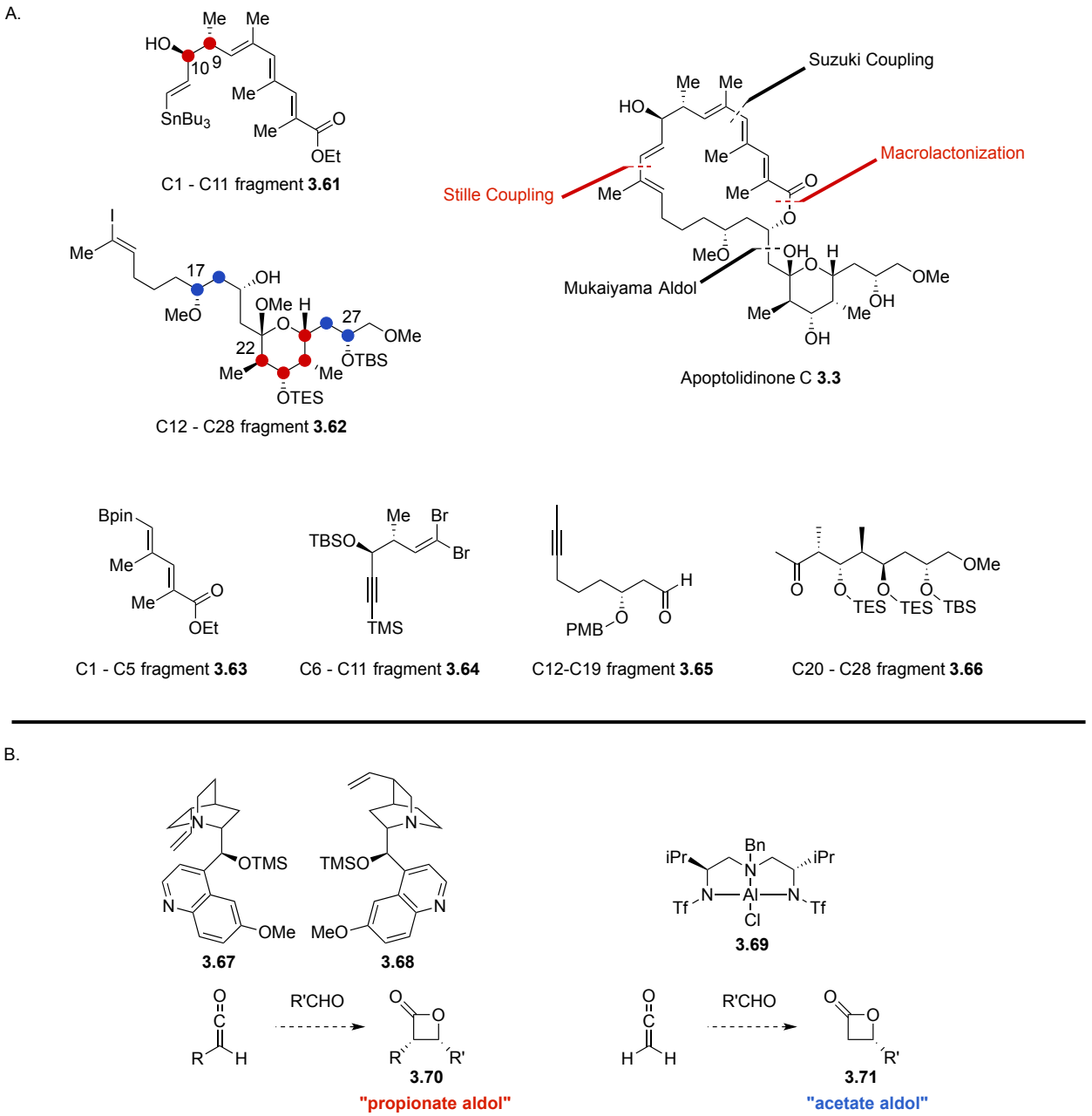

Figure 3.17. Nelson's retrosynthetic analysis of apoptolidinone A.

Mechanistically, the AAC methodology developed by the Nelson group and first reported in 1999, [14] exploits a [2+2] ketene—aldehyde cycloaddition in which the chiral Lewis acid or base can influence the facial selectivity of the approach (Fig. 3.17B). [14-16] The resulting β-lactones can be opened via nucleophillic acyl substitution. Asymmetric acyl

halide-aldehyde cyclocondensation were used to assemble nearly all the stereocenters in the molecule including the upper C8-9 positions, and most of the lower half (Fig. 3.17A, stereocenters set by propionate "aldols" denoted in red and acetate "aldols" denoted in blue). [13]

It is worth noting that of all the reported total syntheses of apoptolidinone A, synthesis of the C11-C19 region has the most variation (Fig. 3.18). The C1-C5 region of apoptolidinone has, for the most part, been reached using a varied order of olefination methods. The C20-C28 region is usually prepared through iterative aldol reactions. No similar process has been developed for the western half of the molecule and represents the last synthetic hurdle towards the efficient production of the aglycone.

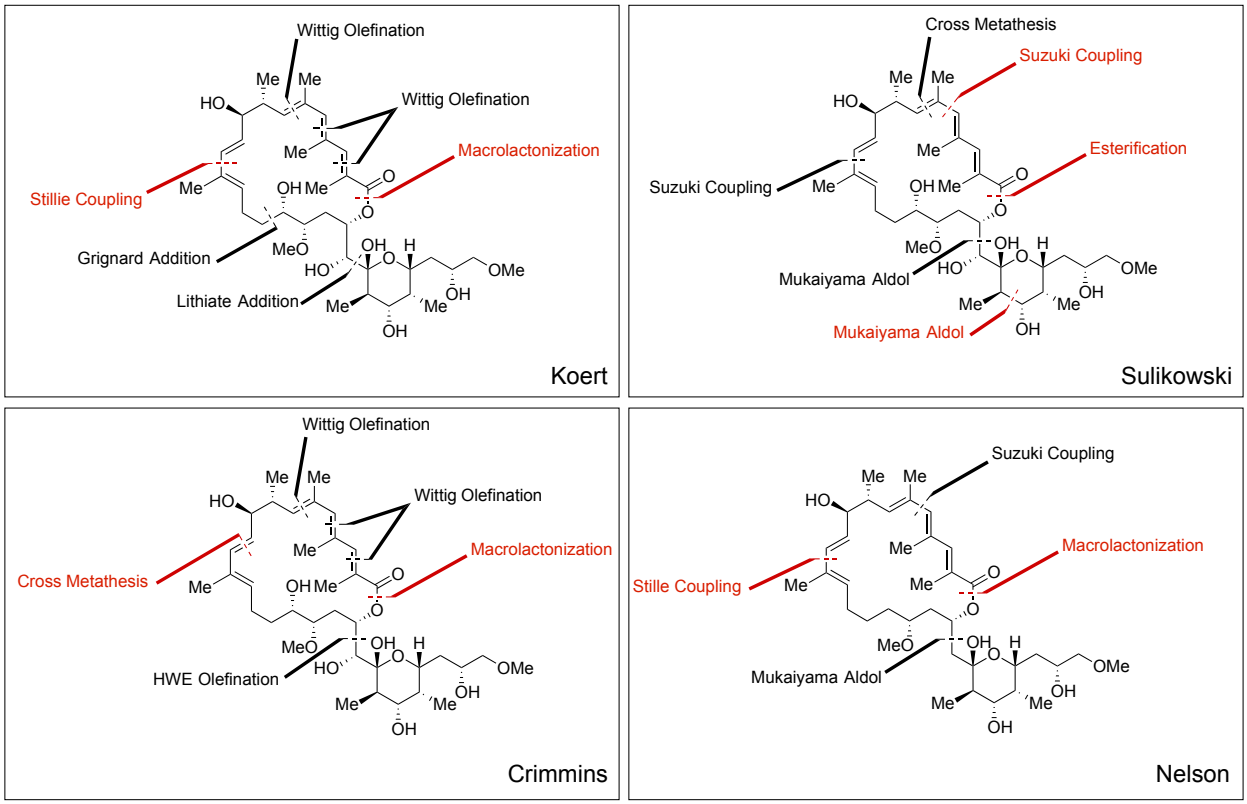

Figure 3.18. Retrosynthetic comparison of completed syntheses of apoptolidinones A and C.

The Nelson group has reported an extremely concise method for synthesizing the two western C6-C10 **3.64** and C11-C19 **3.65** fragments using their catalytic asymmetric aldol methodology via chiral β-lactones **3.70**-**3.71** and chiral catalyst **3.67**-**3.69** (Fig. 3.17A-B), however we sought to create a process toward the western hemisphere of the apoptolidin aglycone that would allow for reliable multi-gram scale synthesis and late stage modifications for future structure-activity relationship (SAR) studies.

3.2 Structure-activity relationship between apoptolidin A and C

Apoptolidin C **3.72** was first isolated by Wender and coworkers [17] from the same producing organism as apoptolidin A **3.1** (*Nocardiopsis sp.* FU40). Apoptolidin C was isolated in less than 5 mg/L as compared to the major metabolite (50-100 mg/L). Apoptolidin A **3.1** and C **3.72** were later isolated by Ismael and coworkers [18] from an *Amycolatopsis sp.* ICBB 8242 (150 mg/L and 2-7 mg/L, respectively). Apoptolidin A **3.1** and C **3.72** differ by two key hydroxyl groups about the center macrolide, yet exhibit reasonably similar bioactivities against H292 human lung cancer cells (Fig. 3.19). [17]

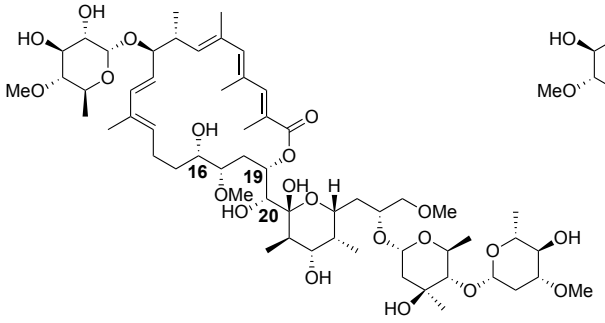

Apoptolidin A **3.1**

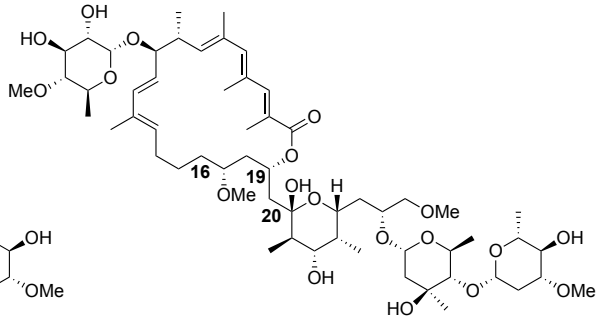

Apoptolidin C **3.72**

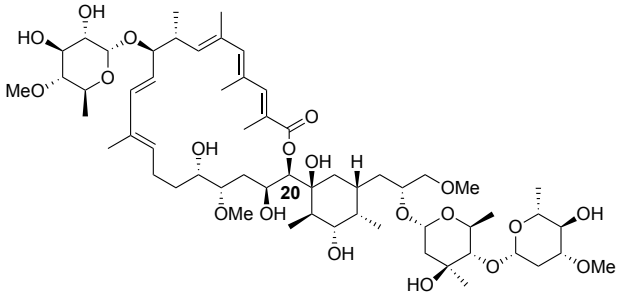

Isoapoptolidin A **3.73**

	GI_{50} (μM) H292	GI_{50} (μM) Ad12-3Y1	GI_{50} (μM) 3Y1	IC_{50} (μM) F_oF_1 ATPase
Apoptolidin A	0.032 ± 0.003	0.0065	> 1.0	0.7
Apoptolidin C	0.024 ± 0.005	-	-	-
Isoapoptolidin A	-	0.009	> 1.0	17

Figure 3.19. Structure-Activity relationship comparisons of apoptolidins.

As compared to apoptolidin A, apoptolidin C does not have a C16- or C20- hydroxyl group. Due to the absence of the C20- alcohol, apoptolidin C is incapable of ring expansion to the isoapoptolidins. It should be noted that apoptolidin A can ring isomerize to isoapoptolidin A and exists in an equilibrium when treating cells for more than 20 minutes of time (less than 12% conversion in 20 minutes, ambient temperature). [19-20] Additionally, the bioactivity of isoapoptolidin A (IC_{50} = 17 μM, F_oF_1-ATPase assay) is somewhat lower than apoptolidin A (IC_{50} = 0.7 μM, F_oF_1-ATPase assay). [19] The removal of the C20- hydroxyl group prevents this ring expansion in apoptolidin C, having apoptolidin exist in its most potent 20-membered macrolide form. The additional removal of the C16- hydroxyl group in apoptolidin C was thought to reduce the overall stereocomplexity of the molecule for ease of synthesis. Thus, apoptolidinone C was chosen as the target for total synthesis.

Overall the synthetic target described herein, apoptolidinone C **3.3**, contains a 20 membered macrocycle, 10 stereocenters, 5 sites of unsaturation, a densely substituted hemiketal ring. Apoptolidin C **3.72** exhibits similar bioactivity to major metabolite apoptolidin A **3.1**, [19] yet increased overall stability and reduced stereocomplexity, making it the ideal target for total synthesis and subsequent precursor directed biosynthetic studies.

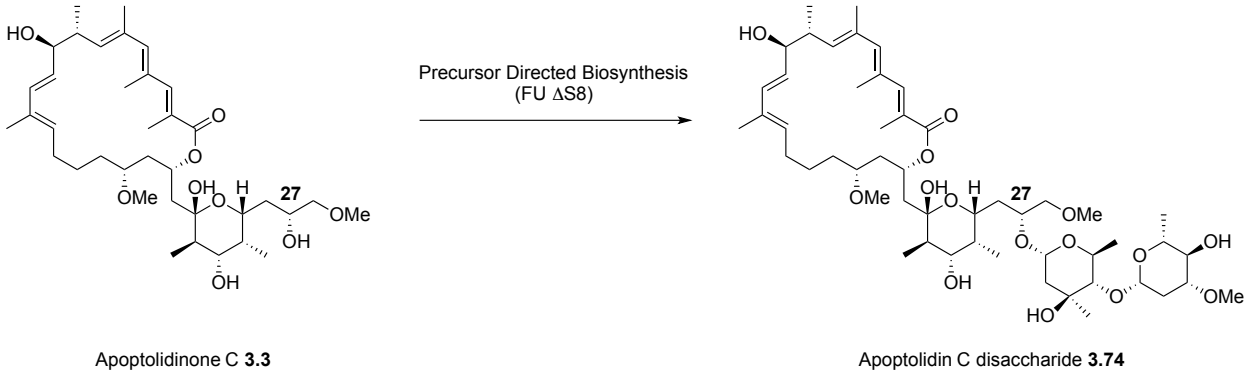

Figure 3.20. Selective C27-glycosylation via precursor directed biosynthesis of apoptolidin C.

3.3 Retrosynthetic analysis of apoptolidinone C

While apoptolidinone C **3.3** was synthesized by the Nelson group in 2010, [13] our goal was to create an efficient, reliable, and scalable process toward the synthesis of apoptolidinone C **3.3**. The proposed precursor directed biosynthetic studies followed by molecular probe synthesis necessitates production of large amounts of apoptolidinone C **3.3**. In order to synthesize such a large quantity of the aglycone through total synthesis, a highly convergent route was explored, utilizing four main fragments **3.75**-**3.78**, and four main disconnections including: Mukaiyama aldol, Suzuki or Stille cross coupling, and Yamaguchi esterification or macrolactonization (Fig. 3.21). Subsequent global deprotection

would concomitantly form the fully substituted hemi-ketal ring to give apoptolidinone C **3.3**.

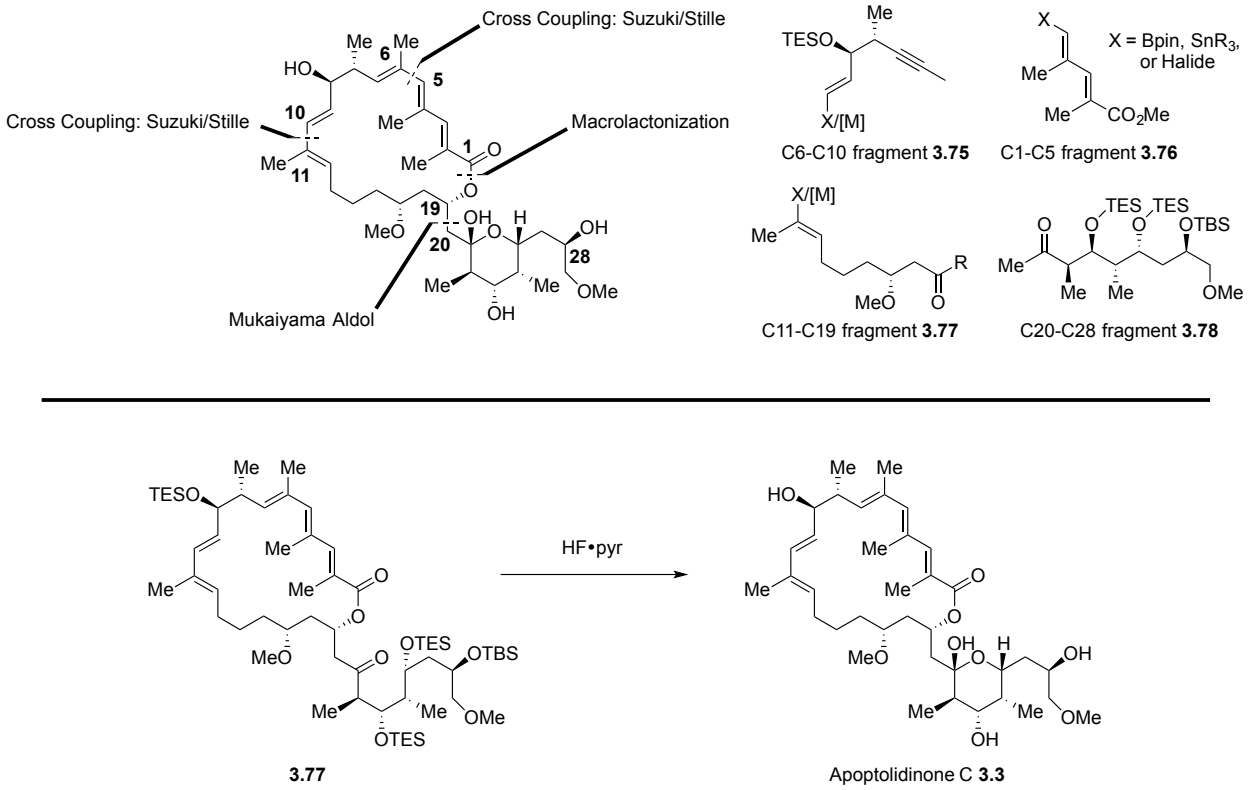

Figure 3.21. First generation retrosynthetic analysis of apoptolidinone C.

Northeastern C1-C5 fragment **3.76** was first reported by Sulikowski and coworkers en route to apoptolidinone A in 2005, [21] and has been used by the Nelson group toward the total synthesis of apoptolidinone C. [13] Other groups [2-9, 12] have opted for iterative Wittig olefination, but the route described by Sulikowski and coworkers [21] was chosen to increase overall synthetic efficiency and convergence. Southeastern C20-C27 fragment **3.78** was first reported by Koert and coworkers in 2001 [8] en route to apoptolidinone A **3.2**, and later used by Nelson and coworkers [13] in their synthesis toward apoptolidinone C **3.3**, representing a second reliable and reproducible route toward a fragment of the apoptolidin macrolide.

3.4 First generation approach toward apoptolidinone C

At the outset, we hoped to generate the C6-C19 framework (depicted in red, Fig. 3.22) through either a Suzuki or Stille coupling to join the C11- and C12- carbons of the macrolide. The northwestern C6-C10 fragment **3.75** could be synthesized in a manner much like our previously published synthesis via crotylation or aldol reaction, [10-11] followed by oxidation-reduction elaboration, homologation, and methylation. However, the C12-C19 fragment **3.77** (Fig. 3.22) proved more difficult to produce, with the largest synthetic hurdle of achieving high stereocontrol of a single stereocenter (C17) with few handles to induce this asymmetry in the fragment, all in highly reproducible yield.

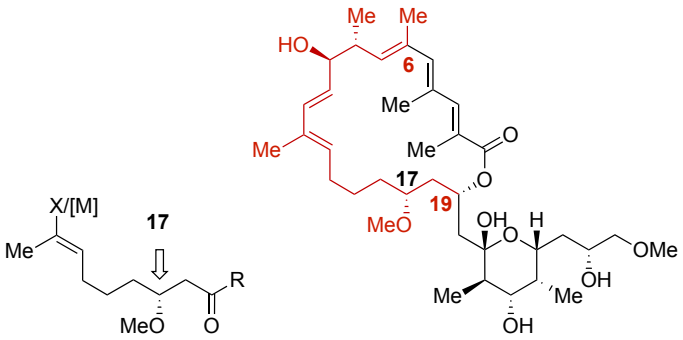

Figure 3.22. Target region of apoptolidinone C for improved synthetic process.

To direct the stereochemistry of the C17 hydroxyl, we set out to complete an acetate aldol between aldehydes **3.78** or **3.81** and either enol silyl ether **3.79** or auxillary **3.82**, under Mukaiyama-Keck [23] or Nagao aldol conditions. [24-25]

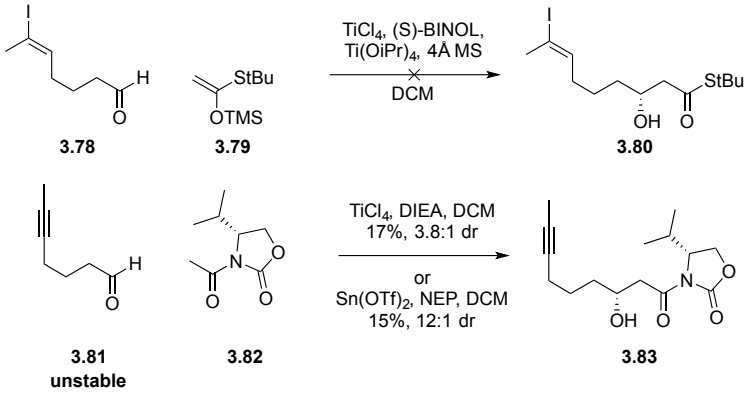

Figure 3.23. Stereoselective acetate aldols to synthesize the C11-C19 fragment of apoptolidinone C.

After much screening, it was determined that the aldol adduct could not be reliably produced and in good yield (table 3.1). This was in part due to the instability of aldehyde **3.81** to purification via column chromatography or distillation. This instability is most likely due to self-condensation and cyclization. Reports by the King and Montgomery groups have shown this type of cyclization is possible under acidic and/or lewis acidic conditions via formal [2+2]—retro [2+2] or 5-exo dig ring cyclizaiton. [25-26] Crude solutions of aldehyde **3.81** were, however, used to successfully obtain the desired aldol adduct, albeit in disappointingly low yield.

Table 3.1. Attempts to optimize Nagao acetate aldol to synthesize C11-19 fragment **3.77**.

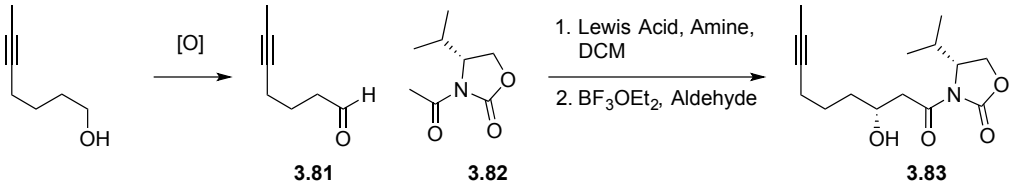

Oxidation	Lewis Acid	Amine	% Yield
TPAP, NMO	$TiCl_4$	DIEA	24
PCC	$TiCl_4$	DIEA	26
SO_3.pyr	$TiCl_4$	DIEA	10
DMP, $NaHCO_3$	$TiCl_4$	DIEA	-
TPAP, NMO	$SnOTf_2$	NEP	19

Investigations into setting the C17- alcohol stereochemistry were then pursued via epoxide opening of **3.86** with 1,3-dithiane (Fig. 3.24). Lithiation of 1,3-dithianes allow for umpolong formation of acyl anion like synthons for an atypical disconnection. Unlike the aldol reaction, the carbonyl carbon becomes the nucleophile. Furthermore, rather than utilize enolate nucleophiles, the enolate becomes the electrophile in the form of an epoxide. By employing epoxide intermediate **3.86**, the C17- hydroxyl could instead be set using an organo-catalyzed asymmetric α-chlorination of aldehyde **3.90**.

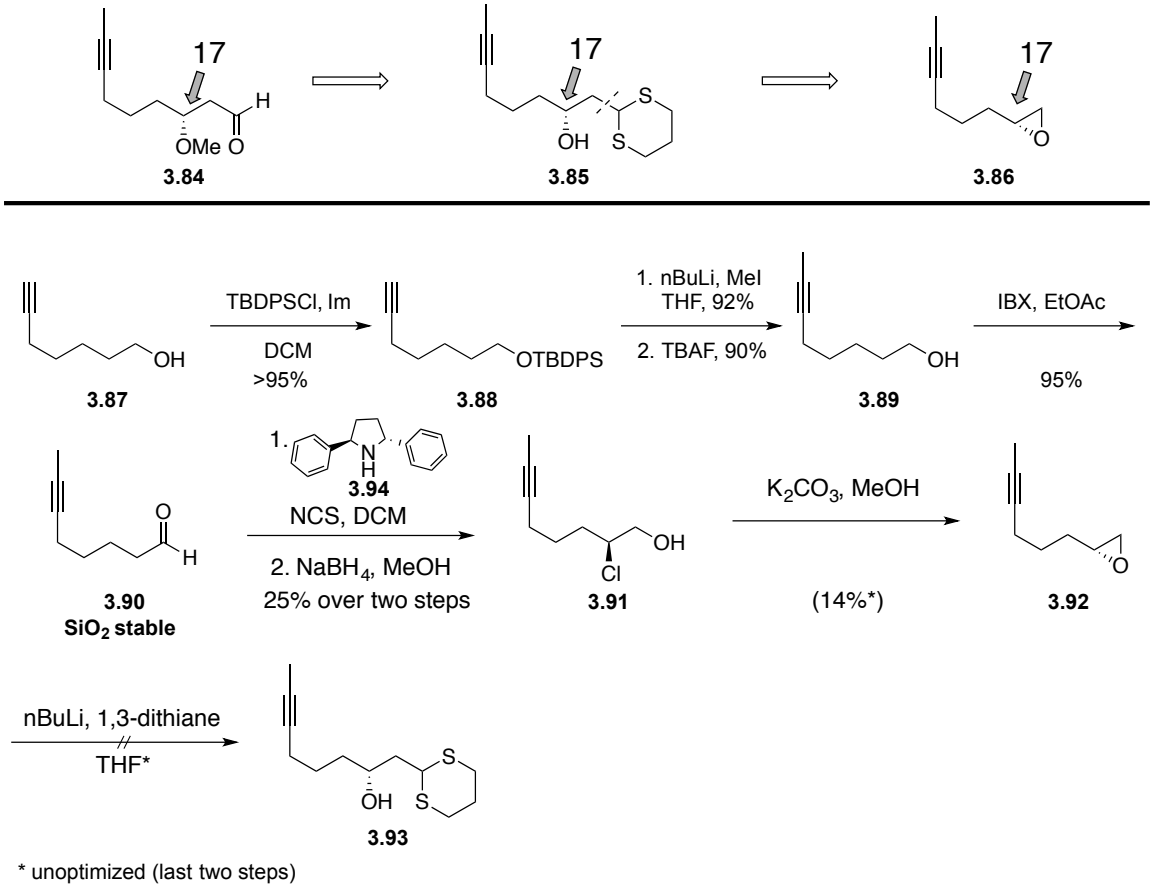

Figure 3.24. Synthesis of C11-C19 fragment via α-chlorination with C2-symmetric pyrrolidine catalyst.

Gratifyingly, unlike aldehyde **3.81** needed for acetate aldol, aldehyde **3.90**, homologated by one carbon, proved to be more stable to silica gel purification. Once in

hand, α-chlorination with C2- symmetric pyrrolidine catalyst **3.94**, developed and used by MacMillan, Jørgensen, and Lindsley groups [27-29] provided an α-chloroaldehyde that could be reduced with sodium borohydride to give the desired halohydrin **3.91**, all in one pot. However, monitoring the reaction by nuclear magnetic resonance (NMR) showed a significant amount of competing dichlorination (Fig. 3.25), despite efforts to minimize the rate of dichlorination via changes in reaction time, temperature, and concentrations. Talks with the Lindsley group at Vanderbilt University, revealed this reaction to be highly substrate dependent, giving sometimes dichlorination over monochlorination.

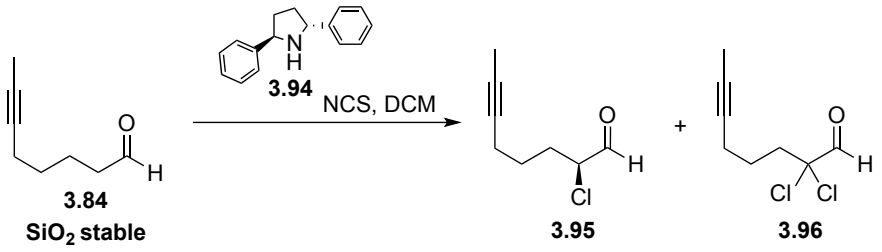

Figure 3.25. α-Chlorination of aldehyde **3.90** gives both mono- and di- chlorinated products.

While this proved to be an inefficient route toward the C12-C19 fragment **3.84**, in order to explore this α-chlorination, large quantities of (2S,5S)-2,5-diphenylpyrrolidine were required. En route to synthesizing the diphenylpyrrolidine **3.94**, a more efficient and facile means of purifying a key intermediate was discovered (Fig. 3.26). [30]

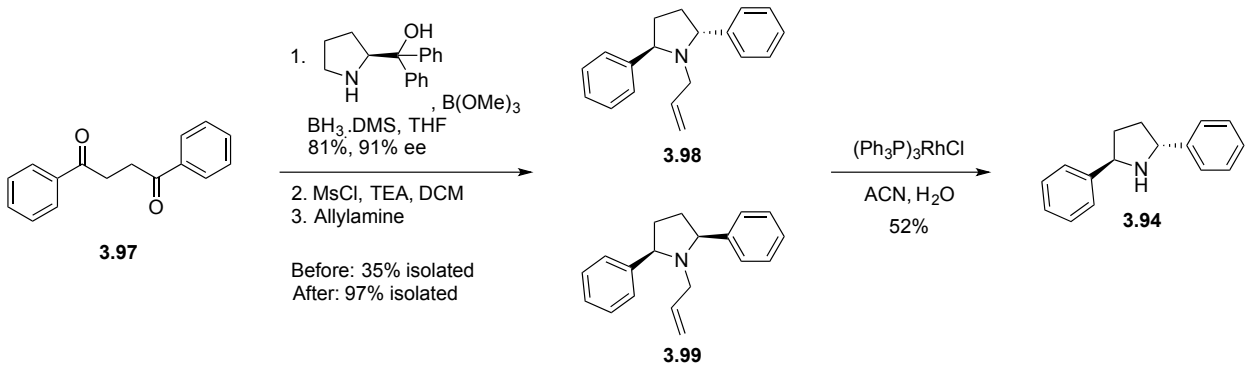

Figure 3.26. Synthetic process toward C2-symmetric catalyst **3.94**.

Previously, separation via column chromatography of diphenyl intermediate **3.98** from the achiral meso byproduct **3.99** required multiple columns using an ethyl acetate/ hexanes solvent system or careful recrystallization in hexanes utilizing a cold room. Discovery of a different solvent system employing toluene (Tol) and hexanes (Hex), 10% Tol/Hex, could be used to achieve complete separation between the desired C2-symmetric catalyst **3.98** and the undesired achiral meso byproduct **3.99**. With this solvent system, the undesired meso byproduct **3.99** has an Rf = 1, while the desired C2- symmetric **3.98**, an Rf = 0. The desired product XX could then be flushed from the column using a mixture of diethyl ether (Et_2O) and hexanes, 30% Et_2O/Hex.

Though the synthesis of the C2-symmetric diphenyl pyrrolidine **3.94** was achieved, due to the large amount of competing dichlorination, an alternative disconnection was made. By migrating the key bond disconnection, we instead sought to utilize a nucleophillic opening of epoxide **3.102** using various lower order cuprates, lower order mixed cuprates, and higher order cuprates (Fig. 3.27).

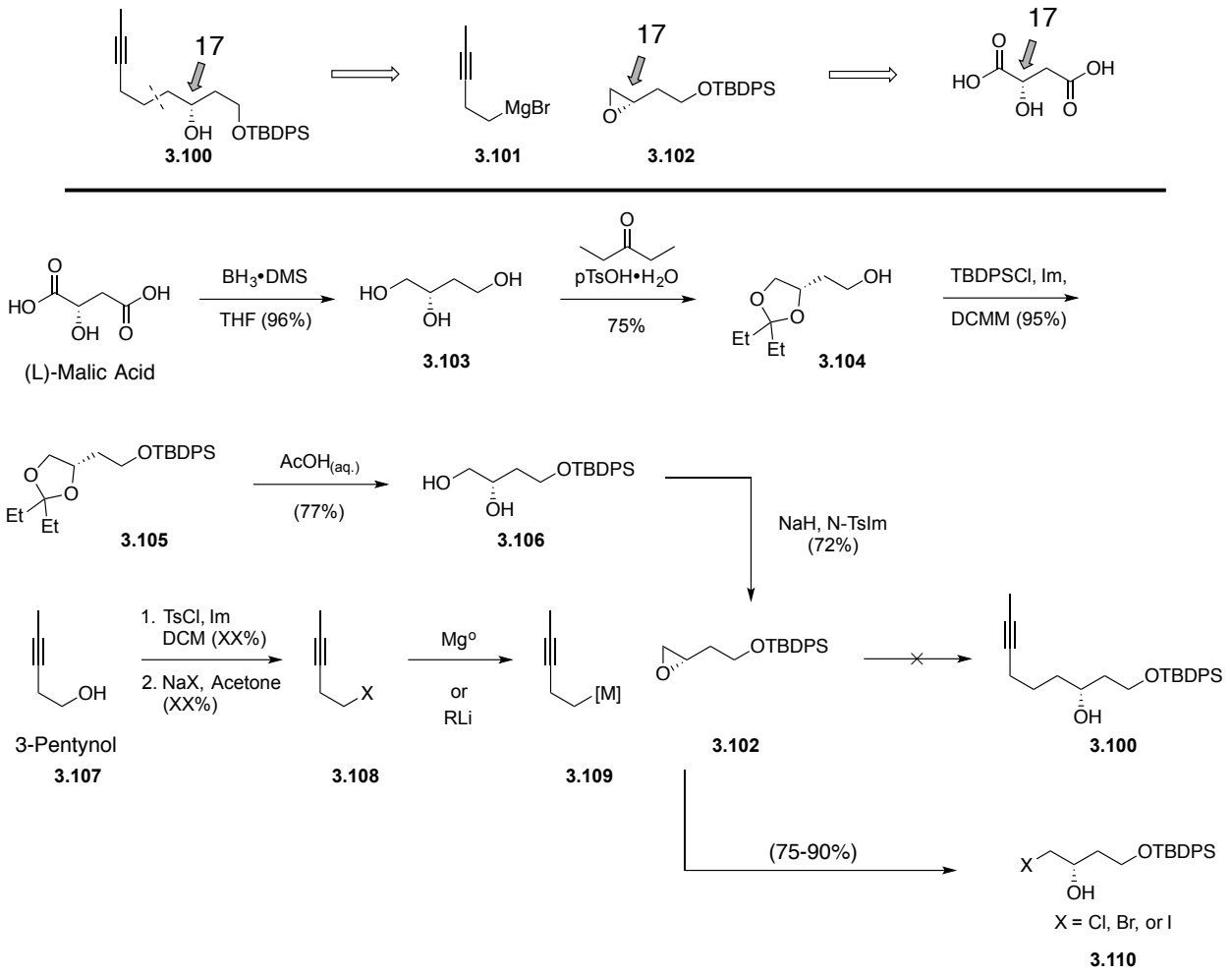

Figure 3.27. Synthesis of C12-C29 fragment via cuprate opening of epoxide **3.102**.

Epoxide **3.102** was synthesized in five steps from (L)-malic acid (Fig. 3.27). (L)-Malic acid was reduced with borane-dimethyl sulfide to the triol **3.103**, selectively protected with 3-pentanone to the five-membered diethyl ketal, and silyl protected to give **3.105**. The diethyl ketal was removed under acidic conditions and the resulting diol **3.106** was treated with sodium hydride and tosyl-imidazole to give the desired epoxide **3.102**, under Forsyth conditions, all in good yield. The necessary alkynyl halide **3.108** to construct the desired cuprate was fashioned from 3-pentynol in two steps through tosyl activation followed by Finkelstein.

With all the necessary components for epoxide opening in hand, several different conditions were screened (table 3.2). However all attempts to synthesize the C12-C19 framework via this route, proved unfruitful. Instead, lower order cuprates and mixed cuprates gave the undesired halohydrin **3.110**, whereas higher order cuprates resulted in decomposition or recovery of starting material. Attempts to resubmit the halohydrin **3.110** with an additional equivalent of cuprate resulted in almost complete recovery of starting halohydrin **3.110**. In order to move away from using alkynes in the presence of a cuprate, cyclic acetal (table 3.2, entry 3) was used, and disappointingly returned the same halohydrin **3.110**. However, upon exposure to 12 equivalents of vinyl magnesium bromide and copper (I) iodide did return the desired secondary alcohol was produced (table 3.2, entry 5). While successful, this route was abandoned due to its inefficient atom economy.

Table 3.2. Attempts to elaborate epoxide **3.102** using cuprates.

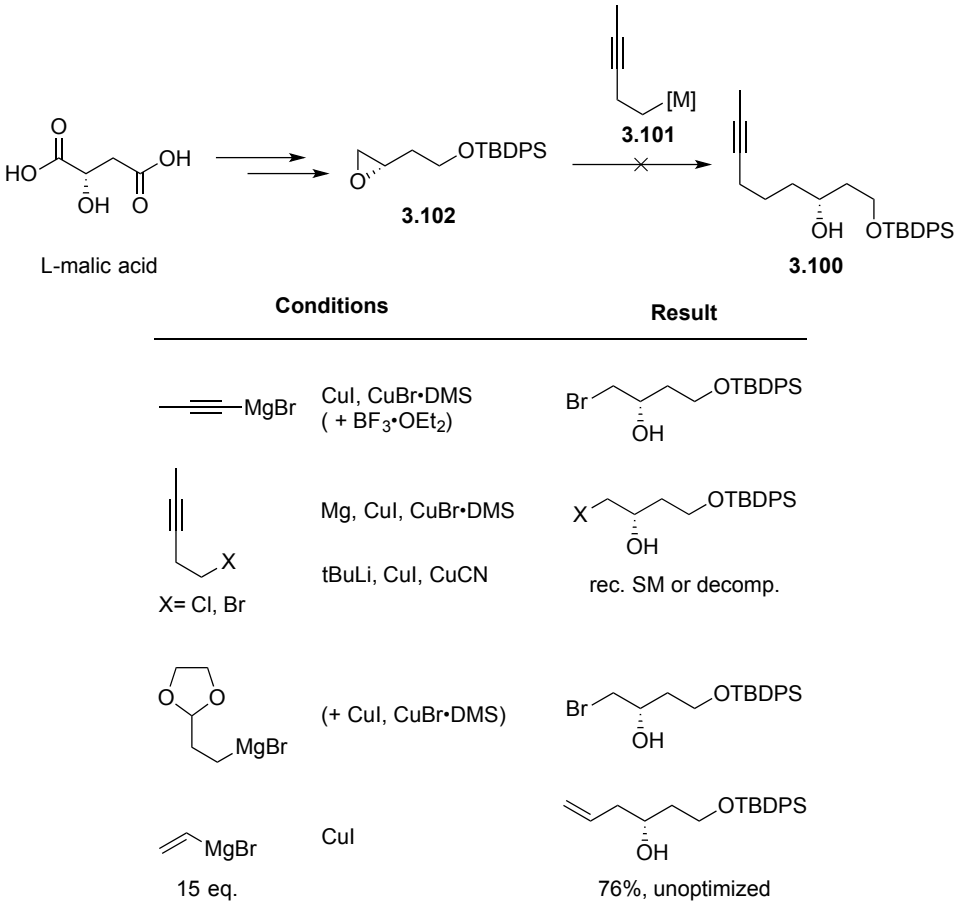

Due to the inability to successfully open epoxide **3.102** in an efficient manner, epoxide **3.102** was shortened by one carbon to give aldehyde **3.111**. The thought process being, that utilizing a route that was similar to the one previously developed for epoxide **3.102**, the more electrophilic aldehyde **3.111** could be synthesized. Aldehyde **3.111** was synthesized in three steps from (L)-malic acid. (L)-Malic acid was reduced to the triol using borane-dimethyl sulfide in > 95% yield. The resulting triol was selectively protected to the five-membered ketal using 3-pentanone and oxidized to give the desired aldehyde **3.116**, all in good yield. Alkynyl bromide **3.115** was acquired through tetrahydropyran (THP) acetal formation of 3-pentynol, followed by methylation, deprotection, mesylation, and

Finkelstein with lithium bromide to give the desired bromide in 70% over all yield. Additionally, all five steps could be conducted by without flash chromatography or additional purification to produce 6-bromohex-2-yne **3.115** in consistent 66% yield over 5 steps, increasing the overall efficiency of the synthetic route.

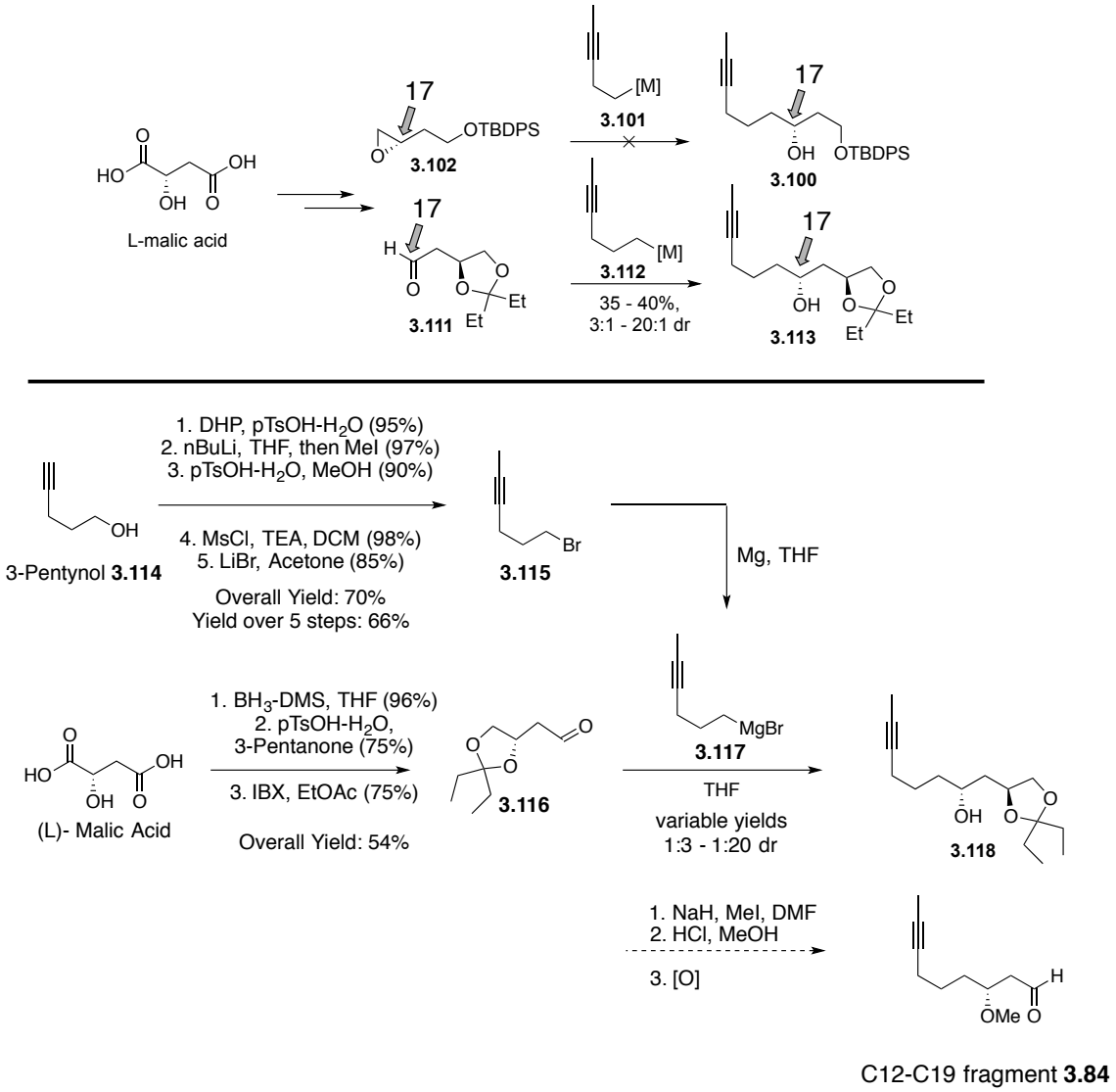

Figure 3.28. Synthesis of C12-C19 fragment via asymmetric induction.

Asymmetric induction from the β-chiral center would infer asymmetry in a nucleophilic opening of the aldehyde via 1,3-chelation control (Fig. 3.29), giving the desired

product. This however, proved to give variable diastereoselectivity (20:1 – 3:1). While asymmetric induction of β-substituted carbonyl compounds has been shown to give great diastereoselectivity (5:1 – 4:1) with β-substituted ketones, [32-33] the variability observed with aldehyde **3.116**, may be substrate dependent. Typically asymmetric induction is obtained with α-substituted aldehydes, through a Cram-chelate-like or Felk-Ahn model rather than a Zimmerman-Traxler-like transition state (Fig. 3.29). [33] Additionally, α-substitution would lower the acidity of the α-hydrogens when using Grignard reagents in the nucleophillic opening.

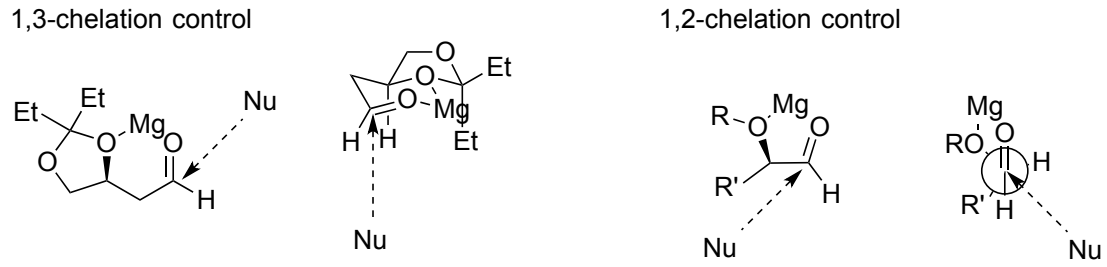

Figure 3.29. Asymmetric induction via 1,3- or 1,2- chelation controlled addition to aldehydes.

Having explored several means of organocatalysis to set the C17 chiral center and utilizing the chiral pool, a more reliable method of inducing asymmetry was pursued. Using inspiration from process chemistry, [34] a route using a Noyori reduction of a β-keto ester was settled upon. In order to reach the desired β-keto ester framework, two routes were simultaneously explored (Fig. 3.30).

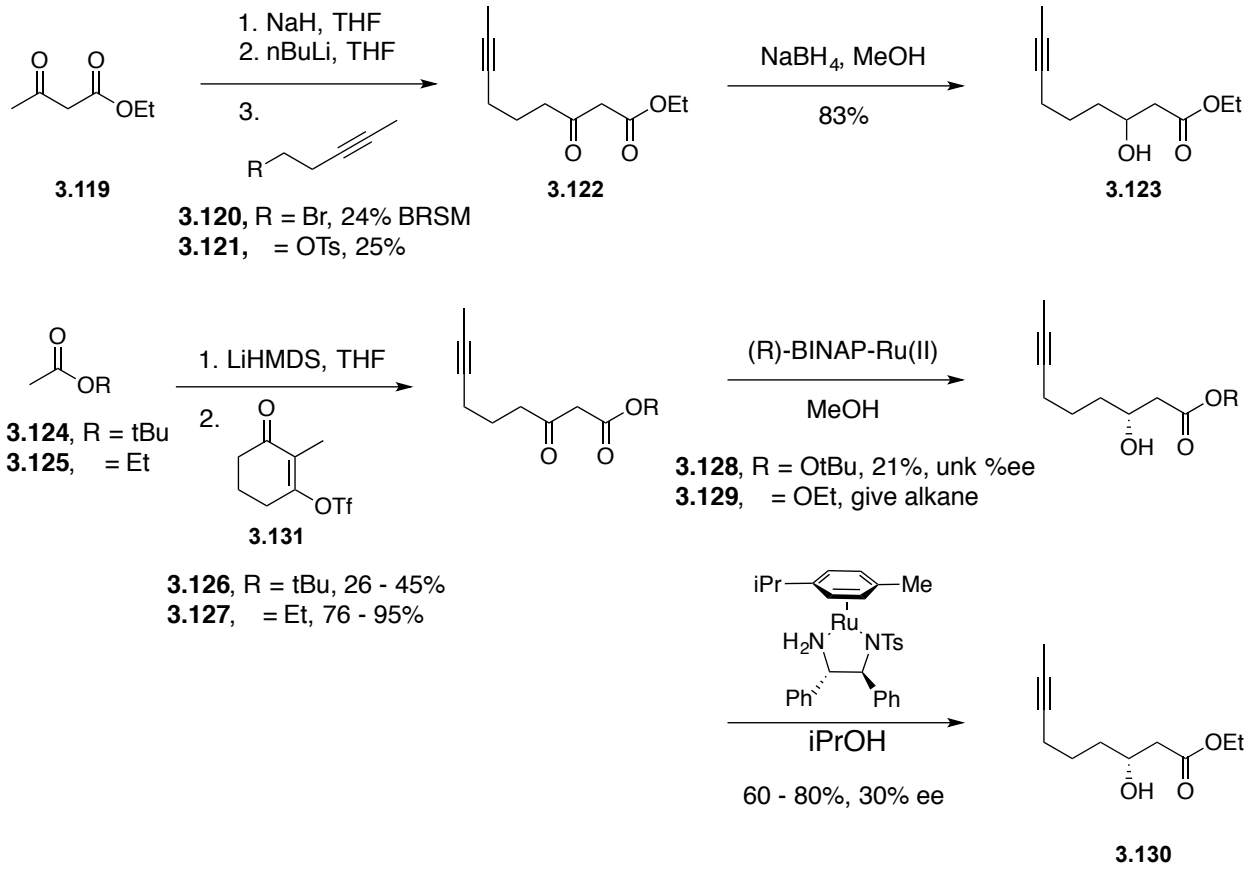

Figure 3.30. Synthesis of C12-C19 fragment via Grobb fragmentation.

Formation of the dianion from **3.119** [35] and alkylation with alkynyl bromide **3.120** (synthesized previously, Fig. 3.28), β-keto ester **3.122** could be obtained in low to modest yield (24-25%). Alternatively, Claisen or Grobb-like fragmentation using vinylogous triflate **3.131** and esters **3.126** or **3.127** could be used to reach the same β-keto esters **3.128** and **3.129**. Subsequent Noyori reduction, however, gave the β-hydroxy t-butyl ester **3.128** in about 21% yield and none of the desired β-hydroxy ethyl ester **3.130**. Presumably, this is due to competing reduction of the alkyne. Substituting the traditional Noyori asymmetric reduction for hydrogen transfer conditions with isopropanol gave the desired β-hydroxy ethyl ester **3.129** in good yield (60-80%), but unfortunately low enantioselectivity (30% ee). The low enantioselectivity observed in this reaction may be due to unfavorable

interactions between the catalyst and alkynyl moiety, as this catalyst has been known to coordinate with ynones to induce selectivity in the reduction. [36]

3.5 Apoptolidinone model system for western C6-C19 fragment

While simultaneously working on the synthesis of the C6-C10 northwestern portion of the aglycone, a model system was developed to explore the C10-C11 bond connection to bring together the western hemisphere of apoptolidinone C (Fig. 3.31). These studies completed in unpublished work by Robert Davis in the Sulikowski group, showed that Stille conditions, even when the vinyl stannane (**3.133**, **3.136**) and vinyl iodide (**3.134**, **3.137**) were reversed, could not yield the desired western framework. However, Suzuki coupling between vinyl boronate ester **3.139** and vinyl iodide **3.140** gave the desired model system skeleton, albeit in modest yield (51%).

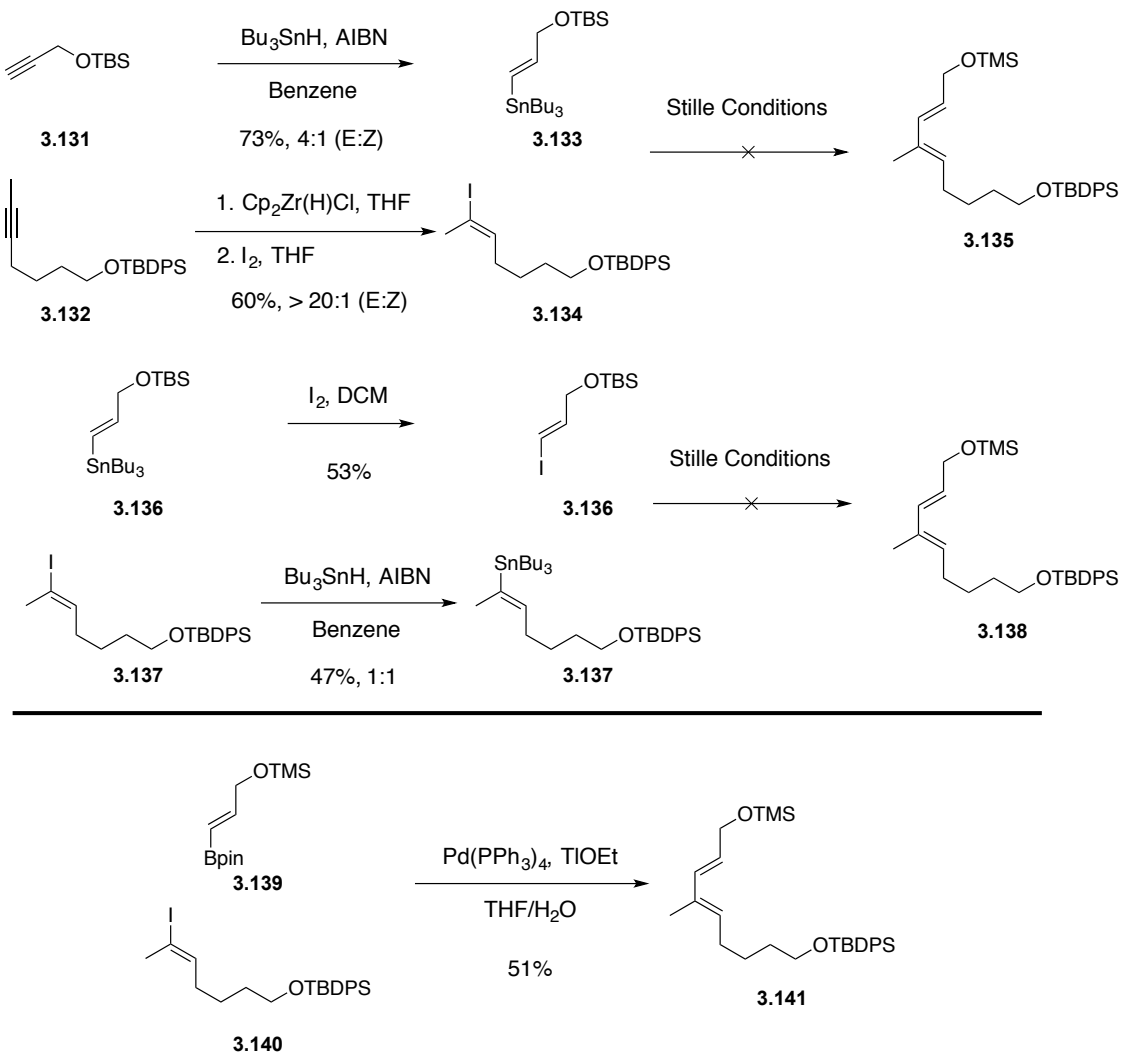

Figure 3.31. Davis' model system studies toward exploration of the C10-C11 bond connection.

In light of these findings, racemic β-hydroxy esters were *O*-methylated to give **3.143** and **3.147**, and the resulting framework was used as a model system to study methods of regioselective hydrometallation (Fig. 3.32). With little differentiation along the internal alkyne, poor selectivity was witnessed under hydrostannylation conditions. Efforts to form the vinyl iodide via hydrozirconation-iodination surprisingly gave the proto-demetallation alkene by-product **3.148** in >95% yield. This result was surprising. However, while lower in yield, ethyl ester **3.146** under the same conditions returned the same proto-

demetallation product. Reduction of ethyl ester **3.143** to the alcohol, followed by triethylsilyl (TES) protection to give silyl ether **3.149**, gave the desired vinyl iodide under hydrozirconation iodination conditions. While low in yield, optimization of the reaction was not pursued as this route would require the excessive use of redox manipulations.

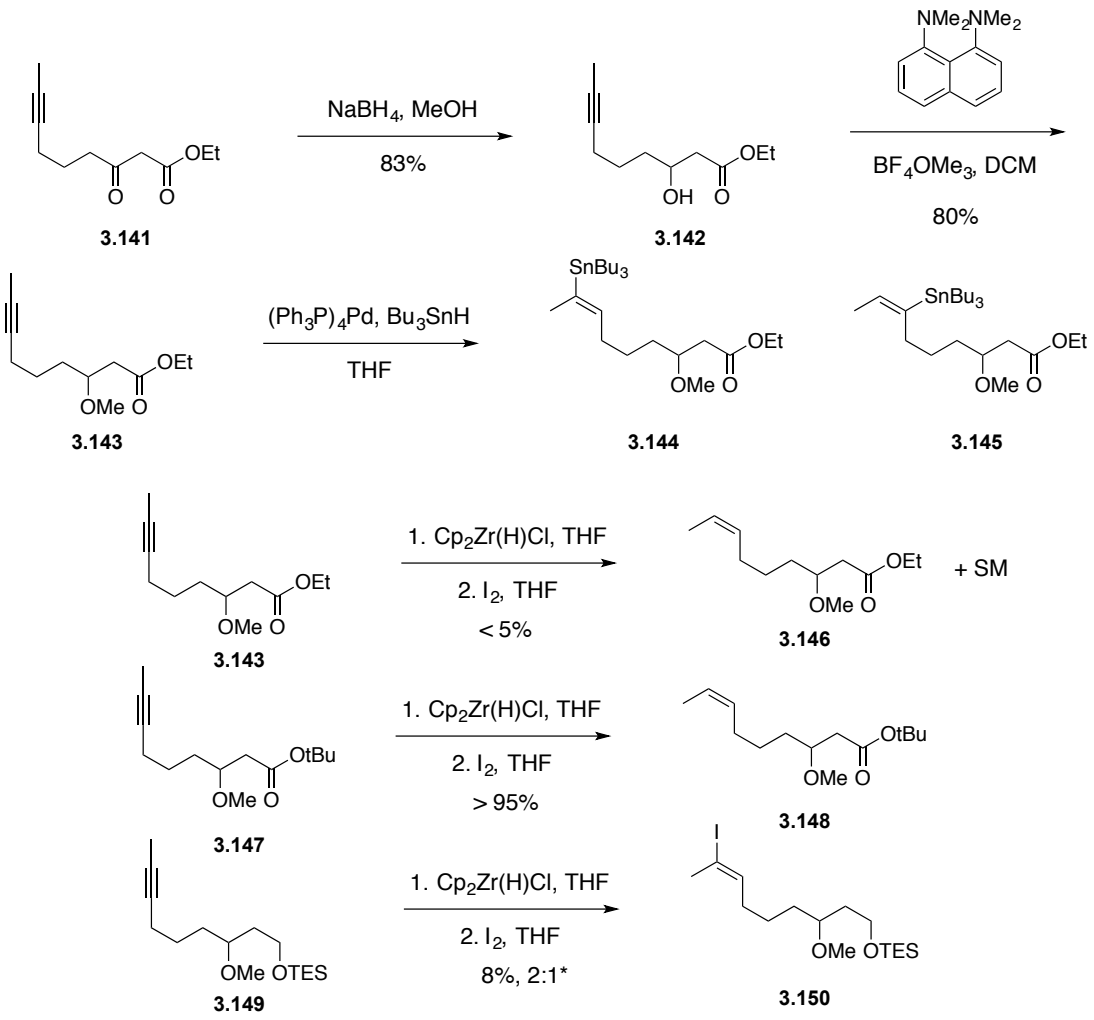

Figure 3.32. Model system hydrometallation of internal alkynes.

Lastly, unpublished work performed by Robert Davis of the Sulikowski group also showed great difficulty in synthesizing the necessary vinyl boronate coupling partner of the C6-C10 fragment, with the highest yielding steps of the process ranging between 39-66%. Additionally, the key aldol to set the C8- and C9- stereocenters gave 39% and 19:1 dr.

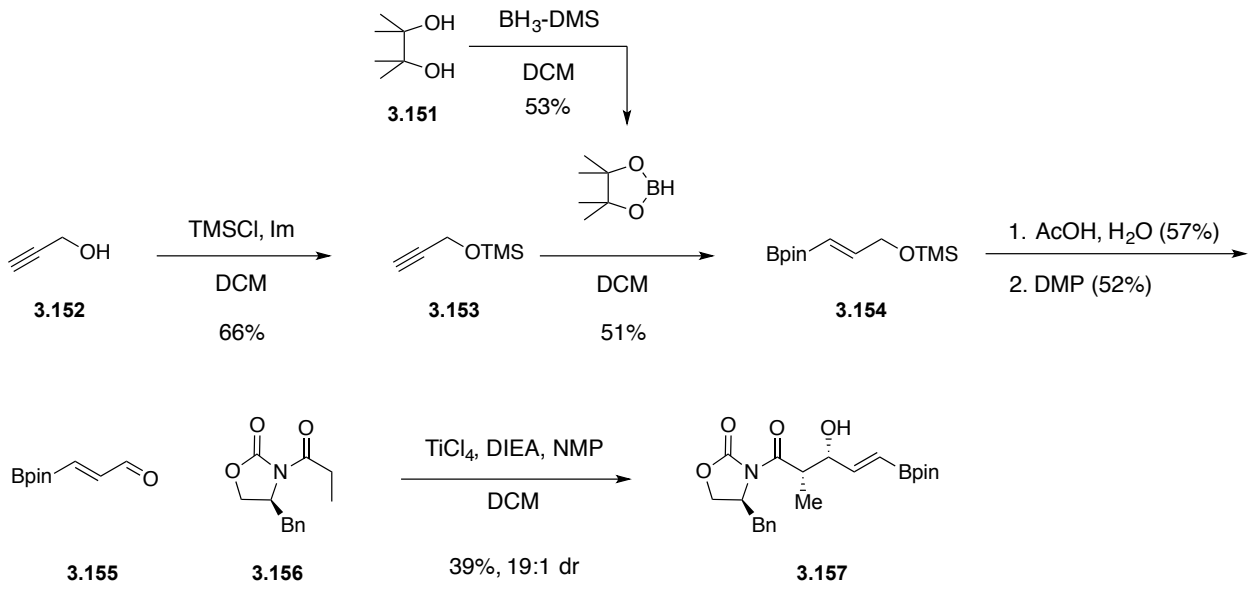

Figure 3.33. Davis' synthesis of the C6-C10 fragment.

3.6 Second generation approach toward apoptolidinone C

Our second-generational approach focused on the forming the bond between the C10- and C11- carbons of the western half, for either cross metathesis or ring closing metathesis (RCM) mediated completion of the macrolide (Fig. 3.34). The use of a cross metathesis to bring together western halves C6-C10 **3.75** and C11-C19 **3.158** would also allow for a Mukaiyama aldol reaction to incorporate C20-C28 fragment **3.78** and Yamaguchi esterification to join the last C1-C5 fragment **3.76**. A one-pot hydrostannylation-Stille coupling, developed in unpublished work by Dr. Steven Chau of the Sulikowski group, [37] could then furnish the resulting macrolide **3.162**. Global deprotection would comprehensively remove the silyl ethers and concomitant ring cyclization to the hemi-ketal ring provides the desired macrolide **3.3**.

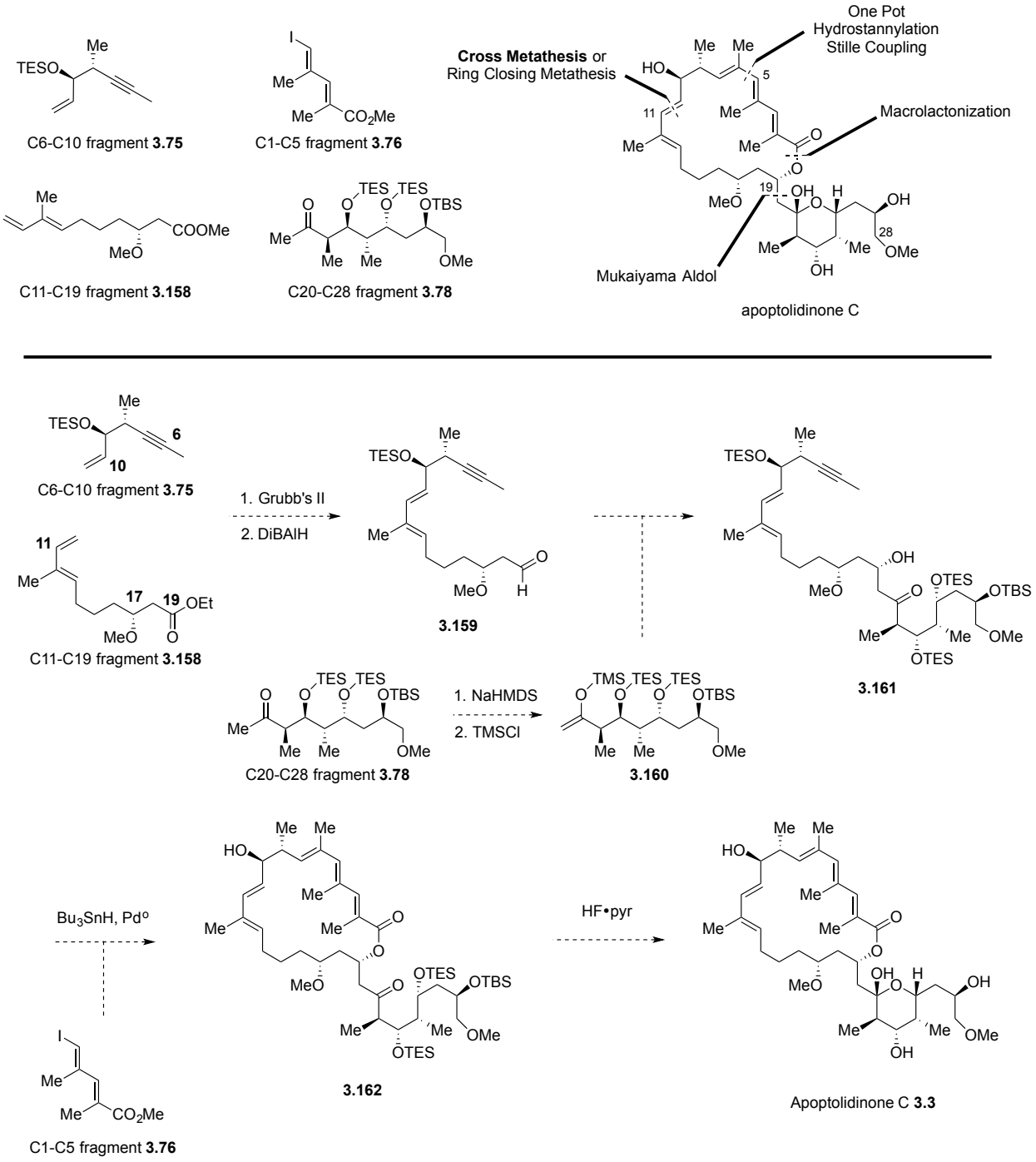

Figure 3.34. Second generation retrosynthetic analysis of apoptolidinone C.

Diene **3.158** could be obtained in 5-7 steps from δ-valerolatone **3.163** (Fig. 3.35). Ring opening to the Weinreb amide **3.165** could be oxidized and homologated to the diene framework **3.166** or t-butyldimethylsilyl (TBS) protected to give **3.167**. Silyl protected

Weinreb amide **3.167** treated with the lithiate of ethoxyacetylene produced alkynone **3.168**. However unexpected hydration during the purification process gave a variable amount of β-keto ester **3.169**.

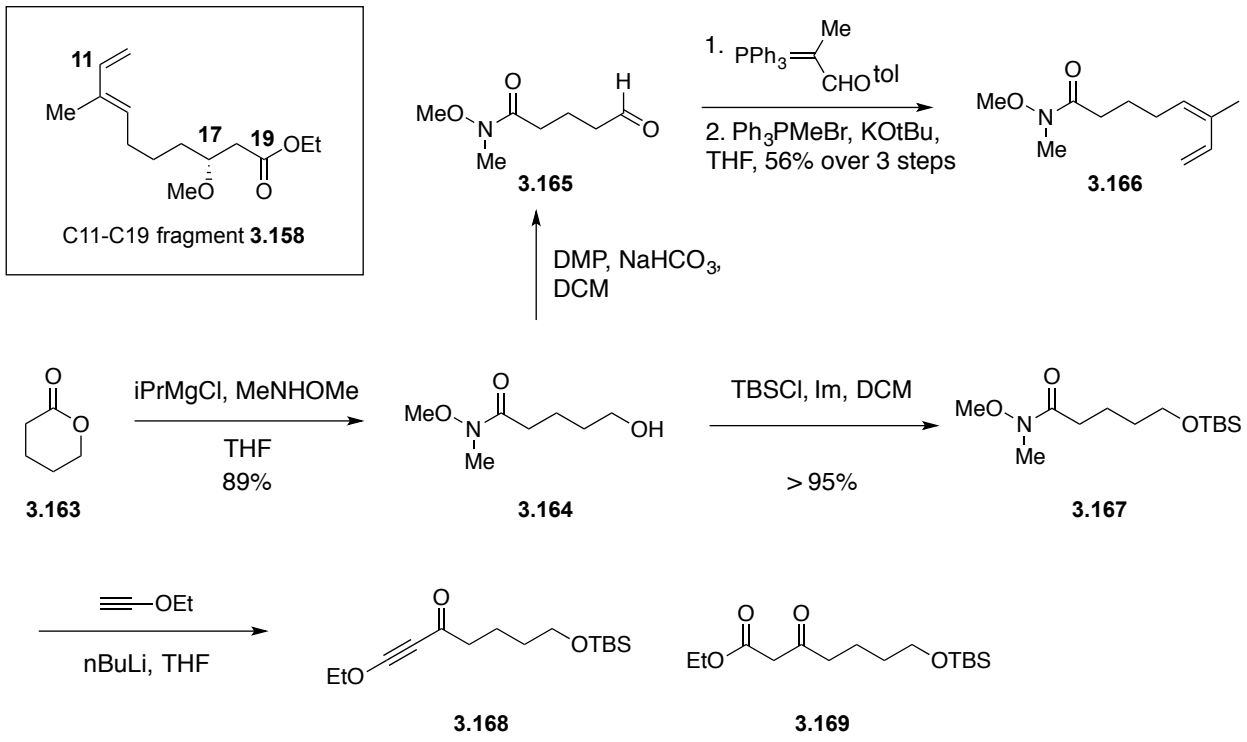

Figure 3.35. Synthesis of C11-C19 fragment via Noyori asymmetric reduction.

To avoid the variable hydration of alkynone **3.168** during pufication, we sought to develop a route that utilized β-keto ester **3.169** as a key intermediate. Instead of using Noyori hydrogen transfer conditions on ynone **3.168**, typical Noyori hydrogenation could be used to establish asymmetry of the C17 hydroxyl from β-keto ester **3.171** (Fig. 3.36). Claisen condensation between δ-valerolatone **3.136** and ethyl acetate gave a mixture of cyclic and acyclic products **3.170**-**3.171** in ca. 2:1 ratio and good yield (88 - 95%). Noyori hydrogenation of the mixture cleanly gave the desired β-hydroxy ester **3.172**, in 92 – 96% yield. Monoprotection with t-butyldiphenylsilyl chloride (TBDPSCl) gave the desired β-

hydroxy ester **3.173**, which could be analyzed for enantiopurity (>99% ee). *O*-methylation, deprotection, oxidation, and double wittig homologation gave the final desired diene, all in excellent yield and reasonably large scale.

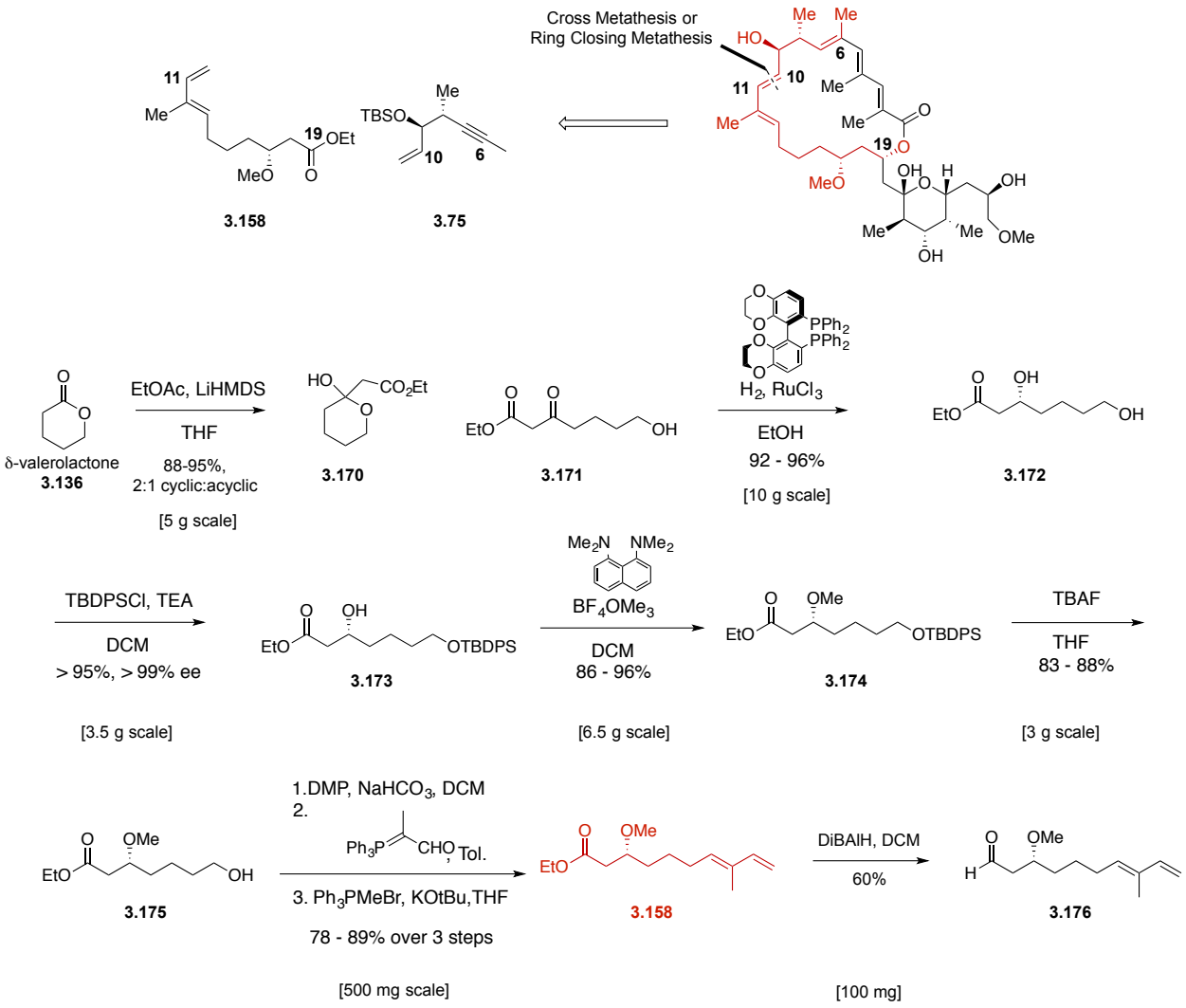

Figure 3.36. Final synthetic process toward C11-C19 western fragment of apoptolidinone C.

3.7 Exploration of cross metatheses to complete western hemisphere of apoptolidinone C

Investigations into the possible cross metatheses between the western hemispheres utilized diene **3.158** and several variations of alkene **3.75**, **3.177**-**3.182** (Table 3.3). While initially promising, these experiments yielded little success, suggesting this to be a suboptimal route. Treatment of diene **3.158** with Grubb's II catalyst, and several variations of allylic alcohol (**3.177**, **3.179**, **3.180-3.181**, Table 3.3) resulted in mostly the recovery of starting material, despite several additional changes in reaction time, solvent, and temperature.

Table 3.3. Attempted cross metatheses to form western hemisphere of apoptolidinone C.

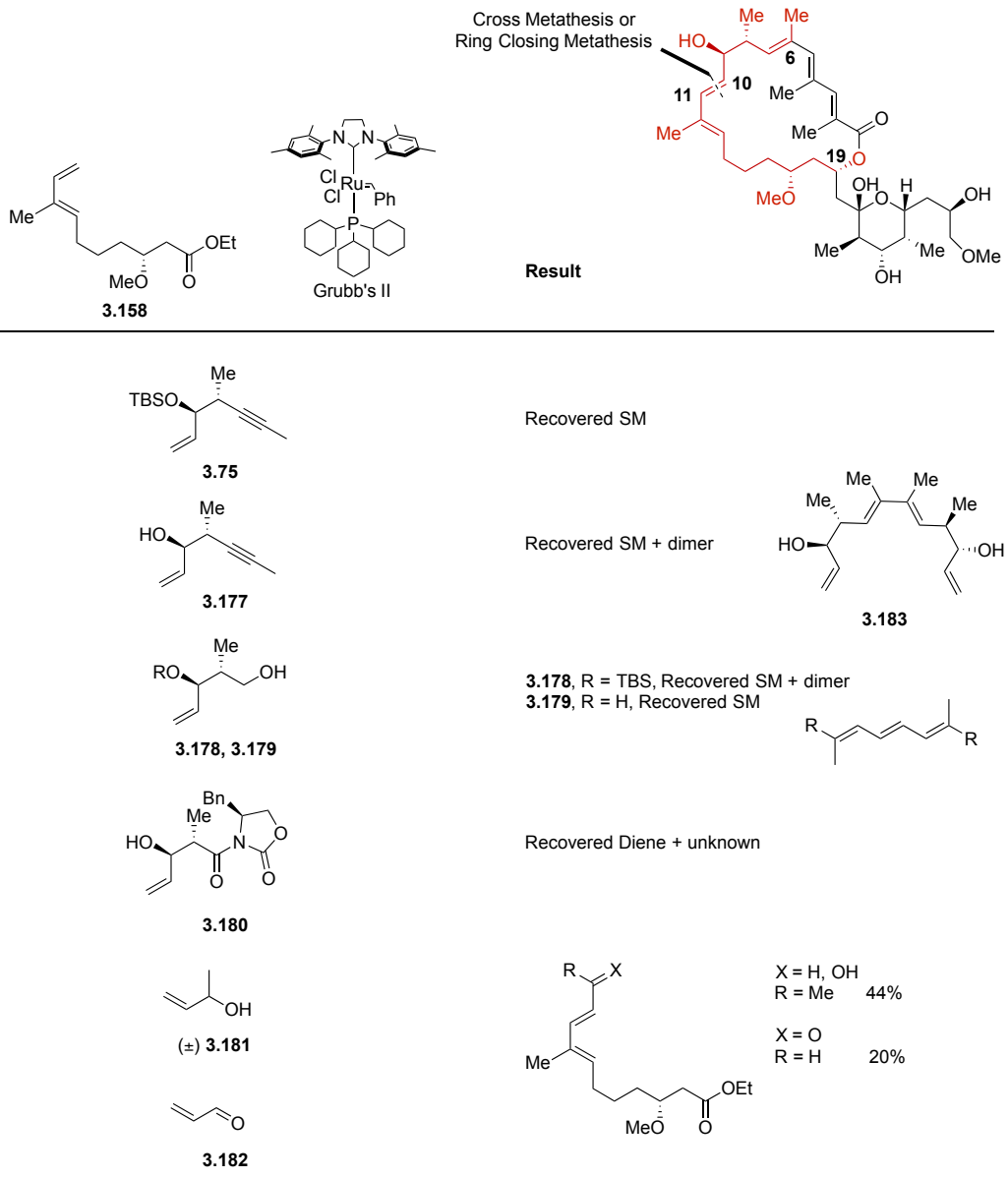

At the outset, we realized the alkynyl moiety of alkenes **3.75** and **3.177** may have been negatively impacting the catalyst, resulting in no reaction. While not fully confirmed, we hypothesized that under forcing conditions, the alkyne may dimerize to form **3.183**. Removing the alkyne moiety and using an alcohol intermediates **3.178**-**3.179** that were used en route to **3.75**, we subjected alcohols **3.178**-**3.179** through the same conditions to give mostly recovered starting material and in some cases, dimerization of diene **3.158**.

Unsurprisingly, aldol adduct **3.180** gave recovery of the diene starting material **3.158** and decomposition of the aldol adduct **3.180**. Finally, crotonaldehyde **3.181** and allylic alcohol **3.182** did yield the desired cross metatheses product, albeit in low yield.

3.8 Conclusion

In the interest of atom economy and the creation of a highly convergent route toward apoptolidinone C, we hoped instead to bring the western haves through a late stage ring closing metathesis. RCM as it would be more entropically favorable than cross metatheses (Fig. 3.37).

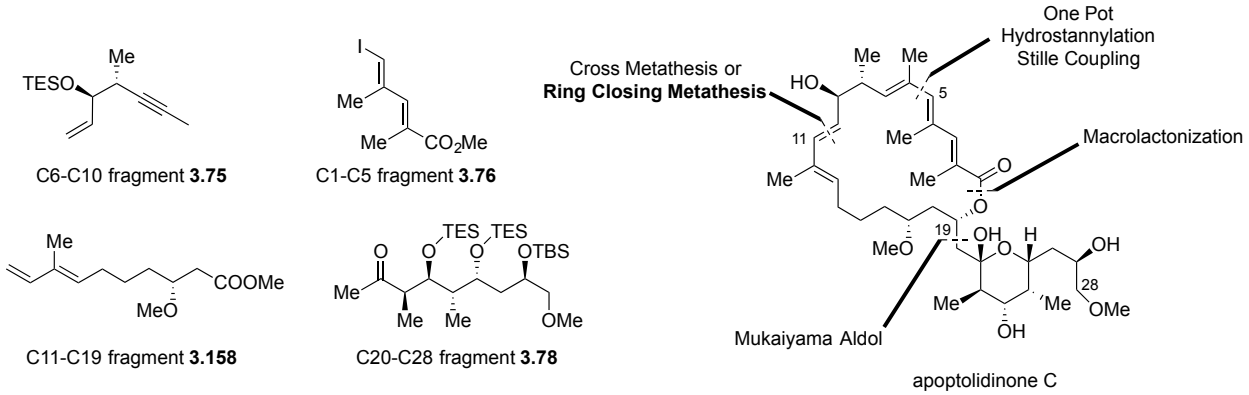

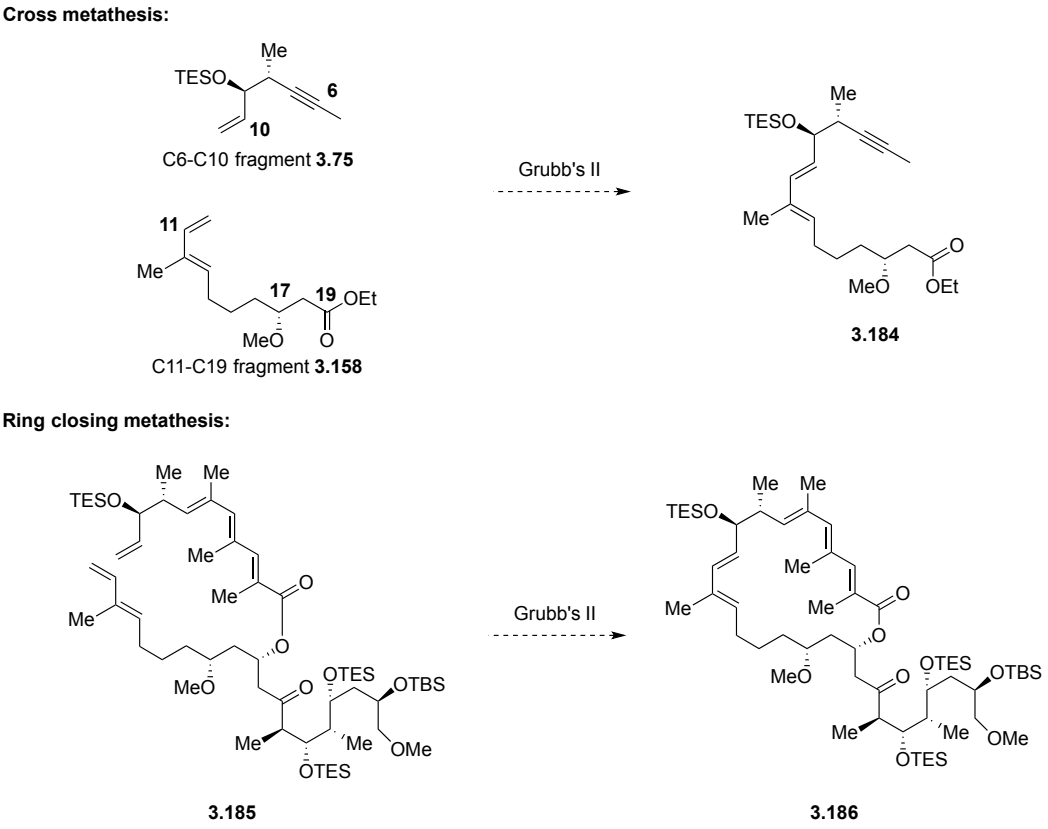

Figure 3.37. Revisiting the second generational retrosynthetic analysis for apoptolidinone C synthesis.

It is important to note that while RCM could possibly close onto the internal olefin of diene moiety of **3.185** (Fig. 3.37), reports by the Danishefsky [39] and Fürstner [40] groups have shown favorable selectivity for terminal olefin ring closure and in high (E)- geometry (**3.186**, Fig. 3.37). Reports by Fürstner, [40] Winssinger, [41] and Porco [42] have shown that (Z)-

alkenes are much more difficult to form via this method, often needing extensive optimization.

3.9 Experimental methods

General Procedure. All glassware used for non-aqueous reactions was flame dried under vacuum. Reactions conducted at ambient temperature were run at approximately 23 °C unless otherwise noted. Reactions were monitored by analytical thin-layer chromatography performed on Analtech silica gel GF 250 micron plates. The plates were visualized with UV light (254 nm) and either potassium permanganate, ceric ammonium molybdate, or *p*-anisaldehyde followed by charring with a heat-gun. Flash chromatography utilized 230-400 mesh silica from Sorbent Technologies or Silica RediSep Rf flash columns on a CombiFlash Rf automated flash chromatography system. Solvents for extraction, washing and chromatography were HPLC grade. Nuclear magnetic resonance (NMR) spectra were acquired on either a 300 MHz Bruker DPX-300 FT-NMR, a 400 MHz Bruker AV-400 FT-NMR, or 500 MHz Bruker DRX-500 FT-NMR Spectrometer at ambient temperature. ^{1}H and ^{13}C NMR data are reported as values relative to $CDCl_3$.^{1}H chemical shifts are reported in δ values in ppm. Data are reported as follows: chemical shift, multiplicity (s = singlet, d = doublet, t = triplet, q = quartet, br = broad, m = multiplet), integration, coupling constant (Hz). ^{13}C chemical shifts are reported in δ values in ppm. Low resolution mass spectra were obtained on an Agilent 1200 series 6130 mass spectrometer with electrospray ionization. High resolution mass spectra were recorded on a Waters Q-TOF API-US.. Analytical HPLC was performed on an Agilent 1200 series with

UV detection at 214 nm and 254 nm along with ELSD detection. Preparative HPLC was conducted on a Gilson 215 Liquid Handler HPLC system using Gemini-NX 50 x 20 mm column. Yields were reported as isolated, spectroscopically pure compounds.

Materials. All reagents and solvents were commercial grade and purified prior to use when necessary. D-Valine was purchased from Combi-blocks. All other reagents unless otherwise stated were purchased from Sigma Aldrich or VWR International. All reactions were performed under argon atmosphere unless otherwise stated. Diethyl ether (Et_2O) and dichloromethane (CH_2Cl_2) were dried by passage through a column of activated alumina using an MBraun MB-SPS dry solvent system. Tetrahydrofuran (THF) was distilled from sodium with benzophenone as indicator prior to use. Solid lithium bis(trimethylsilyl)amide was stored under argon in a glove box and removed prior to use. Freshly distilled ethyl acetate was stirred prior to distillation with activated 4 Å molecular sieves (MS).

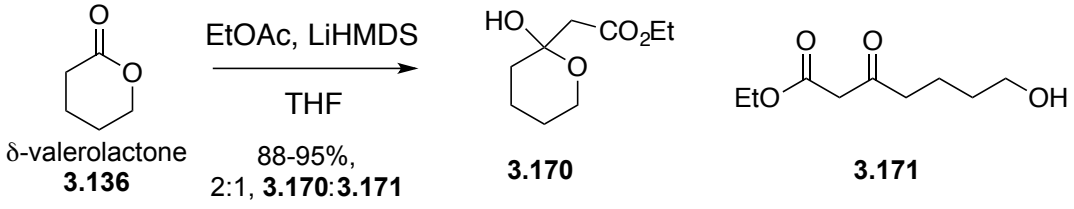

Ethyl 2-(2-hydroxytetrahydro-2*H*-pyran-2-yl)acetate (3.170) and Ethyl 7-hydroxy-3-oxoheptanoate (3.171): To a cooled solution of lithium bis(trimethylsilyl)amide (9.19 g, 54.9 mmol) in THF (40 mL, 1.4 M) at -78 °C, was added a solution of freshly distilled ethyl acetate (4.88 mL, 49.9 mmol) in THF (26 mL, 1.9 M) via addition funnel, dropwise over 2 h. The thick mixture was stirred at -78 °C for 1 h. A solution of freshly distilled δ-valerolactone **3.136** (5.0 g, 49.9 mmol) in THF (21 mL, 2.4M) was added dropwise via addition funnel, and the mixture was stirred at -78 °C for 3 h. Upon completion, the reaction was quenched with glacial acetic acid (ca. 6 mL) and the cloudy white suspension was allowed to warm to RT. The mixture was diluted with brine and Et_2O and the layers were seperated. The crude product was extracted from the aqueous layer with Et_2O (3X) and the combined organic extracts were dried ($MgSO_4$), filtered, and concentrated. The resulting residue was then purified by column chromatography (Hex → 40% EtOAc/Hex, holding at 20% EtOAc/Hex) to give a mixture of the cyclic **3.170** and acyclic **3.171** product as a clear and colorless oil (8.8 g, 94%, 1.2:1.0 cyclic **3.170** : acyclic **3.171**): ^{1}H NMR of cyclic product (400 MHz, $CDCl_3$) δ4.84 (d, *J* = 2.07 Hz, 1H), 4.19 (q, *J* = 7.17 Hz, 2H), 3.97 (m, 1H), 3.61 (m, 1H), 2.62 (d, *J* = 15.6 Hz, 1H), 2.53 (d, *J* = 15.6 Hz, 1H), 1.93 – 1.41 (m, 6H), 1.27 (t, *J* = 7.14 Hz, 3H). ^{1}H NMR of acyclic product (400 MHz, $CDCl_3$) δ4.19 (q, *J* = 7.18 Hz, 2H), 3.57 (t, *J* = 6.26 Hz, 2H), 3.42 (s, 2H), 2.56 (t, *J* = 7.29 Hz, 2H), 1.63 – 1.51 (m, 6H), 1.27 (t, *J* = 7.18 Hz, 3H). Observed spectral properties were identical with those previously reported.

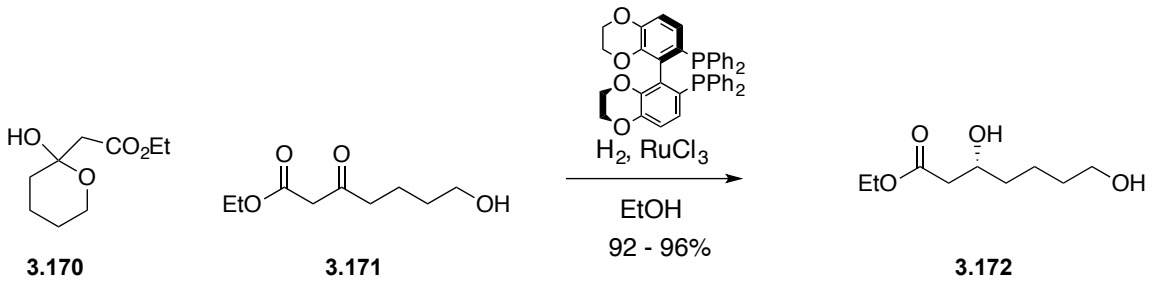

3.170 3.171 3.172

Ethyl (*R*)-3,7-dihydroxyheptanoate (3.172): To a suspension of benzeneruthenium(II) chloride dimer (137 mg, 0.274 mmol) in DMF (1.4 mL, 0.05 M) at 115 °C, was added (S)-BINAP (256 mg, 0.411 mmol). The resulting slurry was stirred for 15 min and then cooled to ambient temperature. The mixture was transferred to a Parr hydrogenation apparatus and a solution of Ethyl 2-(2-hydroxytetrahydro-2H-pyran-2-yl)acetate **3.170** and Ethyl 7-hydroxy-3-oxoheptanoate **3.171** (10 g, 68.4 mmol) in MeOH (30 mL, 2.3 M) was added. The mixture was filled with hydrogen and cycled three times, evacuating the vessel and refilling with hydrogen, behind a blast shield. The mixture was pressurized with an atmosphere of hydrogen (10 bar, 150 psi), warmed to 95 °C, and stirred for 72 h. The mixture was transferred to an RB flask and concentrated. The resulting residue was then purified by column chromatography (Hex → 20% EtOAc/Hex) to give **12** (9.63 g, 95%) as a yellow-green oil: ^{1}H NMR (400 MHz, $CDCl_3$) δ 4.17 (q, *J* = 6.90 Hz, 2H), 4.03 – 3.99 (m, 1H), 3.65 (dd, *J* = 10.16, 5.47 Hz, 2H), 3.06 (d, *J* = 3.57 Hz, 1H), 2.50 (dd, *J* = 16.7, 3.17 Hz, 1H), 2.41 (dd, *J* = 16.7, 8.88 Hz, 1H), 1.66 – 1.41 (m, 6H), 1.27 (t, *J* = 7.14 Hz, 3H). Observed spectral properties were identical with those previously reported.

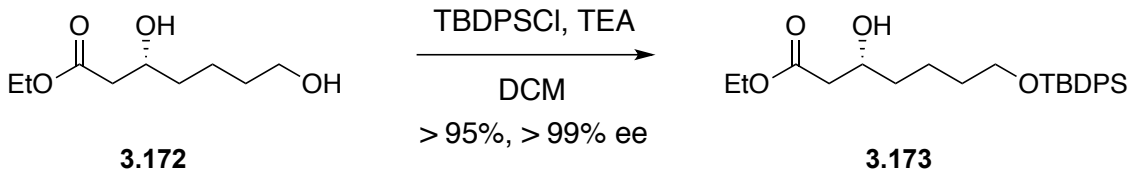

3.172 **3.173**

Ethyl (*R*)-7-((*tert*-butyldiphenylsilyl)oxy)-3-hydroxyheptanoate (3.173): To a solution of ethyl (R)-3,7-dihydroxyheptanoate **3.172** (3.66 g, 19.3 mmol) in DCM (21 mL, 0.9 M), was added tert-butylchlorodiphenylsilane (5.50 mL, 21.2 mmol), followed by triethylamine (2.95 mL, 21.2 mmol) and N,N-dimethylpyridin-4-amine (94 mg, 0.77 mmol). The mixture was stirred at ambient temperature for 48 h and then poured into a mixture of sat. $NH_4Cl_{(aq.)}$ and DCM. The layers were separated and the crude product was extracted from the aqueous with DCM (3X). The combined organic extracts were washed with brine, dried ($MgSO_4$), filtered, and concentrated. The resulting residue was then purified by ISCO (Hex → 20%EtOAc/Hex) to give **3.173** (7.89 g, 96%) as a colorless oil: ^{1}H NMR (600 MHz, $CDCl_3$) δ7.67 – 7.65 (m, 4H), 7.44 – 7.35 (m, 6H), 4.12 (q, *J* = 7.15 Hz, 2H), 4.01 – 3.94 (m, 1H), 3.66, (t, *J* = 6.13 Hz, 2H), 2.90 (m, 1H), 2.49 (dd, *J* = 16.5, 3.07 Hz, 1H), 2.37 (dd, *J* = 9.34, 16.5 Hz, 1H), 1.61 – 1.40 (m, 4H), 1.27 (q, *J* = 7.07, 3H), 1.04 (s, 9H). ^{13}C NMR (600 MHz, $CDCl_3$) δ173.4, 135.9, 134.4, 129.9, 129.9, 68.29, 64.06, 61.01, 41.58, 36.52, 32.71, 27.22, 22.11, 19.55, 14.53. Observed spectral properties were identical with those previously reported.

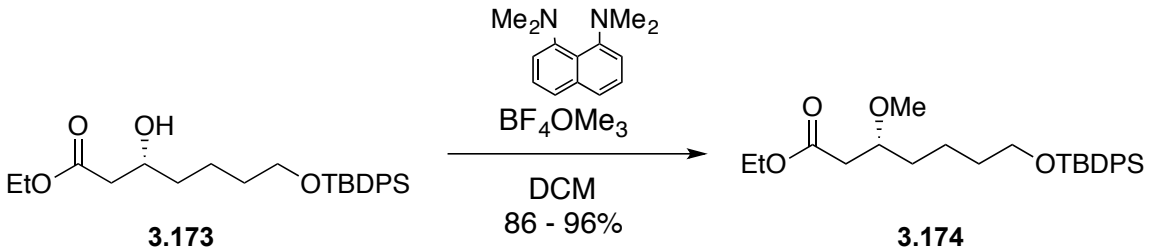

3.173 **3.174**

Ethyl (*R*)-7-((*tert*-butyldiphenylsilyl)oxy)-3-methoxyheptanoate (3.174): To a cooled solution of ethyl (R)-7-((tert-butyldiphenylsilyl)oxy)-3-hydroxyheptanoate **3.173** (6.4 g, 15 mmol) in DCM (30 mL, 0.5M) at 0 °C, was added N,N,N',N'-tetramethyl-1,8-naphthalenediamine (9.61 g, 45 mmol) and trimethyloxonium tetrafluoroborate (4.42 g, 30 mmol). The mixture was warmed to ambient temperature and stirred over 24 h. The reaction was then quenched with sat. NH_4Cl $_{(aq.)}$ DCM and Celite® was added and the mixture was stirred for 15 min and filtered through a plug of Celite®. The sticky white solids were washed with DCM (3X) and the combined filtrate was transferred to a separatory funnel and the layers separated. The organic layer was washed with sat. $NaHSO_3$ (4X) and brine, dried ($MgSO_4$), filtered, and concentrated. The resulting residue was ISCO purified (Hex → 25% EtOAc/Hex) to give **3.147** as colorless oil (5.33 g, 81%): ^{1}H NMR (600 MHz, $CDCl_3$) δ7.67 – 7.65 (m, 4H), 7.44 – 7.35 (m, 6H), 4.15 (q, *J* = 7.11 Hz, 2H), 3.66 (t, *J* = 6.19, 2H), 3.65 – 3.59 (m, 1H), 3.34 (s, 3H), 2.51 (dd, *J* = 15.1, 7.39 Hz, 1H), 2.38 (dd, *J* = 15.1, 5.36 Hz, 1H), 1.59 – 1.41 (m, 6H), 1.26 (t, *J* = 7.15 Hz, 3H), 1.05 (s, 9H). ^{13}C NMR (600 MHz, $CDCl_3$) δ172.2, 136.0, 134.4, 130.0, 127.9, 78.1, 64.1, 60.8, 57.4, 53.8, 39.9, 34.1, 32.9, 27.2, 21.8, 19.6, 14.6. *m/z* calcd. for $C_{26}H_{38}O_4Si$ $[M+H]^+$ 442.25 found 443.2615.

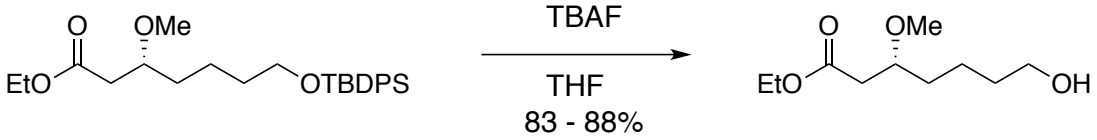

3.174 **3.175**

Ethyl (*R*)-7-hydroxy-3-methoxyheptanoate (3.175): To a cooled solution of ethyl (R)-7-((tert-butyldiphenylsilyl)oxy)-3-methoxyheptanoate **3.174** (2.903 g, 6.56 mmol) in THF (13 mL, 0.5M) at 0 ˚C, was added a solution of tetrabutylammonium fluoride (13 mL, 1.0 M in THF, 13.1 mmol). The reaction mixture was allowed to warm to ambient temperature and stir for 24 h. The reaction mixture was quenched with sat. $NH_4Cl_{(aq.)}$, diluted with water and Et_2O, and the layers were separated. The crude product was extracted from the aqueous with Et_2O (3X) and the combined organic extracts were washed with brine, dried ($MgSO_4$), filtered, and concentrated. The resulting residue was then purified by column chroatography (Hex → 70% EtOAc/Hex) to give **3.175** as a light yellow oil (1.17 g, 87%): ^{1}H NMR (400 MHz, $CDCl_3$) δ4.15 (q, *J* = 7.12 Hz, 2H), 3.65 (t, *J* = 6.45, 2H), 3.64 – 3.61 (m, 1H), 3.35 (s, 3H), 2.51 (dd, *J* = 15.1, 7.08 Hz, 1H), 2.38 (dd, *J* = 15.1, 5.74 Hz, 1H), 1.63 – 1.40 (m, 6H), 1.26, (t, *J* = 7.07 Hz, 3H). ^{13}C NMR (400 MHz, $CDCl_3$) δ172.1, 78.0, 63.1, 60.8, 57.4, 39.7, 34.0, 33.0, 21.7, 14.5. *m/z* calcd. for $C_{10}H_{21}O_4$ $[M+H]^+$ 204.14 found 205.1434.

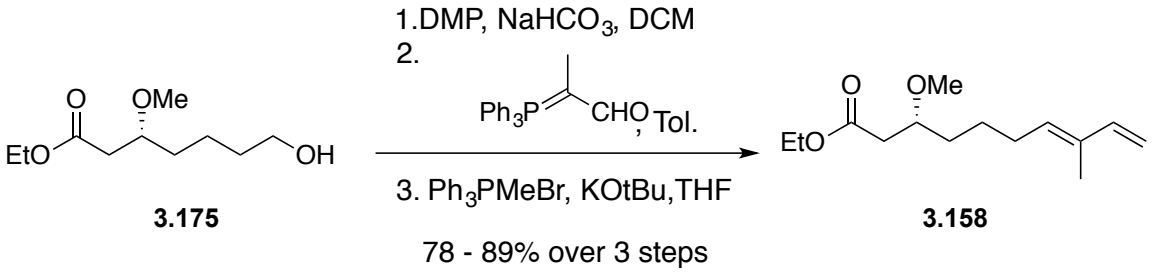

To a solution of ethyl (R)-7-hydroxy-3-methoxyheptanoate **3.175** (966.3 mg, 4.73 mmol) in DCM (12 mL, 0.4M), was added a mixture of Dess-Martin Periodinane (2.41 g, 5.68 mmol) and sodium bicarbonate (1.99 g, 23.7 mmol). The reaction mixture was stirred at ambient temperature for 4 h and quenched with sat. $NaHCO_{3\ (aq.)}$. The mixture was stirred until gas

evolution ceased and then diluted with water and Et_2O. The layers were separated and the crude product was extracted from the aqueous layer with Et_2O (3X). The combined organic extracts were washed with brine, dried ($MgSO_4$), filtered, and concentrated. The resulting sticky white solids were taken up into hexanes and filtered through a plug of Celite®. The white solids were washed with hexanes extensively and the combined filtrate was concentrated. The resulting colorless residue was taken through crude without further purification.

To a solution of crude ethyl (R)-3-methoxy-7-oxoheptanoate (957 mg, 4.73 mmol) in toluene (16 mL, 0.3M), was added solid 2-(triphenylphosphoranylidene)propionaldehyde (2.26 g, 7.10 mmol). The mixture was heated to 85 °C and stirred for 18 h. The reaction mixture was cooled to ambient temperature and concentrated. The resulting brown residue was taken up into a mixture of hexanes and Celite® and carefully heated with a heat gun to a gentle boil, while stirring vigorously. The mixture was allowed to cool to ambient temperature and was filtered through an additional plug of Celite®. The solids were washed with hexanes (3X) and the combined filtrate was concentrated to give a colorless oil which was used crude without further purification in the following reaction.

To a stirring solution of solid methyltriphenylphosphonium bromide (5.07 g, 14.2 mmol) in THF (95 mL, 0.05 M), was added solid potassium *tert*-butoxide (1.59 mg, 14.2 mmol). The bright yellow solution was stirred at ambient temperature for 1 h. Any unreacted

particulates were allowed to settle and the clear yellow-orange solution was taken up and added dropwise to a stirring solution of crude ethyl (R,E)-3-methoxy-8-methyl-9-oxonon-7-enoate (1.15 g, 4.73 mmol) in THF (9.5 mL, 0.5M) dropwise until a bright yellow-orange suspension was observed (or 1.1 eq was added). The reaction mixture was immediately quenched with NH_4Cl and diluted with Et_2O and water. The layers were separated and the crude product was extracted from the aqueous layer with Et_2O (3X). The combined organic extracts were washed with brine, dried ($MgSO_4$), filtered, and concentrated. The resulting residue was purified to give **3.158** (692 mg, 60% over 3 steps) as a faint yellow clear oil. ^1H NMR (400 MHz, $CDCl_3$) δ6.36 (dd, *J* = 7.3 Hz, 10.7 Hz, 1H), 5.45 (t, *J* = 7.39 Hz, 1H), 5.08 (d, *J* = 16.9 Hz, 1H), 4.93 (d, *J* = 10.7 Hz, 1H), 4.15 (q, *J* = 7.03 Hz, 2H), 3.35 (s, 3H), 2.53 (dd, *J* = 7.10, 14.8 Hz, 1H), 2.39 (dd, *J* = 5.43, 14.8), 2.15 (m, 2H), 1.73 (s, 3H), 1.26 (t, *J* = 7.23 Hz, 3H).

3.10 Notes and references

1. Daniel, P. T.; Koert, U.; Schuppan, J., Apoptolidin: Induction of Apoptosis by a Natural Product *Angew. Chem. Int. Ed.* **2006**, 45, 872-893.

2. Wehlan, H.; Dauber, M.; Mujica Fernaud, M.-T.; Schuppan, J.; Mahrwald, R.; Ziemer, B.; Juarez Garcia, M.-E.; Koert, U. Total synthesis of Apoptolidin *Angew. Chem. Int. Ed.* **2004**, 43, 4597-4601.

3. Nicolaou, K. C.; Li, Y.; Fylaktakidou, K. C.; Mitchell, H. J.; Wei, H.-X.; Weyershausen, B. Total Synthesis of Apoptolidin: Part 1. Retrosynthetic Analysis and Construction of Building Blocks *Angew. Chem. Int. Ed.* **2001**, 40, 3849-3854.

4. Nicolaou, K. C.; Li, Y.; Fylaktakidou, K. C.; Mitchell, H. J.; Sugita, K. Total Synthesis of Apoptolidin: Part 2. Coupling of Key Building Blocks and Completion of the Synthesis *Angew. Chem. Int. Ed.* **2001**, 40, 3854-3857.

5. Nicolaou, K. C.; Fylaktakidou, K. C.; Monenschein, H.; Li, Y.; Weyershausen, B.; Mitchell, H. J.; Wei, H.-X.; Guntupalli, P.; Hepworth, D.; Sugita, K. Total Synthesis of Apoptolidin: Construction of Enantiomerically Pure Fragments *J. Am. Chem. Soc.* **2003**, 125, 15433-15442.

6. Nicolaou, K. C.; Li, Y.; Sugita, K.; Monenschein, H.; Guntupalli, P.; Mitchell, H. J.; Fylaktakidou, K. C.; Vourloumis, D.; Giannakakou, P.; O'Brate, A. Total Synthesis of Apoptolidin: Completion of the Synthesis and Analogue Synthesis and Evaluation *J. Am. Chem. Soc.* **2003**, 125, 15443-15454.

7. Crimmins, M. T.; Christie, H. S.; Long. A.; Chaudhary, K. Total Synthesis of Apoptolidin A *Org. Lett.* **2009**, 11, 831-834.

8. Schuppan, J.; wehlan, H.; Keper, S.; Koert, U. Synthesis of Apoptolidinone *Angew. Chem. Int. Ed.* **2001**, 40, 2063-2066.

9. Schuppan, J.; Wehlan, H.; Keiper, S.; Koert, U. Apoptolidinone A: Synthesis of the Apoptolidin A Aglycone *Chem. Eur. J.* **2006**, 12, 7364-7377.

10. Wu, B.; Liu, Q.; Sulikowski, G. A. Total Synthesis of Apoptolidinone *Angew. Chem. Int. Ed.* **2004**, 43, 6673-6675.

11. Ghidu, V. P.; Wang, J.; Wu, B.; Liu, Q.; Jacobs, A.; Marnett, L. J.; Sulikowski, G. A. Synthesis and Evaluation of the Cytotoxicity of Apoptolidinones A and D *J. Org. Chem.* **2008**, 73, 4949-4955.

12. Crimmins, M. T.; Christie, H. s.; Chaudhary, K.; Long. A. Enantioselective Synthesis of Apoptolidinone: Exploiting the Versatility of Thiazolidinethione Chiral Auxiliaries *J. Am. Chem. Soc.* **2005**, 127, 13810-13812.

13. Vargo, T. R.; Hale, J. S.; Nelson, S. G. Catalytic Asymmetric Aldol Equivalents in the Enantioselective Synthesis of the Apoptolidin C Aglycone *Angew. Chem. Int. Ed.* **2010**, 49, 8678-8681.

14. Nelson, S. G.; Peelen, T. J.; Wan, Z. Catalytic Asymmetric Acyl Halide—Adehyde Cyclocondensations. A Strategy for Enantioselective Catalyzed Cross Aldol Reactions *J. Am. Chem. Soc.* **1999**, 121, 9742-9743.

15. Nelson, S. G.; Zhu, C.; Shen, X. Catalytic Asymmetric Acyl—Halide Aldehyde Cyclocondensation Reactions of Substituted Ketenes *J. Am. Chem. Soc.* **2004**, 126, 14-15.

16. Shen, X.; Wasmuth, A. S.; Zhao, J.; Zhu, G.; Nelson, S. G. Catalytic Asymmetric Assembly of Stereodefined Propionate Units: An Enantioselective Total Synthesis of (-)-Pironetin *J. Am. Chem. Soc.* **2006**, 128, 7438-7439.

17. Wender, P. A.; Sukopp, M.; Longcore, K. Apoptolidins B and C: Isolation, Structure Deterimination, and Biological Activity *Org. Lett.* **2005**, 7, 3025-3028.

18. Serrill, J. D.; Tan, M.; Fotso, S.; Sikorska, J.; Kasanah, N.; Hau, A. M.; McPhail, K. L.; Santosa, D. A.; Zabiskie, T. M.; Mahmud, T.; Viollet, B.; Proteau, P. J.; Ishmael, J. E. Apoptolidins A and C activate AMPK in metabolically sensitive cell types and are mechanistically distinct from oligomycin A. *Biochem. Pharmacol.* **2015**, 3, 251-265.

19. Wender, P. A.; Gulledge, A. V.; Jankowski, O. D.; Seto, H., Isoapoptolidin: Structure and Activity of the Ring-Expanded Isomer of Apoptolidin *Org. Lett.* **2002**, 4, 3819-3822.

20. Pennington, J. D.; Williams, H. J.; Salomon,A. R.; Sulikowski, G. A., Toward a Stable Apoptolidin Derivative: Identification of Isoapoptolidin and Selective Deglycosylation of Apoptolidin *Org. Lett.* **2002**, 4, 3823-3825.

21. Jin, B.; Liu, Q.; Sulikowski, G. A. Development of an end-game strategy towards apoptolidin: a sequential Suzuki coupling approach *Tetrahedron* **2005**, 61, 401-408.

22. Ghidu, V. P.; Wang, J.; Wu, B.; Liu, Q.; Jacobs, A.; Marnett, L. J.; Sulikowski, G. A. Synthesis and Evaluation of the Cytotoxicity of Apoptolidinones A and D *J. Org. Chem.* **2008**, 73, 4949-4955.

23. Keck, G. E.; Tarbet, K. H.; Geraci, L. S. Catalytic asymmetric allylation of aldehydes *J. Am. Chem. Soc.* **1993**, 115, 8467-8468.

24. Nagao, Y.; Hagiwara, Y.; Kumagai, T.; Ochiai M.; Inoue, T.; Hashimoto, K.; Fujit, E. New C-4-chiral 1,3-thiazolidine-2-thiones: excellent chiral auxiliaries for highly diastereo-controlled aldol-type reactions of acetic acid and α, β-unsaturated aldehydes *J. Org. Chem.* **1985**, 51, 2391-2393.

25. Harding, C. E.; King, S. L. Mechanism of Intramolecular Cyclization of Acetylenic Ketones *J. Org. Chem.* **1992**, 57, 883-886.

26. Oblinger, E.; Montgomery, J. A New Stereoselective Method for the Preparation of Allyl Alcohols *J. Am. Chem. Soc.* **1997**, 119, 9065-9066.

27. Brochu, M. P.; Brown, S. P.; MacMillan, D. W. C. Direct and Enantioselective Organocatalytic α-Chlorination of Aldehydes *J. Am. Chem. Soc.* **2004**, 126, 4108-4109.

28. Halland, N.;Braunton, A.; Bachmann, S.; Marigo, M.; Jørgensen, K. A. Direct Organocatalytic Asymmetric α-Chlorination of Aldehydes *J. Am. Chem. Soc.* **2004**, 126, 4790-4791.

29. Fadeyi, O. O.; Schulte, M. L.; Lindsley, C. W. General Access to Chiral *N*-Alkyl Terminal Aziridines via Organocatalysis *Org. Lett.* **2010**, 12, 3276-3278.

30. Senter, T. J.; O'Reilly, M. C.; Chong, K. M.; Sulikowski, G. A.; Lindsley, C. W. A general, enantioselective synthesis of *N*-alkyl terminal aziridines and C2-functionalized azetidines via organocatalysis *Tet. Lett.* **2015**, 56, 1276-1279.

31. Doroh, B.; Sulikowski, G. A. Progress toward the Total Synthesis of Bielschowskysin: A Stereoselective [2+2] Photocycloaddition *Org. Lett.* **2006**, 8, 903-906.

32. Townsend, S. D.; Sulikowski, G. A. Progress toward the Total Synthesis of Bielschowskyskin *Org. Lett.* **2013**, 15, 5096-5098.

33. Guillarme, S.; Plé K.; Banchet, A.; Liard, A.; Haudrechy, A. Alkynylation of Chiral Aldehydes: Alkoxy-, Amino-, and Thio-Substituted Aldehydes

34. Netscher, T.; Scalone, M.; Schmid, R. Enantioselective Hydrogenation: Towards a Large-Scale Total Synthesis of (R,R,R)-α-Tocopherol. In *Asymmetric Catalysis on Industrial Scale: Challenges, Approaches and Solutions;* Blaser, H.-U.; Schmidt, E., Ed; Wiley-VCH Verlag GmbH & Co. KGaA: 2004, 71.

35. Hauser, C. R.; Harris, T. M. Condensations at the Methyl Group Rather than the Methylene Group of Benzoyl-and Acetylacetone Through Intermediate Dipotassio Salts *J. Am. Chem. Soc.* **1958**, 6360-6363.

36. Ikariya, T.; Blacker, J. Asymmetric Transfer Hydrogenation of Ketones with Bifunctional Transition Metal-Based Molecular Catalysts *Acc. Chem. Res.* **2007**, 40, 1300-1308.

37. Chau, S. T. Progress Toward the Total Synthesis of Ammocidin D, Vanderbilt Univeresity, Nashville, TN, 2011.

38. Zerong Wang, Evan's Aldol Reaction, Comprehensive Organic Name Reactions and Reagents (http://onlinelibrary.wiley.com/doi/10.1002/9780470638859.conrr223/abstract)

39. Biswas, K.; Lin, H.; Njardason, J. T.; Chappel, M. D.; Chou, T.-C.; Guan, Y.; Tong, W. P.; He, L.; Horwitz, S. B.; Danishefsky, S. J. Highly Concise Routes to Epothilones: The Total Synthesis and Evaluation of Epothilone 490 *J. Am. Chem. Soc.* **2002**, 124, 9825-9832.

40. Gallenkamp, D.; Fürstner, A. Stereoselective Synthesis of *E,Z*-Configured 1,3-Dienes by Ring-Closing Metathesis. Application to the Total Synthesis of Lactimidomycin *J. Am. Chem. Soc.* **2011**, 133, 9232-9235.

41. Barluenga, S.; Lopez, P.; Moulin, E.; Winssinger, N. Modular Asymmetric Synthesis of Pochonin C *Angew. Chem. Int. Ed.* **2004**, 116, 3549-3552.

42. Wang, X.; Bowman, E. J.; Bowman, B. J.; Porco Jr., J. A. Total Synthesis of the Salicylate Enamide Macrolide Oximidine III: Application of Relay Ring-Closing Metathesis *Angew. Chem. Int. Ed.* **2004**, 43, 3601-3605.

43. Roche, C.; Desroy, N.; Haddad, M.; Phansavath, P.; Genet, J.-P. Ruthenium-SYNPHOS-Catalyzed Asymmetric Hydrogenations: an Entry to Highly Stereoselective Synthesis of the C15-C30 Subunit of Dolabelide A *Org. Lett.* **2008**, 10, 3911-3914.

Appendix A1:

Spectra relevant to chapter III

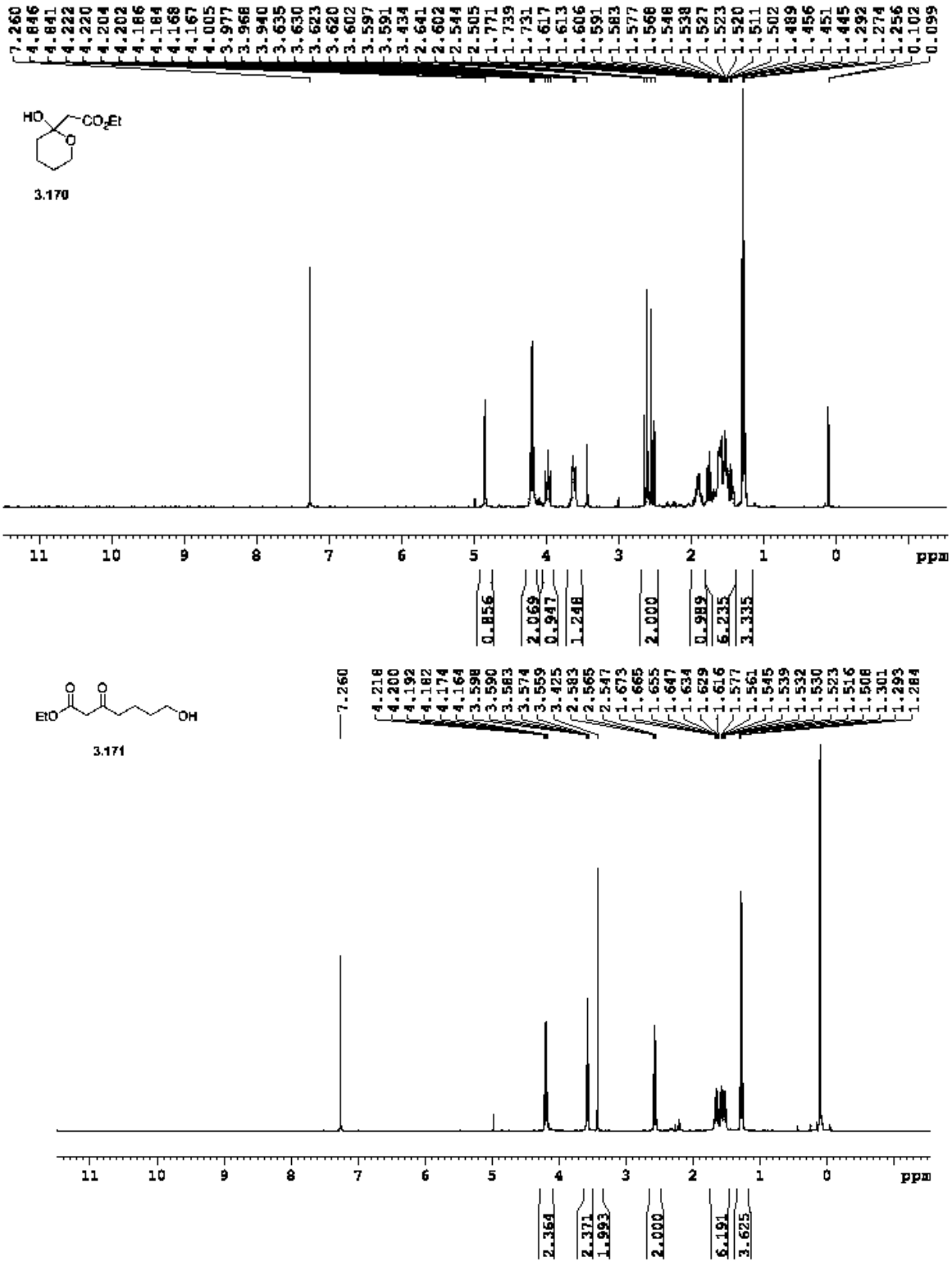

Figure A1.1. ^{1}H NMR (400 MHz, $CDCl_3$) of **3.170** and **3.171.**

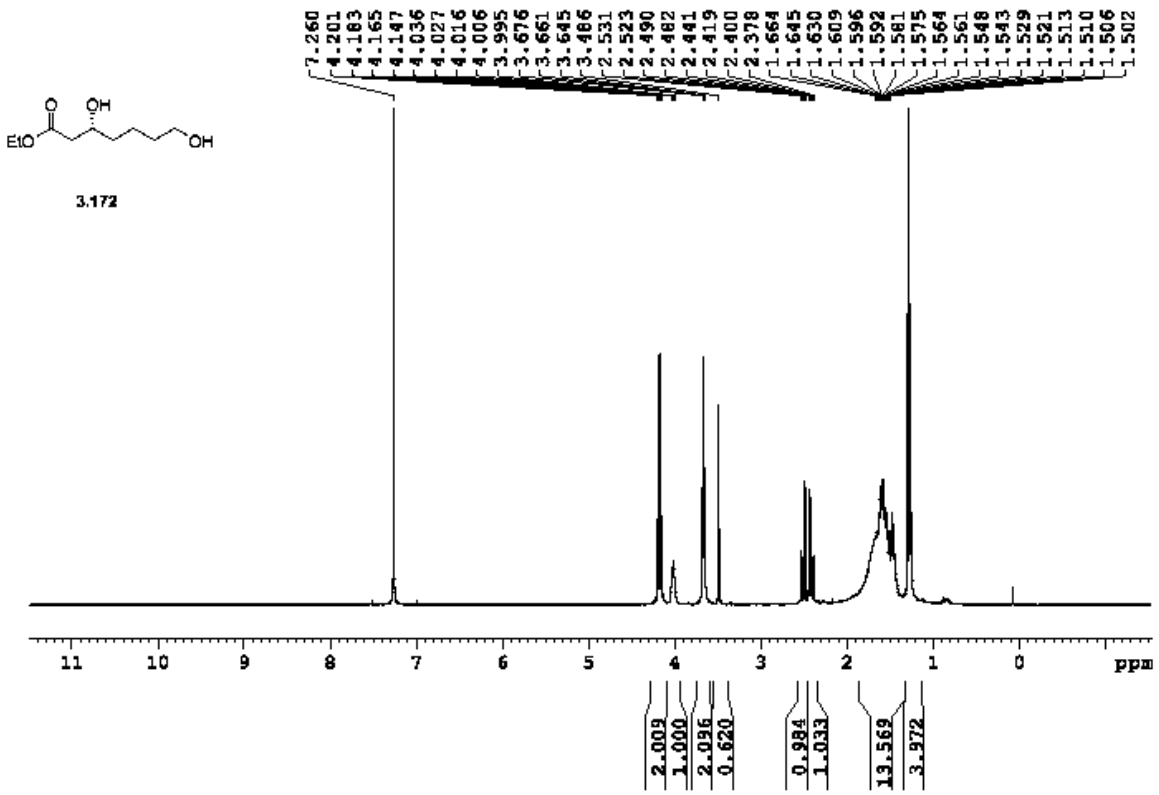

Figure A1.2. ^{1}H NMR (400 MHz, $CDCl_3$) of **3.172**.

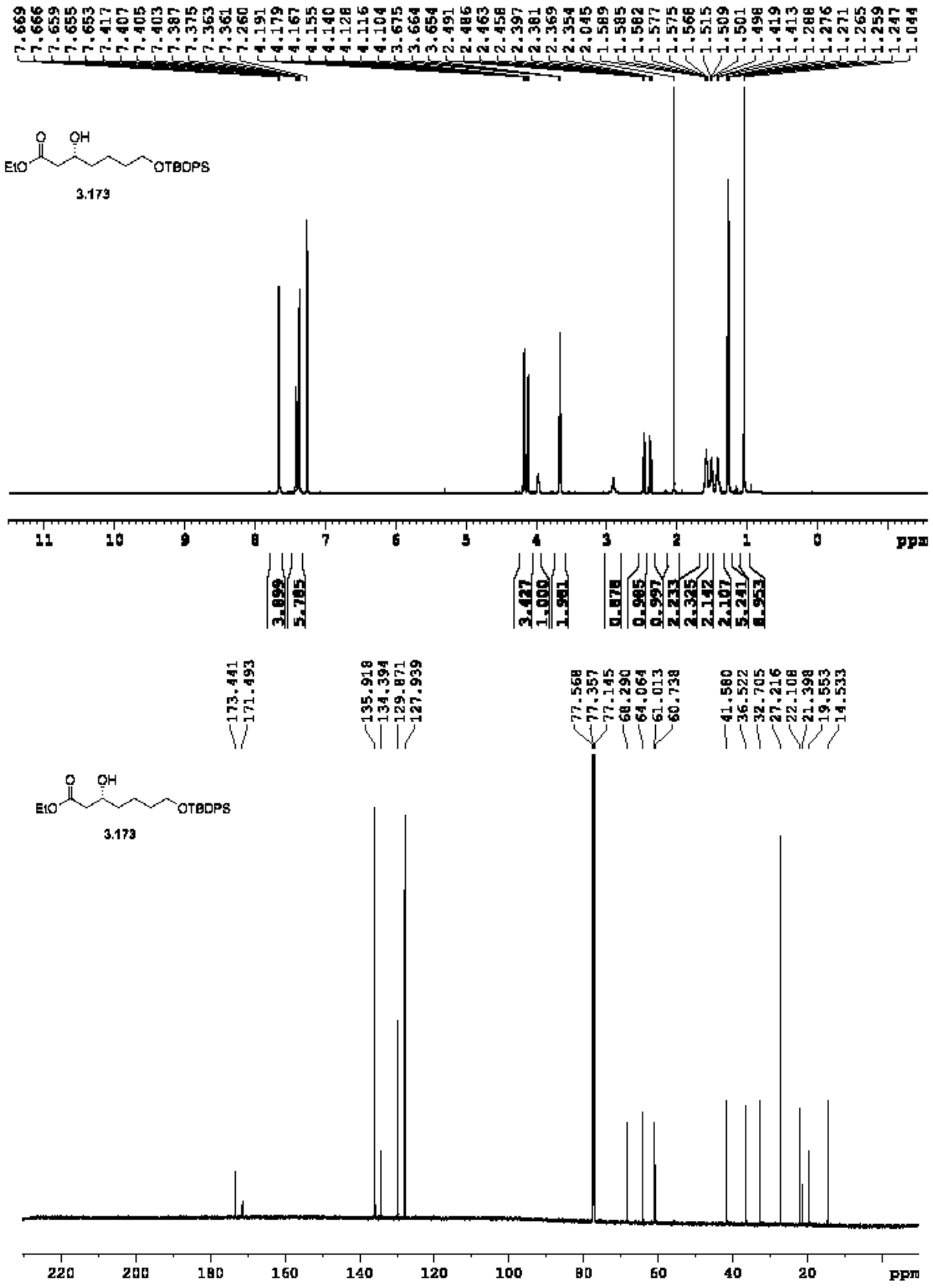

Figure A1.3. ^{1}H NMR (400 MHz, $CDCl_3$) and ^{13}C NMR (400 MHz, $CDCl_3$) of **3.173**.

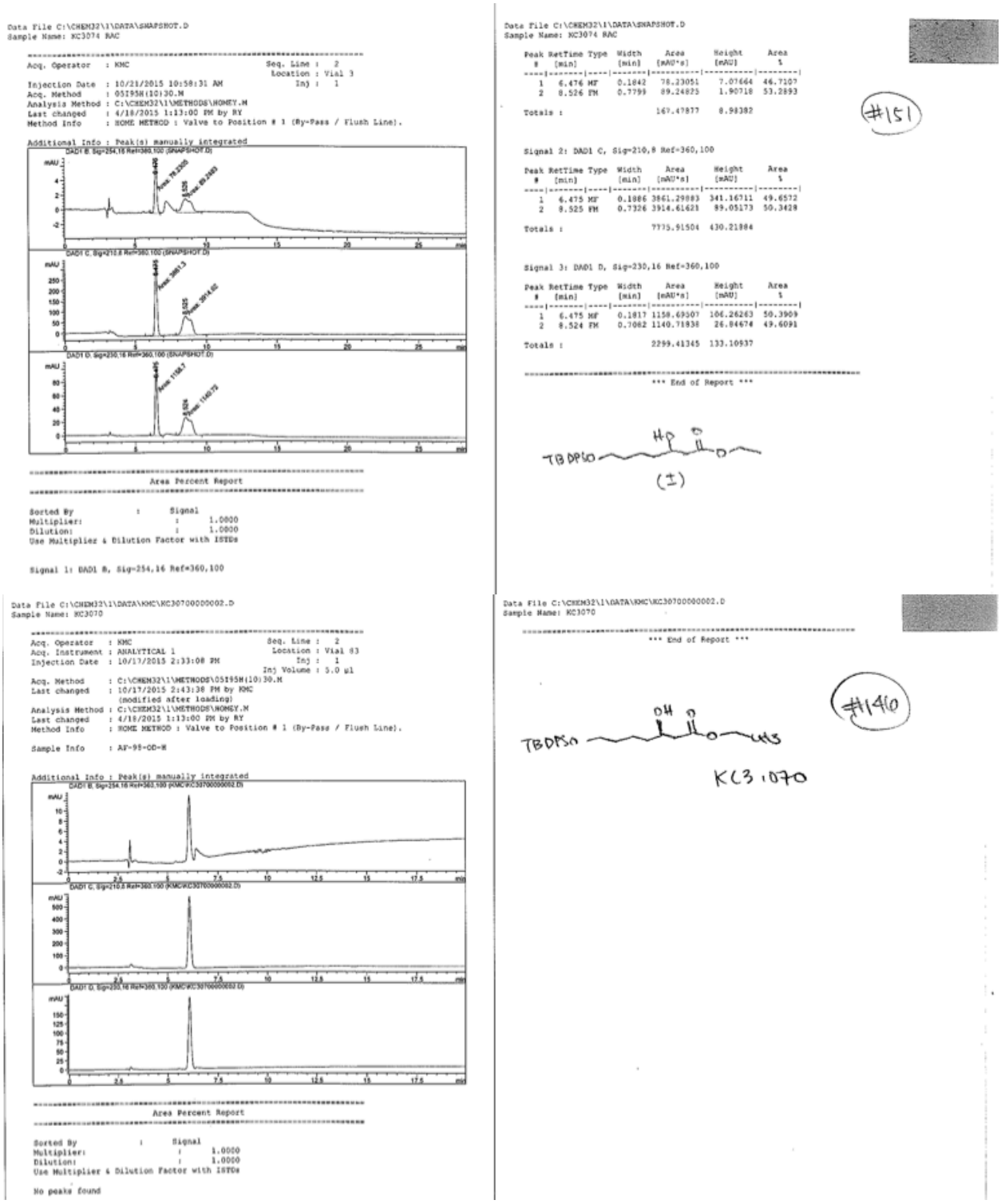

Figure A1.4. HPLC trace for racemic asymmetric **3.173**.

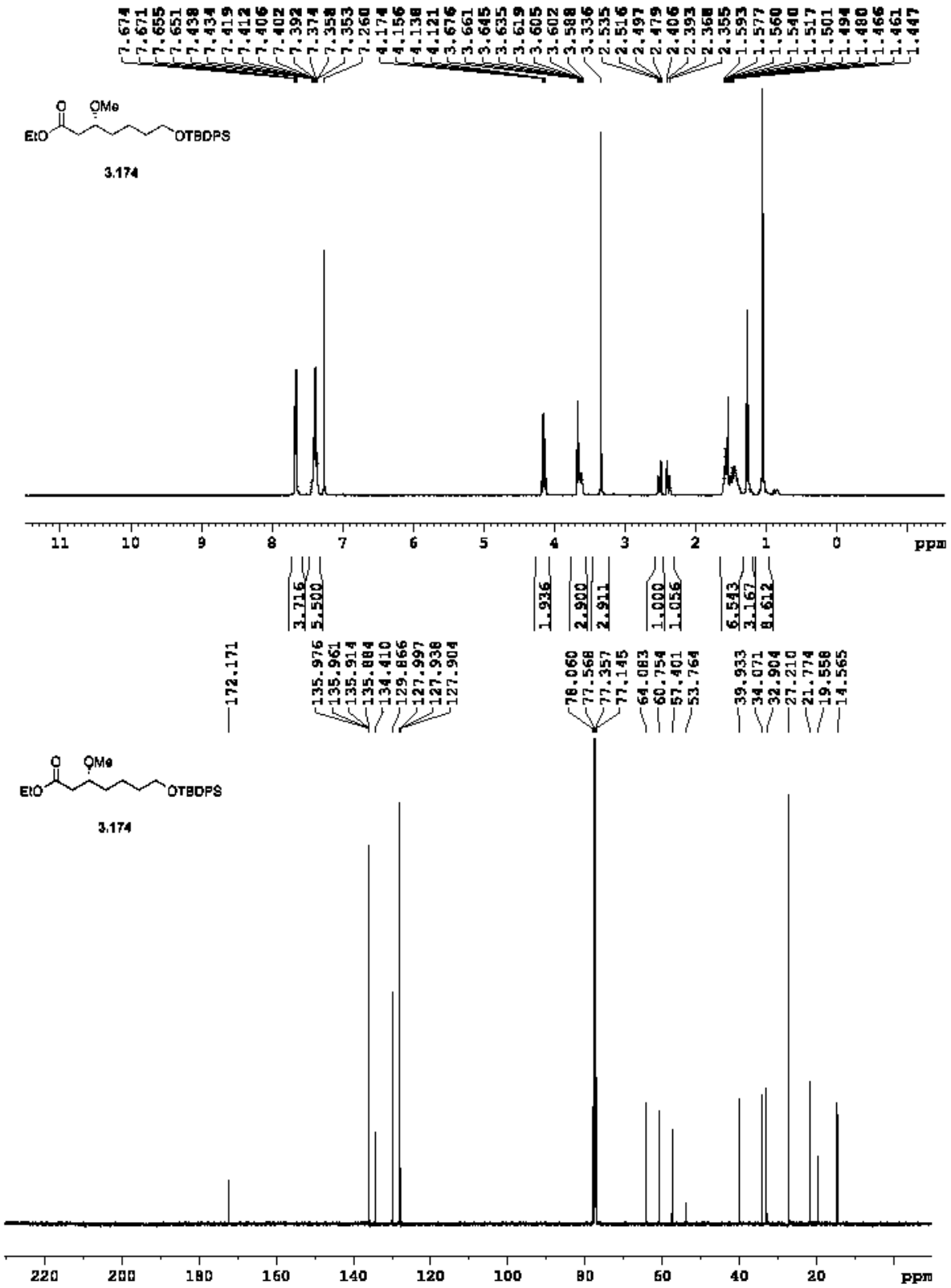

Figure A1.5. ^{1}H NMR (400 MHz, $CDCl_3$) and ^{13}C NMR (400 MHz, $CDCl_3$) of **3.174**.

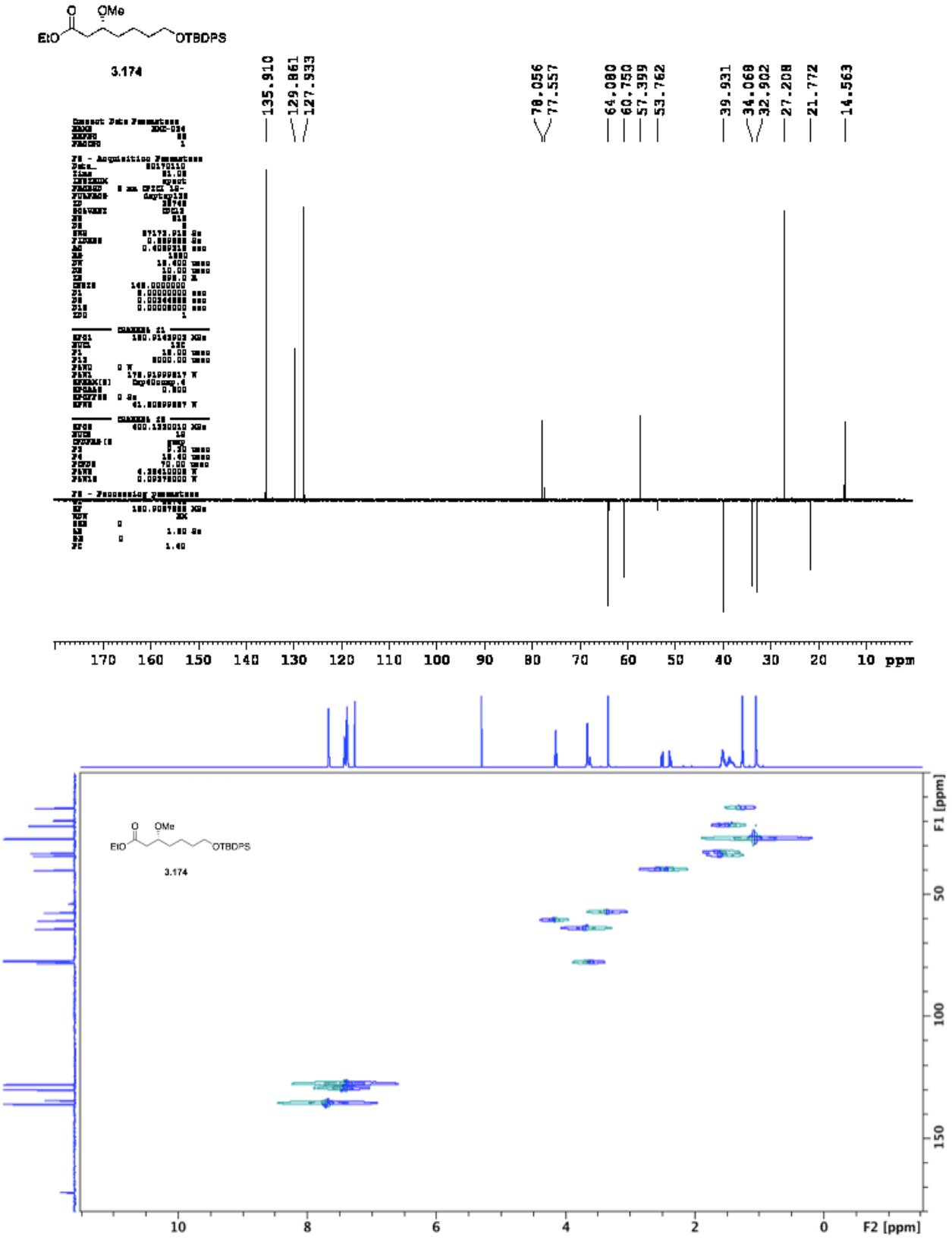

Figure A1.6. DEPT-135 (400 MHz, $CDCl_3$) and HSQC (600 MHz, $CDCl_3$) of **3.174**.

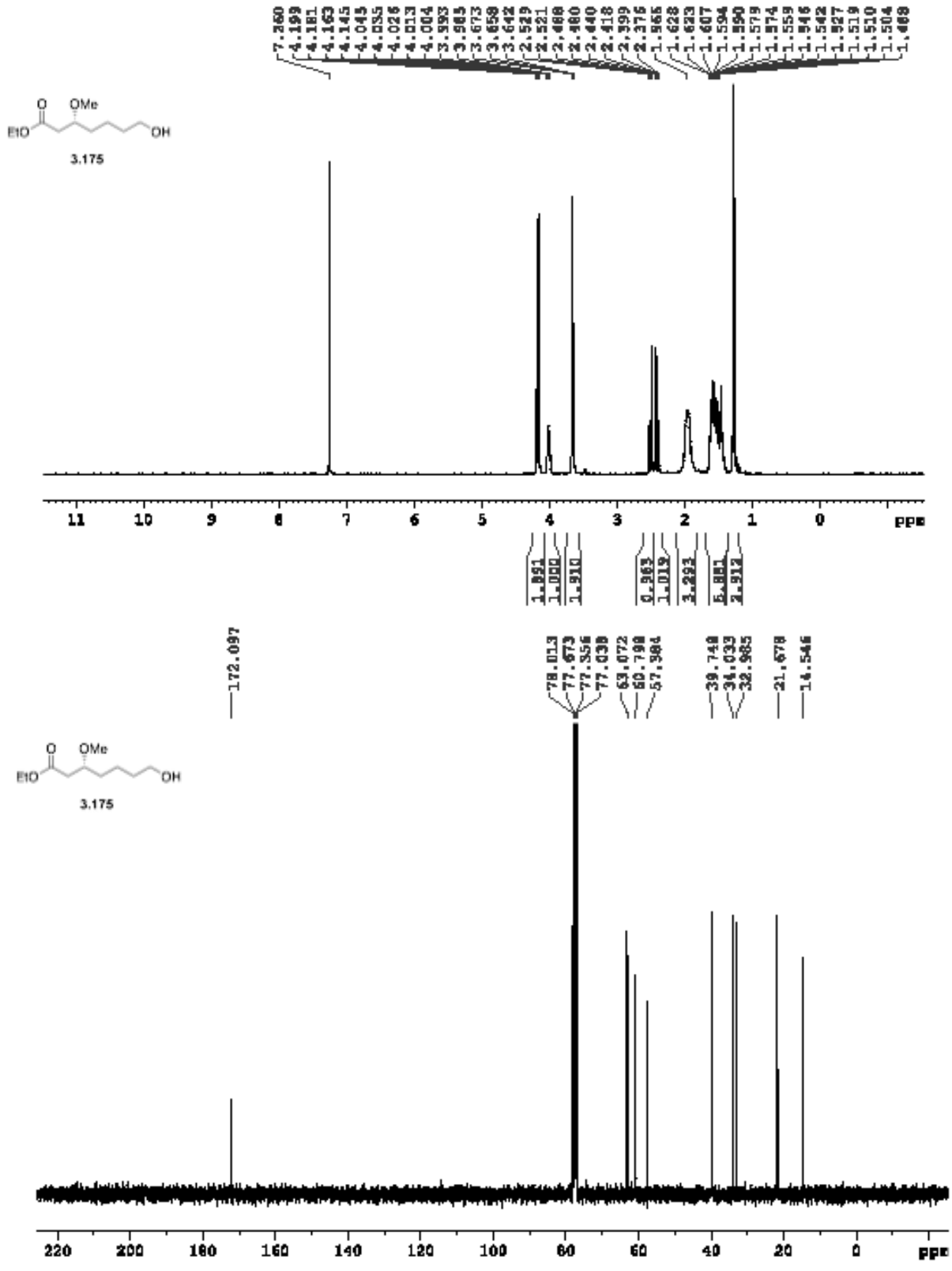

Figure A1.7. ^{1}H NMR (400 MHz, $CDCl_3$) and ^{13}C NMR (400 MHz, $CDCl_3$) of **3.175**.

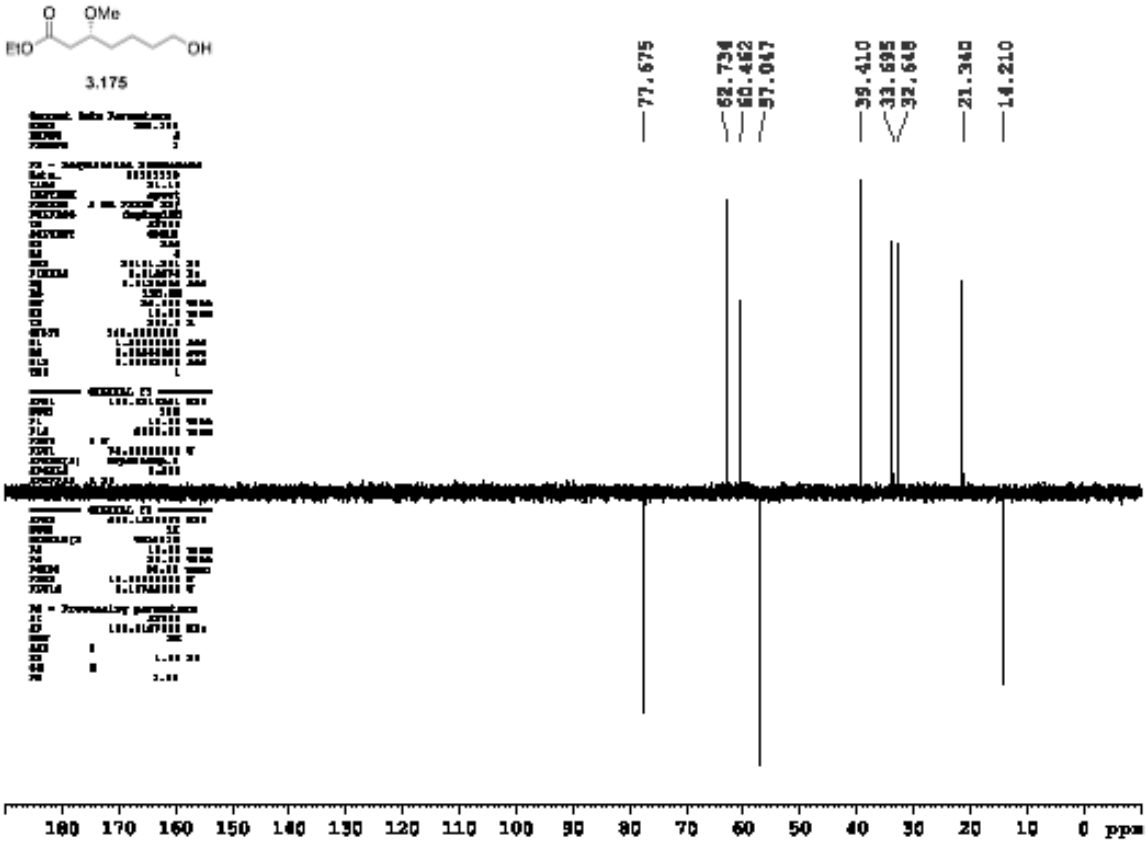

Figure A1.8. DEPT-135 (400 MHz, $CDCl_3$) of **3.174**.

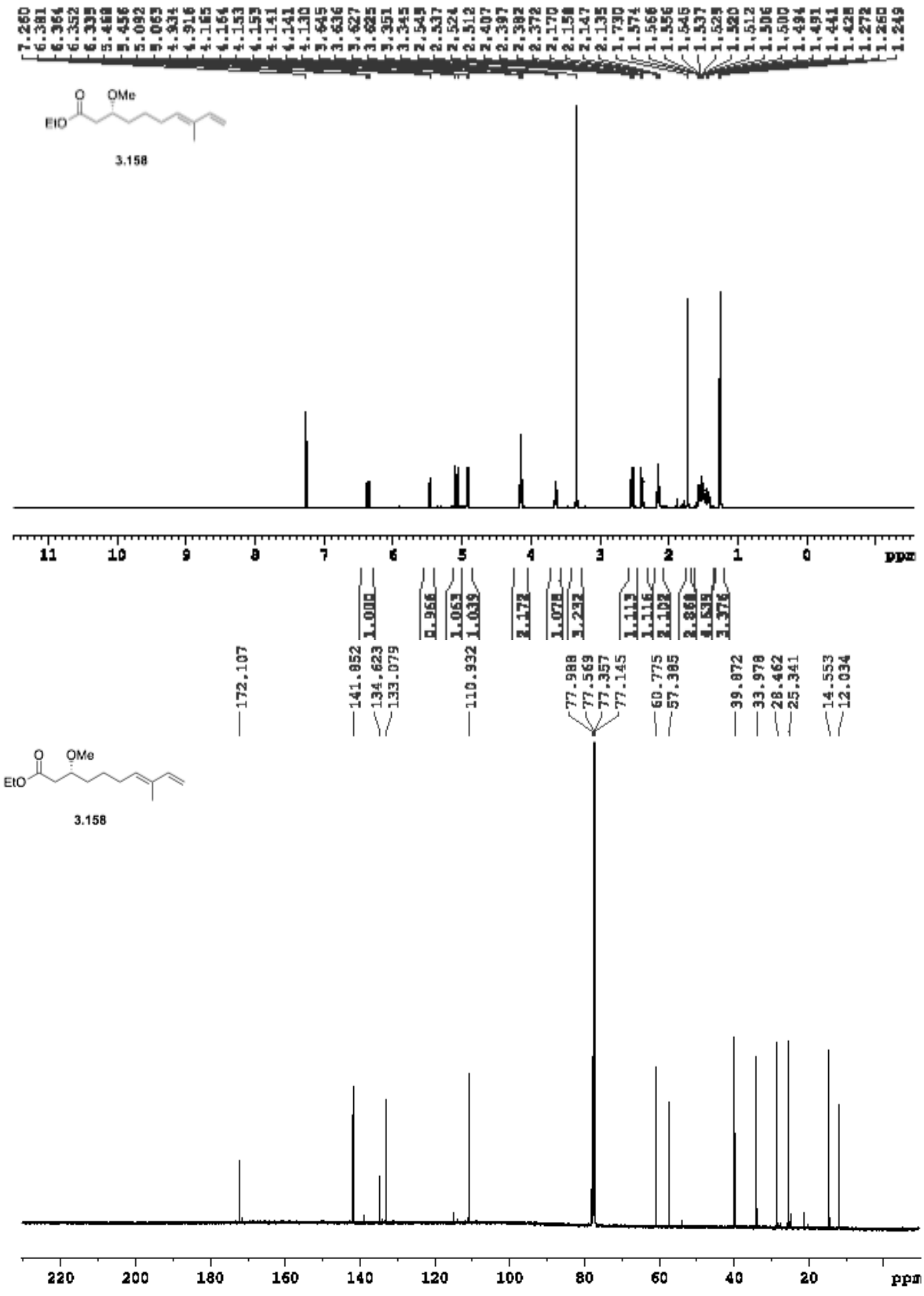

Figure A1.9. ^{1}H NMR (400 MHz, $CDCl_3$) and ^{13}C NMR (400 MHz, $CDCl_3$) of **3.178**.

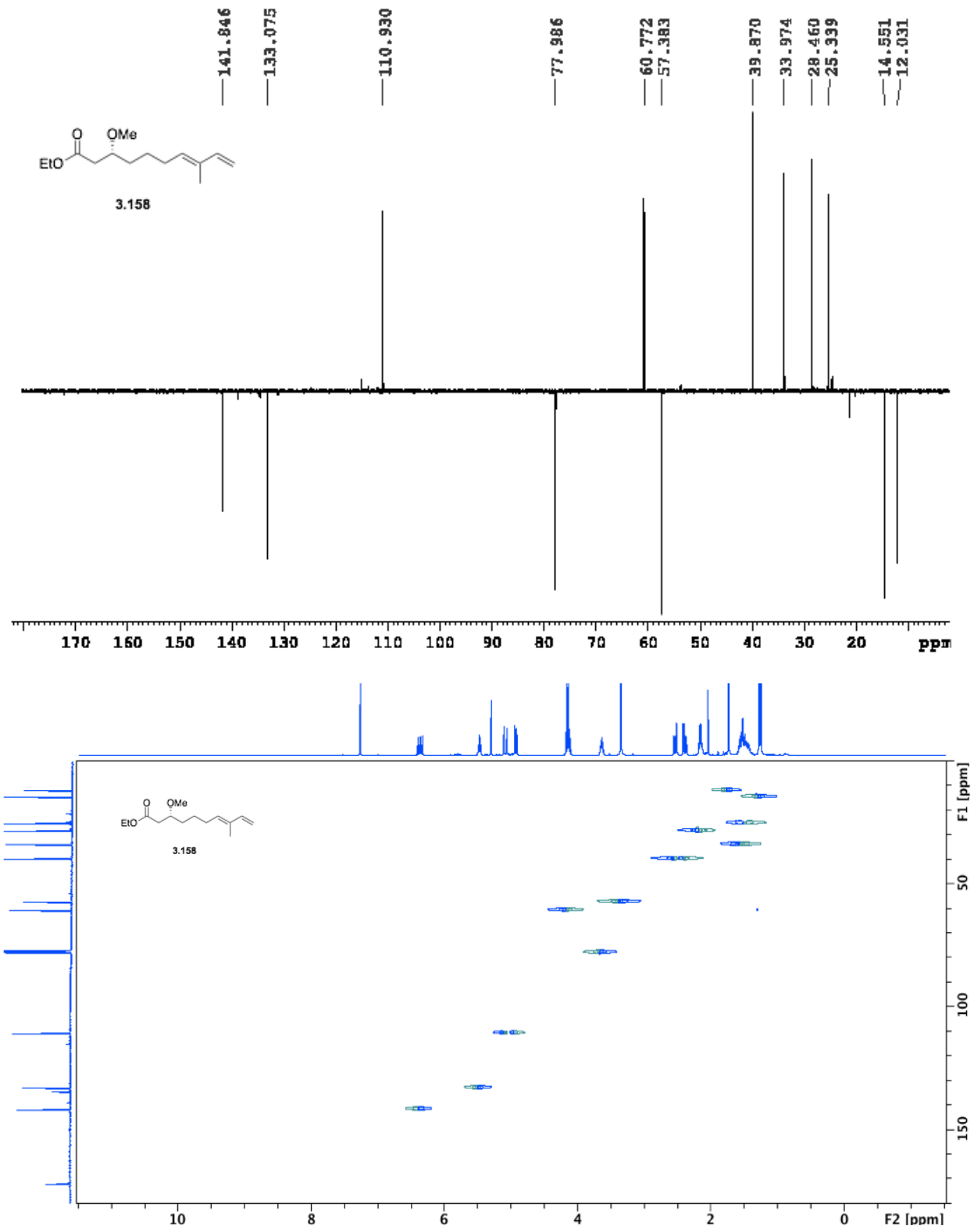

Figure A1.10. DEPT-135 (400 MHz, $CDCl_3$) and HSQC (600 MHz, $CDCl_3$) for **3.158**.

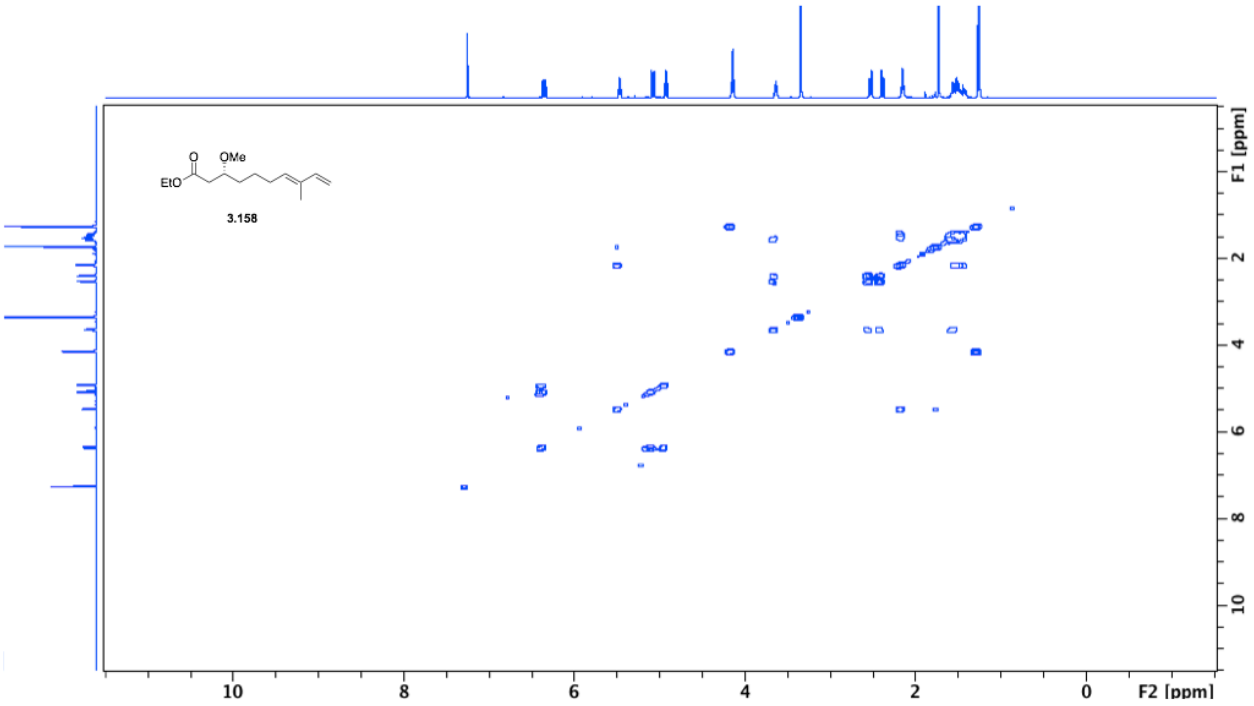

Figure A.11. COSY (600 MHz, $CDCl_3$) for **3.158**.

CHAPTER IV

A ROBUST PROCESS TOWARD THE TOTAL SYNTHESIS OF APOPTOLIDINONE C AND FORMATION OF APOPTOLIDIN C DISACCHARIDE

4.1 Synthesis of northern hemispheric apoptolidinone C fragments

At this point in our work, a robust and reliable route to the southwestern C11-C19 fragment **4.2** was established (Fig. 4.1), and the remaining objectives were to construct a synthetic process toward the northwestern C6-C10 fragment **4.1**, and produce gram quantities of each of the four fragments **4.1**-**4.4** to form the apoptolidin C aglycone **4.5**.

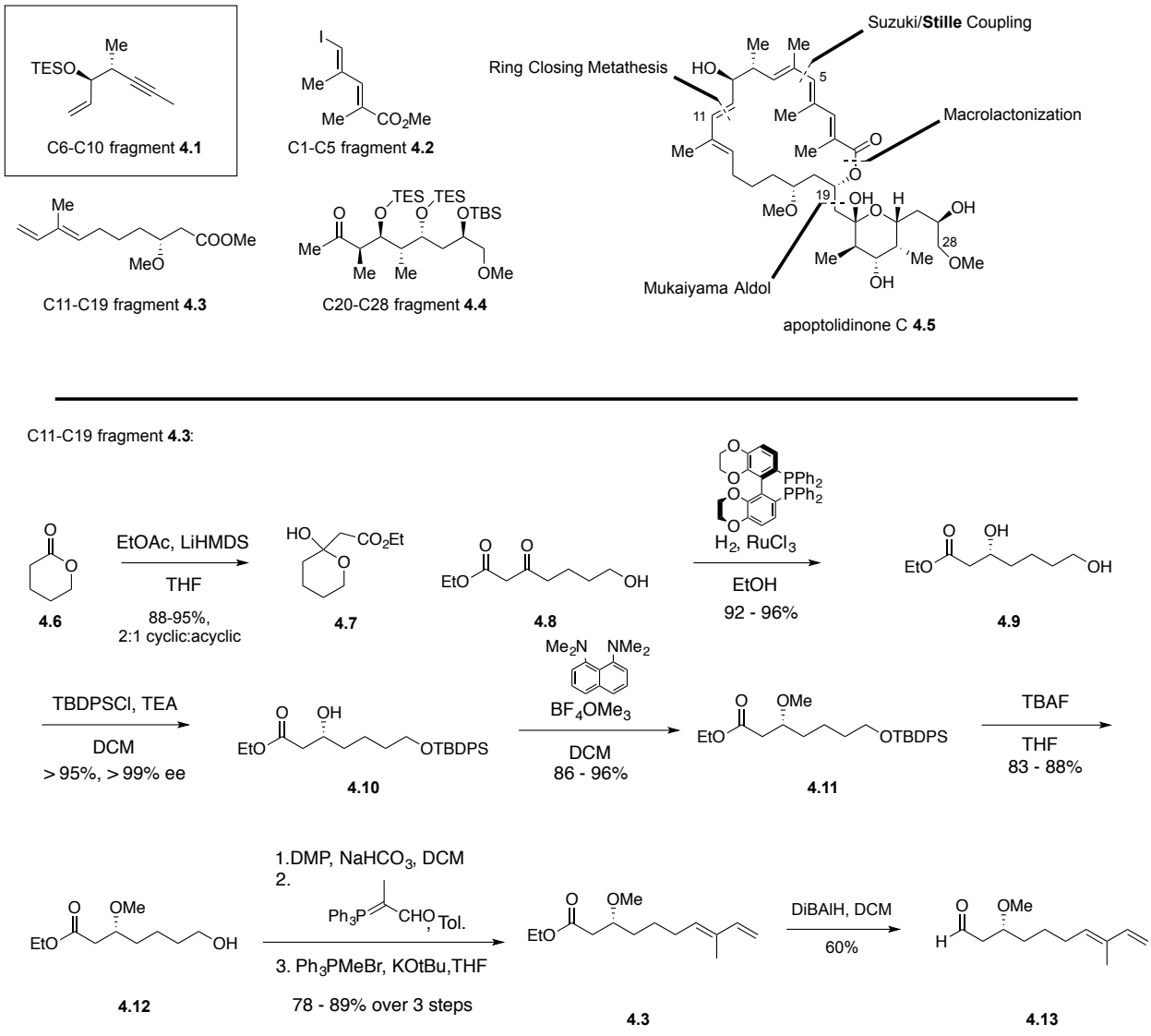

Figure 4.1. Retrosynthetic strategy to reach apoptolidinone C and synthesis of C11-C19 fragment.

Northern C6-C10 fragment **4.1** was modified from a synthetic route developed in unpublished work by Robert Davis of the Sulikowski group, used to create alkyne **4.17** for cross metatheses studies (Fig. 4.2).

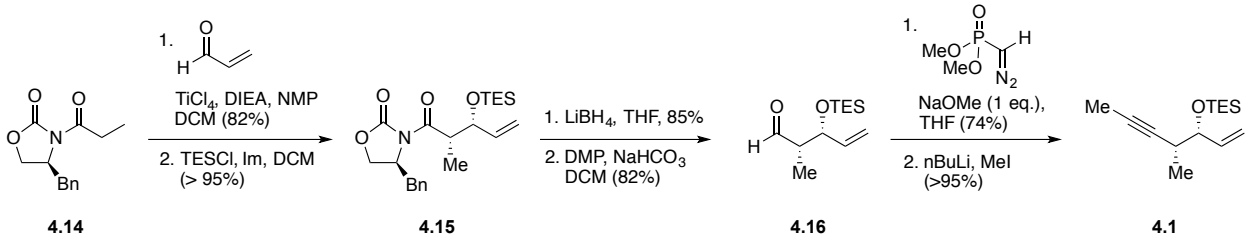

Figure 4.2. Davis' synthesis of alkyne C6-C11 fragment **4.17**.

In order to construct the necessary C6-C10 fragment **4.1**, selective hydrometallation of the alkyne rather than the alkene, would need to be implemented (Fig. 4.3). Unfortunately, studies completed by Davis and coworkers show that methods developed by Lipshultz and Lindley failed to produce vinyl stannane **4.17**. Efforts to functionalize the alkyne through radical and palladium-mediated hydrostannylation conditions also failed.

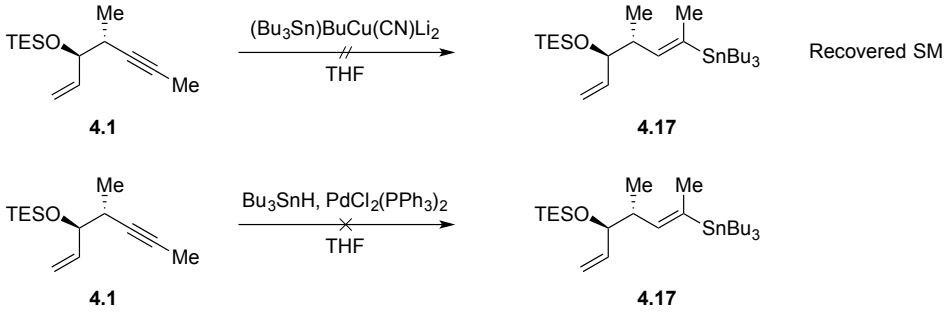

Figure 4.3. Davis' hydrostannylation of alkynyl fragment **4.1**.

In the interest of exploring new synthetically useful methods for the formation of complex targets, we sought to develop an alternative approach to vinyl stannane **4.17** directly from aldehyde **4.16**. Originally the route aimed to synthesize vinyl stanne **4.17** through alkynyl intermediate **4.1**, adding 3-4 steps. If we could instead utilize phosphonate **4.19**, a Horner-Waddsworth-Emmons-like olefination could be developed and employed toward the synthesis of C6-C10 fragment **4.17** (Fig. 4.4).

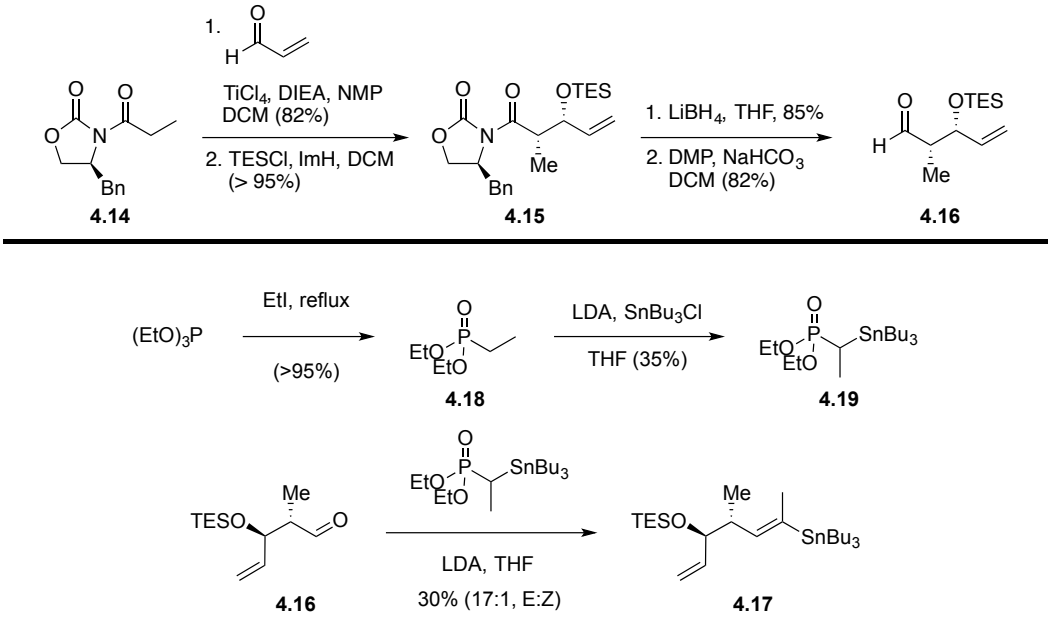

Figure 4.4. Modified HWE olefination to construct vinyl stannane **4.17**.

Gratifyingly vinyl stannane **4.17** could be produced from the aldehyde intermediate **4.16**, although in modest yield yet excellent geometric selectivity (30%, 17:1 E:Z, Fig. 4.4). Interestingly, lithium diisoporpyl amine (LDA) was not formed prior to deprotonation of the phosphonate **4.19**. Instead, a solution of diisopropylamine and phosphonate **4.19** were added simultaneously to a solution of n-butyl lithium (nBuLi) at -60 °C and then allowed to warm to ambient temperature over the course of 20 hours (Table 4.1). When not warmed to ambient temperature, starting material was recovered. At higher temperatures, decomposition was observed. In situ formation of LDA did not yield the desired vinyl stannane, presumably due to the steric bulk of both the base and the phosphonate. Treatment of phosphonate **4.19** with solely nBuLi or sodium hydride (NaH), followed by the addition of a model aldehyde (benzaldehyde) also failed to yield the desired vinyl stannane **4.20** (Table 4.2).

Table 4.1. Methodology toward modified HWE to synthesize vinyl stannane **4.17**.

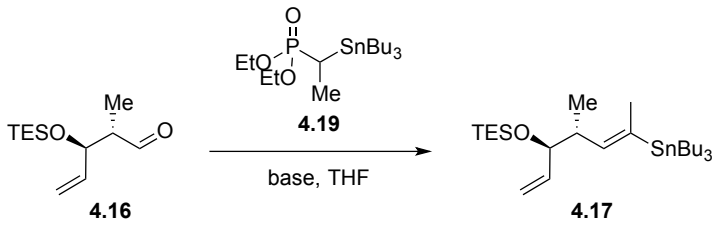

4.16 **4.17**

Base	Addition Conditions	Temperature	Time	Result
nBuLi, iPr_2NH	Simultenous addition to phosphonate @ -60 °C	-60 °C → RT	18 - 20 hr	30% (17:1, E:Z)
nBuLi, iPr_2NH	Simultenous addition to phosphonate @ -60 °C	-60 °C → 80 °C	8 hr	decomp.
nBuLi, iPr_2NH	Simultenous addition to phosphonate	-60 °C	18 - 20 hr	no reaction
nBuLi, iPr_2NH	Formation of LDA added to phosphonate @ -60 °C	-60 °C → RT	18 - 20 hr	no reaction

Table 4.2. Exploration of modified HWE olefination with model system.

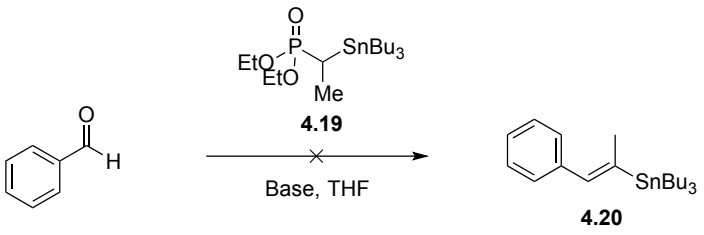

4.20

Base	Temperature	Time	Result
nBuLi	-60 °C	15 min	decomp.
nBuLi	-78 °C → -60 °C	30 min	decomp.
NaH	0 °C → RT	1 hr	no reaction

Next, Stille cross coupling was pursued between vinyl stannane **4.17** and vinyl iodide **4.2**. Despite in depth screening, the fully elaborated northern framework could not be produced (Fig 4.5). While reports have shown that more difficult Stille couplings can be

achieved with the addition of tetrabutylammonium phosphinate salt $[Ph_2PO_2][NBu_4]$. [2-6] This strategy was not pursued due to the prohibitive cost of the reagent.

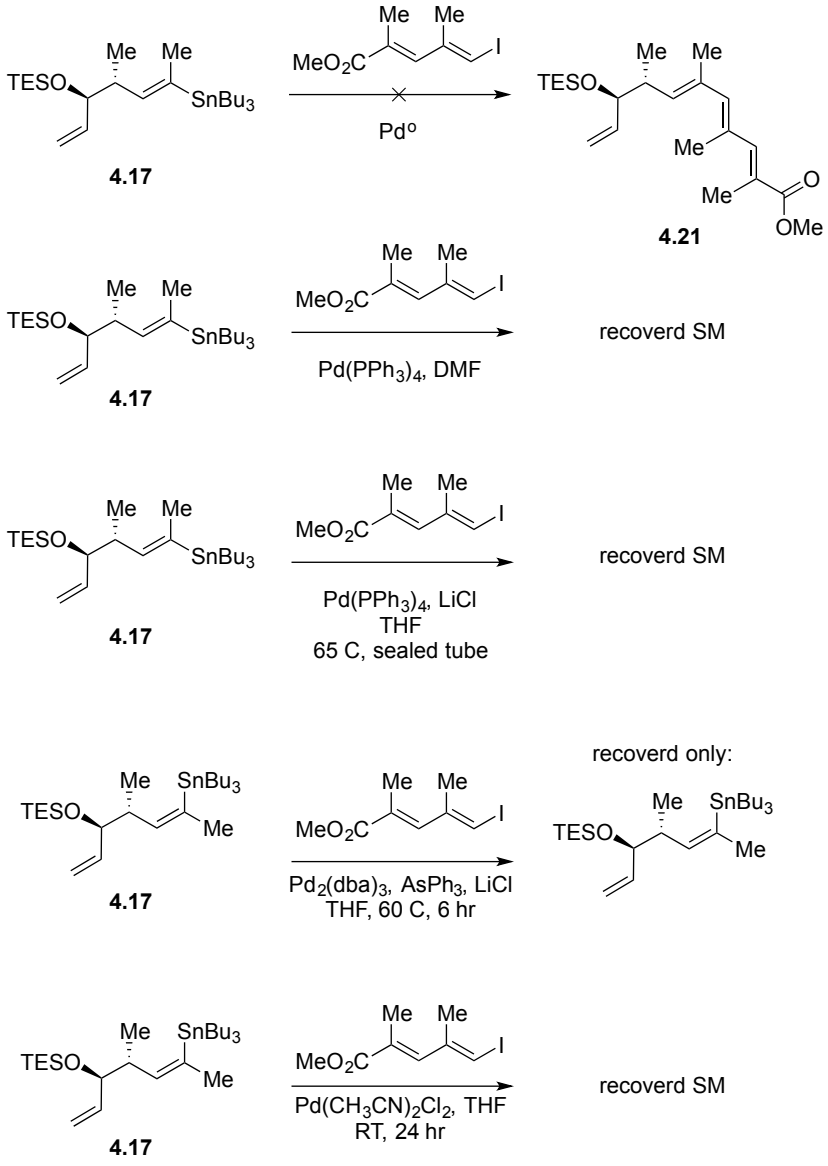

Figure 4.5. Attempts to construct apoptolidinone C northern hemisphere via Stille cross coupling.

Revisiting other possible disconnections, we thought to complete the northern framework of apoptolidinone C via Suzuki cross coupling from vinyl dibromide **4.22** (Fig. 4.6). In order to access vinyl dibromide **4.22**, modified Wittig olefination with triphenylphosphonium bromide could be used to intercept aldehyde **4.16**, in >95% yield.

Interestingly, standard Ramirez conditions [7] to form the vinyl dibromide from bromotriphenylphosphonium bromide and carbon tetrabromide resulted in the concomitant deprotection of the silyl ether followed by elimination and decomposition of the starting material.

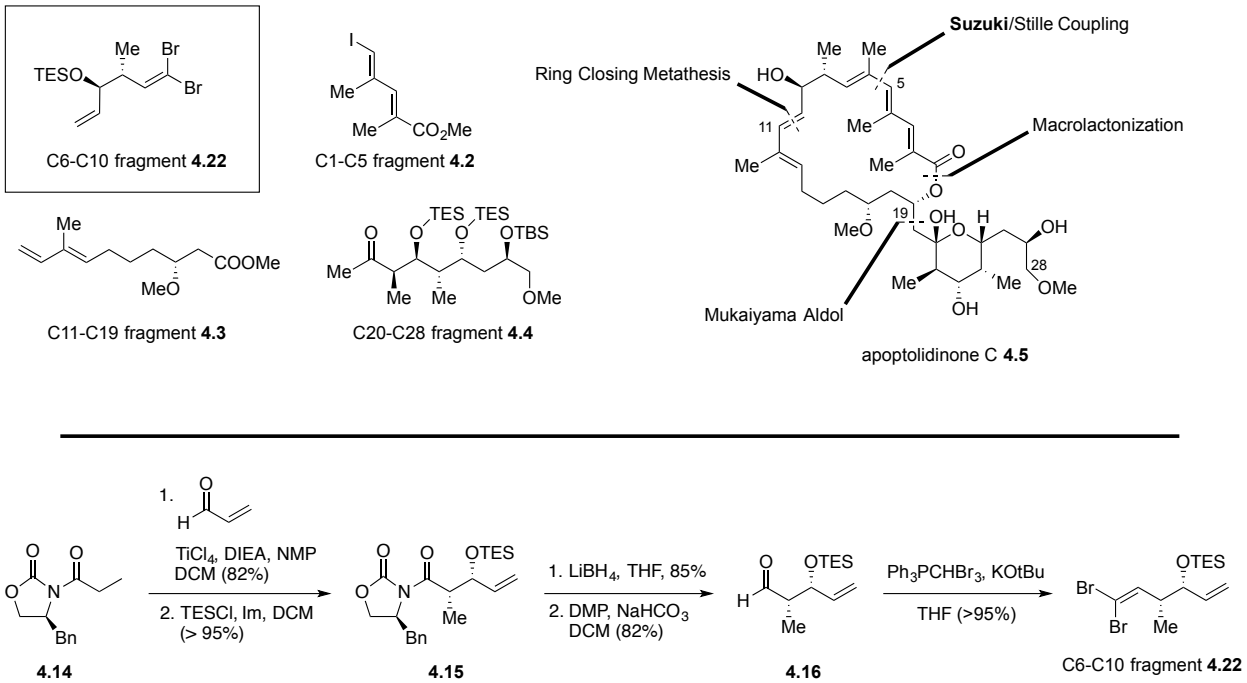

Figure 4.6. Revisiting retrosynthetic analysis of apoptolidinone northern hemisphere, synthesis of vinyl dibromide C6-C10 fragment **4.22**.

With vinyl dibromide **4.22** in hand, the C1-C5 fragment **4.2** was synthesized according to Sulikowski and coworkers original report, [8] beginning with diethyl 2-methyl malonate **4.23** (Fig.4.7). Malonate **4.23** was subjected through alkylation conditions with iodoform and treated with three equivalents of potassium hydroxide to furnish the desired vinyl iodide **4.25** by simultaneous saponification, decarboxylation, and elimination. Carboxylic acid intermediate **4.25** was then reduced, oxidized and homologated with phosphonate **4.26** to give the desired C1-C5 fragment **4.2**.

Figure 4.7. Synthesis of northeastern C1-C5 fragment **4.2**.

Suzuki cross coupling from the vinyl iodide to vinyl Bpin boronate gave the coupling partner for northern hemispheric elaboration (Fig. 4.8). Cross coupling between northern fragments C1-C5 **4.2** and C6-C10 **4.22** proceeded smoothly in 42% yield to give vinyl bromide **4.27**. Completion of the C1-C10 fragment requires a second cross-coupling with a methyl-metal reagent. This could be completed through additional Suzuki (Me-BBN, Me-$B(OH)_2$), Negishi (Me_2Zn), or cuprate coupling.

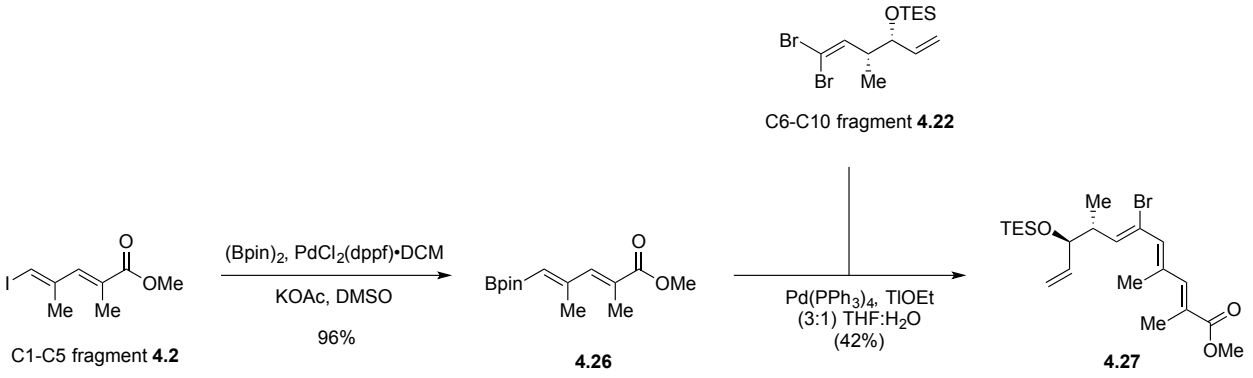

Figure 4.8. Synthesis of northern hemisphere of apoptolidinone C.

4.2 Synthesis of southern hemispheric apoptolidinone C fragments

The synthesis of the southern hemisphere of apoptolidinone C **4.5**, the synthesis of C20-C28 fragment **4.4** was first approached employing the highly convergent route described by Koert and coworkers (Fig. 4.9). [9] However, in work conducted by Robert Davis

and Binhua Li of the Sulikowski group, the β-keto-imide **4.31** used to synthesize the C20-C28 fragment **4.34**, underwent a substantial amount of epimerization at the α-carbon.

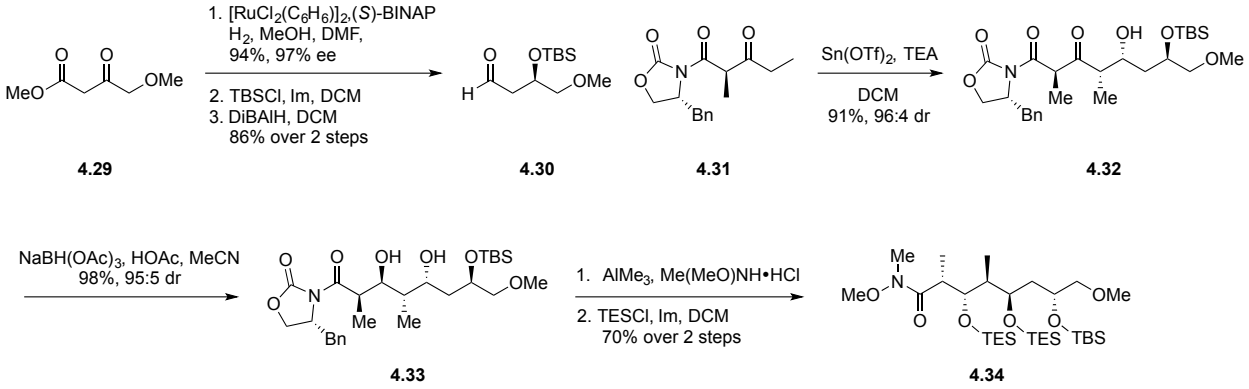

Figure 4.9. Koert's synthesis of C20-C28 fragment **4.34** of apoptolidinone A.

Attention was turned toward an iterative titanium-mediated aldol assembly beginning with methyl 4-methoxy-3-oxobutanoate **4.35** (Fig. 4.10). β-keto ester **4.35** was subjected through Noyori hydrogenation conditions to furnish the β-hydroxy ester **4.36**. β-hydroxy ester **4.36** was then protected as a tert-butyl dimethyl silyl (TBS) ether, semi-reduced to aldehyde **4.38** and subjected through its first titanium-mediated aldol with auxillary **4.39**. The resulting aldol adduct was triethyl silyl (TES) protected, reduced and oxidized to give aldehyde **4.41**. Aldehyde **4.41** was submitted through a second titanium-mediated aldol with auxillary **4.42**. Aldol adduct **4.43** was treated with the HCl salt of *N*,*O*-Dimethylhydroxylamine and trimethyl aluminum to produce the Weinreb salt and then TES protected. Treatment of **4.44** with methyl magnesium chloride gave the final methyl ketone **4.4**, all in good yield and diastereoselectivity.

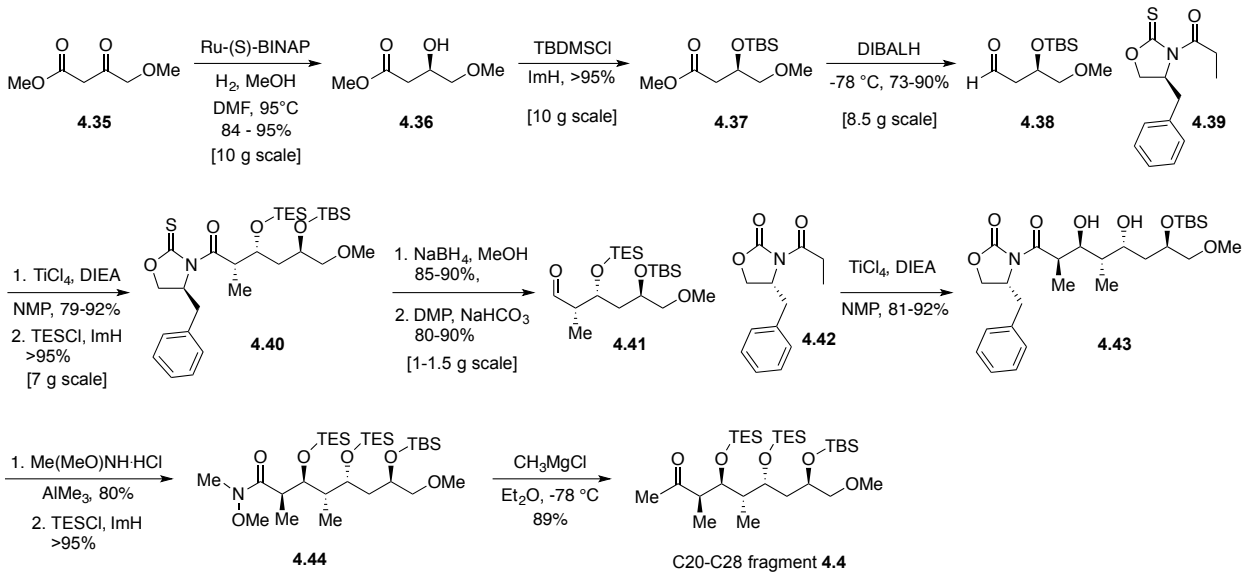

Figure 4.10. Synthesis of southwestern C20-C28 fragment **4.4**.

It is interesting to note, that for the first titanium-mediate aldol between aldehyde **4.38** and auxillary **4.39**, depending on the type of auxillary, differing diastereoselectivity can be achieved. Oxazolidinone **4.45**, thiazolidinthione **4.46**, and oxazolidinthione **4.39** auxiliaries were examined. Oxazolidinthione **4.39** gave the best overall consistent yield and diastereoselectivity, under titanium-mediated aldol conditions with aldehyde **4.38**. The reason for this selectivity based on auxiliary is most likely due to binding with the titanium metal during the Zimmerman Traxler transition state. [10]

Table 4.3. Exploration of first aldol in synthesis of C20-C28 apoptolidinone C fragment **4.4**.

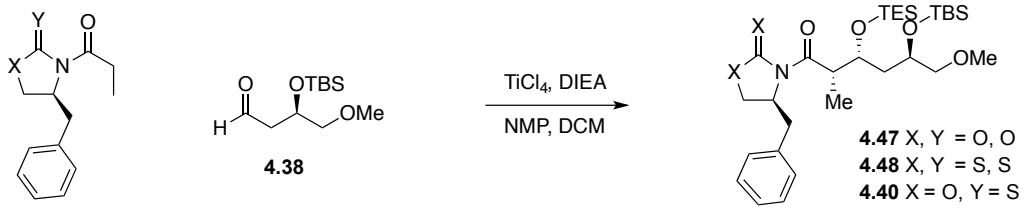

Auxiliary	% Yield	Diastereoselectivity (dr)
4.45 X, Y = O, O	46 - 67	9:1
4.46 X, Y = S, S	52	>95:5
4.39 X = O, Y = S	72	> 95:5

The second similarly conducted aldol in constructing the C20-C28 fragment **4.4** (Fig. 4.10) is not as sensitive to the identity of the auxiliary as can be evidenced by the use of commercially available oxazolidinone auxillary **4.42**, in great yield and diastereoselectivity, as this is a matched case in terms of substrate control in the auxiliary **4.42** and chiral aldehyde **4.41**. In addition, oxazolidinthione **4.39** was used as an auxiliary in the first aldol to synthesize aldol adduct **4.40** due to its more efficient and mild cleavage as compared to the oxazolidinone auxiliary **4.47** (Fig. 4.11).

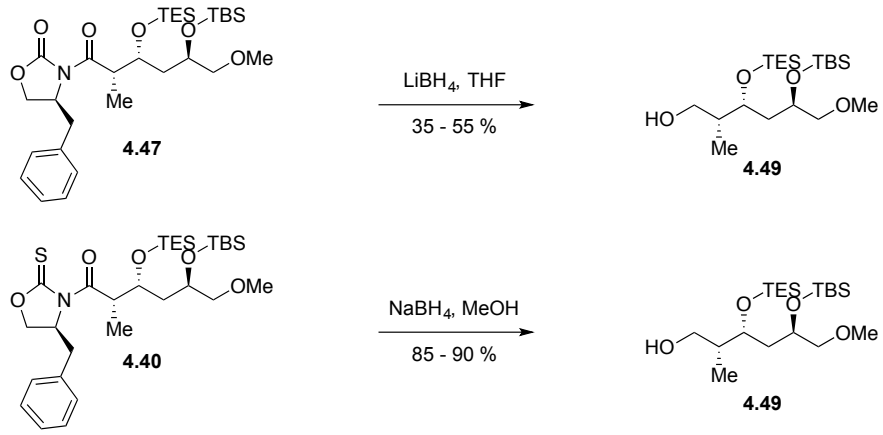

Figure 4.11. Comparison of conditions for auxiliary removal of aldol adduct variants.

Having developed a route toward C11-C19 fragment **4.3** (Fig. 4.12), semi-reduction using diisobutylaluminum hydride(DIBAlH) arrived at desired aldehyde **4.13** in 60% yield.

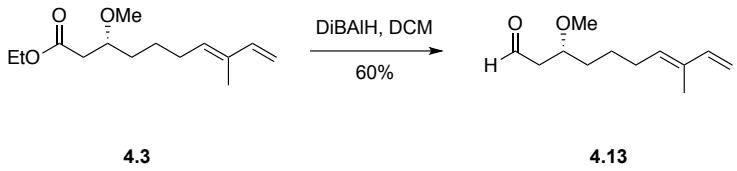

4.3 **4.13**

Figure 4.12. Semi-reduction of β-methoxy ester **4.3**.

4.3 Toward the total synthesis of apoptolidinone C

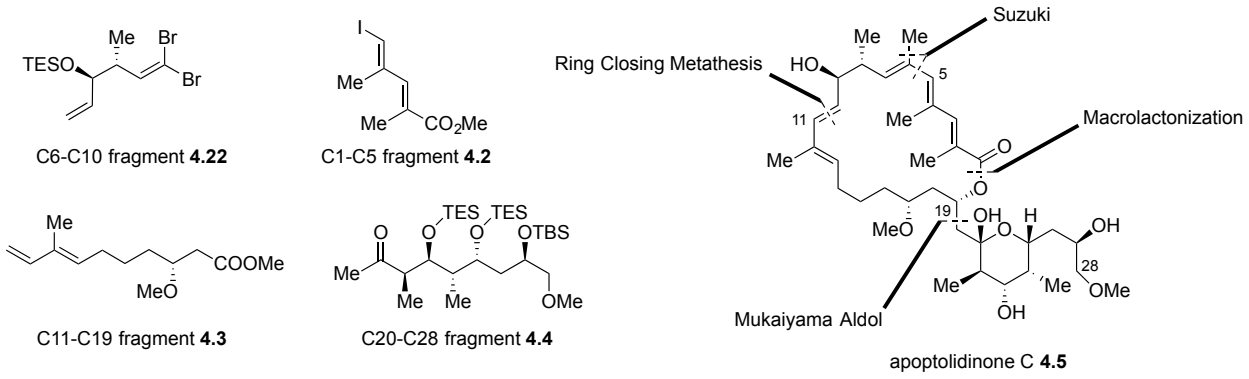

Figure 4.13. Summary retrosynthetic analysis of apoptolidinone C construction.

In summary, an efficient route toward each of the four apoptolidinone C fragments **4.2**-**4.4** and **4.22** were developed (Fig. 4.13). Gram quantities of each of the four fragments have been produced and efforts will be made toward the full elaboration of the northern hemisphere **4.53** of apoptolidinone C from vinyl bromide **4.51** through methyl coupling screening and saponification (Fig. 4.14). Synthesis of southern hemisphere **4.55** via Mukaiyama aldol between the semi-reduced form of **4.3** to give aldehyde **4.56** and enol silyl ether **4.54**, formed from methyl ketone **4.4**. Yamaguchi esterification would give the

linear framework **4.56** and RCM could furnish the full macrolide core. Global deprotection and simultaneous hemi-ketal formation would arrive at the final apoptolidinone C target **4.5**.

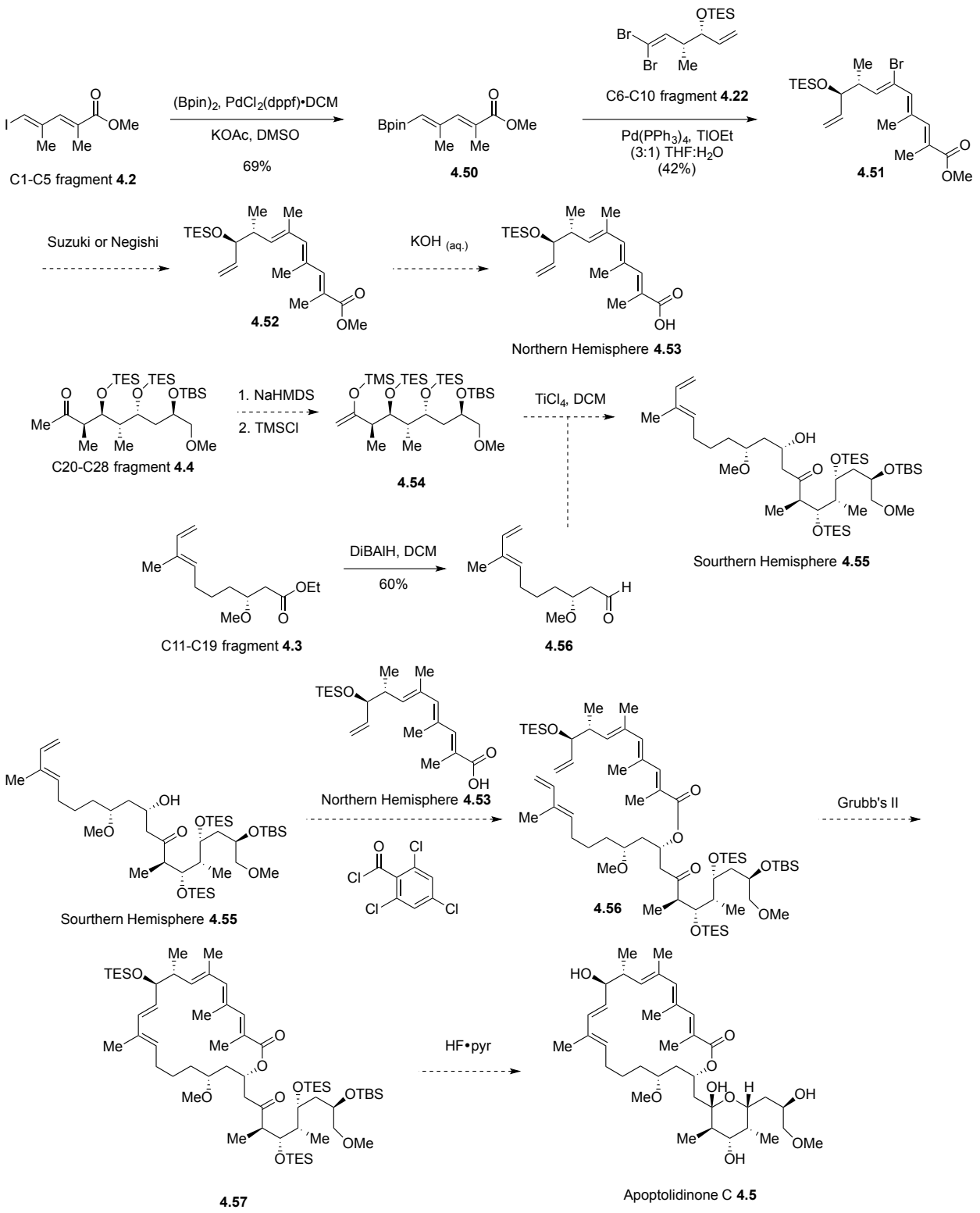

Figure 4.14. Final synthetic strategy to reach apoptolidinone C.

4.4 Conclusion

In summary, we have completed the synthesis of each of the necessary fragments for the completion of apoptolidinone C. This highly convergent route should produce the aglycone in large quantities allowing for future precursor directed biosynthesis to access every glycosylation state of apoptolidin **4.5** and **4.58**-**4** (Fig. 4.17).

4.5 Experimental methods

General Procedure. All glassware used for non-aqueous reactions was flame dried under vacuum. Reactions conducted at ambient temperature were run at approximately 23 °C unless otherwise noted. Reactions were monitored by analytical thin-layer chromatography performed on Analtech silica gel GF 250 micron plates. The plates were visualized with UV light (254 nm) and either potassium permanganate, ceric ammonium molybdate, or *p*-anisaldehyde followed by charring with a heat-gun. Flash chromatography utilized 230-400 mesh silica from Sorbent Technologies or Silica RediSep Rf flash columns on a CombiFlash Rf automated flash chromatography system. Solvents for extraction, washing and chromatography were HPLC grade. Nuclear magnetic resonance (NMR) spectra were acquired on either a 300 MHz Bruker DPX-300 FT-NMR, a 400 MHz Bruker AV-400 FT-NMR, or 500 MHz Bruker DRX-500 FT-NMR Spectrometer at ambient temperature. ^{1}H and ^{13}C NMR data are reported as values relative to $CDCl_3$.^{1}H chemical shifts are reported in δ values in ppm. Data are reported as follows: chemical shift, multiplicity (s = singlet, d = doublet, t = triplet, q = quartet, br = broad, m = multiplet), integration, coupling constant (Hz). ^{13}C chemical shifts are reported in δ values in ppm.

Low resolution mass spectra were obtained on an Agilent 1200 series 6130 mass spectrometer with electrospray ionization. High resolution mass spectra were recorded on a Waters Q-TOF API-US.. Analytical HPLC was performed on an Agilent 1200 series with UV detection at 214 nm and 254 nm along with ELSD detection. Preparative HPLC was conducted on a Gilson 215 Liquid Handler HPLC system using Gemini-NX 50 x 20 mm column. Yields were reported as isolated, spectroscopically pure compounds.

Materials. All reagents and solvents were commercial grade and purified prior to use when necessary. All reagents unless otherwise stated were purchased from Sigma Aldrich or VWR International. All reactions were performed under argon atmosphere unless otherwise stated. Diethyl ether (Et_2O) and dichloromethane (CH_2Cl_2) were dried by passage through a column of activated alumina using an MBraun MB-SPS dry solvent system. Tetrahydrofuran (THF) was distilled from sodium with benzophenone as indicator prior to use.

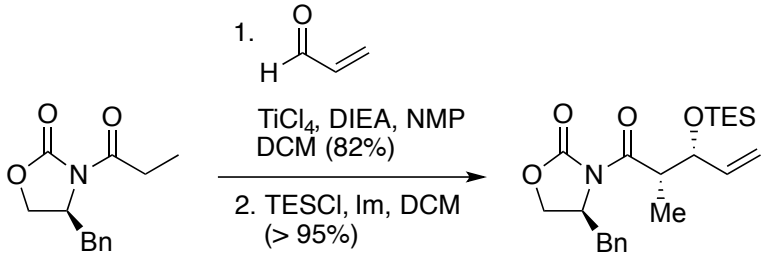

4.14 **4.15**

(S)-4-benzyl-3-((2S,3R)-2-methyl-3-((triethylsilyl)oxy)pent-4-enoyl)oxazolidin-2-one (4.15): To a solution of (S)-4-benzyl-3-propionyloxazolidin-2-one **4.14** (3.00 g, 12.86 mmol) in DCM (535 mL) at 0 ˚C, was added a solution of titanium tetrachloride (14.4 mL, 1M in DCM, 14.4 mmol) dropwise. The resulting yellow slurry was stirred for 15 min and freshly distilled diispropylethylamine (2.3 mL, 13.1 mmol). The mixture was allowed to stir for 40 min and N-methylpyrrolidinone (1.3 mL, 12.8 mmol) was added and allowed to stir for 5 min. A solution of freshly distilled acrolein (0.961 mL, 14.4 mmol) in DCM (5 mL) was added and the mixture was allowed to stir for an additional 1.5 h. The reaction was then quenched with sat. $NH_4Cl_{(aq.)}$ and diluted with water and DCM. The layers were separated and the crude product was extracted from the aqueous with DCM (3X). The combined organic extracts were washed with brine, dried ($MgSO_4$), filtered, and concentrated. The resulting residue was then purified by column chromatography (Hex → 20% EtOAC/Hex) to give the syn aldol adduct (S)-4-benzyl-3-((2S,3R)-3-hydroxy-2-methylpent-4-enoyl)oxazolidin-2-one as a yellow oil (3.3 g, 87%). ^{1}H NMR (400 MHz, $CDCl_3$): δ = 7.18-7.32 (m, 5H), 5.84 (m, 1H), 5.37 (d, J = 17.24, 1H), 5.23 (d, J = 10.6 Hz, 1H), 4.70 (m, 1H), 4.50 (br. S, 1H), 4.19 (m, 2H), 3.87 (m, 1H), 3.26 (d, J = 10.4 Hz, 1H), 2.79 (m, 1H), 1.25 (d, J = 7.0 Hz, 3H*);* ^{13}C NMR (100 MHz, $CDCl_3$): δ = 176.35, 153.08, 137.42, 135.01, 129.36, 128.87, 127.32, 116.12, 72.61, 66.15, 55.07, 42.50, 37.66, 11.05.

To a solution of (S)-4-benzyl-3-((2S,3R)-3-hydroxy-2-methylpent-4-enoyl)oxazolidin-2-one (1.34 g, 4.60 mmol) in DCM (34 mL, 0.15 M), was added triethylsilyl chloride (2.32 mL, 13.8 mmol) followed by imidazole (940 mg, 13.8 mmol). The mixture was stirred for 18 h

and quenched with sat. $NH_4Cl_{(aq.)}$. The mixture was diluted with water and DCM and the layers were separated. The crude product was extracted from the aqueous with DCM (3X) and the combined organic extracts were washed with brine, dried ($MgSO_4$), filtered, and concentrated. The resulting residue was then purified by column chromatography (Hex → 20% EtOAc/Hex) to give **4.15** as a colorless oil (1.83, >95%). ^{1}H NMR (400 MHz, $CDCl_3$): δ = 7.15-7.25 (m, 5H), 5.79 (m, 1H), 5.14 (d, J = 17.2, 1H), 5.04 (d, J = 10.36, 1H), 4.53 (ddd, 1H), 4.24 (t, 1H), 4.06 (m, 2H), 3.95 (m, 1H), 3.18 (d, J = 16.48 Hz, 1H), 2.69 (m, 1H), 1.14 (d, 3H), 0.86 (m, 9H), 0.51 (m, 6H), ; ^{13}C NMR ($CDCl_3$, 100 MHz): δ = 174.67, 153.16, 139.09, 135.34, 129.38, 128.85, 127.24, 115.73, 75.45, 65.89, 55.57, 43.94, 37.78, 29.62, 12.72, 6.70, 4.76.

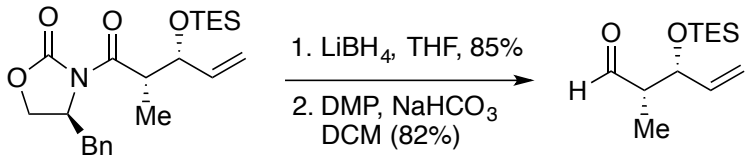

4.15 **4.16**

(2S,3R)-2-methyl-3-((triethylsilyl)oxy)pent-4-enal (4.16): To a solution of (S)-4-benzyl-3-((2S,3R)-2-methyl-3-((triethylsilyl)oxy)pent-4-enoyl)oxazolidin-2-one **4.15** (700 mg, 1.74 mmol) in THF (16 mL) stirring at 0 °C was added $LiBH_4$ (3.47 mL, 2.0 M in THF, 1.74 mmol) dropwise. The mixture was allowed to warm to room temperature and stirred for 5 h. The reaction was then cooled to 0 °C and quenched by dropwise addition of water. The aqueous layer was extracted with diethyl ether (3 x 10 mL). The combined organic extracts were dried (MgSO4), filtered, and concentrated. The residue was purified by flash chromatography (8:1 hexanes/ethyl acetate) to give (2R,3R)-2-methyl-3-((triethylsilyl)oxy)pent-4-en-1-ol (340 mg, 85%) as a colorless oil. 1H NMR (400 MHz,

CDCl3): δ = 5.88 (m, 1H), 5.24 (d, *J* = 17.3 Hz, 1H), 5.19 (d, *J* = 10.5 Hz, 1H), 4.24 (t, 1H), 3.65 (m, 1H), 3.49 (m, 1H), 3.02 (br s, 1H), 2.01 (m, 1H), 0.94 (m, 9H), 0.78 (d, 3H), 0.59 (m, 6H); 13C NMR (CDCl3, 100 MHz): δ = 137.36, 115.99, 65.69, 40.64, 12.37, 6.66, 4.68.

To a solution of (2R,3R)-2-methyl-3-((triethylsilyl)oxy)pent-4-en-1-ol (100 mg, 0.434 mmol) in DCM (8.7 mL, 0.05 M), was added a mixture of Dess-Martin periodinane (276 mg, 0.651 mmol) and sodium bicarbonate (31 mg, 0.373 mmol). The mixture was stirred for 1 h and quenched with sat. $Na_2SO_{3\ (aq.)}$. The reaction mixture was diluted with water and DCM and the layers were separated. The crude product was extracted from the aqueous with DCM (3X) and the combined organic extracts were washed with brine, dried ($MgSO_4$), filtered, and concentrated. The resulting residue was then purified by column chromatography (Hex → 10 % EtOAc/Hex) to give **4.16** as a colorless oil (113 mg, > 95%). ^{1}H NMR (400 MHz, $CDCl_3$): *δ* = 9.76 (d, *J* = 1.3 Hz, 1H), 5.82 (m, 1H), 5.26 (d, 1H), 5.17 (d, 1H), 4.52 (t, 1H), 2.47 (m, 1H), 1.05 (d, J = 6.8 Hz, 3H), 0.91 (m, 9H), 0.58 (m, 6H); ^{13}C NMR ($CDCl_3$, 100 MHz): δ = 204.57, 138.25, 115.89, 73.68, 52.48, 8.39, 6.65, 4.78.

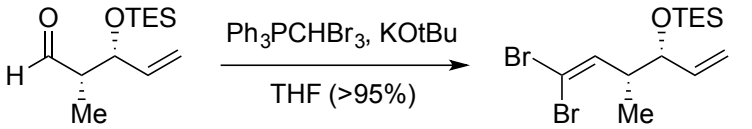

4.16 C6-C10 fragment **4.22**

(((3R,4R)-6,6-dibromo-4-methylhexa-1,5-dien-3-yl)oxy)triethylsilane (4.22): To a suspension of (dibromomethyl)triphenylphosphonium bromide (1.49 g, 2.89 mmol) in THF

(2.9 mL, 1M), was added solid potassium t-butoxide (181 mg, 1.62 mmol) at RT. The mixture was allowed to stir for 1 min and cooled to 0 °C. The mixture gold-brown suspension was stirred for an additional 15 min and a solution of (2S,3R)-2-methyl-3-((triethylsilyl)oxy)pent-4-enal **9** (60.01 mg, 0.263 mmol) in THF (10 mL) was added dropwise. The remaining residue was dissolved in THF (3 mL) and the resulting solution was added dropwise to the dark orange/brown suspension. The reaction was stirred at 0 ˚C for 3 h and quenched with brine. The mixture was diluted with water and Et_2O and the layers were separated. The crude product was extracted from the aqueous layer with Et_2O (3X). The combined organic extracts were washed with brine, dried ($MgSO_4$), filtered, and concentrated. The resulting residue was then purified through a plug of silica gel and washed with hexanes (3X), followed by DCM (3X) to give **4.22** as a light orange oil (100.41 mg, > 95%).

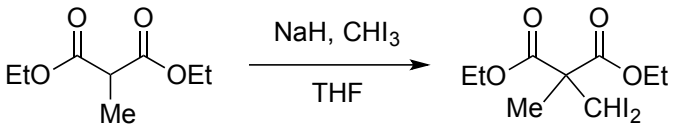

4.23 **4.24**

diethyl 2-(diiodomethyl)-2-methylmalonate (**4.24**): To a suspension of sodium hydride (2.3 g, 58 mmol, 60% dispersion) in ether (70 mL) was added diethyl methylmalonate (9.9 mL, 57 mmol) dropwise over 30 min via addition funnel. The resulting thick white slurry was refluxed for 2.5 h before iodoform (22.4 g, 57 mmol) was added. The reaction mixture was refluxed for an additional 21 h and cooled to 0°C. HCl (20 mL, 10% aqueous) was added and the mixture was stirred for 10 min. The aqueous layer was separated and

extracted with ether (2 x 200 mL). The combined organic layers were dried ($MgSO_4$), filtered, and concentrated, and purified by simple distillation (128-148°C) to give **4.24** as a colorless liquid (22.4 g, 89%). Observed spectral properties were identical with those previously reported. [8]

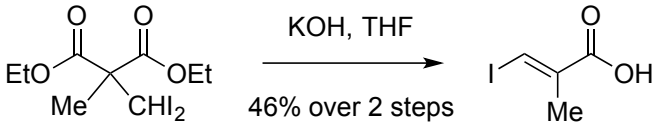

4.24 **4.25**

(E)-3-iodo-2-methylacrylic acid (4.24): To a solution of diethyl 2-(diiodomethyl)-2-methylmalonate **4.24** (22.4 g, 51 mmol) in EtOH-H_2O (60 mL, 3:1) was added KOH (8.8 g, 156 mmol). The reaction mixture was refluxed for 24 h and cooled to ambient temperature. The reaction mixture was concentrated and solid K_2CO_3 (30 mL, 10%) was added. The layers were separated and the crude product was extracted from the aqueous layer with DCM (2X) and then acidified with concentrated HCl (pH = 4). The acidified aqueous layer was extracted with CH_2Cl_2 (7X). The combined organic layers were dried ($MgSO_4$), filtered, and concentrated to give **4.25** as a brown solid (10.4 g, 96%). Observed spectral properties were identical with those previously reported. [8]

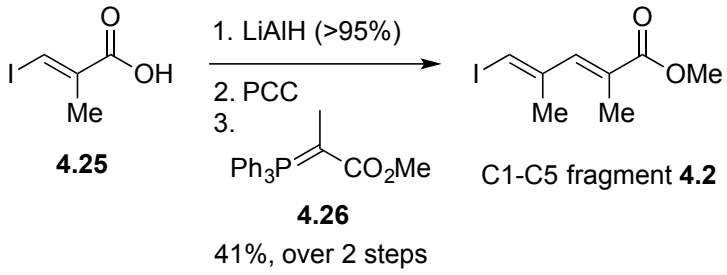

Methyl (2E,4E)-5-iodo-2,4-dimethylpenta-2,4-dienoate (4.2): To a solution of (E)-3-iodo-2-methylacrylic acid **4.24** (10.4 g, 49 mmol) in THF (80 mL) at 0°C was slowly added lithium aluminumhydride (1.86 g, 49 mmol) via a solid addition funnel over 20 min. The mixture was warmed to ambient temperature and stirred for 3 h then cooled to 0°C. A saturated solution of Na_2SO_4 (30 mL) was added slowly, followed by ether (50 mL) and H_2SO_4 (70 mL, 2.0 M). The aqueous layer was separated and extracted with DCM (2X). The combined organic layers were washed with K_2CO_3 (20 mL, 10%) and dried ($MgSO_4$), and concentrated. The resulting residue was purified by column chromatography (Hex -> 25% EtOAc/Hex) to give (E)-3-iodo-2-methylprop-2-en-1-ol as a pale yellow oil (9.3 g, 96%). Observed spectral properties were identical with those previously reported. [8]

To a solution of (E)-3-iodo-2-methylprop-2-en-1-ol (9.3 g, 47 mmol) in DCM (350 mL) at 0 °C was added Celite® (21 g) and pyridinium chlorochromate (15 g, 70 mmol). The mixture was stirred at 0 °C for 3.5 h and filtered through a bed of silica gel, rinsed with Et_2O (500 mL), and concentrated to give a volatile brown crude oil. To a solution of the crude oil in DCM (50 mL) at 0 °C was added Ph3P=C(CH3)COOMe (10.6 g, 30 mmol). The solution was stirred at ambient temperature for 1.5 h and concentrated. The resulting residue was

filtered through a bed of silica gel and rinsed with ether (500 mL) and the combined filtrate concentrated. The resulting residue was purified by column chromatography (5% Et_2O/petroleum ether) to give **4.2** as a pale yellow oil (5.1 g, 41%). Observed spectral properties were identical with those previously reported.

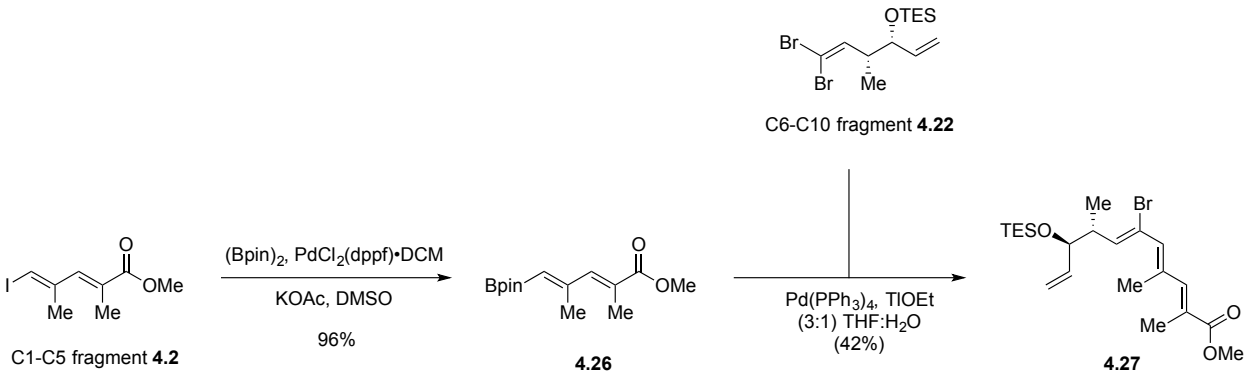

methyl (2E,4E)-2,4-dimethyl-5-(4,4,5,5-tetramethyl-1,3,2-dioxaborolan-2-yl)penta-2,4-dienoate (4.26): To a solution of methyl (2E,4E)-5-iodo-2,4-dimethylpenta-2,4-dienoate **4.2** (100 mg, 0.376 mmol) in DMSO (1.3 mL, 0.3 M), was added bis(pinacolato)diboron (286 mg, 1.13 mmol), followed by $PdCl_2$(dppf) (8.3 mg, 0.011 mmol) and potassium acetate (111 mg, 1.13 mmol). The mixture was heated to 85 °C and stirred for 35 min. The reaction mixture was cooled to ambient temperature and diluted with Et_2O and water. The layers were separated and the organic layer was washed with water (2X). The combined organic extracts were dried ($MgSO_4$), filtered, and concentrated. The resulting residue was then purified by column chromatography (Hex → 10 %

EtOAc/Hex) to give **4.26** as a colorless-white amorphous solid (94.74 mg, 95%). Observed spectral properties were identical with those previously reported. [8, 12]

Methyl (2E,4E,6Z,8R,9R)-6-bromo-2,4,8-trimethyl-9-((triethylsilyl)oxy)undeca-2,4,6,10-tetraenoate (4.27): To a solution of (((3R,4R)-6,6-dibromo-4-methylhexa-1,5-dien-3-yl)oxy)triethylsilane (46 mg, 0.119 mmol) and methyl (2E,4E)-2,4-dimethyl-5-(4,4,5,5-tetramethyl-1,3,2-dioxaborolan-2-yl)penta-2,4-dienoate (95 mg, 0.357 mmol) in (3:1) THF/H_2O (0.63 mL, 0.19 M, 0.47 mL/0.16 mL) at ambient temperature, was added $Pd(PPh_3)_4$ (14 mg, 0.012 mmol). The suspension was stirred for 5 min and TlOEt (15 µL, 0.21 mmol). The suspension was stirred for an additional 40 min and then diluted with Et_2O (1.2 mL) and $NaHSO_4$ (1 mL). The layers were shaken and separated. The organic portion was filtered through a Celite® plug and then washed with brine, dried ($MgSO_4$), filtered, and concentrated. The resulting residue was then purified by column chromatography (10% Tol/Hex with 1% EtOAc → 5% EtOAc/Hex) to give 4.27 as a light yellow oil (22.2 mg, 42%). ^{1}H NMR (600 MHz, $CDCl_3$) δ7.12 (s, 1H), 6.08 (s, 1H), 5.90-5.82 (m, 1H), 5.70 (dd, *J* = 1.07, 9.08 Hz), 5.16 (overlapping dd, 2H), 4.10 (apparent t, *J* = 5.57 Hz), 3.77 (s, 3H), 2.04 (d, *J* = 1.34 Hz), 1.98 (d, *J* = 1.34 Hz), 1.04 (d, *J* = 7.09 Hz), 0.95 (t, *J* = 7.82 Hz), 0.59 (q, *J* = 7.82).

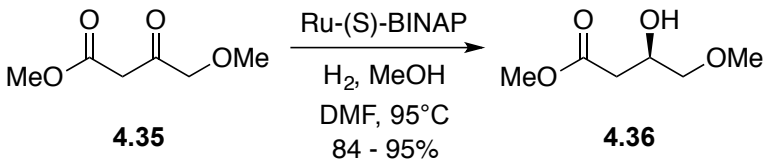

4.35 **4.36**

Methyl (R)-3-hydroxy-4-methoxybutanoate (4.36): To a suspension of benzeneruthenium (II) chloride dimer (137 mg, 0.274 mmol) in DMF (1.4 mL, 0.05 M) at 115 °C, was added (S)-BINAP (256 mg, 0.411 mmol). The resulting slurry was stirred for 15 min and then cooled to ambient temperature. The mixture was transferred to a Parr hydrogenation apparatus and a solution of methyl 4-methoxy-3-oxobutanoate **4.35** (10 g, 68.4 mmol) in MeOH (30 mL, 2.3 M) was added. The mixture was filled with hydrogen gas (10 bar, 150 psi) and cycled three times evacuating the vessel and refilling with hydrogen gas. The mixture was left under an atmosphere of hydrogen (10 bar, 150 psi) and stirred at 95 °C for 72 h. The reaction mixture was transferred to a RB flask and concentrated. The resulting residue was purified by flash chromatography (Hex → 40% EtOAc/Hex) to give **4.36** (8.5g, 84%) as a yellow oil. ^{1}H NMR (400 MHz, $CDCl_3$): δ = 4.13 (m, 1H), 3.71 (s, 3H), 3.42 (m, 2H), 3.40 (s, 3H), 2.95 (d, 1H), 2.54 (d, 2H); ^{13}C NMR (100 MHz, $CDCl_3$): δ = 171.7, 75.3, 66.2, 58.3, 51.0, 37.7. Observed spectral properties were identical with those previously reported. [9]

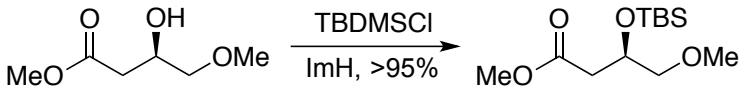

4.36 **4.37**

Methyl (*R*)-3-((*tert*-butyldimethylsilyl)oxy)-4-methoxybutanoate (4.37): To a suspension of benzeneruthenium (II) chloride dimer (137 mg, 0.274 mmol) in DMF (1.4 mL, 0.05 M) at 115 °C, was added (S)-BINAP (256 mg, 0.411 mmol). The resulting slurry was stirred for 15 min and then cooled to ambient temperature. The mixture was transferred to

a Parr hydrogenation apparatus and a solution of methyl 4-methoxy-3-oxobutanoate **4.36** (10 g, 68.4 mmol) in MeOH (30 mL, 2.3 M) was added. The mixture was filled with hydrogen gas (10 bar, 150 psi) and cycled three times evacuating the vessel and refilling with hydrogen gas. The mixture was left under an atmosphere of hydrogen (10 bar, 150 psi) and stirred at 95 °C for 72 h. The reaction mixture was transferred to a RB flask and concentrated. The resulting residue was purified by flash chromatography (Hex → 35% EtOAc/Hex) to give **4.37** (8.5g, 84%) as a yellow oil. ^{1}H NMR (400 MHz, $CDCl_3$): δ = 4.13 (m, 1H), 3.71 (s, 3H), 3.42 (m, 2H), 3.40 (s, 3H), 2.95 (d, 1H), 2.54 (d, 2H); ^{13}C NMR (100 MHz, $CDCl_3$): δ = 171.7, 75.3, 66.2, 58.3, 51.0, 37.7. Observed spectral properties were identical with those previously reported.[9]

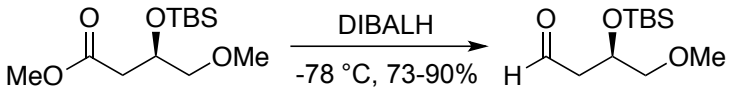

4.37 **4.38**

(*R*)-3-((*tert*-butyldimethylsilyl)oxy)-4-methoxybutanal (4.38): To a solution of methyl (R)-3-hydroxy-4-methoxybutanoate **4.37** (8.4 g, 56.7 mmol) in DMF (81 mL, 0.7 M), was added *tert*-butyldimethylsilyl chloride (11.1 g, 73.7 mmol) followed by imidazole (8.9 g, 130 mmol). The mixture was stirred for 18 h and quenched with sat. NH_4Cl $_{(aq.)}$. The reaction mixture was diluted with DCM and water and the layers were separated. The crude product was extracted from the aqueous with DCM (3X). The combined organic extracts were washed with brine, dried (MgSO4), filtered, and concentrated. The resulting residue was then purified through a plug of silica gel (Hex → 15% EtOAc/Hex) to give

silylether **22** (13.8 g, 93%) as a light yellow oil. ^{1}H NMR (400 MHz, $CDCl_3$): δ = 4.25 (m, 1H), 3.65 (s, 3H), 3.31 (s, 3H), 3.27 (dd, 1H), 2.58 (dd, 1H), 2.44 (dd, 1H) 0.84 (s, 9H), 0.06, 0.03 (2s, 6H); ^{13}C NMR (100 MHz, $CDCl_3$): δ = 171.7, 76.5, 68.2, 58.8, 51.3, 40.1, 25.6, 17.9, -4.7, -5.3. Observed spectral properties were identical with those previously reported. [9]

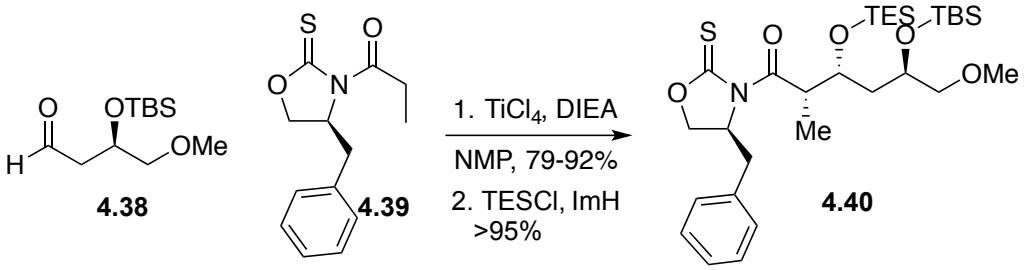

(2*S*,3*R*,5*R*)-1-((*S*)-4-benzyl-2-thioxooxazolidin-3-yl)-5-((*tert*-butyldimethylsilyl)oxy)-6-methoxy-2-methyl-3-((triethylsilyl)oxy)hexan-1-one (4.40): To a solution of propionyloxazolidinethione **4.39** (6.82 g, 27.4 mmol) in DCM (110 mL) at 0 °C was added a solution of titanium tetrachloride (30.2 mL, 1.0 M in DCM, 30.2 mmol). The yellow slurry was stirred for 15 min at 0 °C. Diisopropylethylamine (4.77 mL, 27.4 mmol) was added slowly and the reaction was stirred for 40 min at 0 °C. Added N-methylpyrrolidinone (2.64 mL, 27.4 mmol) and stirred for 10 min. A solution of (R)-3-((tert-butyldimethylsilyl)oxy)-4-methoxybutanal **4.38** (7.0 g, 30.2 mmol) in DCM (10 mL) was added dropwise. After complete addition, the reaction was stirred at 0 °C for 1.5 h. The reaction was quenched with sat. $NH_4Cl_{(aq.)}$ and diluted with water and DCM. The layers were separated and the crude product was extracted from the aqueous with DCM (3 x 150 mL). The combined organic layers were dried ($MgSO_4$), filtered, and concentrated. The residue was purified by flash chromatography (Hex → 15% EtOAc/Hex) to give (2S,3R,5R)-1-((S)-4-benzyl-2-

thioxooxazolidin-3-yl)-5-((tert-butyldimethylsilyl)oxy)-6-methoxy-2-methyl-3-((triethylsilyl)oxy)hexan-1-one as a yellow oil (12.2 g, 92%, >95:5 dr). ^{1}H NMR (400 MHz, $CDCl_3$): δ = 7.37-7.22 (m, 5H), 4.96 (m, 1H), 4.72 (m, 1H), 4.32 (m, 3H), 4.11 (m, 1H), 3.40 (m, 2H), 3.36 (s, 3H), 3.29 (dd, 1H), 2.80 (dd, 1H), 1.80 (m, 1H), 1.68 (m, 1H), 1.33 (d, 3H), 0.90 (s, 9H), 0.12, 0.11 (2s, 6H); ^{13}C NMR (100 MHz, $CDCl_3$): δ =185.1, 177.0, 135.1, 129.3, 128.9, 127.3, 70.0, 69.6, 68.6, 65.7, 60.2, 59.0, 53.3, 43.0, 38.3, 37.4, 25.7, 18.0, 15.1, 10.7, -4.66, -5.04. Observed spectral properties were identical with those previously reported. [12]

To a cooled solution of (2S,3R,5R)-1-((S)-4-benzyl-2-thioxooxazolidin-3-yl)-5-((tert-butyldimethylsilyl)oxy)-3-hydroxy-6-methoxy-2-methylhexan-1-one (2.08 g, 4.32 mmol) in DMF (7.2 mL), at 0 °C, was added triethylsilylchloride (1.95 g, 12.95 mmol, 2.2 mL) followed by imidazole (882 mg, 12.95 mmol). The mixture was stirred at 0 °C for 3 h and then quenched with water. The layers were separated and crude product was extracted from the aqueous layer with DCM (3X). The combined organic extracts were washed with water and brine, dried ($MgSO_4$), filtered, and concentrated. The resulting residue was then ISCO purified (Hex → 10% EtOAc/Hex) to give silyl ether **4.40** (2.37 g, 92%) colorless oil. ^{1}H NMR (400 MHz, $CDCl_3$): δ = 7.37-7.22 (m, 5H), 4.83 (m, 2H), 4.29 (m, 1H), 4.19 (m, 2H), 3.95 (m, 1H), 3.33 (m, 4H), 2.78 (m, 1H), 1.69 (m, 2H), 1.37 (d, 3H), 0.99 (s, 9H), 0.60 (m, 15H), 0.11, 0.10 (2s, 6H); ^{13}C NMR (100 MHz, $CDCl_3$): δ =185.0, 175.9, 135.3, 129.3, 128.8, 127.2, 71.4, 69.0, 68.6, 60.7, 59.0, 43.4, 37.2, 25.8, 22.5, 13.9, 12.3, 6.81, 6.43, -3.94, -4.71. Observed spectral properties were identical with those previously reported. [12]

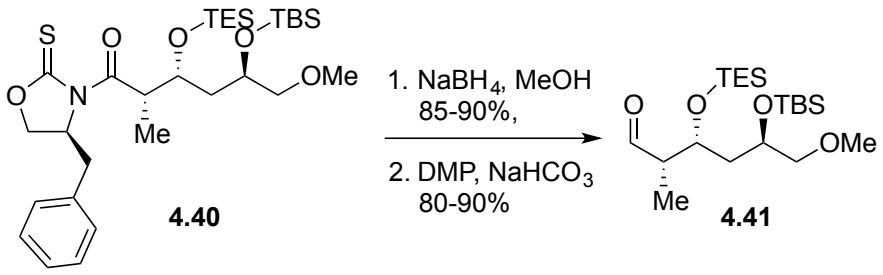

(2*S*,3*R*,5*R*)-5-((*tert*-butyldimethylsilyl)oxy)-6-methoxy-2-methyl-3-((triethylsilyl)oxy)hexanal (4.41): To a cooled solution of (2S,3R,5R)-1-((S)-4-benzyl-2-thioxooxazolidin-3-yl)-5-((tert-butyldimethylsilyl)oxy)-6-methoxy-2-methyl-3-((triethylsilyl)oxy)hexan-1-one **4.40** (2.37 g, 3.98 mmol) in MeOH (40 mL, 0.1 M) at 0 °C, was added sodium borohydride (903 mg, 23.9 mmol). The mixture was stirred at 0 °C for 3 h and then concentrated. The resulting residue was taken up into water and DCM and the layers were separated. The crude product was extracted from the aqueous with DCM (3X) and the combined organic extracts were washed with brine, dried (MgSO4), filtered, and concentrated. The resulting residue was then purified by column chromatography (Hex -> 15% Et_2O/Hex) to give (2*R*,3*R*,5*R*)-5-((*tert*-butyldimethylsilyl)oxy)-6-methoxy-2-methyl-3-((triethylsilyl)oxy)hexan-1-ol (1.38 g, 86%) as a colorless oil. ^{1}H NMR (400 MHz, $CDCl_3$): δ = 4.13 (m, 1H), 3.99 (m, 1H), 3.87 (m, 1H), 3.68 (m, 1H), 3.32 (s, 3H), 3.30 (m, 2H), 2.74 (m, 1H), 2.00 (m, 1H), 1.69 (t, 2H), 0.98 (s, 9H), 0.87 (m, 12H), 0.64 (m, 6H), 0.08, 0.07 (2s, 6H); ^{13}C NMR (100 MHz, $CDCl_3$): δ = 77.6, 73.1, 69.2, 65.6, 58.5, 40.0, 38.0, 25.7, 18.0, 11.9, 6.68, 6.43, 5.68, 5.00, -3.94, -4.86. Observed spectral properties were identical with those previously reported. [12]

To a stirred solution of (2R,3R,5R)-5-((tert-butyldimethylsilyl)oxy)-6-methoxy-2-methyl-3-((triethylsilyl)oxy)hexan-1-ol (215.21 mg, 0.529 mmol) in DCM (5.3 mL, 0.1 M), was added a mixture of Dess-Martin Periodinane (269 mg, 0.635 mmol) and sodium bicarbonate (222 mg, 2.65 mmol). The mixture was stirred for 4 h at ambient temperature. The reaction was quenched with sat. $NaHCO_{3\,(aq.)}$ and diluted with water and DCM. The layers were separated and the crude product was extracted from the aqueous layer with DCM (3X). The combined organic extracts were washed with brine, dried ($MgSO_4$), filtered, and concentrated. The resulting residue was then purified by column chromatography (Hex → 15% EtOAc/Hex) to give aldehyde **4.41** (210 mg, > 95%) as a colorless oil. ^{1}H NMR (400 MHz, $CDCl_3$): δ = 9.81 (s, 1H), 4.31 (m, 1H), 3.88 (m, 1H), 3.35 (s, 3H), 3.31 (d, 2H), 2.53 (m, 1H), 1.68 (m, 2H), 1.08 (d, 3H), 0.96 (s, 9H), 0.90 (m, 12H), 0.63 (m, 6H), 0.10 (s, 6H); ^{13}C NMR (100 MHz, $CDCl_3$): δ = 205.0, 77.5, 69.7, 69.1, 58.7, 52.1, 40.0, 25.8, 18.0, 6.76, 6.49, 5.37, 5.08, -4.00, -4.75. Observed spectral properties were identical with those previously reported.

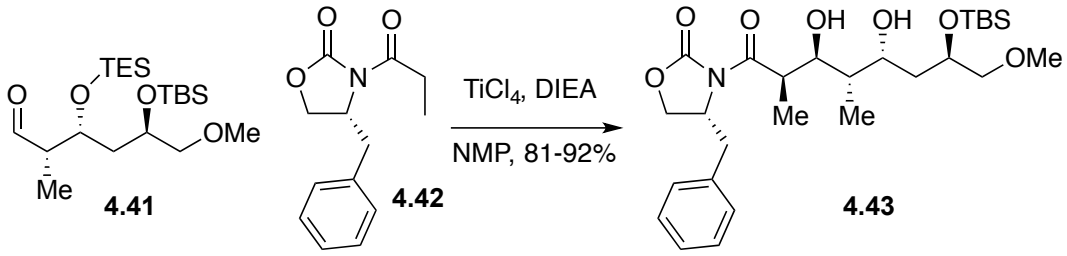

To a cooled solution of (R)-4-benzyl-3-propionyloxazolidin-2-one **4.42** (201 mg, 0.86 mmol) in DCM (3.7 mL, 0.23 M) at 0 °C, was added a solution of $TiCl_4$ (0.95 mL, 1.0 M in DCM, 0.95 mmol). The yellow slurry was stirred for 15 min and freshly distilled diisopropylethylamine (0.15 mL, 0.86 mmol) was added and the reaction was stirred over

40 min. N-methylpyrrolidine (0.083 mL, 0.86 mmol) was added and stirred for 10 min. A solution of (2S,3R,5R)-5-((tert-butyldimethylsilyl)oxy)-6-methoxy-2-methyl-3-((triethylsilyl)oxy)hexanal **4.41** (383.4 mg, 0.95 mmol) in DCM (1 mL, 0.95 M) was added dropwise. The reaction was stirred for 1.5 h and then quenched with sat. $NH_4Cl_{(aq.)}$ and allowed to stir for 30 min before the reaction mixture was diluted water and DCM. The layers were separated and the crude product was extracted from the aqueous with DCM (3X). The combined organic extracts were washed with water, dried ($MgSO_4$), filtered, and concentrated. The resulting residue was then purified by column chromatography (15% EtOAc/Hex → 30% EtOAc/Hex) to give **4.43** (320.3 mg, 71%, > 95:5 dr) as a colorless oil. ^{1}H NMR (400 MHz, $CDCl_3$): δ = 7.33-7.21 (m, 5H), 4.69 (m, 1H), 4.19 (m, 2H), 4.11 (m, 2H), 4.09 (m, 2H), 3.39 (m, 2H), 3.33 (s, 3H), 3.29 (dd, 1H), 2.80 (dd, 1H), 1.84 (m, 2H), 1.60 (m, 1H), 1.25 (d, 3H), 0.87 (s, 9H), 0.09, 0.08 (2s, 6H); ^{13}C NMR (100 MHz, $CDCl_3$): δ =176.9, 152.9, 135.2, 129.3, 128.8, 127.2, 77.3, 73.6, 71.8, 70.7, 66.0, 60.2, 55.4, 40.0, 39.3, 37.62, 36.4, 25.7, 17.9, 11.8, 9.73, -4.68, -5.01. Observed spectral properties were identical with those previously reported. [9]

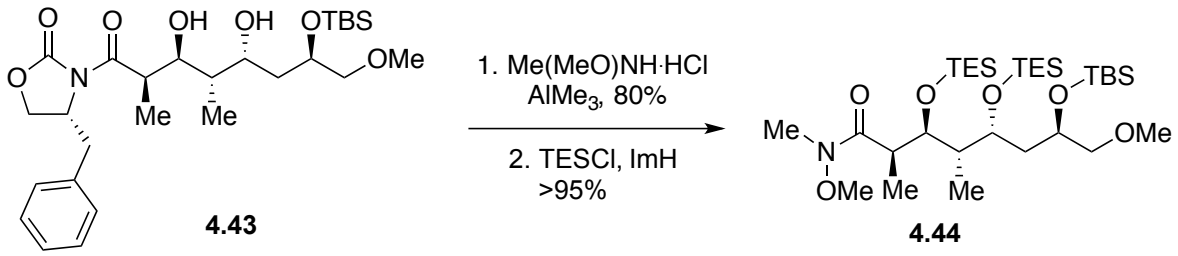

To a solution of *N*,*O*-Dimethylhydroxylamine hydrochloride (519 mg, 5.32 mmol) in DCM (8.0 mL) at -10°C was added $AlMe_3$ (2.66 mL, 2.0 M in hexanes). The mixture was allowed

to stir at room temperature for 1 h. The reaction was cooled to -10 °C and a solution of adduct **4.43** (400 mg, 0.76 mmol) in CH_2Cl_2 (8 mL) was added. The reaction was stirred at -10 °C for 4 h. The mixture was then transferred to a solution of aq. Rochelle's salt (60 mL, 1.0 M) via cannula and the solution was stirred overnight. The two layers were separated and the aqueous layer was extracted with DCM (3 x 60 mL). The combined organic layers were washed with brine, dried ($MgSO_4$), filtered, and concentrated. The residue was purified by flash chromatography (25% EtOAc/Hex → 50% EtOAc/Hex) to give (2*R*,3*S*,4*S*,5*R*,7*R*)-7-((*tert*-butyldimethylsilyl)oxy)-3,5-dihydroxy-*N*,8-dimethoxy-*N*,2,4-trimethyloctanamide (310 mg, 80%) as a colorless oil. ^{1}H NMR (400 MHz, $CDCl_3$): δ = 4.37 (s, 1H), 4.10 (m, 1H), 4.09 (1H), 3.85 (m, 1H), 3.71 (br s, 1H), 3.68 (s, 3H), 3.38 (m, 2H), 3.33 (s, 3H), 3.17 (s, 3H), 3.07 (br m, 1H), 1.81 (m, 2H), 1.50 (m, 1H), 1.17 (d, 3H), 0.87 (s, 9H), 0.09, 0.07 (2s, 6H); ^{13}C NMR (100 MHz, $CDCl_3$): δ = 178.2, 77.2, 74.3, 69.9, 69.3, 60.8, 58.9, 39.2, 37.4, 32.3, 25.9, 18.0, 11.9, 10.0, -4.56, -5.06. Observed spectral properties were identical with those previously reported. [13]

To a solution of (2R,3S,4S,5R,7R)-7-((tert-butyldimethylsilyl)oxy)-3,5-dihydroxy-N,8-dimethoxy-N,2,4-trimethyloctanamide (250 mg, 0.61 mmol) in DCM (10 mL) stirring at 0 °C was added imidazole (332 mg, 4.9 mmol) and trimethylsilyl chloride (0.62 mL, 3.7 mmol). The solution was stirred at 0 °C for 3 h. The reaction was quenched with pH = 7 phosphate buffer (10 mL). The two layers were separated and the aqueous layer was extracted with Et_2O (3X). The combined organic layers were dried ($MgSO_4$), filtered, and concentrated. The residue was purified by column chromatography (Hex → 5% EtOAc/Hex) to afford the

product **4.44** (370 mg, > 95%) as a colorless oil. ^{1}H NMR (400 MHz, $CDCl_3$): δ = 4.14 (m, 1H), 3.99 (m, 1H), 3.74 (m, 1H), 3.66 (s, 3H), 3.32 (s, 3H), 3.31 (m, 2H), 3.16 (s, 3H), 2.97 (m, 1H), 1.80 (m, 2H), 1.47 (m, 1H), 1.03 (d, 3H), 0.92 (s, 9H), 0.88 (m, 12H), 0.52 (m, 6H), 0.07 (s, 6H). ^{13}C NMR (100 MHz, $CDCl_3$): δ = 176.2, 77.2, 73.71, 69.6, 69.3, 60.4, 58.6, 42.1, 40.3, 38.7, 31.4, 25.7, 22.5, 18.0, 13.9, 9.71, 10., 10.5, -4.48, -4.87. Observed spectral properties were identical with those previously reported. [13]

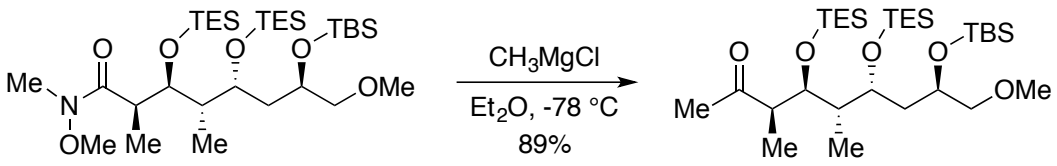

4.44 C20-C28 fragment **4.4**

To a solution of amide **4.44** (250 mg, 0.39 mmol) in THF (0.39 mL) at 0^{o}C was added CH_3MgCl (0.39 mL, 3.0 M in THF) dropwise. After complete addition, the reaction was allowed to stir for 30 mins, before quenching with sat. aq. NH_4Cl (10 mL). The aqueous layer was extracted with CH_2Cl_2 (3 x 10 mL). The combined organic layers were dried ($MgSO_4$), filtered, and concentrated *in vacuo*. The residue was purified by flash chromatography (Hex → 5% EtOAc/Hex) to afford the product **4.4** (208 mg, 89%) as a colorless oil. ^{1}H NMR (400 MHz, $CDCl_3$): δ = 4.26 (m, 1H), 3.95 (m, 1H), 3.71 (m, 1H), 3.33 (s, 3H), 3.29 (m, 2H), 2.70 (m, 1H), 2.15 (s, 3H), 1.78 (m, 2H), 1.62 (m, 1H), 1.09 (d, 3H), 0.92 (s, 9H), 0.88 (m, 12H), 0.52 (m, 6H), 0.69 (s, 6H); ^{13}C NMR (100 MHz, $CDCl_3$): δ = 210.1, 73.0,

70.1, 69.3, 58.8, 50.2, 42.8, 40.5, 28.5, 25.8, 11.9, 9.72, 9.41, 7.00, 5.91, 5.33, -4.36, -4.75. Observed spectral properties were identical with those previously reported. [13]

4.6 Notes and references

1. Lipshutz, B. H.; Lindsley, C. A Streamlined Route to Highly Conjugated, *All-E* Polyenes Characteristic of Oxo Polyene Macrolide Antibiotics *J. Am. Chem. Soc.* **1997**, 119, 4555-4556.

2. Srogl, J.; Allred, G. D.; Liebeskind, L. S. Sulfonium Salts. Participants *par* Excellence in Metal-Catalyzed Carbon-Carbon Bond-Forming Reactions *J. Am. Chem. Soc.* **1997**, 119, 12376-12377.

3. Smith, III, A. B.; Minbiole, K. P.; Verhoest, P. R.; Schelhaas, M. Total Synthesis of (+)-Phorboxazole A Exploiting the Petasis—Ferrier Rearrangment *J. Am. Chem. Soc.* **2001**, 123, 10942-10953.

4. Durham, T. B.; Blanchard, N.; Savall, B. M.; Powell, N. A.; Roush, W. R. Total Synthesis of Formacin *J. Am. Chem. Soc.* **2004**, 124, 9307-9317.

5. Fürstner, A.; Funel, J.-A.; Tremblay, M.; Bouchez, L. C.; Nevado, C.; Waser, M.; Ackerstaff, J.; Stimson, C. C. A versatile protocol for Stille-Migita cross coupling reactions *Chem. Commun.* **2008**, 2873-2875.

6. Williams, S.; Jin, J.; Kan, S. B. J.; Li, M.; Gibson, L. J.; Paterson, I. An Expedient Total Synthesis of Chivosazole F: an Actin-Binding Antimitotic Macrolide from the Myxobacterium *Sorangium Cellulosum Angew Chem. Int. Ed.* **2017**, 56, 645-649.

7. Desai, N. B.; McKelvie, N.;Ramirez, F. A New Synthesis of 1,1-Dibromoölefins *via* Phosphine-Dibromomethylenes. the Reaction of Triphenylphosphine with Carbon Tetrabromide *J. Am. Chem. Soc.* **1962**, 84, 1745-1747.

8. Jin, B.; Liu, Q.; Sulikowski, Q. A. Development of an end-game strategy towards apoptolidin: a sequential Suzuki coupling approach *Tetrahedron* **2005**, 61, 401-408.

9. Schuppan, J.; wehlan, H.; Keper, S.; Koert, U. Synthesis of Apoptolidinone *Angew. Chem. Int. Ed.* **2001**, 40, 2063-2066.

10. Crimmins, M. T.; King, B. W.; Tabet, E. A.; Chaudhary, K. Asymmetric Aldol Additions: Use of Titanium Tetrachloride and (-)-Sparteine for the Soft Enolization of *N*-Acyl Oxazolidinones, Oxazolidinthiones, and Thiazolidinthiones *J. Org. Chem.* **2001**, 66, 894-902.

11. Du, Y.; Derewacz, D. K.; Deguire, S. M.; Teske, J.; Ravel, J.; Sulikowski, G. A.; Bachmann, B. O. Biosynthesis of apoptolidins in *Nocardiopsis* sp. FU 40 *Tetrahedron*, **2011**, 67, 6568-6575.

12. Wu, B.; Liu, Q.; Sulikowski, G. A. Total Synthesis of Apoptolidinone *Angew. Chem. Int. Ed.* **2004**, 43, 6673-6675.

13. Vargo, T. R.; Hale, J. S.; Nelson, S. G. Catalytic Asymmetric Aldol Equivalents in the Enantioselective Synthesis of the Apoptolidin C Aglycone *Angew. Chem. Int. Ed.* **2010**, 49, 8678-8681.

Appendix A2:
Spectra relevant to chapter IV

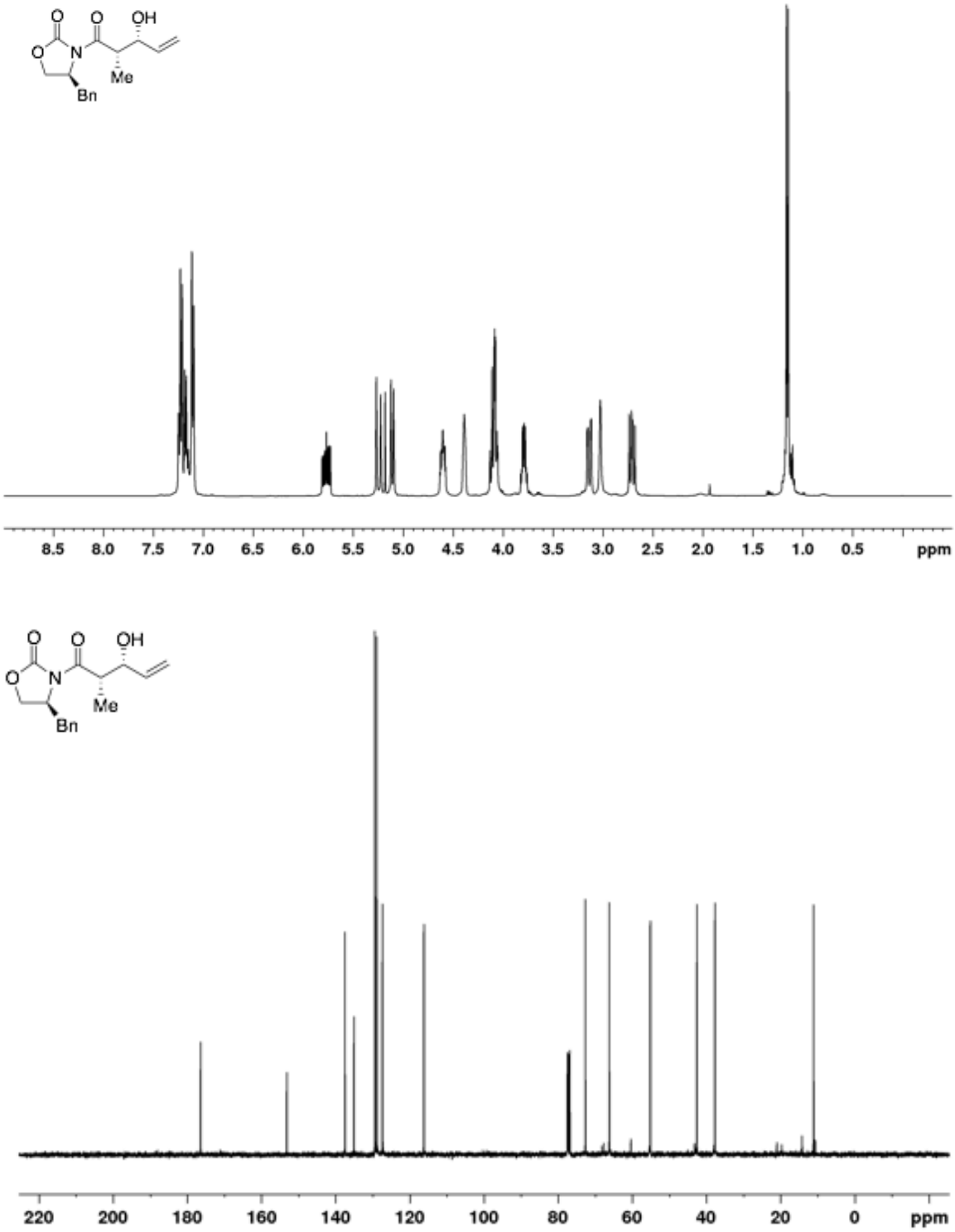

Figure A2.1. ^{1}H NMR (400 MHz, $CDCl_3$) of (S)-4-benzyl-3-((2S,3R)-3-hydroxy-2-methylpent-4-enoyl)oxazolidin-2-one

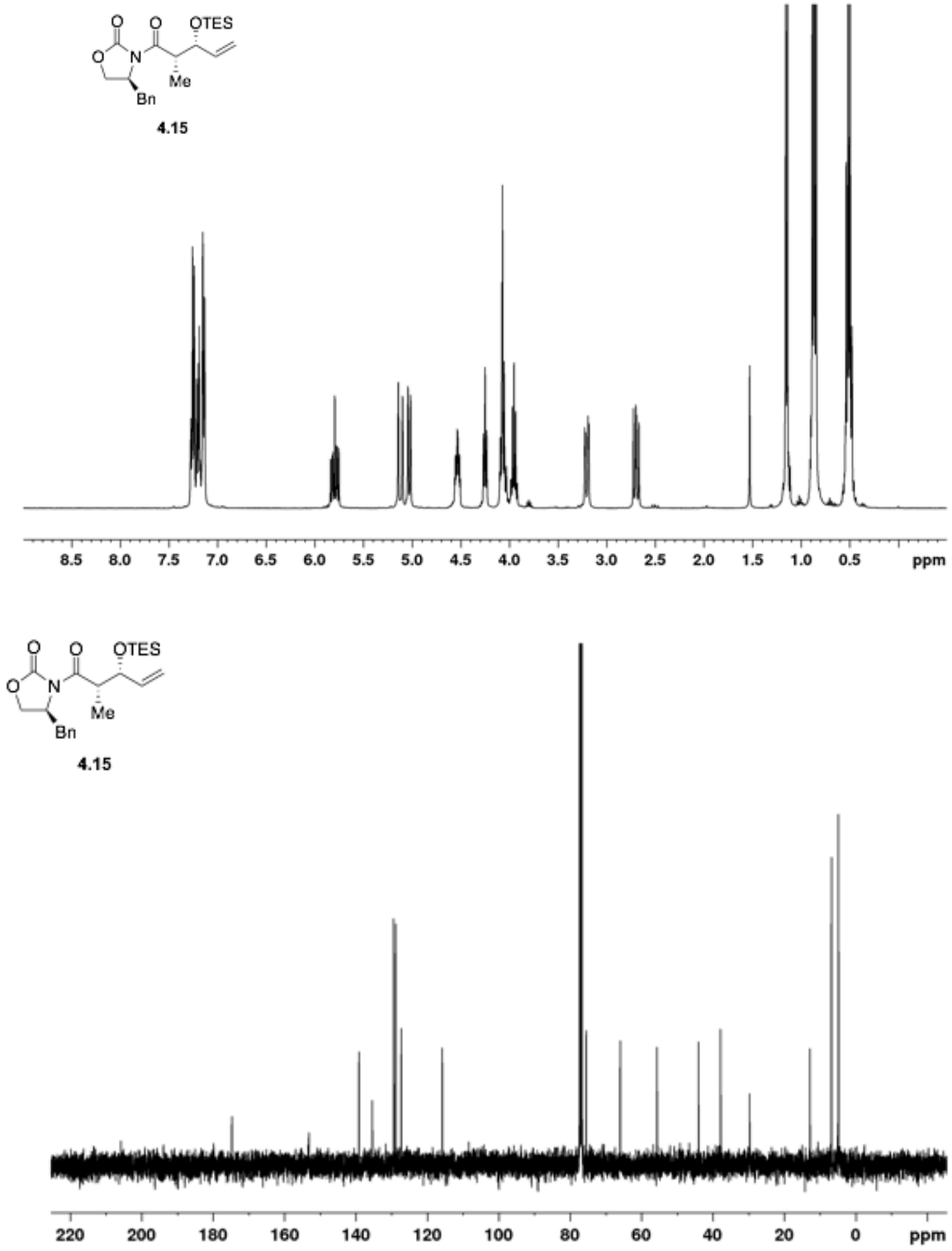

Figure A2.2. ^{1}H NMR (400 MHz, $CDCl_3$) and ^{13}C NMR (400 MHz, $CDCl_3$) of **4.15**.

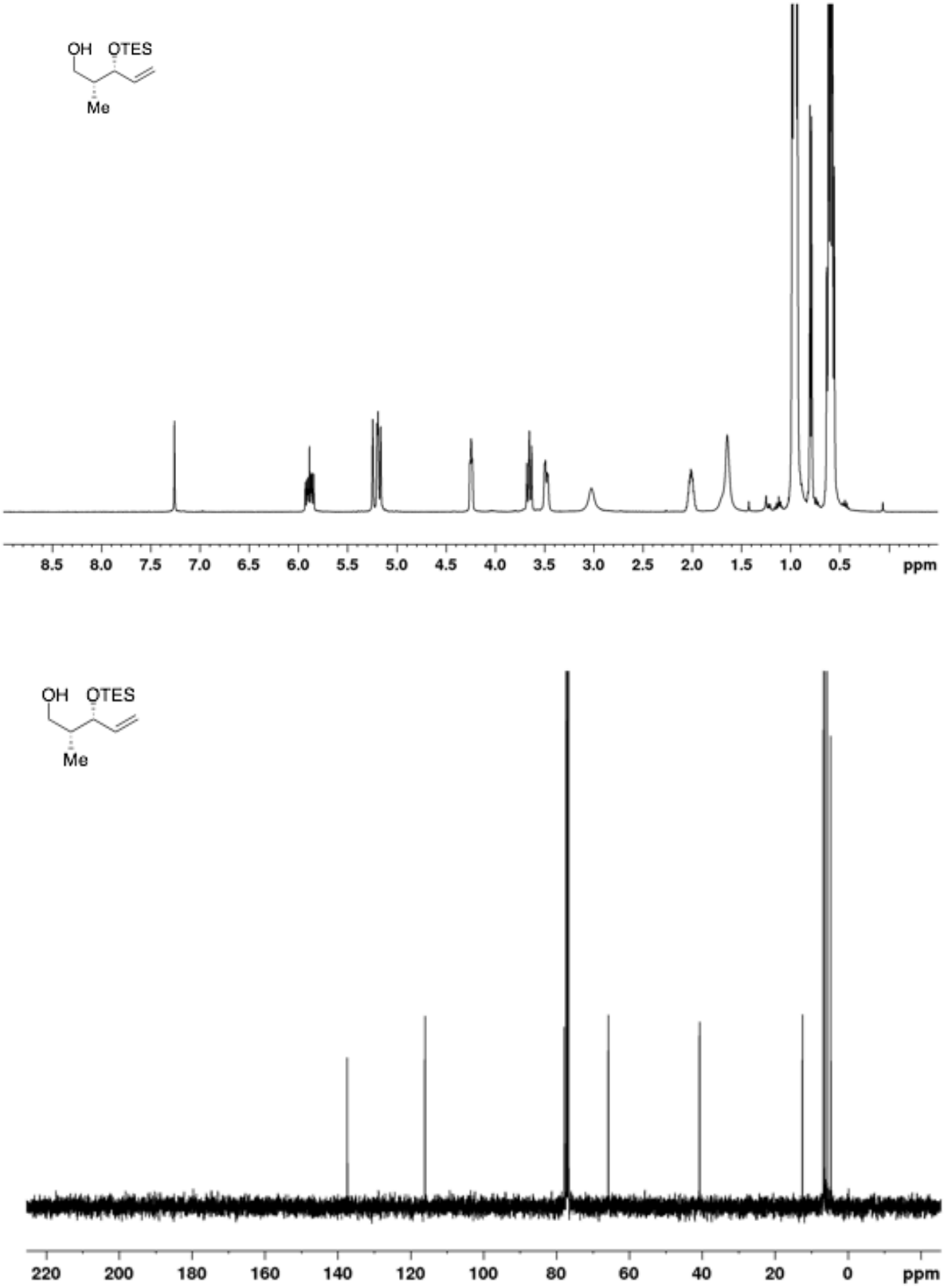

Figure A2.3. ^{1}H NMR (400 MHz, $CDCl_3$) and ^{13}C NMR (400 MHz, $CDCl_3$) of (2R,3R)-2-methyl-3-((triethylsilyl)oxy)pent-4-en-1-ol.

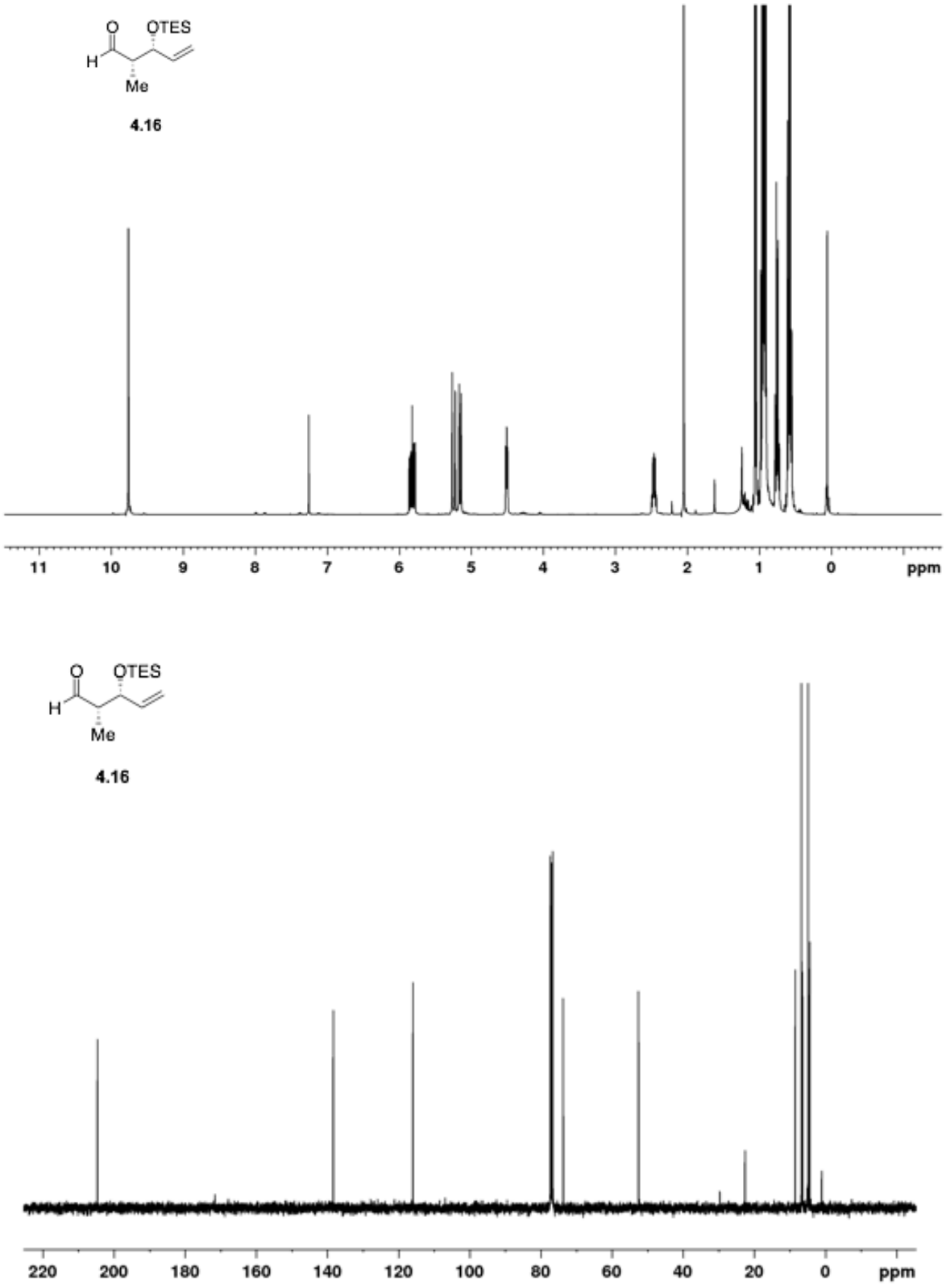

Figure A2.4. ^{1}H NMR (400 MHz, $CDCl_3$) and ^{13}C NMR (400 MHz, $CDCl_3$) of **4.16**.

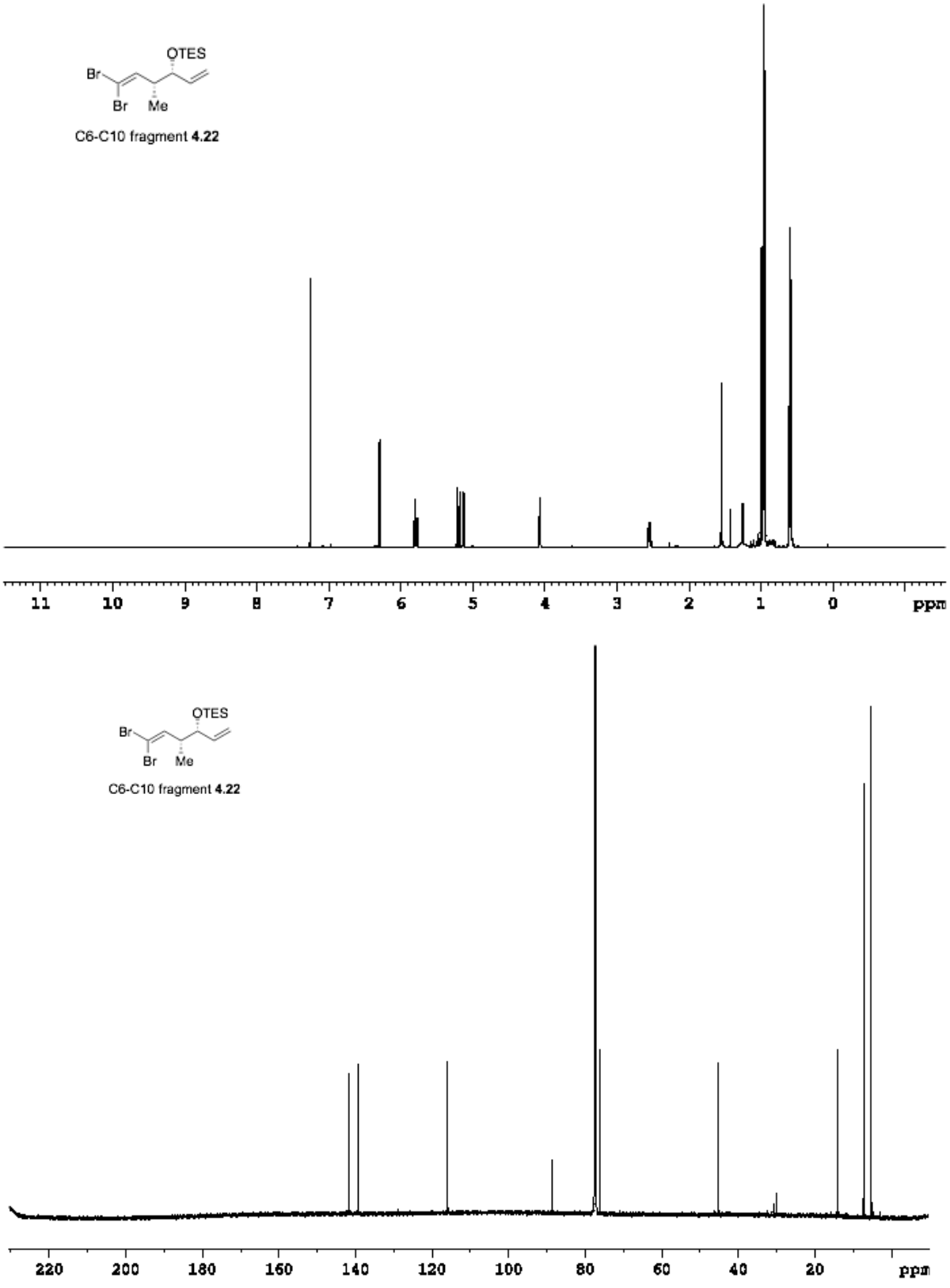

Figure A2.5. ^{1}H NMR (600 MHz, $CDCl_3$) and ^{13}C NMR (600 MHz, $CDCl_3$) of **4.22**

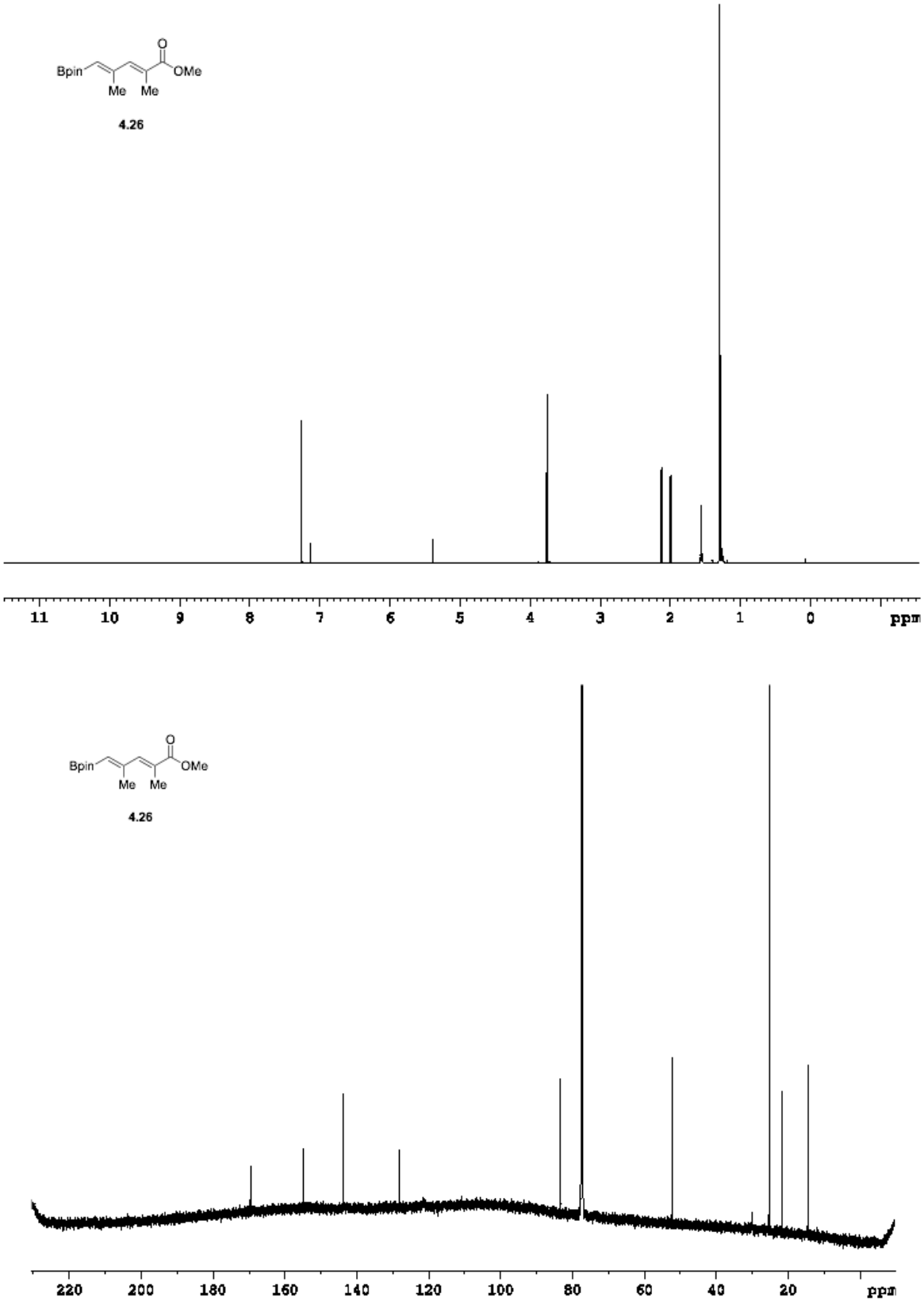

Figure A2.6. ^{1}H NMR (600 MHz, $CDCl_3$) and ^{13}C NMR (600 MHz, $CDCl_3$) of **4.26.**

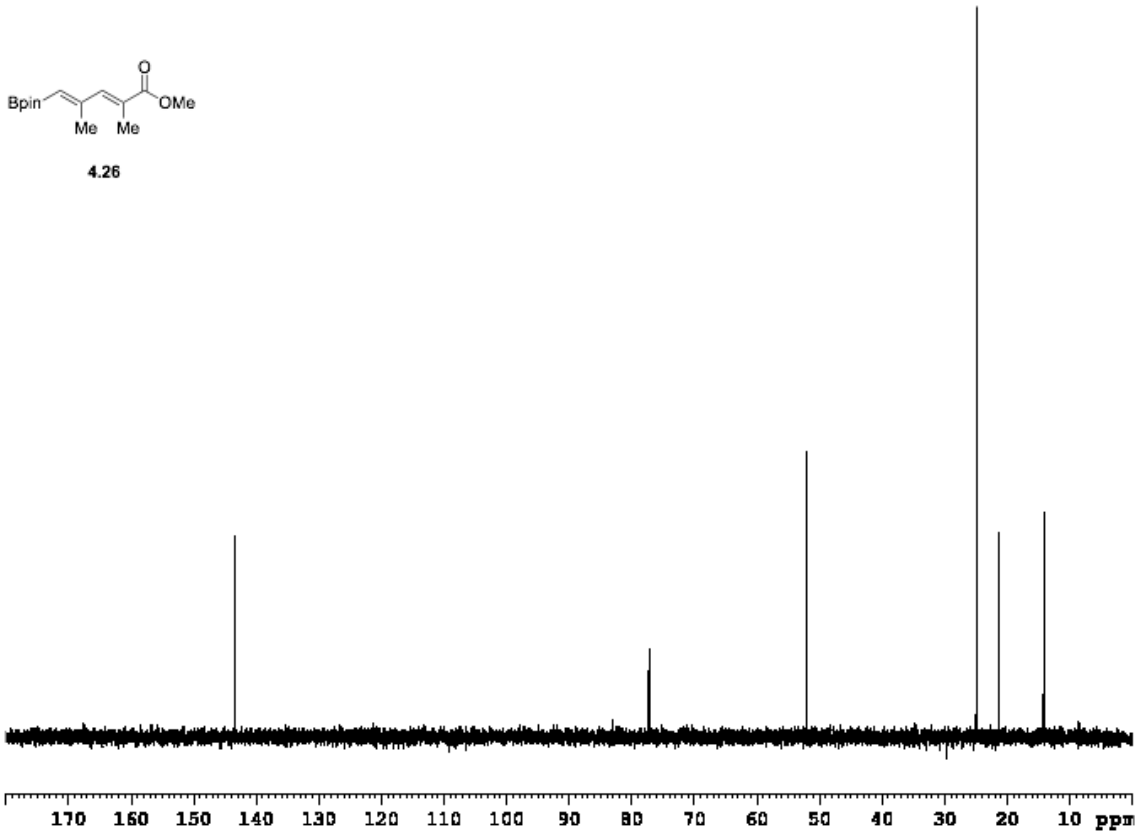

Figure A2.7. DEPT-135 (600 MHz, $CDCl_3$) of **4.26**.

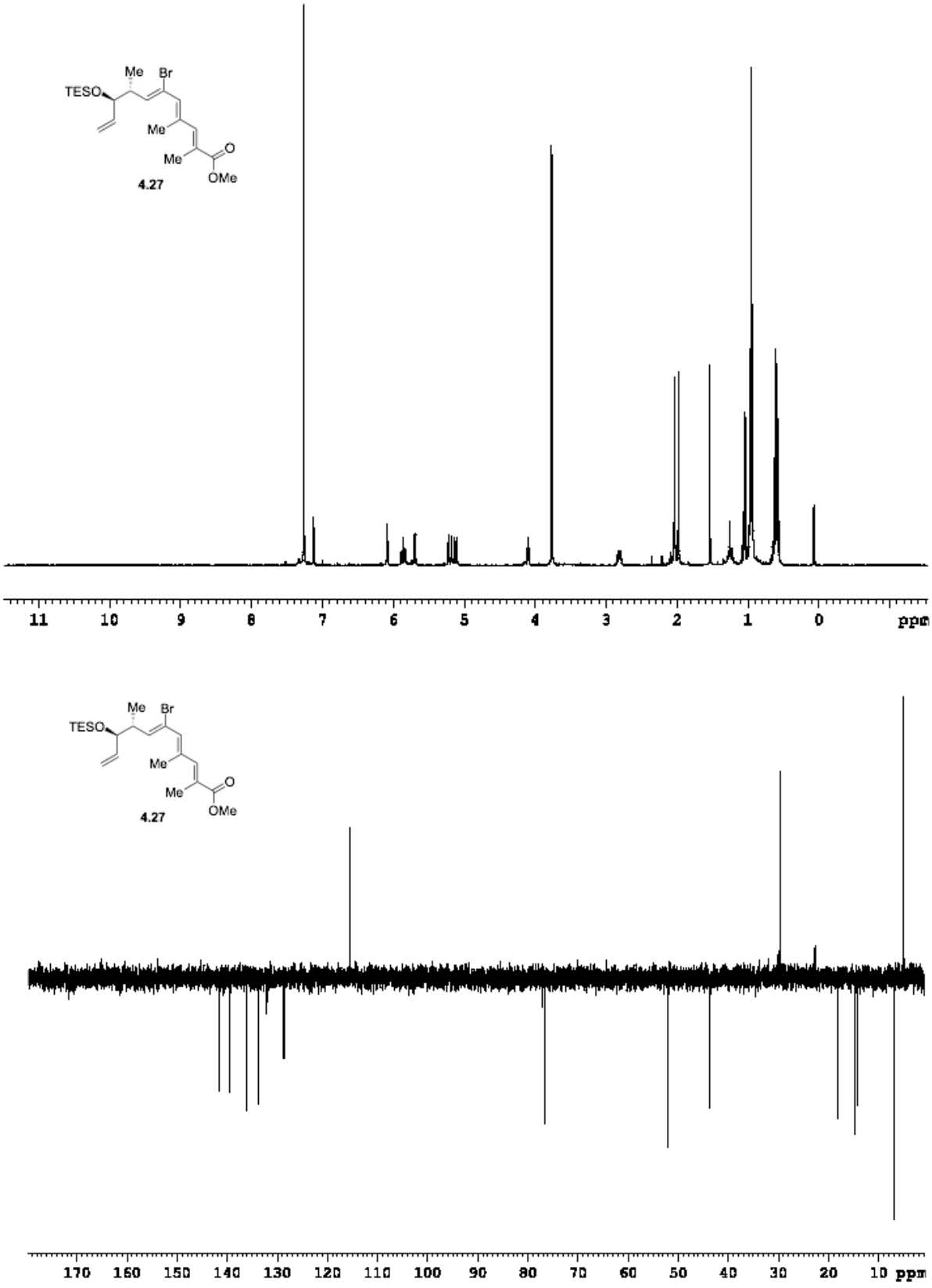

Figure A2.8. ^{1}H NMR (400 MHz, $CDCl_3$) and DEPT-135 (400 MHz, $CDCl_3$) of **4.27**.

CHAPTER V

TOWARD THE COMPREHENSIVE SYNTHEIS OF FLUORESCENT APOPTOLIDIN GLYCOVARIANTS

5.1 Progress toward evaluating cell uptake and localization of fluorescent apoptolidin glycovariants

In previous work, [1] our group has shown that apoptolidin **5.1**-**5.4** displays an interesting cell confluence and glycosylation dependency for cytotoxic activity (Fig. 5.1). At levels of high cell confluence and glycosylation state, apoptolidin is a substantial cancer cell toxin against human lung cancer cells (H292).

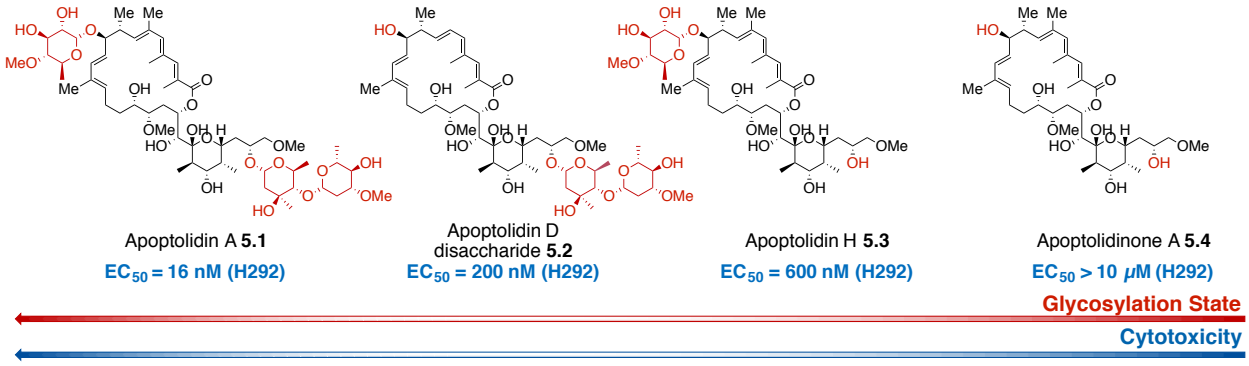

Figure 5.1. Comparison of cytotoxicity as a function of apoptolidin glycosylation state.

Sulikowski and coworkers [1] further explored this trend by visualizing the cellular localization of fluorescent apoptolidin A **5.1** and H **5.3** in H292 cells. Apoptolidin A **5.1** and H **5.3** were functionalized via selective C2' esterification with 5-azidopentanoic acid

followed by copper-free click conditions with fluorescent bicyclononyne linker (BNE-Cy3, **5.7**) to give Cy3 functionalized apoptolidin A (Cy3 Apo A, **5.5**) and H (Cy3 Apo H, **5.6**, Fig. 5.2).

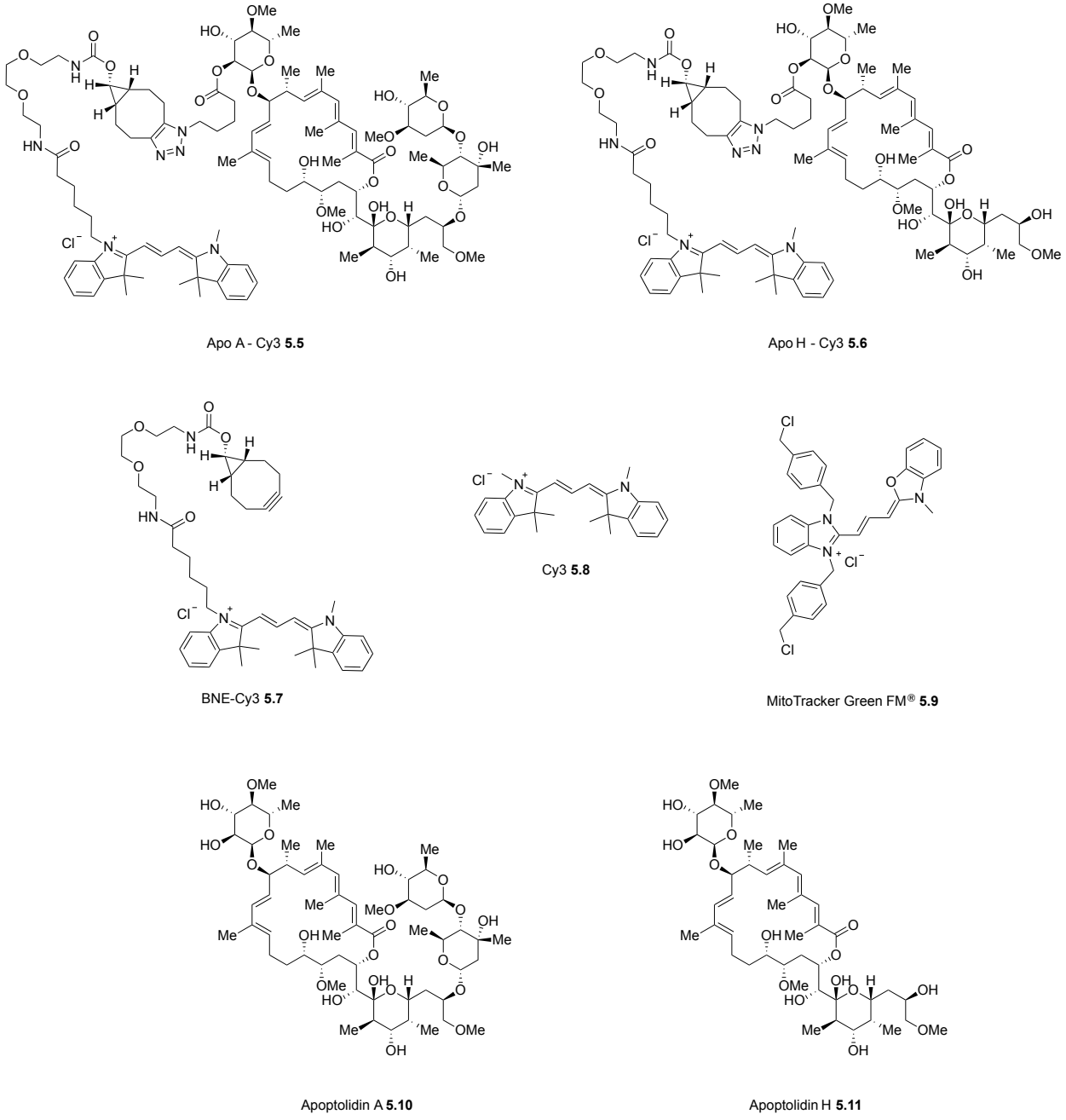

Figure 5.2. Chemical structures of fluorescent and non-fluorescent apoptolidins.

Imaging of the H292 cells after treatment with either Cy3 Apo A **5.5** or Cy3 Apo H **5.6** showed significant staining of the mitochondria and overlap with a known mitochondrial dye: MitoTracker® **5.9** (Pearson coefficient 0.90 – 0.88, Fig. 5.3). Fluorescent Cy3 functionalized apoptolidins **5.5**-**5.6** also retain much of their activity as compared to their non-fluorescent parents **5.10-5.11**. These findings are consistent with a proposed mitochondrial target, such as F_oF_1-ATPase.

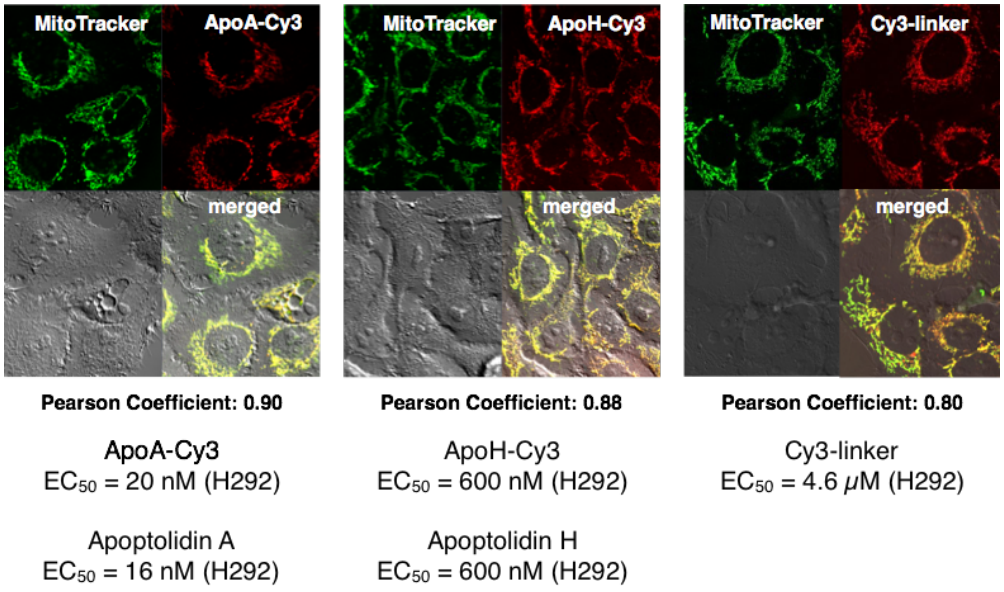

Figure 5.3. Deguire's confocal microscopy images of fluorescent apoptolidins.

However in these studies, Sulikowski and coworkers did find that fluorescent cationic bicyclononyne linker (BNE-Cy3, **5.7**) does show significant selective localization to the mitochrondria and overlap with MitoTracker® **5.9** (Pearson coefficient = 0.80). While cationic dyes have been known to localize to the mitochondria due to its large electrochemical gradient, the BNE-Cy3 linker **5.7** does not show significant cytotoxicity towards H292 cells (EC_{50} = 4.6 μM), revealing that Cy3- labeled apoptolidin glycovariants **5.5**-**5.6**, supporting previous studies proposing a mitochondrial apoptolidin molecular

target. While the Cy3-BNE linker **5.7** exhibited little to no activity against the lung cancer cells (4.6 μM, H292 cells), this work necessitates follow-up studies utilizing a non-mitochondrial staining fluorescent linker.

Cationic amphiphilic small molecules readily localize to the mitochondria. One of the first dyes reported to exhibit mitochondrial selectivity and fluorescent staining was Janus green B **5.12** (Fig. 5.3). Janus green B **5.12**, along with several other later reported dyes: rhodamine 123 (Rh123) **5.13** and cresyl blue **5.14**, have been shown to target the mitochondria due to its transmembrane potential. [2]

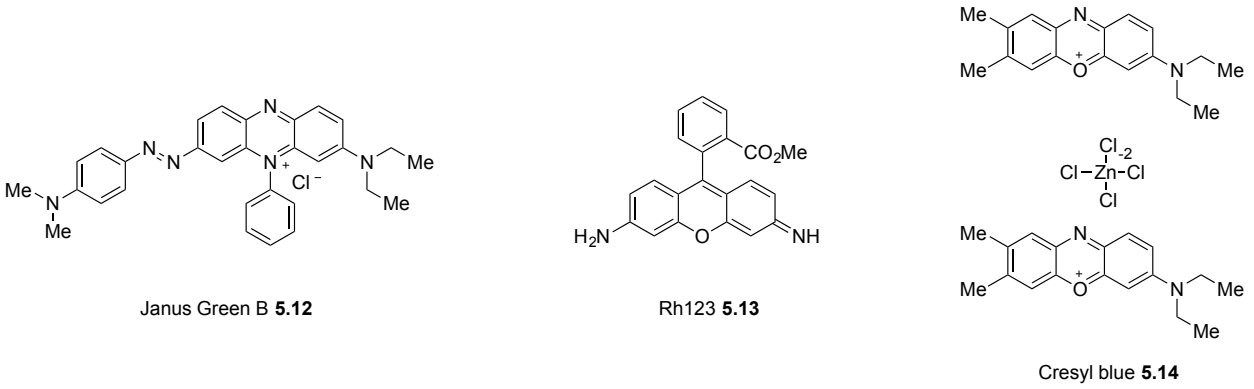

Figure 5.4. Cationic mitochondrion staining dyes.

Mitochondria are the energy power plants of the cell and generate adenine triphosphoate (ATP) by utilizing a large electrochemical gradient potential across its membrane (Fig. 5.4). The respiratory electron transport chain (ETC) drives protons (H^+) against their natural concentration gradient to the outer membrane of the mitochondria. The accumulation of H^+ results in the flow of protons into the mitochondria through the F_oF_1-ATPase complex to complete the ETC and produce ATP. [3] This charge gradient of

positive charge into the mitochondria explains how cationic dyes can result in specific mitochondrial staining. [2]

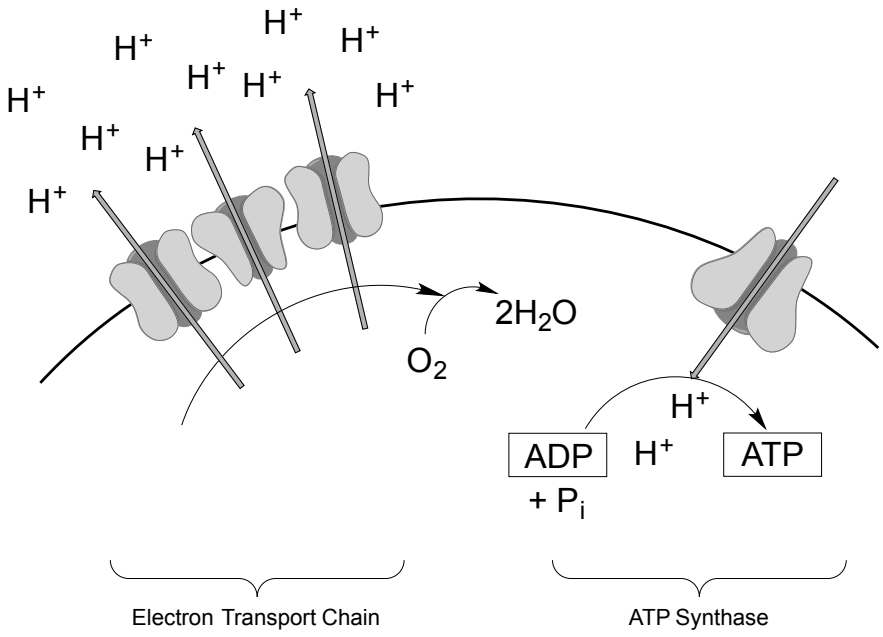

Figure 5.5. General mechanism for electrochemical gradient across mitochondrial membrane.

While there are still means of utilizing Cy3- labeled apoptolidins A **5.5** and H **5.6** and decoupling the Cy3 dye activity from the parent apoptolidins by using small molecule protonophore mitochondrial inhibitors such as 2,4-dinitrophenol **5.15**, [4] p-trifluoromethoxy carbonyl cyanide phenyl hydrazine (FCCP) **5.16**, and carbonyl cyanide m-chloro phenyl hydrazine (CCCP) **5.17** (Fig. 5.5). [5] These mitochondrial inhibitors work by rapidly dissipating the mitochondrial gradient by targeting F_oF_1-ATP synthase. Because these these inhibitors directly impact the proposed target of apoptolidin, F_oF_1-ATPase, we cannot rule out the possibility that this could somehow disrupt apoptolidin's mechanism of action.

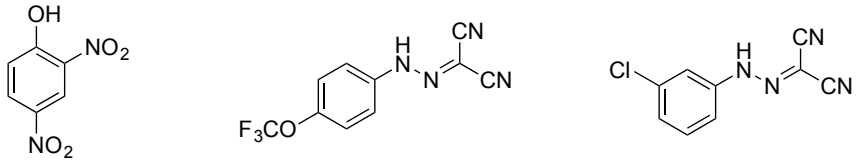

2,4-Dinitrophenol **5.15** FCCP **5.16** FCCP **5.17**

Figure 5.6. Small molecule protonophore mitochondrial decouplers.

5.2 Synthesis of fluorescent non-cationic apoptolidin glycovariants

In order to observe apoptolidin cell localization as a function of glycosylation state, we propose to synthesize non-cationic fluorescent apoptolidin glycovariants, based on the fluorescent scaffold difluoro-boraindacene **5.18**, otherwise known as BODIPY (Fig. 5.6A). The synthesis of BODIPY was first reported in 1968 by Triebs and Kreuzer. However, little attention was given until the mid 1990's, as it became popularized as an effective label for biological studies. [6]

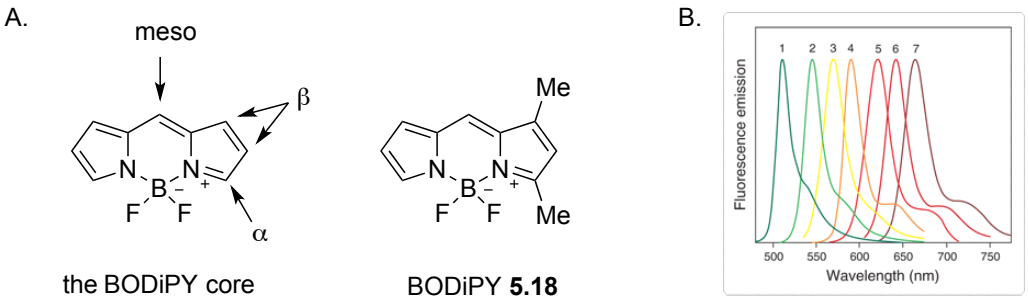

the BODiPY core BODiPY **5.18**

Figure 5.7. BODIPY scaffold and spectral properties. A. Chemical structure of BODIPY core and relevant dyes. B. Example spectral properties of dyes available through ThermoFisher for purchase.

The BODIPY scaffold exhibits immense versatility with finely tunable photochemical properties, excellent thermal and photostability, high fluorescent and quantum yield,

negligible triplet state formation, intense absorption profile, good solubility, and chemical robustness. Depending on its substitution pattern, BODIPY dyes can absorb light anywhere from 370 nm to 770 nm and emit from 500 nm to 830 nm (Fig. 5.6B). These dyes typically have sharp absorption bands (half-widths typically ranging from 25-35 nm), high molar absorption coefficients (between 40,000 – 110, 000 $M^{-1}cm^{-1}$), high quantum yield (60 – 90%), long excited singlet-state lives (1 to 10 ns), are resistant to aggregation in solution, and good solubility in most solvents (except water). [6-8] Additionally, BODIPY dyes been shown to somewhat localize to lipophilic compartments of the cell including the golgi apparatus and endoplasmic reticulum, however multiple reports have been shown that redirecting BODIPY cell localization to specific cellular compartments is possible. [9-10]

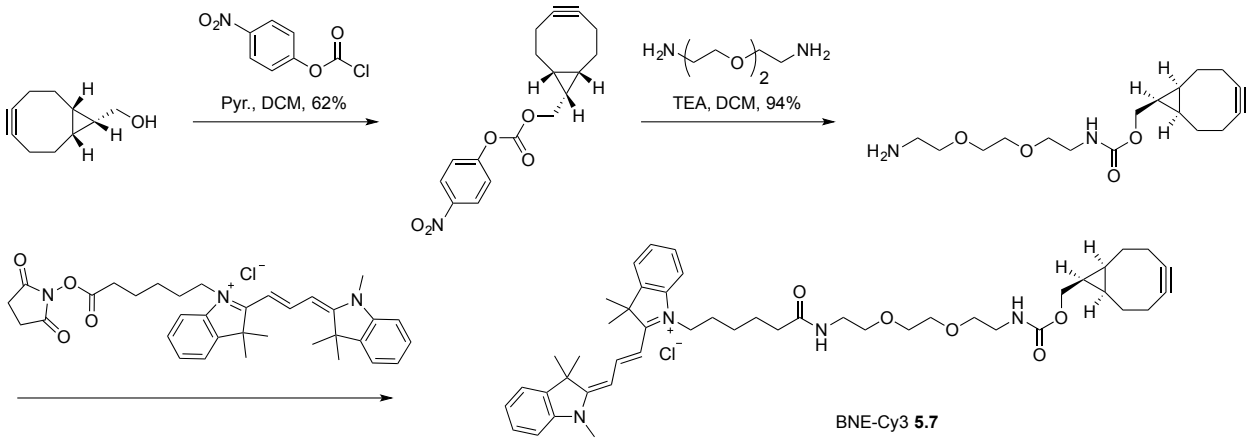

Figure 5.8. Deguire's synthesis of fluorescent Cy3 bicyclononyne linker (BNE-Cy3, **5.7**).

The synthesis of Cy3- fluorescent apoptolidin glycovariants, originally developed by Sean Deguire of the Sulikowski group (Fig. 5.7 and 5.8), [1] was modified to allow for the incorporation of non-cationic fluorescent BODIPY **5.18**. In the work described by Sulikowski and coworkers, apoptolidins A **5.10** and H **5.11** are selectively esterified at the C2' hydroxyl according to conditions first reported by Wender and coworkers (Fig. 5.8). [11-

[12] This selective esterification allows for "clicking" of the fluorescent BNE linker for synthetic flexibility in fluorescent dye choice.

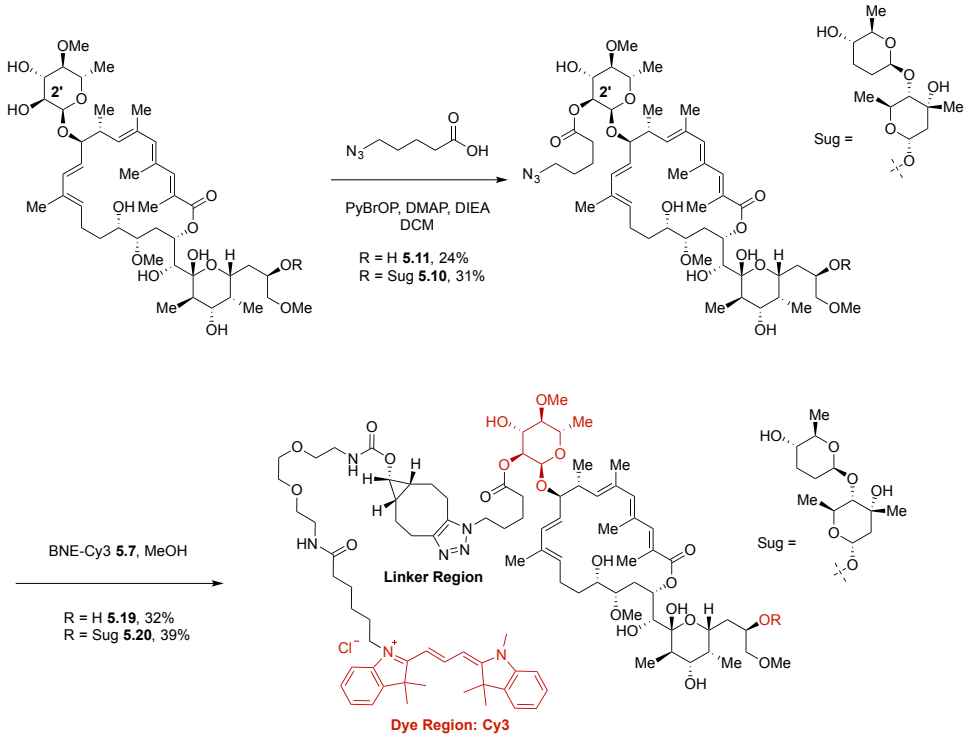

Figure 5.9. Deguire's synthesis of fluorescent Cy3 labeled apoptolidins A and H.

Sulikowski and coworkers [1] detail selective C2' glycosylation of C9- glycosylated apoptolidin A and H **5.10** and **5.11** with 5-azidopenatoic acid to form azido apoptolidins A **5.20** and H **5.19** (Fig. 5.8). The azido apoptolidins can then be introduced to Cy3-BNE **5.7** through copper-free "click" conditions to produce the fully fluorescent apoptolidins A **5.5** and H **5.6**. BODIPY tagged apoptolidins A **5.27** and H **5.28** can be synthesized in much the same way using azido apoptolidins A **5.20** and H **5.19** in [3+2] cycloaddition with BODIPY tagged BNE linker **5.26** (Fig. 5.9).

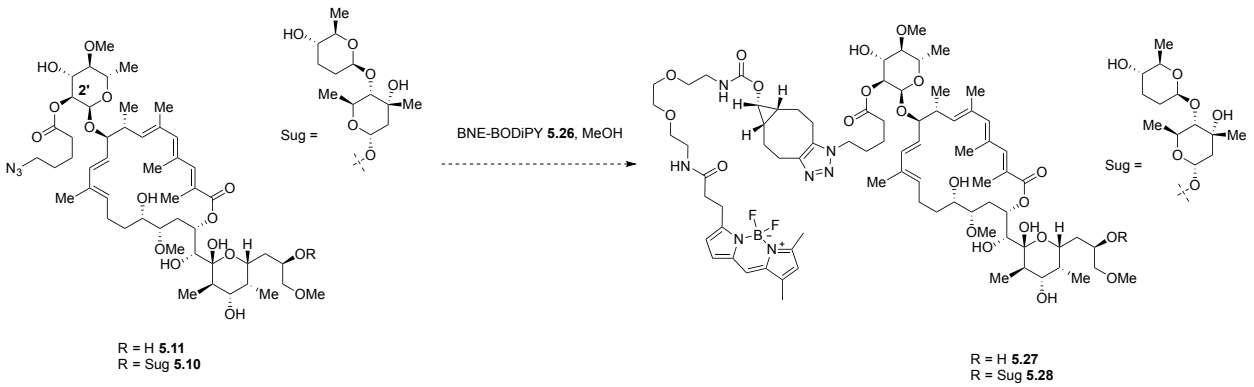

Figure 5.10. Proposed synthesis of BODIPY tagged apoptolidins A and H.

In order to synthesize BODIPY BNE linker **5.26**, BODIPY was synthesized according to a procedure described by Richert and coworkers (Fig. 5.10). [13] Cyclization with phosphoryl chloride, triethylamine, and boron trifluoride etherate gave intermediate **5.24**, which was saponified and esterified to give the N-hydroxy succinimide ester (NHS) derivative **5.25**.

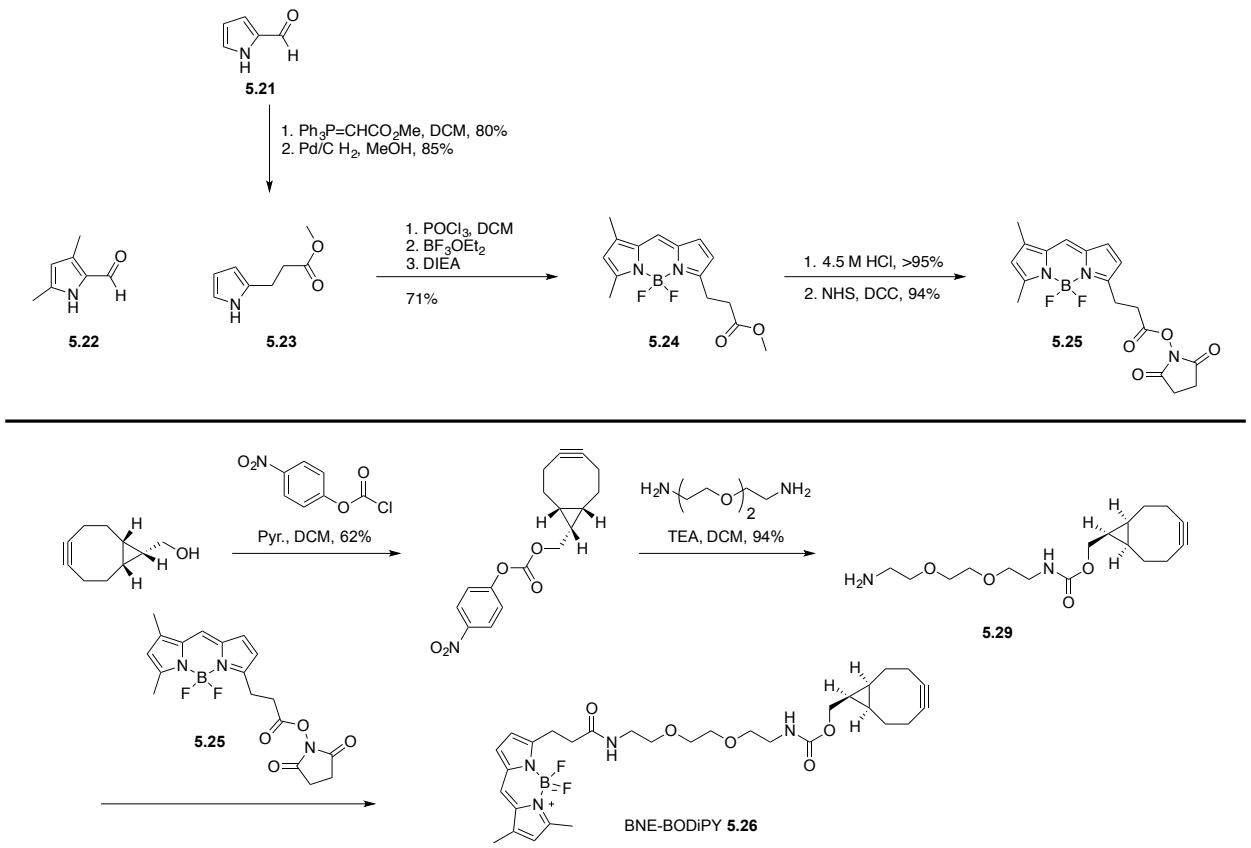

Figure 5.11. BODIPY tagged bicyclononyne linker BNE-BODIPY.

With BODIPY-NHS **5.25** ester in hand, amidation with bicyclononyne (BNE) amino linker **5.29** could arrive at BODIPY-BNE linker **5.26.** Finally, copper-free "click" conditions, or [3+2] cycloaddition, [1] between azido-apoptolidins would produce the desired fluorescent apoptolidin glycovariants **5.27**-**5.28** (Fig. 5.9).

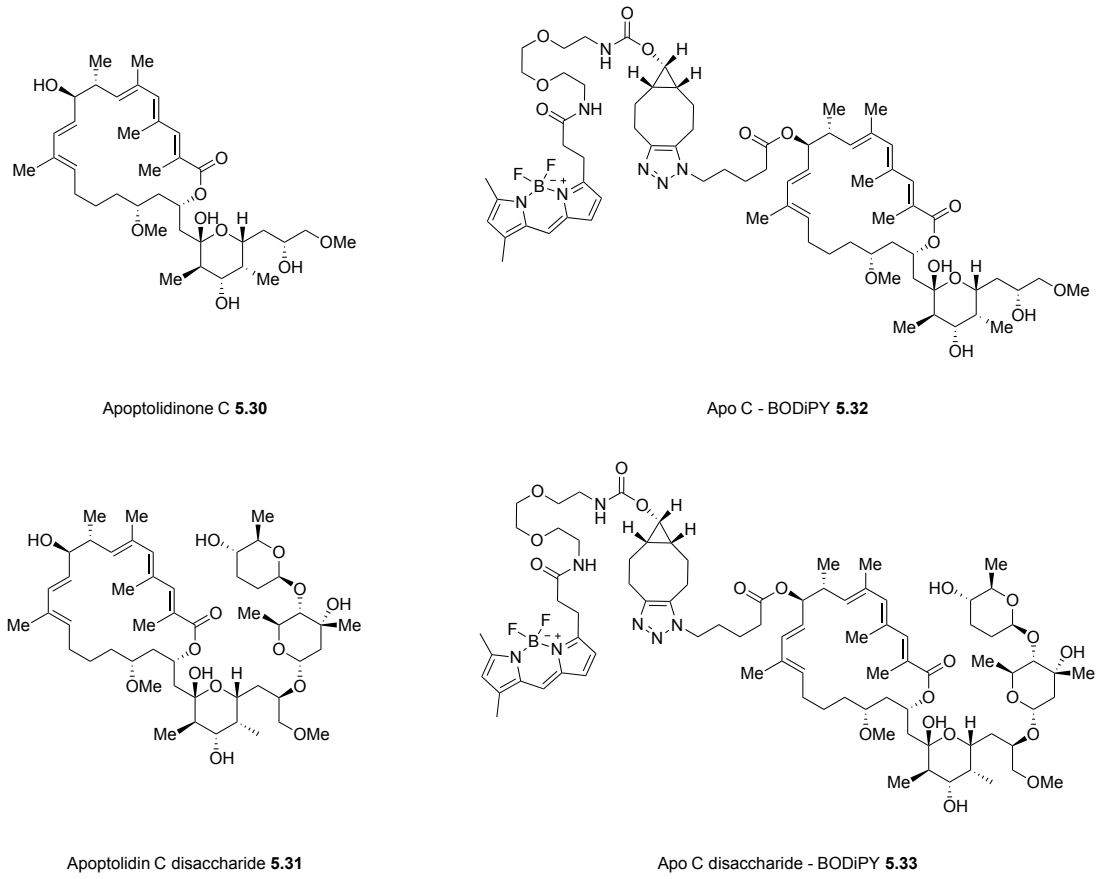

Figure 5.12. Chemical structures of BODIPY tagged apoptolidinone C and apoptolidin C disaccharide.

Apoptolidinone C **5.30** and apoptolidin C disaccharide **5.31** lacking the C9- sugar can be selectively esterified prior to late stage formation of the macrolide ring (Fig. 5.12). Deprotection of the C9- silyl ether of the northern hemisphere of apoptolidinone C **5.34** would allow for selective incorporation of the 5-azido ester **5.35**. Alternatively careful control of the global deprotection of **5.36**, leaving t-butyl dimethyl silyl (TBS) ether in place at the C27- position to give **5.37**, could also be used to selectively esterify at the C9-hydroxyl. This would allow access to azido apoptolidinone C **5.11** and azido apoptolidin C disaccharide **5.10**.

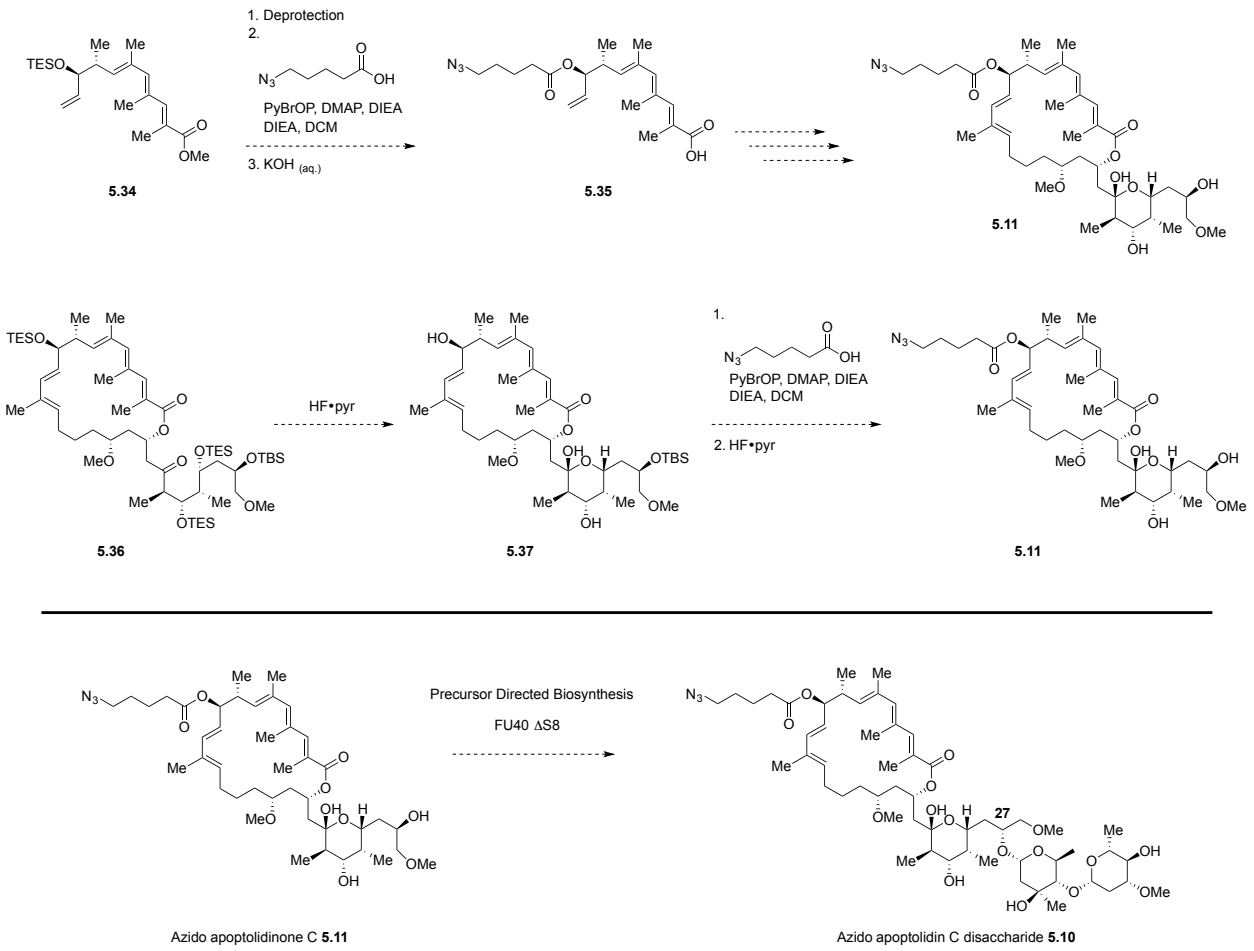

Figure 5.13. Proposed synthesis of azido apoptolidinone C and azido apoptolidin C disaccharide.

5.3 Understanding cellular uptake and response of fluorescent apoptolidins

Preliminary studies completed through collaboration between the Sulikowski, Bachmann, and Irish groups [14] has shown that fluorescent apoptolidin glycovariants can be used to study cellular uptake, localization, and response of cancer and healthy cells. Utilizing Cy3- conjugated apoptolidins A **5.20** and H **5.19**, cell microscopy can be used to better understand the effect of the apoptolidin glycosides on cellular uptake into specific cancer cells. Phospho- specific flow cytometry in a single-cell format allows for

quantification of apoptolidin cellular uptake and subsequent response by analyzing up-regulation of specific phosphorylation events. [15-17] In preliminary studies, we have shown that a panel of cancer cells (SW620, U87-MG, LN229, and A549) can be simultaneously analyzed for cellular uptake and response toward activation of the AMPK pathway. Specifically we chose to focus on the up-regulation of phosphorylated acetyl-CoA-carboxylase (ACC), an important biomarker for autophagy, [18] as previous reports by Ishmael and coworkers [19] demonstrated apoptolidin-induced autophagic cell death in several lines of lung cancer cells (H292, HCT-116), gliablastoma cells (U87-MG and SW), and mouse embryonic cells (MEF's).

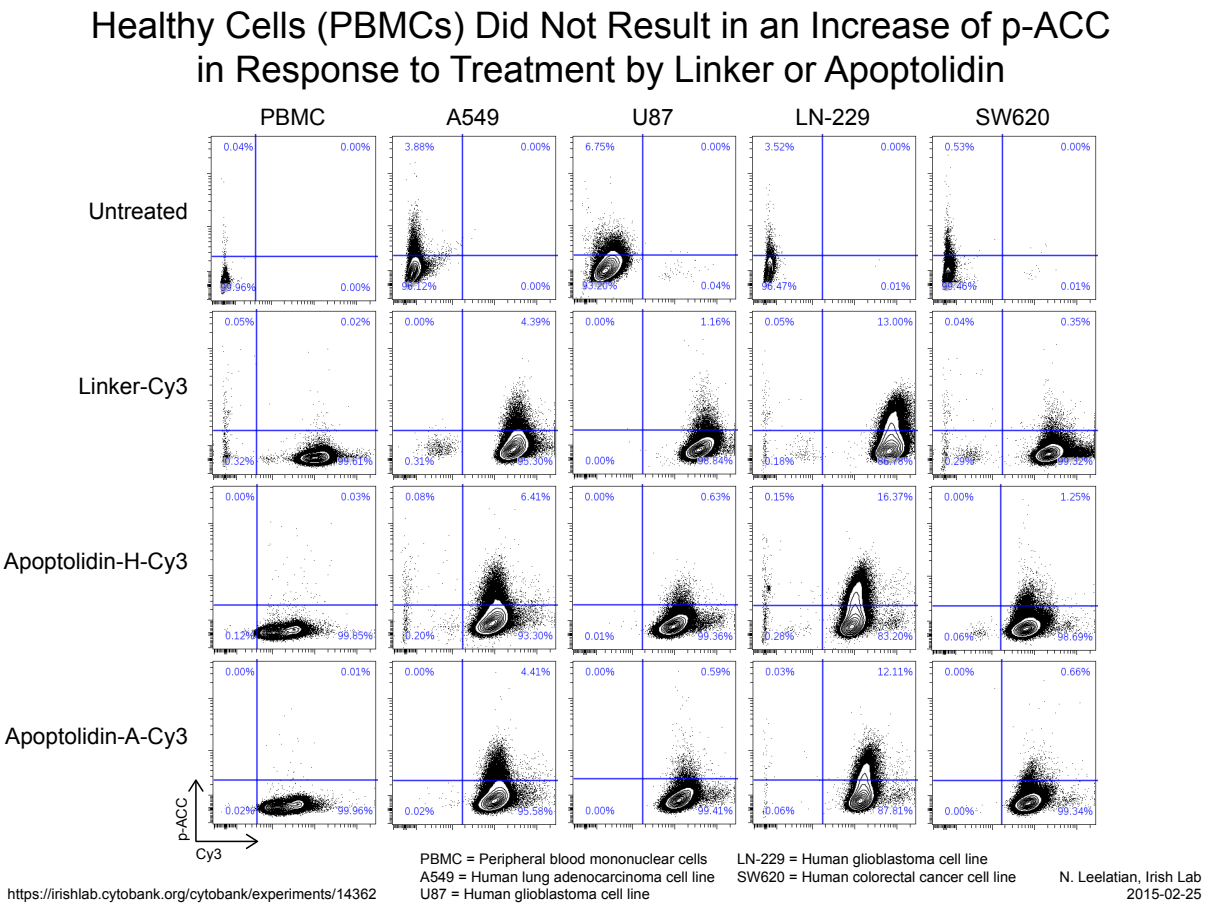

Figure 5.14. Fluorescent flow cytometry used to monitor cellular uptake of Cy3 apoptolidins A and H and phosphorylation of ACC.

In addition, Cy3 tagged apoptolidins A **5.20** and H **5.19** were used to monitor cellular uptake qualitatively in tumor cells (A549 lung cancer cell line, U87 gliablastoma cell line) as compared to healthy cells (PBMC's) via confocal microscopy (Fig. 5.14). The confocal images showed minimal uptake of the Cy3 apoptolidins by healthy PBMC's but higher uptake of Cy3 apoptolidins A **5.20** and H **5.19**.

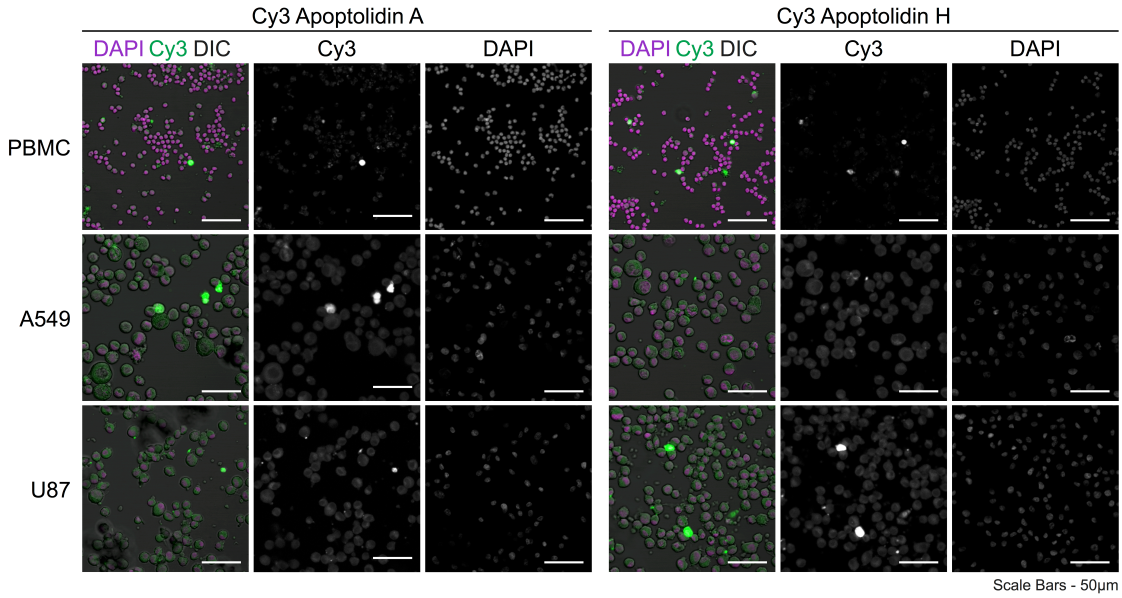

Figure 5.15. Confocal images demonstrate differential uptake of Cy3 apoptolidins in tumor cells relative to healthy cells.

5.4 Future works

Comprehensive access to fluorescent non-cationic apoptolidin glycovariants at each glycosylation state could be used for exhaustive study of the apoptolidin sugars' mechanistic effect on apoptolidin induced cancer cell death. With each apoptolidin glycovariant in hand, fluorescent probes can be created to further explore apoptolidin cellular localization, specific uptake into certain cancer cells, and cell response, including its induction of apoptosis and/or autophagy, as a function of glycosylation state. Fluorescent apoptolidins can be tracked and visualized via confocal microscopy using a non-cationic dye, according to glycosylation state. Cellular uptake and subsequent response studies can

be performed using single-cell fluorescent phospho-specific flow cytometry to understand up-regulation of specific phosphorylation events.

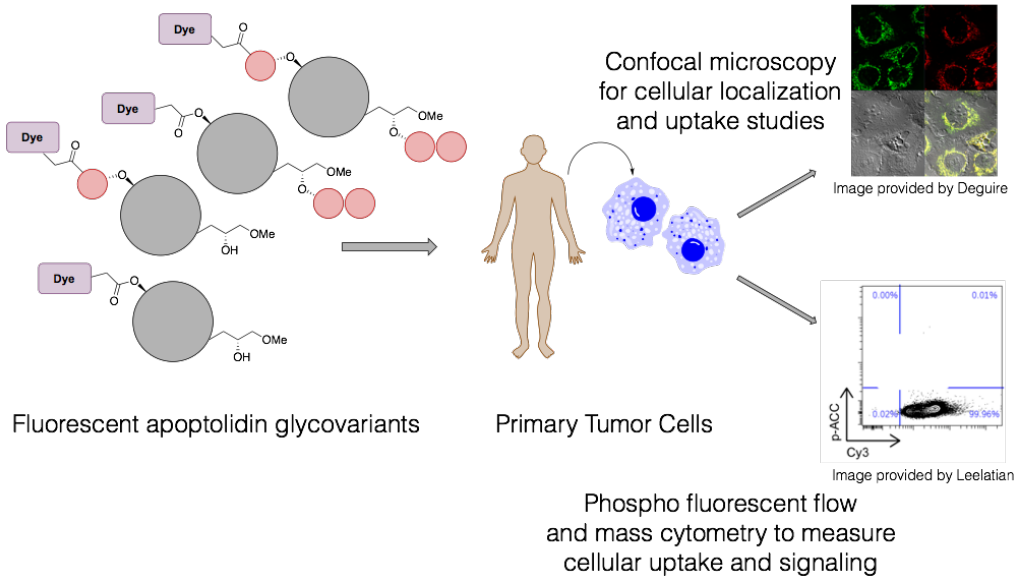

Figure 5.16. Graphical representation of proposed future work.

5.5 Experimental methods

Production and chemical synthesis of apoptolidins and fluorescent derivatives: Apoptolidins A and H were produced by fermentation of the apoptolidin producer FU 40 and a mutant strain (ApoGT2 knockout) at Vanderbilt University. Cyanine-3 derivatives of apoptolidin A and H were prepared by semi synthesis as described earlier.

Uptake of apoptolidins A and H in various cell types: Human cancer cell lines and peripheral blood mononuclear cells (PBMCs) were used to characterize uptake of apoptolidin A and apoptolidin H. The following cell lines were included: SW620 (colon cancer), U87-MG

(glioblastoma), LN229 (glioblastoma), and A549 (lung adenocarcinoma). Cell lines were cultured under ATCC recommended protocols. Cells were detached using Trypsin and resuspended in recommended culture media at 1x106 cells/mL prior to drug treatment. Human PBMCs were collected from a healthy donor following protocols approved by Vanderbilt University Medical Center Institutional Review Board, processed by standard Ficoll preparation protocol, and cryopreserved in liquid nitrogen. PBMCs were thawed and resuspended in warm RPMI 1640 media containing 10% FBS at 1x106 cells/mL prior to drug treatment. Cells were treated with either vehicle (DMSO), 1 μM of Cy3 apoplolidin A, or 1 μM of Cy3 apoptolidin H for 1 hour at 37°C. Cells were washed twice in PBS and fixed with 1.6% paraformaldehyde for 10 minutes at room temperature, and were permeabilized with ice-cold methanol for 30 minutes.

Fluorescent flow cytometry: After methanol permeabilization, cells were stained with 1:250 anti p-ACC antibody (Cell Signaling) for 30 minutes in the dark at room temperature. Cells were then stained with 1:1000 Donkey anti-Rabbit Ax647 (Life Technologies) for 30 minutes in the dark at room temperature, and were washed and resuspended in PBS for analysis on 5-laser BD LSRII (BD Biosciences, San Jose, CA) at the Vanderbilt Flow Cytometry Shared Resource and evaluated using Cytobank software. Untreated cells were stained with only the secondary antibody and used as negative control.

Confocal microscopy: The stained cell suspensions described above were incubated with diaminophenylindole (DAPI) at 1 μg/mL for 10 minutes at room temperature, and placed

on glass slides for imaging on an LSM 710 META inverted microscope (Zeiss) at the Vanderbilt Cell Imaging Shared Resource. Data were analyzed using

Zen 2011 software.

5.6 Notes and references

1. Deguire, S. M.; Earl, D. C.; Du, Y.; Crews, B. A.; Jacobs, A. T.; Ustione, A.; Daniel, C.; Chong, K. M.; Marnett, L. J.; Piston, D. W.; Bachmann, B. O.; Sulikowski, G. A., Fluorescent Probes of the Apoptolidins and their Utility in Cellular Localization Studies *Angew. Chem. Int. Ed.* **2015**, 54, 961-964.

2. Bunting, J. R.; Phan, T. V.; Kamali, E.; Dowbwen, R. M. Fluorescent cationic probes of mitochondria *Biophys. J.* **1989**, 56, 979-993.

3. Perry, S. W.; Norman, J. P.; Barbieri, J.; Brown, E. B.; Gelbard, H. A. Mitochondrial membrane potential probes and the proton gradient: a practical usage guide *BioTechniques* **2011**, 50, 98-115.

4. Patel, S. P.; Sullivan, P. G.; Pandya, J. D.; Rabchevsky, A. G. Differential Effects of the Mitochondrial Uncoupling Agent, 2,4-Dinitrophenol, or the Nitroxide Antioxidant, Tempol, on Synaptic or Nonsynaptic Mitochondria After Spinal Cord Injury *J. Neurosci. Res.* **2009**, 87, 130-140.

5. Pietrobon, D.; Luvisetto, S.; Azzone, G. F. Uncoupling of Oxidative Phosphorylation. 2. Alternative Mechanisms: Intrinsic Uncoupling or Decoupling? *Biochemistry* **1987**, 26, 7339-7347.

6. Loudet, A.; Burgess, K. BODIPY Dyes and Their Derivaties: Syntheses and Spectroscopic Properties *Chem. Rev.* **2007**, 107, 4891-4932.

7. Ulrich, G.; Ziessel, R.; Harriman, A. The Chemistry of Fluorescent BODIPY Dyes: Versatility Unsurpassed *Angew. Chem. Int. Ed.* **2008**, 47, 1184-1201.

8. BODIPY Dye Series—Section 1.4 ThermoFisher Scientific (https://www.thermofisher.com/us/en/home/references/molecular-probes-the-handbook/fluorophores-and-their-amine-reactive-derivatives/BODIPY-dye-series.html) Accessed Aug 3, 2017.

9. Probes for the Endoplasmic Reticulum and Golgi Apparatus–Section 12.4 ThermoFisher Scientific (https://www.thermofisher.com/us/en/home/references/molecular-probes-the-handbook/probes-for-organelles/probes-for-the-endoplasmic-reticulum-and-golgi-apparatus.html) Accessed Aug 3, 2017.

10. Chazotte, B. Labeling the Golgi Appartus with BODIPY-FL-Ceramide (C5-DMB-ceramide) for Imaging *CSH Protoc.* **2008**, 3, 1-2.

11. Wender, P. A.; Jankowski, O. D.; Tabet, E. A.; Seto, H. Toward a Structre-Activity Relationship for Apoptolidin: Selective Functionalization of the Hydroxyl Group Array *Org. Lett.* **2003**, 5, 487-490.

12. Lewis, C. A.; Longcore, K. E.; Miller, S. J.; Wender, P. A., An Approach to the Site-Selective Diversification of Apoptolidin A with Peptide-Based Catalysts *J. Nat. Prod.* **2009**, 72, 1864-1869.

13. Giebler, K.; Griesser, H.; Göhringer, D.; Sabirov, T.; Richert, C. Synthesis of 3'-BODIPY-Labeled Active Esters of Nucleotides and a Chemical Primer Extension Assay on Beads *Eur. J. Org. Chem.* **2010**, 3611-3620.

14. Chong, K. M.; Leelatian, N.; Deguire, S. M.; Brockman, A. A.; Earl, D.; Ihrie, R. A.; Irish, J. M.; Bachmann, B. O.; Sulikowski, G. A. The use of fluorescently-tagged apoptolidins in cellular uptake and response studies *J. Antibiot.* **2016**, 69, 327-330.

15. Krutzik, P. O.; Nolan, G. P. Intracellular phospho-protein staining techniques for flow cytometry: Monitoring single cell signaling events *Cytometry A* **2003**, 55, 61-70.

16. Schultz, K. R.; Danna, E. A.; Krutzik, P. O.; Nolan, G. P. Single-cell phospho-protein analysis by flow cytometry *Curr. Protoc. Immunol.* **2007**, 78, 17.1-17.7.

17. Krutzik, P. O.; Clutter, M. R.; Trejo, A.; Nolan, G. P. Fluorescent Cell Barcoding for Multiplex Flow Cytometry, *Curr. Protoc. Cytom.* **2011**, 55, 31.1-31.6

18. Meley, D.; Bauvy, C.; Houben-Weerts, J. H. P. M.; Dubbelhuis, P. F.; Helmond, M. T. J.; Codogno, P.; Meijer, A. J. AMP-activated Protein Kinase and the Regulation of Autophagic Proteolysis *J. Biol. Chem.* **2006**, 281, 34870-34879.

19. Serrill, J. D.; Tan, M.; Fotso, S.; Sikorska, J.; Kasanah, N.; Hau, A. M.; McPhail, K. L.; Santosa, D. A.; Zabiskie, T. M.; Mahmud, T.; Viollet, B.; Proteau, P. J.; Ishmael, J. E. Apoptolidins A and C activate AMPK in metabolically sensitive cell types and are mechanistically distinct from oligomycin A. *Biochem. Pharmacol.* **2015**, 3, 251-265.